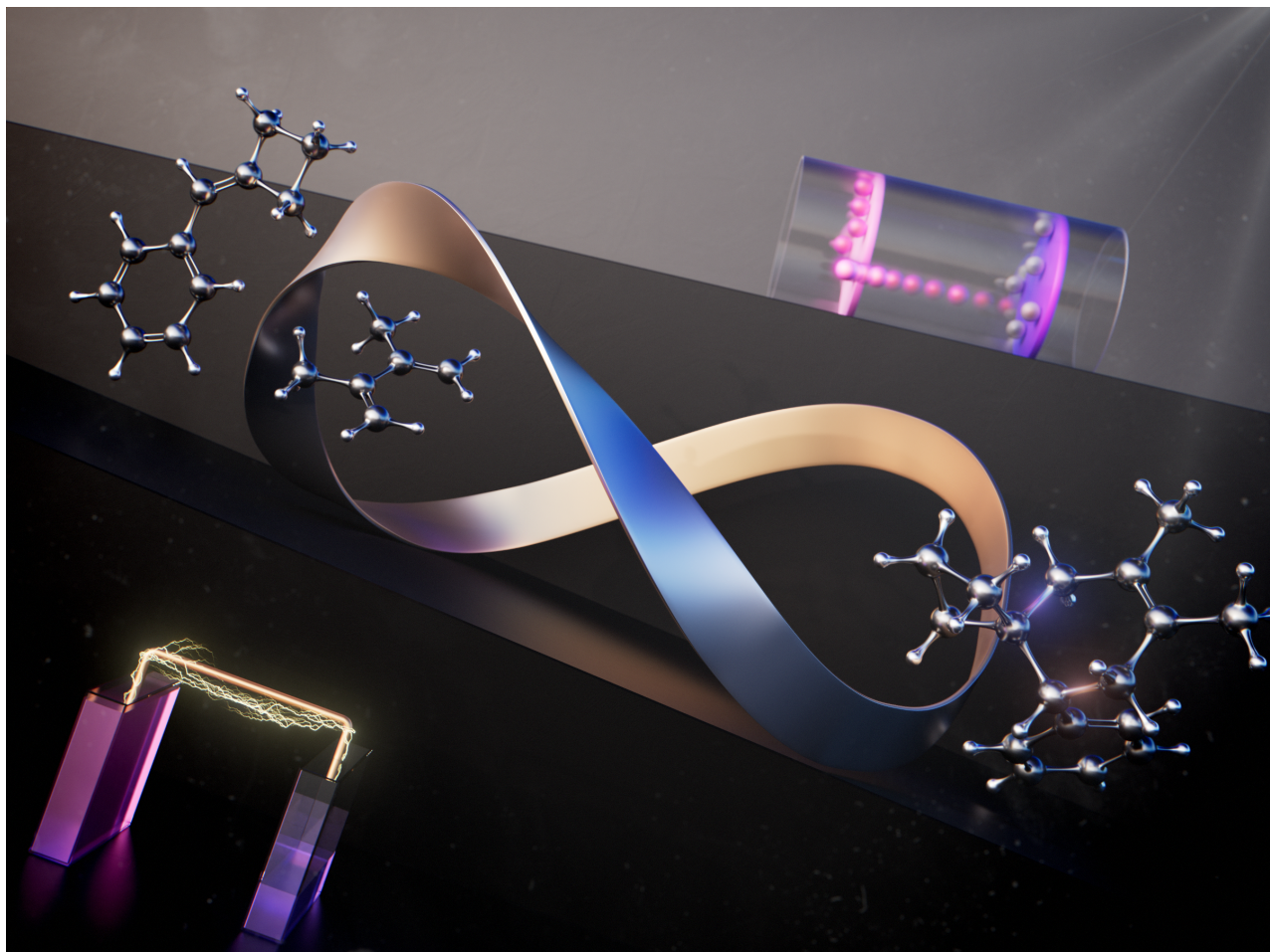




Molecular and macromolecular electrochemistry: synthesis, mechanism, and redox properties

Edited by Shinsuke Inagi and Mahito Atobe



Imprint

Beilstein Journal of Organic Chemistry
www.bjoc.org
ISSN 1860-5397
Email: journals-support@beilstein-institut.de

The *Beilstein Journal of Organic Chemistry* is published by the Beilstein-Institut zur Förderung der Chemischen Wissenschaften.

Beilstein-Institut zur Förderung der Chemischen Wissenschaften
Trakehner Straße 7–9
60487 Frankfurt am Main
Germany
www.beilstein-institut.de

The copyright to this document as a whole, which is published in the *Beilstein Journal of Organic Chemistry*, is held by the Beilstein-Institut zur Förderung der Chemischen Wissenschaften. The copyright to the individual articles in this document is held by the respective authors, subject to a Creative Commons Attribution license.

The cover image, copyright 2022 Yohei Okada, is licensed under the Creative Commons Attribution 4.0 license (<https://creativecommons.org/licenses/by/4.0>). The reuse, redistribution or reproduction requires that the author, source and license are credited.



Molecular and macromolecular electrochemistry: synthesis, mechanism, and redox properties

Shinsuke Inagi^{*1} and Mahito Atobe^{*2}

Editorial

Open Access

Address:

¹Department of Chemical Science and Engineering, Tokyo Institute of Technology, 4259 Nagatsuta-cho, Midori-ku, Yokohama 226-8502, Japan and ²Department of Chemistry and Life Science, Yokohama National University, 79-5 Tokiwadai, Hodogaya-ku, Yokohama 240-8501, Japan

Email:

Shinsuke Inagi^{*} - inagi@cap.mac.titech.ac.jp; Mahito Atobe^{*} - atobe@ynu.ac.jp

* Corresponding author

Keywords:

electron transfer; electrosynthesis; organic electrochemistry; redox-active materials

Beilstein J. Org. Chem. **2022**, *18*, 1505–1506.

<https://doi.org/10.3762/bjoc.18.158>

Received: 13 October 2022

Accepted: 21 October 2022

Published: 26 October 2022

This article is part of the thematic issue "Molecular and macromolecular electrochemistry: synthesis, mechanism, and redox properties".

Guest Editor: S. Inagi

© 2022 Inagi and Atobe; licensee Beilstein-Institut.

License and terms: see end of document.

Electrochemistry is now a powerful tool in organic chemistry not only for analyzing the electron transfer behavior of organic molecules and macromolecules, but also for driving organic reactions to produce value-added products. Electrochemical synthesis (or simply electrosynthesis) is increasingly recognized for the high academic and industrial importance, in line with the concept of green chemistry proposed in 1998 and the Sustainable Development Goals (SDGs) adopted by the United Nations in 2015. This is evidenced by the recent publication of special issues on organic electrosynthesis in various academic journals [1-5].

In addition to the conventional two- or three-electrode batch-type electrolytic cells, recent developments include microflow electrolytic reactors, polymer electrolyte membrane electrolysis technology, and new methods coupled with photoredox catalysts or transition metal catalysis, resulting in remarkable progress in organic electrosynthetic processes. Theoretical calculations have also led to a better understanding of the electron transfer behavior of organic molecules and the

estimation of subsequent reactions, resulting in a much better understanding of the reaction mechanism. Furthermore, because organic electrosynthesis requires the setting of many complex parameters, such as applied potential, current density, electrolyte, temperature, and so on, it has a high affinity to informatics approaches, e.g., machine learning, which is expected to become an increasingly important tool in the future.

Progress in the design of organic molecules and polymers and the understanding of the redox behavior of these compounds has led to the development of organic electrochemistry for energy material applications. Organic semiconductor design for electron or hole transport is important for transistor and solar cell applications, and redox-active (but stable) organic and polymeric materials are promising for secondary batteries and redox flow batteries. By understanding organic electron transfer reactions, we can face the challenge of how to design materials with better cycle properties by suppressing undesired side reactions.

To showcase this area of research, the present thematic issue focuses on the recent advances in molecular and macromolecular electrochemistry. The scope of this interdisciplinary issue ranges from synthetic aspects (such as electrosynthesis and reaction mechanisms) to materials science (including redox properties and devices).

Shinsuke Inagi and Mahito Atobe

Yokohama, October 2022

ORCID® IDs

Shinsuke Inagi - <https://orcid.org/0000-0002-9867-1210>

Mahito Atobe - <https://orcid.org/0000-0002-3173-3608>

References

1. Waldvogel, S. R. *Beilstein J. Org. Chem.* **2015**, *11*, 949–950. doi:10.3762/bjoc.11.105
2. Francke, R.; Little, R. D.; Inagi, S. *ChemElectroChem* **2019**, *6*, 4065–4066. doi:10.1002/celc.201901175
3. Little, R. D.; Moeller, K. D. *Chem. Rev.* **2018**, *118*, 4483–4484. doi:10.1021/acs.chemrev.8b00197
4. Minteer, S. D.; Baran, P. *Acc. Chem. Res.* **2020**, *53*, 545–546. doi:10.1021/acs.accounts.0c00049
5. Fuchigami, T. *Chem. Rec.* **2021**, *21*, 2079. doi:10.1002/tcr.202100232

License and Terms

This is an open access article licensed under the terms of the Beilstein-Institut Open Access License Agreement (<https://www.beilstein-journals.org/bjoc/terms>), which is identical to the Creative Commons Attribution 4.0 International License (<https://creativecommons.org/licenses/by/4.0>). The reuse of material under this license requires that the author(s), source and license are credited. Third-party material in this article could be subject to other licenses (typically indicated in the credit line), and in this case, users are required to obtain permission from the license holder to reuse the material.

The definitive version of this article is the electronic one which can be found at:

<https://doi.org/10.3762/bjoc.18.158>



Synthesis of piperidine and pyrrolidine derivatives by electroreductive cyclization of imine with terminal dihaloalkanes in a flow microreactor

Yuki Naito, Naoki Shida^{*} and Mahito Atobe^{*}

Full Research Paper

Open Access

Address:

Graduate School of Science and Engineering, Yokohama National University, Yokohama, Kanagawa 240-8501, Japan

Email:

Naoki Shida^{*} - shida-naoki-gz@ynu.ac.jp; Mahito Atobe^{*} - atobe@ynu.ac.jp

^{*} Corresponding author

Keywords:

electrochemical synthesis; electrocyclization; flow microreactor; heterocyclic amines; imine

Beilstein J. Org. Chem. **2022**, *18*, 350–359.

<https://doi.org/10.3762/bjoc.18.39>

Received: 13 January 2022

Accepted: 21 March 2022

Published: 29 March 2022

This article is part of the thematic issue "Molecular and macromolecular electrochemistry: synthesis, mechanism, and redox properties".

Associate Editor: J. A. Murphy

© 2022 Naito et al.; licensee Beilstein-Institut.

License and terms: see end of document.

Abstract

We have successfully synthesized piperidine and pyrrolidine derivatives by electroreductive cyclization using readily available imine and terminal dihaloalkanes in a flow microreactor. Reduction of the substrate imine on the cathode proceeded efficiently due to the large specific surface area of the microreactor. This method provided target compounds in good yields compared to a conventional batch-type reaction. Furthermore, piperidine and pyrrolidine derivatives could be obtained on preparative scale by continuous electrolysis for approximately 1 hour.

Introduction

Heterocycles are a very important class of compounds and make up more than half of all known organic chemicals [1]. Among them, heterocyclic amines, particularly pyrrolidine and piperidine derivatives, have attracted considerable attention because these are important structural motifs in a wide variety of applications including pharmaceuticals, natural products, and biologically active compounds such as pergolide, scopolamine, morphine, nicotine, hygrine, and procyclidine (Figure 1) [2-4]. Therefore, a considerable number of synthetic approaches to pyrrolidines and piperidines have been investigated [5-13].

Conventional synthetic methods for piperidine derivatives include nucleophilic substitution (route (1) in Scheme 1), reduc-

tive amination (route (2)), intramolecular cyclization of amines and alkenes (route (3)), the Diels–Alder reaction and subsequent reduction (route (4)), and the radical cyclization reaction (route (5)). However, these methods involve the use of toxic acids, bases, or transition metal catalysts, and typically require elevated temperatures [14-20]. In addition, very recently, Molander and co-workers have developed a photoredox-mediated radical/polar crossover process which realizes for the construction of medium-sized saturated nitrogen heterocycles [21]. Although the process enables the rapid construction of saturated nitrogen heterocycles from acyclic precursors, it requires homogeneous precious transition metal complexes as photocatalysts.

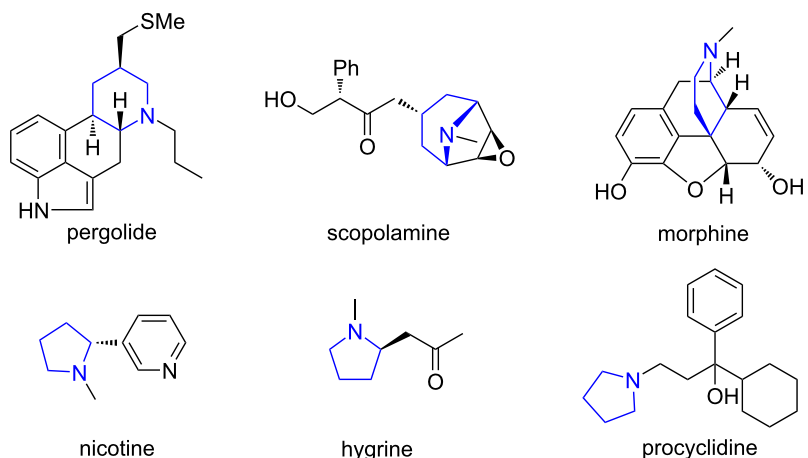
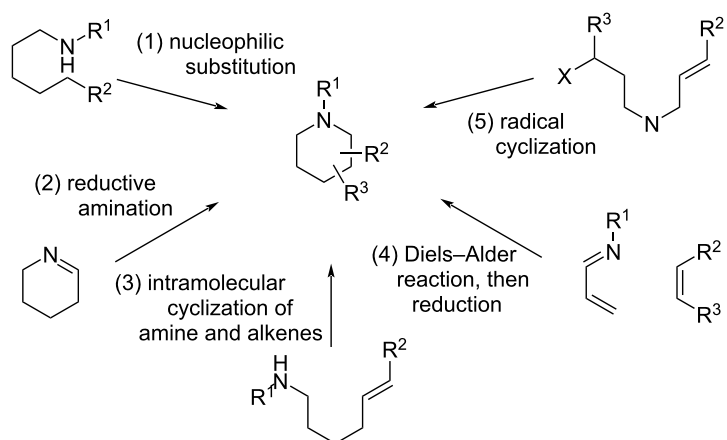


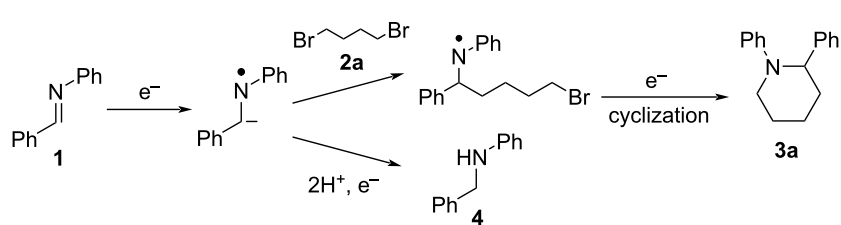
Figure 1: Piperidine and pyrrolidine rings in biologically active compounds.



Scheme 1: Conventional synthetic routes for piperidine derivatives.

On the other hand, organic electrosynthetic reactions, which are driven by direct electron transfer to and from the electrodes, can produce highly reactive species under ambient conditions without the use of harmful and precious chemicals. Therefore, electrosynthesis has been actively researched in recent years as a green and sustainable synthetic method in the face of increasingly stringent environmental and economic constraints. In this

context, several groups have demonstrated the electrochemical synthesis of piperidine and pyrrolidine derivatives by anodic oxidation [22–26]. In contrast, there has been only one report on the electroreductive synthesis of piperidine derivatives: namely Degrand and co-workers demonstrated electroreductive cyclization using imines and terminal dihaloalkanes to provide piperidine derivatives (Scheme 2) [27].



Scheme 2: Synthesis of 1,2-diphenylpiperidine (**3a**) by the electroreductive cyclization mechanism.

In this reaction, a stable radical anion is produced from the starting imine **1** in the first reduction step. The nucleophilic attack of the radical anion on the terminal dihaloalkane **2a** is the second step, which forms a radical. These sequential steps are followed by a further one-electron reduction at the cathode to provide an anion intermediate. The last step is cyclization of the mono-substituted anion to provide the cyclization product **3a**. In addition, the hydromonomeric product **4** was also formed as a byproduct. Although Degrand et al. [27] could successfully obtain the piperidine derivatives by this reductive cyclization; a toxic mercury pool cathode was used in their demonstration. Therefore, it is desirable to conduct the reductive cyclizations without the use of a mercury cathode, and the development of a simple, green, and efficient method for the electrochemical synthesis of heterocyclic amines is an important research target.

The electrochemical flow microreactor has recently attracted attention as an excellent alternative tool to conventional batch-type electrochemical reactors [28–32]. The potential advantages of electrochemical flow microreactors over conventional batch-type reactors are a large surface-to-volume ratio, precise residence time, extremely fast molecular diffusion, and expelling the reaction product to avoid over-oxidation or over-reduction. We have previously reported the electrochemical carboxylation of several imines in a flow microreactor to afford the corresponding α -amino acids in good to moderate yields [33–35]. The key features of this method are the effective cathodic reduction of imines and their rapid use for the subsequent reactions in a microflow system. Successful preliminary results prompted us to perform the electroreductive cyclization of an imine with terminal dihaloalkanes to afford heterocyclic amines in a flow microreactor because the reaction involves cathodic reduction of the imine and its rapid use for the subsequent reaction with the terminal dihaloalkanes.

In this work, we demonstrate the electroreductive cyclization of an imine with terminal dihaloalkanes in a flow microreactor to establish a facile, green, and efficient method for the synthesis of heterocyclic amines such as pyrrolidine and piperidine derivatives.

Results and Discussion

As a model reaction, the electroreductive cyclization of benzylideneaniline with 1,4-dibromobutane to provide 1,2-diphenylpiperidine was selected. The microreactor fabricated for the model reaction had a simple geometry with the cathode and anode directly facing each other at a distance of several tens of micrometers (Figure 2). The electrolyte containing benzylideneaniline (**1**) and 1,4-dibromobutane (**2a**) was pumped into the gap between the two electrodes and subjected to the electrolytic reaction. Tetrahydrofuran (THF), which is easily oxidized, was employed as the electrolytic solvent, so the reaction at the anode (counter electrode) is thought to be preferentially caused by the oxidative decomposition of THF, and the re-oxidation of the cathodic reaction products at the anode would be suppressed.

On the other hand, the cathode material is an important factor in selecting the course of the cathodic reaction and to control the efficiency of the reaction. To select a suitable cathode material for this model reaction, we first investigated the effect of the cathode material on the yield of **3a** using three different cathode materials: platinum (Pt), glassy carbon (GC), and silver (Ag). As shown in Table 1, the yield of **3a** was higher using GC than that of the other cathode materials. The yield of the hydromonomeric product **4** was also highest when GC was used. Both **3a** and **4** are products obtained through the reduction of imine **1**, which suggests that the GC cathode is effective for the reduction of imine **1**. In sharp contrast, the yields of both

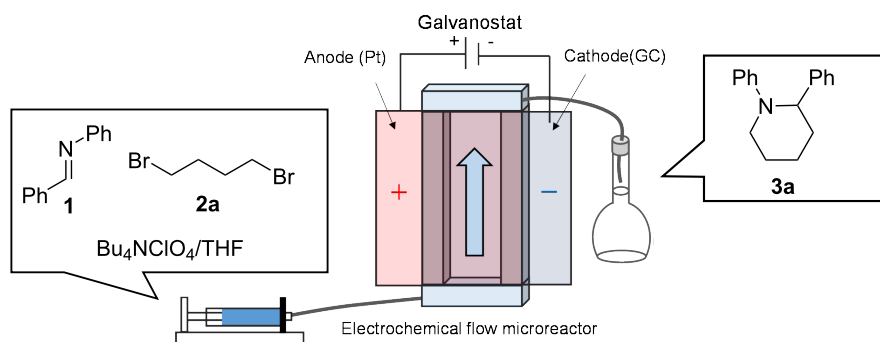


Figure 2: Schematic diagram of the electroreductive cyclization for the synthesis of 1,2-diphenylpiperidine (**3a**) in an electrochemical flow microreactor. Adapted with permission from ref. [33]. Copyright 2021 American Chemical Society. This content is not subject to CC BY 4.0.

3a and **4** were very low when a Ag cathode was used. A Ag cathode has electrocatalytic activity for the reduction of organic halides [35,36]; therefore, 1,4-dibromobutane (**2a**) was more easily reduced than **1** at the Ag cathode, which resulted in the recovery of a large amount of unreacted **1**. Linear sweep voltammetry (LSV) experiments revealed that the reduction of **2a** occurred at a lower potential than the reduction of **1** when the Ag cathode was used (Supporting Information File 1, Figure S7). Furthermore, LSV experiments with various cathodes showed that the reduction of **2a** was significantly dependent on the cathode material, and their overpotentials were larger in the order of Ag < Pt < GC (Supporting Information File 1, Figures S5–S7). Therefore, GC prioritized the reduction of **1**, even in the presence of **2a**, to produce **3a** and **4** efficiently. In the following experiments, GC was used as the cathode material for this reaction.

Table 1: Effect of the cathode material on the reduction products, **3a** and **4**^a.

Entry	Cathode material	Yield of 3a (%) ^b	Yield of 4 (%) ^b
1	Pt	21	27
2	GC	36	53
3	Ag	2	2

^aExperimental conditions: anode, Pt plate; electricity, 2.15 F mol⁻¹; current density, 12.7 mA cm⁻²; electrode distance, 40 µm; solvent, THF; substrate, 0.06 M benzylideneaniline (**1**) and 0.06 M 1,4-dibromobutane (**2a**); supporting electrolyte, 0.14 M *n*-Bu₄N-ClO₄; flow rate, 11 mL h⁻¹ (residence time, 3.9 s). ^bDetermined by HPLC.

The effect of the amount of **2a** addition on the yield of **3a** was then investigated. Table 2 shows that the yield of **3a** increased as the amount of **2a** was increased, and reached a maximum at 2 equiv. The yield of **3a** began to decrease with the addition of more **2a**. This decrease in the yield of **3a** can be attributed to the competition of the cathodic reduction of **2a** caused by the increase in the amount of **2a** addition. On the other hand, as shown in Scheme 2, the desired product **3a** is produced by the reaction of **2a** with the radical anion species of the substrate imine **1**, while the hydromonomeric product **4** is produced by the reaction of protons with the radical anion species of **1**. Therefore, the yield of **4** consistently decreased with the increase in the amount of **2a** addition.

In the model process in an electrochemical flow microreactor, the desired reaction (the reaction of radical anion of imine **1** with **2a** to afford **3a**) at the cathode may be interfered with by the protons generated by the oxidation of the THF solvent at anode, leading to increased formation of **4** because the distance between the electrodes of the reactor is much shorter than that

Table 2: Effect of the amount of 1,4-dibromobutane (**2a**) addition on the yield of the reduction products **3a** and **4**^a.

Entry	1,4-Dibromobutane (equiv)	Yield of 3a (%) ^b	Yield of 4 (%) ^b
1	1.0	36	53
2	1.5	45	40
3	2.0	47	33
4	3.0	28	29
5	5.0	26	24

^aExperimental conditions: cathode, GC plate; anode, Pt plate; electricity, 2.15 F mol⁻¹; current density, 12.7 mA cm⁻²; electrode distance, 40 µm; solvent, THF; substrate, 0.06 M benzylideneaniline (**1**) and 1,4-dibromobutane (**2a**); supporting electrolyte, 0.14 M *n*-Bu₄N-ClO₄; flow rate, 11 mL h⁻¹ (residence time, 3.9 s). ^bDetermined by HPLC.

of conventional batch-type reactors. Therefore, the electrode distance is also an important factor that must be investigated to obtain the desired product **3a** in a high yield. Table 3 shows the effect of the electrode distance on the yield of the reduction products **3a** and **4**. From these results, the optimal electrode distance was determined to be 40 µm (Table 3, entry 2). When the electrode distance was increased to 80 µm, the yield of **3a** decreased (Table 3, entry 1). This may be ascribed to the decrease in the surface-to-volume ratio, which makes it difficult for imine **1** to reach the cathode during the residence time. On the other hand, when the electrode distance was decreased to 20 µm, not only the yield of **3a**, but also the selectivity toward **3a/4** decreased (Table 3, entry 3). As mentioned above, this is probably because the protons generated by the oxidation of the THF solvent at anode could easily meet the radical anions of imine **1** generated at cathode due to the very short interelectrode distance.

Table 3: Effect of the electrode distance on the yield of the reduction products **3a** and **4**^a.

Entry	Electrode distance/µm (residence time/s)	Yield of 3a (%) ^b	Yield of 4 (%) ^b	Selectivity 3a/4
1	80 (7.9)	35	26	1.35
2	40 (3.9)	47	33	1.42
3	20 (2.0)	21	27	0.78

^aExperimental conditions: cathode, GC plate; anode, Pt plate; solvent, electricity, 2.15 F mol⁻¹; current density, 12.7 mA cm⁻²; solvent, THF; substrate, 0.06 M benzylideneaniline (**1**) and 0.12 M 1,4-dibromobutane (**2a**); supporting electrolyte, 0.14 M *n*-Bu₄N-ClO₄; flow rate, 11 mL h⁻¹. ^bDetermined by HPLC.

In the electrochemical reaction, the electrons themselves act as reagents, so electricity affects the degree of reaction progress.

In addition, excessive electricity may also cause undesired electrochemical reactions, and it is thus extremely important to estimate the optimal electricity for the desired reaction. For constant-current electrolysis in a flow microreactor with fixed channel dimensions, the electricity can be controlled by changing the current density or flow rate. As shown in entries 1 and 2 of Table 4, the yield of **3a** increased with the electricity (caused by an increase in the current density) and reached a maximum value at 2.15 F mol^{-1} . The theoretical electricity required for the generation of **3a** is 2 F mol^{-1} ; however, 2 F mol^{-1} of electricity was probably insufficient to fully convert the substrate imine **1** introduced into the reactor. On the other hand, as shown in Table 4, entries 3–5, the yield of **3a** decreased slightly when the electricity was increased from 2.15 F mol^{-1} and above, and in contrast, there was an increasing trend in the yield of **4**. This may be ascribed to an increase in the proton supply resulting from THF oxidation at the anode due to an increase in the electricity, which promoted the formation of **4** by the reaction between protons and the radical anions of **1**. As shown in Table 4, entry 6, the yield of **3a** decreased when the electricity was fixed at 2 F mol^{-1} by increasing the flow rate over the conditions in Table 4, entry 2. On the other hand, as shown in Table 4, entry 7, the yield of **3a** was also decreased compared to entry 2 when the electricity was increased to 3 F mol^{-1} by decreasing the flow rate.

The rate of the nucleophilic reaction between the radical anion intermediate generated reductively from **1** and **2a** would be influenced by the cation size of the supporting electrolyte used because this leads to different ion-pair interactions with the radical anion intermediate. To confirm this conjecture, we carried out the model reaction using perchlorate salts consisting of cations of different sizes. As shown in entry 2 of Table 5, when $\text{Et}_4\text{N}\cdot\text{ClO}_4$ was used as the supporting electrolyte, the electrolysis reaction could not be carried out because $\text{Et}_4\text{N}\cdot\text{ClO}_4$

did not dissolve in the THF solution. On the other hand, $n\text{-Hex}_4\text{N}\cdot\text{ClO}_4$ dissolved easily in THF solution and the electrolysis reaction proceeded smoothly. However, the yield of the desired product **3a** was slightly lower than that using $n\text{-Bu}_4\text{N}\cdot\text{ClO}_4$. Therefore, $n\text{-Bu}_4\text{N}\cdot\text{ClO}_4$ is the most suitable supporting electrolyte for the model reaction among the tested electrolytes.

Table 5: Effect of the supporting electrolyte on the yield of the reduction products **3a** and **4**^a.

Entry	Supporting electrolyte	Yield of 3a (%) ^b	Yield of 4 (%) ^b
1	$n\text{-Bu}_4\text{N}\cdot\text{ClO}_4$	47	33
2	$\text{Et}_4\text{N}\cdot\text{ClO}_4$ ^c	–	–
3	$n\text{-Hex}_4\text{N}\cdot\text{ClO}_4$	39	18

^aExperimental conditions: cathode, GC plate; anode, Pt plate; electricity, 2.15 F mol^{-1} ; current density, 12.7 mA cm^{-2} ; electrode distance, $40 \mu\text{m}$; solvent, THF; substrate, 0.06 M benzylideneaniline (**1**) and 1,4-dibromobutane (**2a**); concentration of supporting electrolyte, 0.14 M ; flow rate, 11 mL h^{-1} (residence time, 3.9 s). ^bDetermined by HPLC. ^c $\text{Et}_4\text{N}\cdot\text{ClO}_4$ did not dissolve in THF solution.

In these investigations, the yield of the desired product **3a** was improved to 47% (entry 1 of Table 5); however, this was still not sufficient. To further improve the yield, it would be effective to suppress the competing formation of **4**. To meet this challenge, we attempted to add various bases to the electrolyte to capture the protons in the reaction system. Table 6 shows that the yields of **3a** and **4** were strongly influenced by the type of base added. When 1,8-diazabicyclo[5.4.0]-7-undecene (DBU), which has the strongest basicity among these bases, was used, the yield of **3a** increased significantly, while the formation of **4** was suppressed. In particular, when more than 1.0 equiv of DBU was added, the yield of **3a** reached almost 80%.

Table 4: Effect of electricity on the reduction products **3a** and **4**^a.

Entry	Electricity / F mol^{-1}	Current density / mA cm^{-2}	Flow rate / mL h^{-1} (residence time/s)	Yield of 3a (%) ^b	Yield of 4 (%) ^b
1	2.0	11.8	11 (3.9)	33	21
2	2.15	12.7	11 (3.9)	47	33
3	2.3	13.6	11 (3.9)	37	37
4	2.5	14.0	11 (3.9)	34	29
5	3.0	17.7	11 (3.9)	35	46
6	2.0	12.7	12 (3.6)	23	13
7	3.0	12.7	8 (5.4)	31	26

^aExperimental conditions: cathode, GC plate; anode, Pt plate; solvent, THF; electrode distance, $40 \mu\text{m}$; substrate, 0.06 M benzylideneaniline (**1**) and 0.12 M 1,4-dibromobutane (**2a**); supporting electrolyte, 0.14 M $n\text{-Bu}_4\text{N}\cdot\text{ClO}_4$. ^bDetermined by HPLC.

Table 6: Effect of the type of added base on the yield of the reduction products **3a** and **4**^a.

Entry	Base		Yield of 3a (%) ^c	Yield of 4 (%) ^c
	Type (<i>pK_a</i> of conjugated acid of base ^b)	equiv		
1	pyridine (5.33)	0.5	33	19
2	2,6-lutidine (6.7)	0.5	38	30
3	piperidine (11.1)	0.5	31	28
4	DBU (12.0)	0.5	61	25
5	DBU (12.0)	1.0	78	11
6	DBU (12.0)	1.5	77	17

^aExperimental conditions: cathode, GC plate; anode, Pt plate; electricity, 2.15 F mol⁻¹; current density, 12.7 mA cm⁻²; electrode distance, 40 µm; solvent, THF; substrate, 0.06 M benzylideneaniline (**1**) and 0.12 M 1,4-dibromobutane (**2a**); base added, 0.06 M DBU; supporting electrolyte, 0.14 M *n*-Bu₄N-ClO₄; flow rate, 11 mL h⁻¹ (residence time, 3.9 s). ^bLiterature data according to ref. [37–41]. ^cDetermined by HPLC.

The reactivity of the radical anions of imine **1** with the terminal dihaloalkane is also considered to be an important factor in the formation of the desired product **3a**. Therefore, a model reaction was conducted using dihaloalkanes with different types of terminal halogens (Cl, Br, and I) (Table 7). When the terminal halogen of the dihaloalkane was changed from Br to Cl, the yield of **3a** decreased significantly (Table 7, entry 2). This is probably due to the poor leaving ability of Cl and its low reactivity with the radical anion species generated from imine **1**. This is supported by the increase in the formation of the competing **4**. On the other hand, the yield of **3a** decreased even when the terminal halogen of the dihaloalkane was changed to iodine (Table 7, entry 3). LSV measurements showed that the reduction potential of 1,4-diodobutane (**2c**) was almost the

same as that of the substrate imine **1** (Supporting Information File 1, Figure S12); therefore, the competition between the reduction of **2c** and that of the imine **1** may have caused the low yield of **3a**. A large amount (50%) of unreacted **1** was recovered in this case. Therefore, it can be stated that Br is appropriate as the terminal halogen of the dihaloalkane in this cyclization reaction.

A model electroreductive cyclization was subsequently conducted in a conventional batch-type reactor and a flow microreactor with the same electrolytic parameters (Table 8). The yield of **3a** was much higher in the electrochemical flow microreactor than in the batch-type reactor. In the batch system, the concentration of substrate imine **1** in the electrolyte decreases as the

Table 7: Yields of **3a** and **4** in the model reductive cyclization using dihaloalkanes with different types of terminal halogens^a.

Entry	Type of X	3a ^b (%)	4 ^b (%)
1	Br (2a)	78	11
2	Cl (2b)	6	72
3	I (2c)	14	13

^aExperimental conditions: cathode, GC plate; anode, Pt plate; electricity, 2.15 F mol⁻¹; current density, 12.7 mA cm⁻²; electrode distance, 40 µm; solvent, THF; substrate, 0.06 M benzylideneaniline (**1**) and 0.12 M 1,4-dihaloalkane (**2a**, **2b**, or **2c**); base added, 0.06 M DBU; supporting electrolyte, 0.14 M *n*-Bu₄N-ClO₄; flow rate, 11 mL h⁻¹ (residence time, 3.9 s). ^bDetermined by HPLC.

electrolysis progresses, which makes it difficult for the reaction to proceed. Therefore, even after passing more than the theoretical amount of electricity, a considerable amount (28%) of imine **1** remained. In contrast, in the flow system, the electrolyte containing a predetermined amount of imine **1** is always supplied from the reactor inlet, and the relatively fast flow in the reactor provides a good supply of imine **1** to the working electrode (cathode), so the steady state may be maintained in the flow microreactor. Such an ideal environment for the reduction of imine **1** is considered to result in the high yield of **3a**.

Table 8: Effect of reactor type on the yield of the reduction products **3a** and **4a**.

Entry	Reactor type	Electrode distance/ μm	Yield of 3a (%) ^b	Yield of 4a (%) ^b
1	batch	2 cm	45	25
2	flow	40 μm	77	20

^aExperimental conditions: cathode, GC plate; anode, Pt plate; electricity, 2.15 F mol⁻¹; current density, 12.7 mA cm⁻²; solvent, THF (10 mL each were used for batch and flow experiments.); substrate, 0.06 M benzylideneaniline (**1**) and 0.12 M 1,4-dibromobutane (**2a**); base added, 0.06 M DBU; supporting electrolyte, 0.14 M *n*-Bu₄N-ClO₄; flow rate, 11 mL h⁻¹ (residence time, 3.9 s). ^bDetermined by HPLC.

To confirm that the reaction environment of the flow system was in the steady state, the electrolyzed solution was collected from the reactor outlet at regular intervals and the yield of **3a** for each fraction was determined (Figure 3). Continuous flow electrolysis could be performed without any problem at least until the fifth fraction collection. The yields of the fractions were almost the same, and the average yield of the five fractions was 77%. In addition, no precipitates were observed on the electrodes after the electrolysis, which suggests that a stable yield could be maintained. Therefore, it can be stated that the reaction environment of the flow system was in the steady state.

Experimental conditions for the collection of each fraction sample: cathode, GC plate; anode, Pt plate; electricity, 2.15 F mol⁻¹; current density, 12.7 mA cm⁻²; solvent, THF; substrate, 0.06 M benzylideneaniline (**1**) and 0.12 M 1,4-dibromobutane (**2a**); base added, 0.06M DBU; supporting electrolyte, 0.14 M *n*-Bu₄N-ClO₄; flow rate, 11 mL h⁻¹ (residence time, 3.9 s); collection volume and time for each fraction, 2 mL, 10 min 55 s. The yield of **3a** was determined by HPLC.

After mixing the five fraction samples, we attempted to isolate **3a** from the mixture, and obtained 78.4 mg (55% isolated yield) of **3a** (entry 1 of Table 9). The desired piperidine derivative could be obtained on a scale of several tens of milligrams in approximately 1 hour of continuous electrolysis; therefore, we

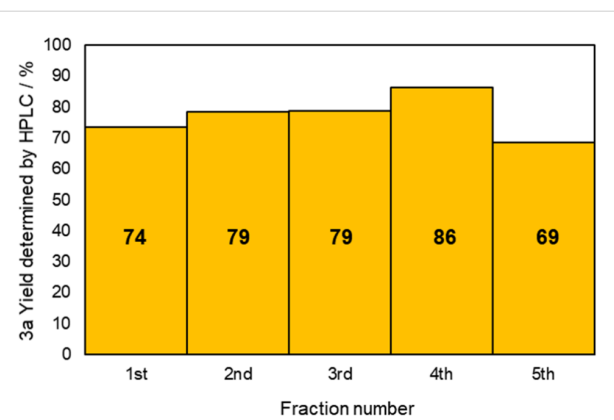


Figure 3: Yield of **3a** for each fraction sample in the continuous flow reductive cyclization.

then attempted to synthesize pyrrolidine and azetidine derivatives (**3b** and **3c**) using the same procedure (entries 2 and 3 of Table 8). **3b** was obtained from imine **1** and dihaloalkane **2d** with a good isolated yield (57%, 75.8 mg). However, the azetidine derivative **3c** was not obtained at all by the reductive cyclization of **1** and **2e**. LSV experiments revealed that the reduction of **2e** occurred at a slightly lower potential than the reduction of **1** (Supporting Information File 1, Figure S14). Therefore, in this case, the competitive reduction of **2e** would inhibit the desired cyclization reaction via the reduction of **1**.

Conclusion

We have demonstrated a facile, green, and efficient method for the synthesis of heterocyclic amines by electroreductive cyclization using a flow microreactor. This method not only allows the synthesis of pyrrolidine and piperidine derivatives from readily available compounds in a single step, but also has the advantage of eliminating the use of expensive or toxic reagents. In addition to optimization of the general parameters for the electrolytic reaction, the effect of base addition was also investigated, and was determined to suppress the formation of the hydromonomeric product, which is a main byproduct. Among the various bases, DBU suppressed the formation of byproducts and the desired cyclization products such as piperidine and pyrrolidine derivatives were obtained in good yields. Moreover, in the electrochemical flow microreactor, the yield of the desired product was much higher than in the batch reactor. These findings provide new insights into the synthetic chemistry of heterocyclic amines.

Experimental General considerations

All chemicals were used without further purification. **1**, **2a–e**, and **4** were purchased from commercial sources. **3a**, **3b**, and **3c** were synthesized according to reported procedures (see Sup-

Table 9: Isolated yield of heterocyclic amines (**3a–c**) obtained by the reductive cyclization of imine **1** with various dihaloalkanes (**2a**, **2d**, and **2e**)^a.

Entry	Terminal dihaloalkane 2	Isolated yield of 3 (%)	Chemical reaction scheme showing the reductive cyclization of imine 1 with dihaloalkane 2 to form heterocyclic amine 3 under the specified conditions.		
			1	2	3
1			<i>n</i> = 3 (2a)	<i>n</i> = 3 (3a)	55%
2			<i>n</i> = 2 (2d)	<i>n</i> = 2 (3b)	57%
3			<i>n</i> = 1 (2e)	<i>n</i> = 1 (3c)	n.d.

^aExperimental conditions: cathode, GC plate; anode, Pt plate; electricity, 2.15 F mol⁻¹; current density, 12.7 mA cm⁻²; electrode distance, 40 µm; solvent, THF; substrate, 0.06 M benzylideneaniline (**1**) and 0.12 M terminal dihaloalkane (**2a**, **2d**, or **2e**); base added, 0.06 M DBU; supporting electrolyte, 0.14 M *n*-Bu₄N·ClO₄; flow rate, 11 mL h⁻¹ (residence time, 3.9 s); collection volume and time for the reaction solution, 10 mL, 54 min 35 s.

porting Information File 1). A silicon oil bath was used as a heat source for the synthesis of **3a**. Flow electrolysis was conducted with an in-house-built electrochemical flow microreactor. The substrate solution was introduced to the microreactor by a syringe pump (KDS100, KdScientific Muromachi Kikai) during the electrosynthesis. Electroreductive cyclization was conducted using a potentiogalvanostat (HABF-501A, Hokuto Denko). High-performance liquid chromatography (HPLC) analysis for **3a** and **4** was performed with a column (Mightysil RP-18 GP II 250-4.6 (5 µm), Cica) using a mixture of H₂O/MeCN/H₃PO₄ (60/40/0.1%) as a mobile phase. All chromatograms were recorded using an LC workstation (LabSolutions DB, Shimadzu). Helium gas was used as a carrier gas for the gas chromatography/mass spectrometry (GC–MS) analyses. ¹H nuclear magnetic resonance (NMR) spectra were recorded on a spectrometer (DRX-500, Bruker; 500 MHz) using tetramethylsilane (TMS) as an internal standard with the solvent resonance (CDCl₃: δ 7.26). The chemical shifts for ¹H NMR spectra are given in δ (ppm) relative to the TMS internal standard. Multiplicities are abbreviated as singlet (s), doublet (d), triplet (t), doublet of triplet (dt), and multiplet (m). Linear sweep voltammetry (LSV) was performed using an electrochemical analyzer (630c, ALS/H CH Instruments).

Fabrication of the electrochemical flow microreactor

The electrochemical flow microreactor was constructed with a platinum plate (3 × 3 cm) and cathode plate (3 × 3 cm) (Supporting Information File 1, Figure S1). A spacer (double faced adhesive type with thicknesses of 20, 40, or 80 µm) was used to leave a rectangular channel exposed (1 × 3 cm), and the two electrodes were simply sandwiched together. After connecting Teflon tubings to the inlets and outlet, the reactor was sealed with epoxy resin (Supporting Information File 1, Figure S2). Thus, the dimensions of the flow channel in the reactor are 1 cm width and 3 cm length, and the channel height corresponds to the thickness of the spacer (20, 40, or 80 µm).

Procedure for the electroreductive cyclization using an electrochemical flow microreactor

The flow microreactor system for the model synthetic reaction was fabricated as illustrated in Supporting Information File 1, Figure S1. The electroreductive cyclization reaction was conducted by introduction of a solution (*n*-Bu₄N·ClO₄ or *n*-Hex₄N·ClO₄ in THF) containing imine **1**, terminal dihaloalkane **2**, and a base into the electrochemical flow microreactor from a syringe pump. Imine **1** is reduced at the cathode in the flow microreactor and then the generated radical anions

of **1** react with the terminal dihaloalkane to produce the corresponding heterocyclic compounds. The THF solvent is oxidized at the anode to generate protons. After electrolysis, 1 mL of the reaction solution was collected from the outlet of the reactor, diluted 5 times with THF, and analyzed using HPLC.

Procedure for the electroreductive cyclization using a batch-type reactor

10 mL of a solution (*n*-Bu₄N-ClO₄ in THF) containing 0.06 M benzylideneaniline (**1**), 0.12 M 1,4-dibromobutane (**2a**), and 0.06 M DBU was prepared. This solution was then added to an undivided cell equipped with a working electrode (GC plate, 1 × 3 cm) and a counter electrode (Pt plate, 1 × 3 cm). The distance between the two electrodes was set to ca. 2 cm. Constant current (12.7 mA cm⁻²) was subsequently applied for the electrolysis reaction. After passage of the electricity (2.15 F mol⁻¹), the electrolyzed solution was diluted 5 times with THF and analyzed using HPLC.

Supporting Information

Supporting Information File 1

Detailed experimental procedures, analytical data, and supplementary figures, and photographs.

[<https://www.beilstein-journals.org/bjoc/content/supplementary/1860-5397-18-39-S1.pdf>]

Acknowledgements

The graphical abstract was adapted with permission from ref. [33]. Copyright 2021 American Chemical Society. This content is not subject to CC BY 4.0.

Funding

This work was financially supported by a grant from the CREST program (No. 18070940) of the Japan Science and Technology Agency (JST) and by Grants-in-Aid for Scientific Research (Nos. 20H02513, 20K21106, and 21H05215) from the Japan Society for the Promotion of Science (JSPS).

ORCID® IDs

Naoki Shida - <https://orcid.org/0000-0003-0586-1216>

Mahito Atobe - <https://orcid.org/0000-0002-3173-3608>

References

1. Eftekhari-Sis, B.; Zirak, M.; Akbari, A. *Chem. Rev.* **2013**, *113*, 2958–3043. doi:10.1021/cr300176g
2. Kaur, N. *Synth. Commun.* **2014**, *44*, 3229–3247. doi:10.1080/00397911.2013.798666
3. Sakulsaknimitr, W.; Kuhakarn, C.; Tuchinda, P.; Reutrakul, V.; Pohmakotr, M. *ARKIVOC* **2009**, No. xii, 81–97. doi:10.3998/ark.5550190.0010.c07
4. Knölker, H.-J.; Reddy, K. R. *Chem. Rev.* **2002**, *102*, 4303–4427. doi:10.1021/cr020059j
5. Wei, D.; Netkaew, C.; Darcel, C. *Adv. Synth. Catal.* **2019**, *361*, 1781–1786. doi:10.1002/adsc.201801656
6. Wurz, R. P.; Fu, G. C. *J. Am. Chem. Soc.* **2005**, *127*, 12234–12235. doi:10.1021/ja053277d
7. Legault, C. Y.; Charette, A. B. *J. Am. Chem. Soc.* **2005**, *127*, 8966–8967. doi:10.1021/ja0525298
8. Zhu, C.-Z.; Feng, J.-J.; Zhang, J. *Chem. Commun.* **2018**, *54*, 2401–2404. doi:10.1039/c8cc00279g
9. Benhaoua, C. *Org. Chem. Int.* **2012**, *1*–6. doi:10.1155/2012/482952
10. Singh, S. *Chem. Rev.* **2000**, *100*, 925–1024. doi:10.1021/cr9700538
11. Baliah, V.; Jeyaraman, R.; Chandrasekaran, L. *Chem. Rev.* **1983**, *83*, 379–423. doi:10.1021/cr00056a002
12. Bull, J. A.; Mousseau, J. J.; Pelletier, G.; Charette, A. B. *Chem. Rev.* **2012**, *112*, 2642–2713. doi:10.1021/cr200251d
13. Yamazaki, K.; Gabriel, P.; Di Carmine, G.; Pedroni, J.; Farizyan, M.; Hamlin, T. A.; Dixon, D. J. *ACS Catal.* **2021**, *11*, 7489–7497. doi:10.1021/acscatal.1c01589
14. Buffat, M. G. P. *Tetrahedron* **2004**, *60*, 1701–1729. doi:10.1016/j.tet.2003.11.043
15. Clemente, F.; Matassini, C.; Cardona, F. *Eur. J. Org. Chem.* **2020**, 4447–4462. doi:10.1002/ejoc.201901840
16. Hong, S.; Kawaoka, A. M.; Marks, T. J. *J. Am. Chem. Soc.* **2003**, *125*, 15878–15892. doi:10.1021/ja036266y
17. Bailey, P. D.; Smith, P. D.; Morgan, K. M.; Rosair, G. M. *Tetrahedron Lett.* **2002**, *43*, 1071–1074. doi:10.1016/s0040-4039(01)02149-9
18. Gandon, L. A.; Russell, A. G.; Güveli, T.; Brodwolf, A. E.; Kariuki, B. M.; Spencer, N.; Snaith, J. S. *J. Org. Chem.* **2006**, *71*, 5198–5207. doi:10.1021/jo060495w
19. Ragoussi, M.-E.; Walker, S. M.; Piccanello, A.; Kariuki, B. M.; Horton, P. N.; Spencer, N.; Snaith, J. S. *J. Org. Chem.* **2010**, *75*, 7347–7357. doi:10.1021/jo101631y
20. Girling, P. R.; Kiyoi, T.; Whiting, A. *Org. Biomol. Chem.* **2011**, *9*, 3105–3121. doi:10.1039/c0ob00996b
21. Pantaine, L. R. E.; Milligan, J. A.; Matsui, J. K.; Kelly, C. B.; Molander, G. A. *Org. Lett.* **2019**, *21*, 2317–2321. doi:10.1021/acs.orglett.9b00602
22. Herold, S.; Bafaluy, D.; Muñiz, K. *Green Chem.* **2018**, *20*, 3191–3196. doi:10.1039/c8gc01411f
23. Ashikari, Y.; Nokami, T.; Yoshida, J.-i. *Org. Biomol. Chem.* **2013**, *11*, 3322–3331. doi:10.1039/c3ob40315g
24. Xu, H.-C.; Moeller, K. D. *J. Am. Chem. Soc.* **2010**, *132*, 2839–2844. doi:10.1021/ja910586v
25. Tokuda, M.; Fujita, H.; Miyamoto, T.; Suginome, H. *Tetrahedron* **1993**, *49*, 2413–2426. doi:10.1016/s0040-4020(01)86320-1
26. Tokuda, M.; Miyamoto, T.; Fujita, H.; Suginome, H. *Tetrahedron* **1991**, *47*, 747–756. doi:10.1016/s0040-4020(01)87064-2
27. Degrand, C.; Compagnon, P. L.; Belot, G.; Jacquin, D. *J. Org. Chem.* **1980**, *45*, 1189–1196. doi:10.1021/jo01295a004
28. Atobe, M.; Tateno, H.; Matsumura, Y. *Chem. Rev.* **2018**, *118*, 4541–4572. doi:10.1021/acs.chemrev.7b00353
29. Plutschack, M. B.; Pieber, B.; Gilmore, K.; Seeberger, P. H. *Chem. Rev.* **2017**, *117*, 11796–11893. doi:10.1021/acs.chemrev.7b00183

30. Noël, T.; Cao, Y.; Laudadio, G. *Acc. Chem. Res.* **2019**, *52*, 2858–2869. doi:10.1021/acs.accounts.9b00412

31. Tanbouza, N.; Ollevier, T.; Lam, K. *iScience* **2020**, *23*, 101720. doi:10.1016/j.isci.2020.101720

32. Pletcher, D.; Green, R. A.; Brown, R. C. D. *Chem. Rev.* **2018**, *118*, 4573–4591. doi:10.1021/acs.chemrev.7b00360

33. Naito, Y.; Nakamura, Y.; Shida, N.; Senboku, H.; Tanaka, K.; Atobe, M. *J. Org. Chem.* **2021**, *86*, 15953–15960. doi:10.1021/acs.joc.1c00821

34. Qu, Y.; Tsuneishi, C.; Tateno, H.; Matsumura, Y.; Atobe, M. *React. Chem. Eng.* **2017**, *2*, 871–875. doi:10.1039/c7re00149e

35. Naito, Y.; Kondo, M.; Nakamura, Y.; Shida, N.; Ishikawa, K.; Washio, T.; Takizawa, S.; Atobe, M. *Chem. Commun.* accepted. doi:10.1039/D2CC00124A.

36. Isse, A. A.; Berzi, G.; Falciai, L.; Rossi, M.; Mussini, P. R.; Gennaro, A. *J. Appl. Electrochem.* **2009**, *39*, 2217–2225. doi:10.1007/s10800-008-9768-z

37. Geboes, B.; Vanreenterghem, B.; Ustarroz, J.; Pauwels, D.; Sotiropoulos, S.; Hubin, A.; Breugelmans, T. *Chem. Eng. Trans.* **2014**, *41*, 73–78. doi:10.3303/cet1441013

38. Luna, O. F.; Gomez, J.; Cárdenas, C.; Albericio, F.; Marshall, S.; Guzmán, F. *Molecules* **2016**, *21*, 1542. doi:10.3390/molecules21111542

39. Fuguet, E.; Reta, M.; Gibert, C.; Rosés, M.; Bosch, E.; Ràfols, C. *Electrophoresis* **2008**, *29*, 2841–2851. doi:10.1002/elps.200700869

40. Iwamoto, K.-i.; Hamaya, M.; Hashimoto, N.; Kimura, H.; Suzuki, Y.; Sato, M. *Tetrahedron Lett.* **2006**, *47*, 7175–7177. doi:10.1016/j.tetlet.2006.07.153

41. Sobkowski, M.; Stawinski, J.; Kraszewski, A. *New J. Chem.* **2009**, *33*, 164–170. doi:10.1039/b812780h

License and Terms

This is an open access article licensed under the terms of the Beilstein-Institut Open Access License Agreement (<https://www.beilstein-journals.org/bjoc/terms>), which is identical to the Creative Commons Attribution 4.0 International License (<https://creativecommons.org/licenses/by/4.0>). The reuse of material under this license requires that the author(s), source and license are credited. Third-party material in this article could be subject to other licenses (typically indicated in the credit line), and in this case, users are required to obtain permission from the license holder to reuse the material.

The definitive version of this article is the electronic one which can be found at:

<https://doi.org/10.3762/bjoc.18.39>



Cathodic generation of reactive (phenylthio)difluoromethyl species and its reactions: mechanistic aspects and synthetic applications

Sadanobu Iwase¹, Shinsuke Inagi² and Toshio Fuchigami^{*1}

Full Research Paper

Open Access

Address:

¹Department of Electronic Chemistry, Tokyo Institute of Technology, Yokohama 226-8502, Japan and ²Department of Chemical Science and Engineering, Tokyo Institute of Technology, Yokohama 226-8502, Japan

Beilstein J. Org. Chem. **2022**, *18*, 872–880.

<https://doi.org/10.3762/bjoc.18.88>

Received: 09 May 2022

Accepted: 12 July 2022

Published: 20 July 2022

Email:

Toshio Fuchigami* - fuchi@echem.titech.ac.jp

This article is part of the thematic issue "Molecular and macromolecular electrochemistry: synthesis, mechanism, and redox properties".

* Corresponding author

Associate Editor: D. Y.-K. Chen

Keywords:

bis(phenylthio)difluoromethane; cathodic reduction; deuteration; *o*-phthalonitrile mediator; (phenylthio)difluoromethylation; (phenylthio)difluoromethyl radical

© 2022 Iwase et al.; licensee Beilstein-Institut.

License and terms: see end of document.

Abstract

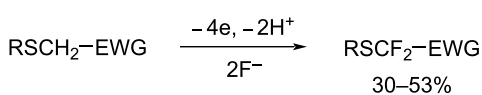
The cathodic reduction of bromodifluoromethyl phenyl sulfide (**1**) using *o*-phthalonitrile as a mediator generated the (phenylthio)difluoromethyl radical, which reacted with α -methylstyrene and 1,1-diphenylethylene to provide the corresponding adducts in moderate and high yields, respectively. In contrast, chemical reduction of **1** with SmI_2 resulted in much lower product yields. The detailed reaction mechanism was clarified based on the cathodic reduction of **1** in the presence of deuterated acetonitrile, CD_3CN .

Introduction

Organofluorine compounds containing a difluoromethylene group have been of much interest from biological aspects since the difluoromethylene group is isopolar and isosteric with an ether oxygen [1,2]. Particularly, organic molecules bearing a (arylthio)difluoromethyl group (ArSCF_2) have potential biological applications such as anti-HIV-1 reverse transcriptase inhibitors and agrochemical applications [3,4]. Reurakul and Pohmakotr et al. carried out the reaction of PhSCF_2Br with SmI_2 in THF/iPrOH to generate PhSCF_2 radicals followed by

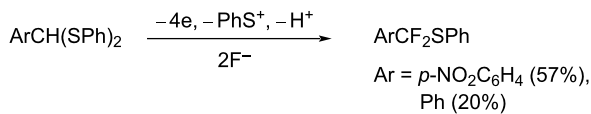
trapping with various olefins in moderate yields [5]. Prakash et al. also achieved fluoride-induced nucleophilic (phenylthio)difluoromethylation of carbonyl compounds using $\text{PhSCF}_2\text{SiMe}_3$ [6]. Quite recently, Shen et al., developed various nucleophilic, electrophilic, and radical difluoromethylthiolating reagents [1]. However, these methods require various metal and organometallic reagents. On the other hand, electrochemical organic synthesis is a metal-free process and does not require any hazardous reagents and it produces

less waste than conventional chemical syntheses. Therefore, electrochemical synthesis is desirable from an aspect of green chemistry [7–10]. In this context, we have developed various electrochemical methodologies for efficient selective fluorination [11,12] and molecular conversion of organofluorine compounds to date [13–18]. We have also achieved the *gem*-difluorination of sulfides bearing various electron-withdrawing groups at the α -position (Scheme 1) [19–21]. Furthermore, we also succeeded in the electrochemical *gem*-difluorodesulfurization of dithioacetals and dithiocarbonate (Scheme 2 and Scheme 3) [22,23].

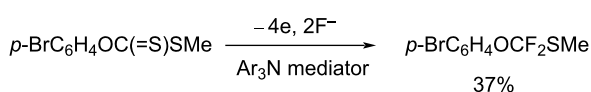


R = Ar, alkyl
EWG = COOEt, PO(OEt)₂, CN, C≡CH

Scheme 1: Electrochemical *gem*-difluorination of sulfides bearing α -electron-withdrawing groups.



Scheme 2: Electrochemical *gem*-difluorodesulfurization of dithioacetals.



Scheme 3: Electrochemical *gem*-difluorodesulfurization of dithiocarbonate.

In this work, we have studied the electrochemical generation of (phenylthio)difluoromethyl reactive species from bromodifluoromethyl phenyl sulfide and their synthetic application as well as mechanistic aspects.

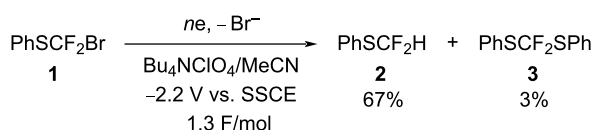
Results and Discussion

Cathodic reduction of bromodifluoromethyl phenyl sulfide (**1**)

At first, the reduction potential (E_p^{red}) of bromodifluoromethyl phenyl sulfide (**1**) was measured by cyclic voltammetry in an anhydrous acetonitrile (MeCN) solution containing Bu₄NClO₄ (0.1 M) using a platinum electrode. One irreversible reduction peak was observed at -2.4 V vs SSCE at a scan rate of 100 mV/s. Even at a much higher scan rate of 500 mV/s, the

reduction peak was irreversible. Since the reduction potentials (E_p^{red}) of CF₃Br and PhCF₂Cl are -1.55 V (Pt cathode) and -2.11 V vs SCE (hanging Hg drop cathode), respectively [24,25], the reduction potential of **1** was found to be similar to that of PhCF₂Cl.

Next, we carried out the constant potential cathodic reduction of **1** at a platinum cathode in Bu₄NClO₄/MeCN. Notably, when 1.3 F/mol were passed, starting compound **1** was consumed completely. As shown in Scheme 4, difluoromethyl phenyl sulfide (**2**) was mainly formed as well as bis(phenylthio)difluoromethane (**3**) as a minor product. From these results, one-electron and two-electron reductions of **1** seem to take place simultaneously to generate radical and anionic intermediates.



Scheme 4: Cathodic reduction of **1**.

In order to trap the radical intermediate, the constant potential cathodic reduction of **1** was performed in the presence of various olefins such as α -methylstyrene, cyclohexene, and dihydrofuran. The results are summarized in Table 1.

Regardless of trapping reagents, 1.3–1.4 F/mol of electricity was required to consume the starting material **1**. The required electricity was similar to the electrolysis in the absence of the trapping reagent. Only when α -methylstyrene was used as the radical trapping reagent, the expected radical adduct **4** was formed in reasonable yield of ca. 30% (Table 1, run 1). A platinum cathode is more suitable for the formation of adduct **4** compared to a glassy carbon cathode (Table 1, run 2). Dolbier et al. reported that electron-poor perfluoroalkyl radicals such as *n*-perfluoropropyl radical have high reactivity to electron-rich olefins such as α -methylstyrene and styrene [26]. In fact, our cathodically generated reactive species also reacted with α -methylstyrene. However, electron-rich dihydrofuran did not provide any radical adduct at all (Table 1, run 4). The reason is not clear at present. Thus the obtained results indicate that the cathodically generated reactive species would be the (phenylthio)difluoromethyl radical. In order to increase the yield of adduct **4**, the cathodic reduction of **1** was performed in other solvents such as DMF and CH₂Cl₂ using 20 equiv of α -methylstyrene. However, the yield of **4** did not increase.

The cathodic reduction of perfluoroalkyl halide generates radical and/or anionic species in general [24]. In order to

Table 1: Cathodic reduction of bromodifluoromethyl phenyl sulfide (**1**) in the presence of various olefins as a trapping reagent.

1	$n\text{e}^- - \text{Br}^-$	2	3	4 : Y = $\text{CH}_2\text{CH}(\text{Me})\text{Ph}$ 4' : Y = cyclohexyl 4'' : Y = 2-tetrahydrofuryl
Run	Olefin	Charge passed (F/mol)		Yield (%) ^a
			2	3
1		1.4	65 (60) ^b	trace
2 ^c		1.4	64	trace
3		1.3	55	trace
4		1.4	65	trace
				4 4' 4''
				29 (23) ^b
				12
				0
				0

^aDetermined by ¹⁹F NMR; ^bisolated yield is shown in parentheses; ^cglassy carbon cathode was used.

generate radical species selectively, indirect cathodic reduction using various mediators has been often employed. Médebielle et al. successfully carried out the cathodic reduction of ArCF_2X and RCOCl_2X with nitrobenzene as a mediator to generate the corresponding difluoromethyl radicals selectively, and they applied this electrocatalytic system to the synthesis of various heterocyclic compounds bearing a perfluoroalkyl or perfluoroacyl group [27–30]. Furthermore, they extended this methodology to tandem cyclization to provide fused difluoromethylene-containing heterocycles [31]. In consideration of

these facts, we studied the cathodic reduction of **1** using a mediator.

Indirect cathodic reduction of **1** using *o*-phthalonitrile as mediator

At first, cyclic voltammetry was carried out to investigate the electrocatalytic reduction of bromodifluoromethyl phenyl sulfide (**1**) with *o*-phthalonitrile as a mediator. The cyclic voltammograms of *o*-phthalonitrile in the absence and presence of compound **1** are shown in Figure 1.

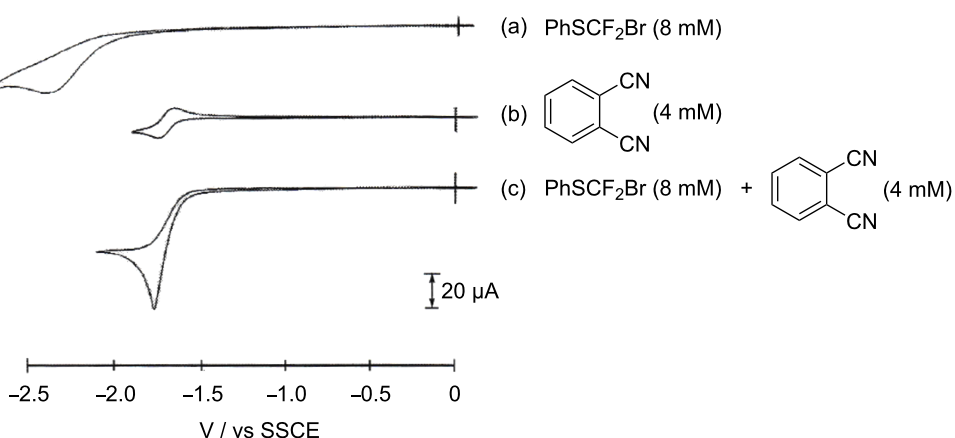


Figure 1: Cyclic voltammograms of (a) PhSCF_2Br (8 mM) in 0.1 M $n\text{-Bu}_4\text{NClO}_4/\text{MeCN}$; (b) *o*-phthalonitrile (4 mM), and (c) *o*-phthalonitrile (4 mM) + **1** (8 mM). Scan rate: 100 mV/s.

As shown in Figure 1b, a typical reversible redox couple ($E_{1/2}^{\text{red}} = -1.69$ V vs. SSCE) of *o*-phthalonitrile was clearly observed. A significantly enhanced cathodic peak current was observed after addition of compound **1** to the solution containing *o*-phthalonitrile while the anodic peak current disappeared completely as shown in Figure 1c. The reduction peak potential of **1** is -2.4 V vs. SSCE, which excludes the reduction of **1** at this potential. Therefore, the enhanced cathodic current of *o*-phthalonitrile clearly suggests that a typical electrocatalytic reduction reaction takes place. Thus, it was found that *o*-phthalonitrile should work as an electron transfer catalyst, i.e., a redox mediator.

On the bases of the cyclic voltammetric measurements, the cathodic reduction of **1** was carried out at a constant potential using *o*-phthalonitrile as mediator. As shown in Scheme 5, the total yield of products **2** and **3** increased appreciably to ca. 80% compared to the direct cathodic reduction of **1** (70% yield in Scheme 4).

Next, the indirect cathodic reduction of compound **1** was carried out similarly in the presence of α -methylstyrene and the results are summarized in Table 2.

When 0.2 equiv of the mediator were used, the yields of both products **2** and **4** were decreased compared to the direct cathodic reduction (Table 2, run 1). Increasing the amount of the mediator to 0.5 equiv resulted in an increase of the yield of **4** to 35% (Table 2, run 3) while the yield of **2** was decreased significantly. In this case, the required electricity was increased to 1.8 F/mol.

From these results, we anticipate that a one-electron reduction of compound **1** takes place to generate the PhSCF₂ radical, which is further reduced affording the PhSCF₂ anion when a trapping reagent is absent. The resulting anion seems to undergo elimination of difluorocarbene to generate a phenylthiolate anion which reacts with compound **1** to form product **3** as shown in Scheme 6.

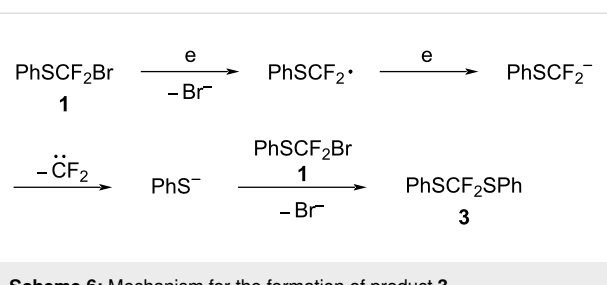
Table 2: Indirect cathodic reduction of compound **1** using *o*-phthalonitrile as mediator in the presence of α -methylstyrene.

PhSCF_2Br 1		<i>ne, -Br⁻</i> <i>o</i> -phthalonitrile mediator <i>Bu</i> ₄ NClO ₄ /solvent <i>α</i> -methylstyrene -1.7 V vs. SSCE	PhSCF_2H + PhSCF_2SPh + $\text{PhSCF}_2\text{CH}_2\text{CH}(\text{Me})\text{Ph}$ 2 3 4			
Run	Solvent	Mediator	Charge passed (F/mol)	2	3	4
1	MeCN	—	1.4	65	trace	29
2	MeCN	0.2 equiv	1.5	44	trace	15
3	MeCN	0.5 equiv	1.8	26	trace	35
4	DMF	—	1.6	67	trace	16
5	DMF	0.5 equiv	1.9	31	trace	28

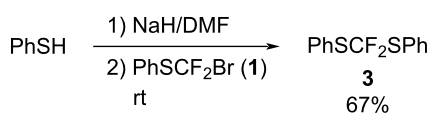
^aDetermined by ¹⁹F NMR.



Scheme 5: Indirect cathodic reduction of **1** using *o*-phthalonitrile as mediator.

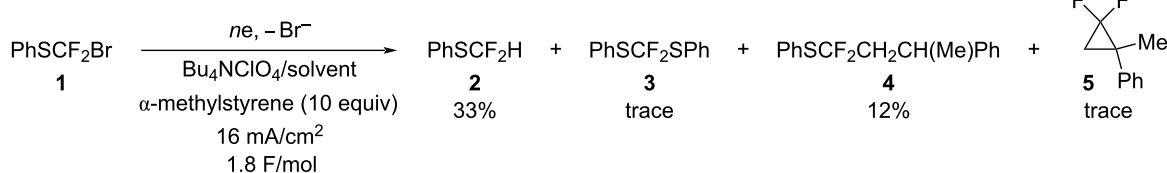
**Scheme 6:** Mechanism for the formation of product 3.

In order to confirm the proposed reaction pathway to product 3, the reaction of bromodifluoromethyl phenyl sulfide (1) with phenylthiolate anion was performed at room temperature. As expected, product 3 was formed in moderate yield of 67% as shown in Scheme 7.

**Scheme 7:** Reaction of compound 1 with PhS anions.

It is known that difluorocarbene has generally low reactivity towards olefins; however, it can be trapped with electron-rich olefins [32]. In order to trap difluorocarbene with an olefin, we tried to increase the amount of generated difluorocarbene by increasing the current density for the cathodic reduction of compound 1. Thus, the cathodic reduction of 1 was carried out completely at a high current density of 16 mA/cm^2 in the presence of α -methylstyrene. As shown in Scheme 8, the expected difluorocarbene adduct 5 was detected by high resolution mass spectrometry in addition to products 2, 3, and 4.

As already mentioned, SmI_2 is a well-known one-electron reducing reagent, and has been used to generate PhSCF_2 radicals and perfluoroalkyl radicals from PhSCF_2Br and perfluoroalkyl halides, respectively. The generated radicals undergo addition to olefins and acetylenes [5,33]. Pohmakotr et al. and Yoshida et al. reported that the reaction of PhSCF_2Br and PhCF_2Cl with SmI_2 generated PhSCF_2 and PhCF_2 radicals, which were trapped with styrene [5,34,35]. Therefore, we carried out the reaction of compound 1 with SmI_2 in the absence and presence of α -methylstyrene, which is more electron-rich compared to styrene. The results are summarized in Table 3.

**Scheme 8:** Cathodic reduction of compound 1 in the presence of α -methylstyrene at a high current density.**Table 3:** Reaction of compound 1 with SmI_2 in the presence and absence of α -methylstyrene.

Run	Solvent	SmI_2 (2 equiv) 	Conversion (%)	Yield (%) ^a		
				2	3	4
1	THF	0	34	12	trace	–
2	HMPA (7.5 equiv)/THF	0	66	5	32	–
3	HMPA (7.5 equiv)/THF	10	76	5	32	0
4	MeOH (10 equiv)/THF	10	45	5	0	14

^aDetermined by ^{19}F NMR.

As shown in Table 3, even when two equivalents of SmI_2 were used in the absence of α -methylstyrene, the conversion of compound **1** was low and a large amount of starting material **1** was recovered (Table 3, run 1). In this case, simple reduction product **2** was formed together with trace amounts of product **3**. Since HMPA is known to enhance the reducing ability of SmI_2 [36], we performed the reaction of compound **1** in THF containing 7.5 equiv HMPA. As expected, the conversion of **1** increased from 34% to 66%, and product **3** was formed in 32% yield (Table 3, run 2). However, the yield of product **2** decreased from 12% to 5%. Then, the reaction of **1** with SmI_2 was carried out similarly in the presence of α -methylstyrene (Table 3, run 3). However, the result was almost the same as that in the absence of α -methylstyrene: the yields of products **2** and **3** remained unchanged and the expected adduct **4** was not formed at all although the conversion of compound **1** increased. In both cases (Table 3, runs 2 and 3), unidentified products were formed. Thus, it was found that the chemical reduction of compound **1** with SmI_2 was quite different from the electrochemical reduction. However, notably, when THF containing MeOH (10 equiv with regard to compound **1**) was used, adduct **4** was formed in 14% yield (Table 3, run 4). In this case, product **3** was not formed.

In order to determine the hydrogen source of the products **2** and **4**, indirect cathodic reduction of **1** was carried out in deuterated acetonitrile, CD_3CN (Scheme 9).

As shown in Scheme 9, deuterated products **2** and **4** were formed. In the case of product **2**, almost complete deuteration was observed, which clearly indicates that product **2** should be formed via a PhSCF_2 radical intermediate. Thus, the main hydrogen source for the formation of product **2** was determined to be MeCN. On the other hand, in the case of adduct **4**, deuterated and protonated **4** were formed in a similar yield, which suggests that **4** would be formed via both radical and anionic intermediates.

In order to further clarify the reaction mechanism, the indirect cathodic reduction of compound **1** was performed in the pres-

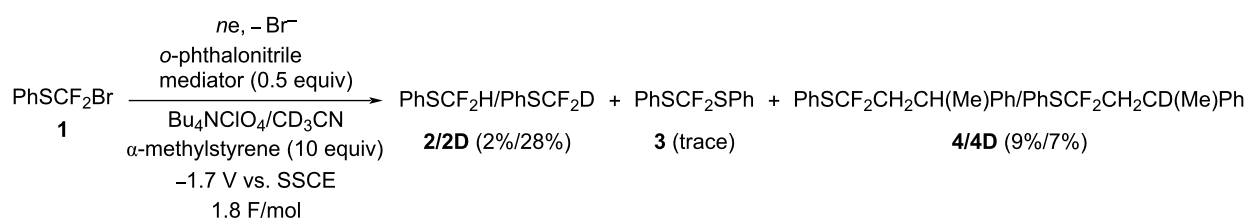
ence of α -methylstyrene in MeCN containing cumene (iPrC_6H_5) and isopropyl alcohol (iPrOH). The former works as a hydrogen radical source while the latter works as both a hydrogen radical and proton source. The results are summarized in Table 4.

Although it was expected that the yield of product **4** would be increased in the presence of cumene as a hydrogen radical source, the yield was decreased (Table 4, run 2) compared to the electrolysis in the absence of cumene (Table 4, run 1). On the other hand, the yield of product **4** increased in the presence of iPrOH (Table 4, run 3), and the yield further increased to 60% at a higher content of iPrOH of 50% (Table 4, run 4). In the latter case, the required electricity was increased to 2.7 F/mol. Reutrakul and Pomakotr et al. also reported that iPrOH is an effective additive for the addition of PhSCF_2 radical to olefins [5]. Since the presence of a large amount of a proton source such as iPrOH increased the yield of adduct **4** significantly, the electrolysis of compound **1** in the presence of 1,1-diphenylethylene as a more electron-rich olefin compared to α -methylstyrene was carried out similarly. As expected, the adduct **6** was formed in a high yield of 90% as shown in Scheme 10.

Isopropanol can serve as both a proton and a hydrogen radical source while cumene serves only as a hydrogen radical source. The indirect cathodic reduction of compound **1** in the presence of cumene decreased the yield of adduct **4** while the use of iPrOH instead of cumene increased the yield markedly. As already mentioned, in the chemical reduction of compound **1** with SmI_2 , only 10 equiv of MeOH to **1** also enhanced the formation of adduct **4** to some extent (from 0% to 14% yield) as shown in Table 3. Therefore, iPrOH seems to promote the radical addition rather than reduction although the reason has not been clarified yet.

Reaction mechanism

Although the cathodic reduction of perfluoroalkyl halides usually involves one- and two-electron transfer, their indirect cathodic reduction using mediators undergoes one-electron

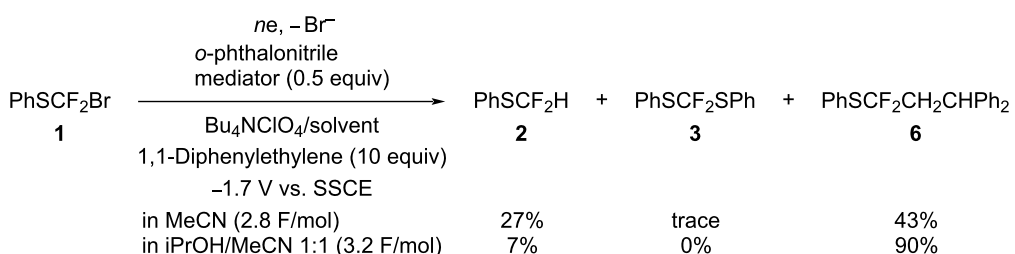


Scheme 9: Indirect cathodic reduction of compound **1** in CD_3CN .

Table 4: Indirect cathodic reduction of compound **1** with *o*-phthalonitrile in the presence of α -methylstyrene in MeCN containing cumene or isopropyl alcohol.

Run	Solvent (hydrogen source)	Charge passed (F/mol)	Yield (%) ^a		
			2	3	4
1	MeCN	1.8	26	trace	35
2	MeCN/iPr ₂ C ₆ H ₅ (10 equiv)	1.7	27	trace	23
3	MeCN/iPrOH (10:1)	1.7	15	0	44
4	MeCN/iPrOH (1:1)	2.7	20	0	60 (53) ^b

^aDetermined by ¹⁹F NMR; ^bisolated yield is shown in parentheses.

**Scheme 10:** Indirect cathodic reduction of compound **1** in the presence of 1,1-diphenylethylene.

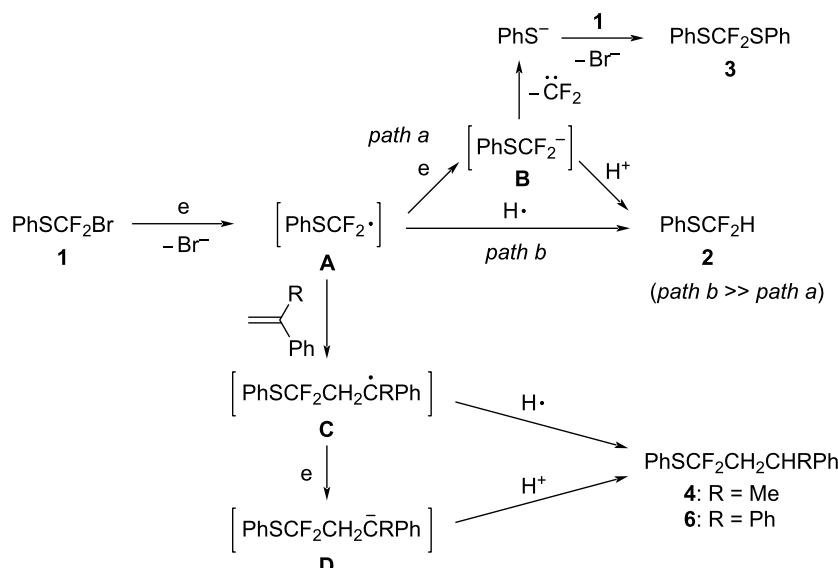
reduction selectively as reported by Saveant et al. [24]. In this study, we also confirmed that the *o*-phthalonitrile-mediated reduction of PhSCF₂Br (**1**) in the absence of radical trapping reagents consumed much less than 2 F/mol of electricity. Furthermore, the indirect cathodic reduction of compound **1** in CD₃CN formed the deuterated product, PhSCF₂D (**2D**) as a major product. On the other hand, the indirect cathodic reduction of compound **1** in CD₃CN containing a radical trapping reagent such as α -methylstyrene consumed less than 2 F/mol of electricity to provide protonated and deuterated adducts **4/4D** in almost same yields. Similar indirect electrolysis of compound **1** in iPrOH/MeCN in the presence of 1,1-diphenylethylene consumed much more than 2 F/mol of electricity to afford adduct **6** in high yield.

Moreover, the indirect cathodic reduction of compound **1** at high current density in the presence of α -methylstyrene formed

a trace amount of 1,1-difluorocyclopropane derivative **5**, which is an evidence of the generation of difluorocarbene from **1**.

In consideration to these facts, we propose the following reaction mechanism as shown in Scheme 11.

The one-electron reduction of **1** generates the PhSCF₂ radical **A**, which abstracts a hydrogen radical from MeCN to give product **2** (path b). The radical **A** undergoes further reduction to generate anion **B** (path a). Elimination of difluorocarbene from anion **B** forms a phenylthiolate anion, which reacts with the starting material **1** to form product **3**. In the presence of radical trapping reagents such as styrene derivatives, radical **A** reacts with styrenes to form radical intermediate adduct **C**. The radical **C** abstracts a hydrogen radical to form products **4** and **6**. Alternatively, the radical intermediate **C** is further reduced to

**Scheme 11:** Reaction mechanism.

generate anion **D** followed by protonation to give products **4** and **6**.

Conclusion

We have successfully carried out catalytic electrochemical reduction of bromodifluoromethyl phenyl sulfide using *o*-phthalonitrile as mediator to generate (phenylthio)difluoromethyl radicals selectively. The generated radicals were efficiently trapped with electron-rich olefins such as α -methylstyrene and 1,1-diphenylstyrene. The reaction mechanism was also disclosed by using the deuterated solvent CD_3CN .

Supporting Information

Supporting Information File 1

Experimental section: general information, materials, and general procedure for cathodic reduction of compound **1**. [<https://www.beilstein-journals.org/bjoc/content/supporting/1860-5397-18-88-S1.pdf>]

Acknowledgements

We thank Dr. Seichiro Higashiya of Tokyo Institute of Technology for measurements of mass spectra and valuable suggestions.

Funding

This study was supported by Kakenhi Grants-in-Aid (JP20350071) from the Japan Society of Promotion of Science (JSPS) and a Support for Tokyo Tech Advanced Researchers

[STAR] grant funded by the Tokyo Institute of Technology Fund (Tokyo Tech Fund).

ORCID® iDs

Toshio Fuchigami - <https://orcid.org/0000-0002-1905-5656>

References

- Wu, J.; Shen, Q. *Acc. Chem. Res.* **2021**, *54*, 2946–2958. doi:10.1021/acs.accounts.1c00252
- Inoue, M.; Sumii, Y.; Shibata, N. *ACS Omega* **2020**, *5*, 10633–10640. doi:10.1021/acsomega.0c00830
- Burkholder, C. R.; Dolbier, W. R., Jr.; Médebielle, M. *J. Fluorine Chem.* **2000**, *102*, 369–376. doi:10.1016/s0022-1139(99)00314-0
- Burkholder, C.; Dolbier, W. R., Jr.; Médebielle, M.; Ait-Mohand, S. *Tetrahedron Lett.* **2001**, *42*, 3459–3462. doi:10.1016/s0040-4039(01)00513-5
- Reutrakul, V.; Thongpaisanwong, T.; Tuchinda, P.; Kuhakarn, C.; Pohmakot, M. *J. Org. Chem.* **2004**, *69*, 6913–6915. doi:10.1021/jo0489768
- Prakash, G. K. S.; Hu, J.; Wang, Y.; Olah, G. A. *J. Fluorine Chem.* **2005**, *126*, 527–532. doi:10.1016/j.jfluchem.2004.12.005
- Fuchigami, T.; Atobe, M.; Inagi, S. *Fundamentals and Applications of Organic Electrochemistry: Synthesis, Materials, Devices*; Wiley: Chichester, 2014.
- Little, R. D.; Moeller, K. D. *Chem. Rev.* **2018**, *118*, 4483–4484. doi:10.1021/acs.chemrev.8b00197
- Pollock, D.; Waldvogel, S. R. *Chem. Sci.* **2020**, *11*, 12386–12400. doi:10.1039/d0sc01848a
- Francke, R.; Little, R. D. *Chem. Soc. Rev.* **2014**, *43*, 2492–2521. doi:10.1039/c3cs60464k
- Fuchigami, T.; Inagi, S. *Chem. Commun.* **2011**, *47*, 10211–10223. doi:10.1039/c1cc12414e
- Fuchigami, T.; Inagi, S. *Acc. Chem. Res.* **2020**, *53*, 322–334. doi:10.1021/acs.accounts.9b00520

13. Fuchigami, T.; Ichikawa, S. *J. Org. Chem.* **1994**, *59*, 607–615. doi:10.1021/jo00082a018
14. Fuchigami, T. Electrochemistry applied to the synthesis of fluorinated organic substances. In *Advances in Electron Transfer Chemistry*; Mariano, P. S., Ed.; JAI Press: Connecticut, 1999; Vol. 6, pp 41–130.
15. Isokawa, M.; Sano, M.; Kubota, K.; Suzuki, K.; Inagi, S.; Fuchigami, T. *J. Electrochem. Soc.* **2017**, *164*, G121–G127. doi:10.1149/2.1601713jes
16. Sano, M.; Inagi, S.; Fuchigami, T. *J. Electrochem. Soc.* **2018**, *165*, G171–G175. doi:10.1149/2.0141816jes
17. Fuchigami, T.; Inagi, S. *Curr. Opin. Electrochem.* **2020**, *24*, 24–30. doi:10.1016/j.coelec.2020.05.012
18. Imai, N.; Inagi, S.; Fuchigami, T. *Electrochemistry* **2021**, *89*, 104–110. doi:10.5796/electrochemistry.21-65002
19. Konno, A.; Fuchigami, T. *J. Org. Chem.* **1997**, *62*, 8579–8581. doi:10.1021/jo971248i
20. Riyadh, S. M.; Ishii, H.; Fuchigami, T. *Tetrahedron* **2002**, *58*, 5877–5883. doi:10.1016/s0040-4020(02)00559-8
21. Kurabayashi, S.; Shida, N.; Inagi, S.; Fuchigami, T. *Tetrahedron* **2016**, *72*, 5343–5349. doi:10.1016/j.tet.2016.07.016
22. Yoshiyama, T.; Fuchigami, T. *Chem. Lett.* **1992**, *21*, 1995–1998. doi:10.1246/cl.1992.1995
23. Okuda, H.; Taniguchi, K.; Inagi, S.; Fuchigami, T. *Electroanalysis* **2021**, *33*, 2296–2301. doi:10.1002/elan.202100070
24. Andrieux, C. P.; Gelis, L.; Médebielle, M.; Pinson, J.; Saveant, J. M. *J. Am. Chem. Soc.* **1990**, *112*, 3509–3520. doi:10.1021/ja00165a040
25. Lund, H.; Jensen, J. N. *Acta Chem. Scand., Ser. B* **1974**, *28*, 263–265. doi:10.3891/acta.chem.scand.28b-0263
26. Dolbier, W. R. *Top. Curr. Chem.* **1997**, *192*, 97–163. doi:10.1007/bfb0119266
27. Médebielle, M.; Pinson, J.; Saveant, J. M. *J. Am. Chem. Soc.* **1991**, *113*, 6872–6879. doi:10.1021/ja00018a025
28. Médebielle, M. *Tetrahedron Lett.* **1995**, *36*, 2071–2075. doi:10.1016/0040-4039(95)00222-x
29. Burkholder, C.; Dolbier, W. R.; Médebielle, M. *J. Org. Chem.* **1998**, *63*, 5385–5394. doi:10.1021/jo980201+
30. Médebielle, M.; Fujii, S.; Kato, K. *Tetrahedron* **2000**, *56*, 2655–2664. doi:10.1016/s0040-4020(00)00154-x
31. Adouama, C.; Keyrouz, R.; Pilet, G.; Monnereau, C.; Gueyrard, D.; Noël, T.; Médebielle, M. *Chem. Commun.* **2017**, *53*, 5653–5656. doi:10.1039/c7cc02979a
32. Dolbier, W. R., Jr.; Wojtowicz, H.; Burkholder, C. R. *J. Org. Chem.* **1990**, *55*, 5420–5422. doi:10.1021/jo00306a027
33. Ma, S.; Lu, X. *Tetrahedron* **1990**, *46*, 357–364. doi:10.1016/s0040-4020(01)85421-1
34. Yoshida, M.; Morishima, A.; Suzuki, D.; Iyoda, M.; Aoki, K.; Ikuta, S. *Bull. Chem. Soc. Jpn.* **1996**, *69*, 2019–2023. doi:10.1246/bcsj.69.2019
35. Yoshida, M.; Suzuki, D.; Iyoda, M. *J. Chem. Soc., Perkin Trans. 1* **1997**, 643–648. doi:10.1039/a606048j
36. Szostak, M.; Spain, M.; Procter, D. *J. Chem. Soc. Rev.* **2013**, *42*, 9155–9183. doi:10.1039/c3cs60223k

License and Terms

This is an open access article licensed under the terms of the Beilstein-Institut Open Access License Agreement (<https://www.beilstein-journals.org/bjoc/terms>), which is identical to the Creative Commons Attribution 4.0

International License

(<https://creativecommons.org/licenses/by/4.0>). The reuse of material under this license requires that the author(s), source and license are credited. Third-party material in this article could be subject to other licenses (typically indicated in the credit line), and in this case, users are required to obtain permission from the license holder to reuse the material.

The definitive version of this article is the electronic one which can be found at:

<https://doi.org/10.3762/bjoc.18.88>



Electroreductive coupling of 2-acylbenzoates with α,β -unsaturated carbonyl compounds: density functional theory study on product selectivity

Naoki Kise^{*} and Toshihiko Sakurai

Full Research Paper

Open Access

Address:

Department of Chemistry and Biotechnology, Graduate School of Engineering, Tottori University, 4-101, Koyama-cho Minami, Tottori 680-8552, Japan

Email:

Naoki Kise^{*} - kise@tottori-u.ac.jp

* Corresponding author

Keywords:

2-acylbenzoates; chlorotrimethylsilane; 3-(3-cyanoethyl)phthalides; 2-cyanonaphthalen-1-ols; electroreductive coupling

Beilstein J. Org. Chem. **2022**, *18*, 956–962.

<https://doi.org/10.3762/bjoc.18.95>

Received: 26 May 2022

Accepted: 20 July 2022

Published: 02 August 2022

This article is part of the thematic issue "Molecular and macromolecular electrochemistry: synthesis, mechanism, and redox properties".

Guest Editor: S. Inagi

© 2022 Kise and Sakurai; licensee Beilstein-Institut.

License and terms: see end of document.

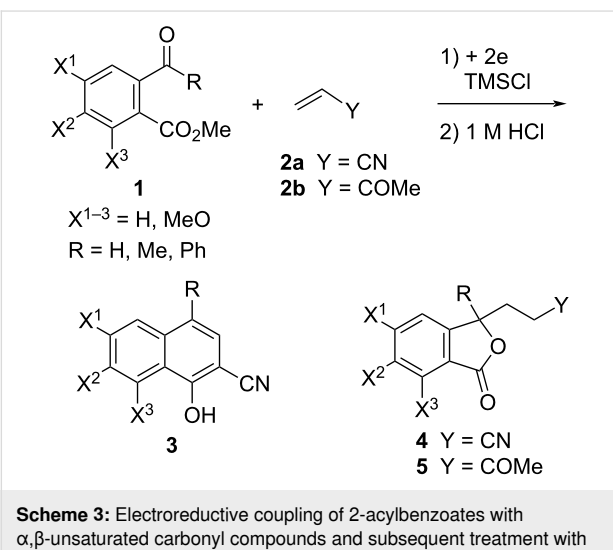
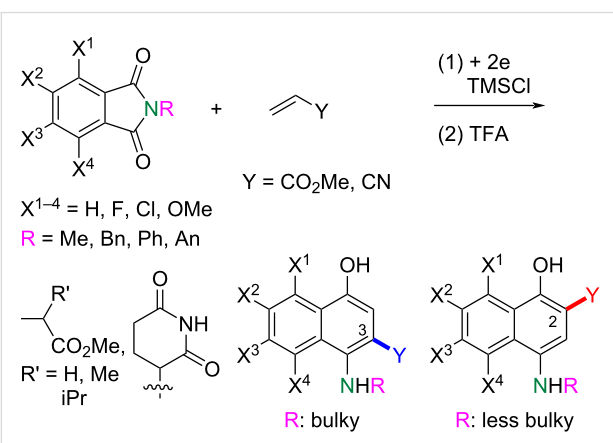
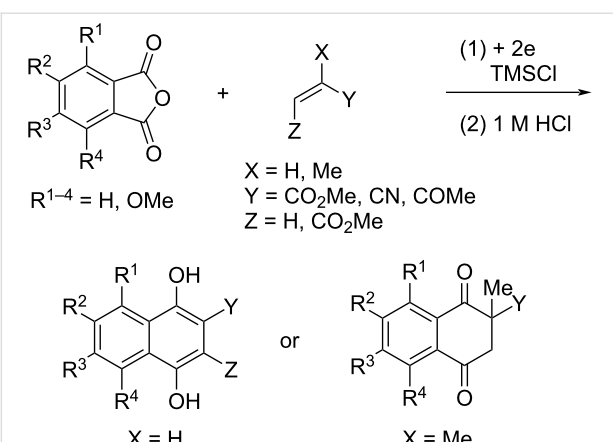
Abstract

The electroreductive coupling of 2-acylbenzoates with acrylonitrile in the presence of TMSCl and successive treatment with 1 M HCl gave 2-cyanonaphthalen-1-ols or 3-(3-cyanoethyl)phthalides. On the other hand, the reaction of 2-acylbenzoates with methyl vinyl ketone under the same conditions produced 3-(3-oxobutyl)phthalides as the sole products. What determines the product selectivity was studied using DFT calculations.

Introduction

The electroreductive coupling between carbon–heteroatom and carbon–carbon double bonds is one of the promising methods for carbon–carbon bond formation [1–4]. Recently, we reported the electroreductive coupling of phthalic anhydrides with α,β -unsaturated carbonyl compounds in the presence of chlorotrimethylsilane (TMSCl) and subsequent treatment with 1 M HCl to give 1,4-dihydroxynaphthalenes and 2-methyl-2,3-dihydro-naphthalene-1,4-diones (Scheme 1) [5]. In addition, we disclosed that the electroreduction of phthalimides with α,β -unsaturated carbonyl compounds under the same conditions and subsequent treatment with trifluoroacetic acid (TFA) produced

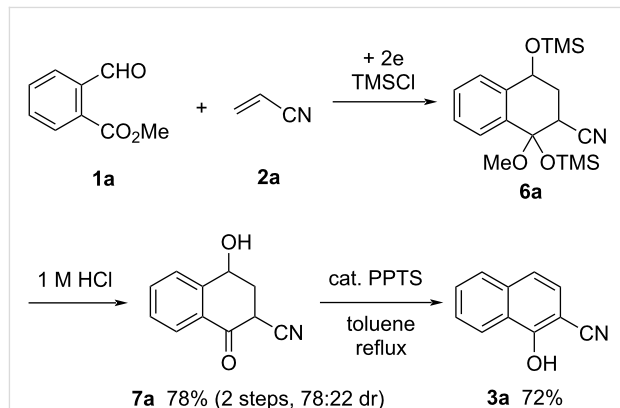
3- and 2-substituted 4-aminonaphthalen-1-ols (Scheme 2) [6]. In this context, we report here that the electroreduction of *o*-acylbenzoates **1** with acrylonitrile (**2a**) in the presence of TMSCl and subsequent treatment with 1 M HCl gives 2-cyanonaphthalen-1-ols **3** or 3-(3-cyanoethyl)phthalides **4** (Scheme 3). The product selectivity depends on the position of the methoxy substituents on the aromatic ring in substrate **1**. On the other hand, 3-(3-oxobutyl)phthalides **5** are obtained by the reaction of compound **1** with methyl vinyl ketone (**2b**) as the sole products (Scheme 3). The synthesis of naphthalene-1-ols [7–9] and 3-substituted phthalides [10–16] is attracting much



attention, since bioactive compounds possessing these structures are known. This method has the potential to be applied to synthesize bioactive 2-cyanonaphthalen-1-ols [8,9] and 3-substituted phthalides [12–16]. The reaction mechanisms of the electroreductive coupling of **1** with **2** and subsequent rearrangement to **3** are also discussed. In particular, the latter mechanism was studied using density functional theory (DFT) calculations and it was suggested that the ΔG for the cyclization step of an intermediate enolate anion determines the product selectivity.

Results and Discussion

The electroreduction of methyl 2-formylbenzoate (**1a**) with acrylonitrile (**2a**) was carried out in 0.3 M Bu_4NClO_4 /THF in the presence of TMSCl at 0.1 A (2.5 F/mol). From the crude product, cyclized product **6a** was obtained by column chromatography as a complex mixture of stereoisomers. Since compound **6a** could not be purified, it was treated with 1 M HCl/dioxane 1:1 at 25 °C for 1 h to give desilylated alcohol **7a** in 78% yield (2 steps) as a mixture of two diastereomers (78:22 dr). Dehydration of compound **7a** in refluxing toluene in the presence of cat. PPTS produced 2-cyanonaphthalene-1-ol (**3a**) in 72% yield (Scheme 4).



Scheme 4: Electroreductive coupling of **1a** with **2a** and subsequent transformation to 2-cyanonaphthalene-1-ol (**3a**).

Next, the crude products of the electroreduction of methyl 2-acylbenzoates **1a–h** with **2a** were successively treated with 1 M HCl/dioxane 1:1 at 25 °C for 1 h and the results are summarized in Table 1. Dehydrated 2-cyanonaphthalene-1-ols **3b–d,g** were obtained only by treatment with 1 M HCl without dehydration in refluxing cat. PPTS/toluene (Table 1, entries 2–4 and 7). From 5,6-dimethoxy substrate **1d**, phthalide **4d** was also formed together with naphthol **3d** (Table 1, entry 4). In contrast, phthalides **4e** and **4f** were the sole products in the reactions of 6-methoxy and 4,5,6-trimethoxy substrates **1e** and **1f** (Table 1, entries 5 and 6). In the reaction of methyl 2-benzoylbenzoate

Table 1: Electroreductive coupling of **1a–h** with **2a** and subsequent treatment with 1 M HCl.

1a–h
 $X^{1-3} = H, MeO$
 $R = H, Me, Ph$

Entry	1	R	X^1	X^2	X^3	% Yield ^a
1	1a	H	H	H	H	3a , 56 ^b
2	1b	H	H	MeO	H	3b , 71
3	1c	H	MeO	MeO	H	3c , 62
4	1d	H	H	MeO	MeO	3d , 36 4d , 26
5	1e	H	H	H	MeO	4e , 48
6	1f	H	MeO	MeO	MeO	4f , 41
7	1g	Me	H	H	H	3g , 73 ^c
8	1h	Ph	H	H	H	4h , 24 ^d

^aIsolated yields. ^bAfter dehydration of **7a** by refluxing in cat. PPTS/toluene for 1 h. ^cThe reaction time for treatment with 1 M HCl was extended to 10 h. ^d3-Phenylphthalide (**i**) was obtained as main product (42% yield).

(**1h**), the reduced product, 3-phenylphthalide (**i**), was formed mainly in 42% yield accompanied by phthalide **4h** in 24% yield (Table 1, entry 8).

On the other hand, the electroreduction of **1a–h** with methyl vinyl ketone (**2b**) and subsequent treatment with 1 M HCl

afforded phthalides **5a–h** in moderate to good yields and naphthalene-1-ols **3'** corresponding to cyclized products **3** were not formed at all (Table 2).

The E_p values of substrates **1a–h** were observed to be in the range from -1.74 to -1.96 V versus SCE by cyclic voltammetry.

Table 2: Electroreductive coupling of **1a–h** with methyl vinyl ketone (**2b**) and subsequent treatment with 1 M HCl.

1a–h

Entry	1	R	X^1	X^2	X^3	% Yield ^a
1	1a	H	H	H	H	5a , 85
2	1b	H	H	MeO	H	5b , 77
3	1c	H	MeO	MeO	H	5c , 88
4	1d	H	H	MeO	MeO	5d , 67
5	1e	H	H	H	MeO	5e , 66
6	1f	H	MeO	MeO	MeO	5f , 73
7	1g	Me	H	H	H	5g , 74
8	1h	Ph	H	H	H	5h , 74

^aIsolated yields.

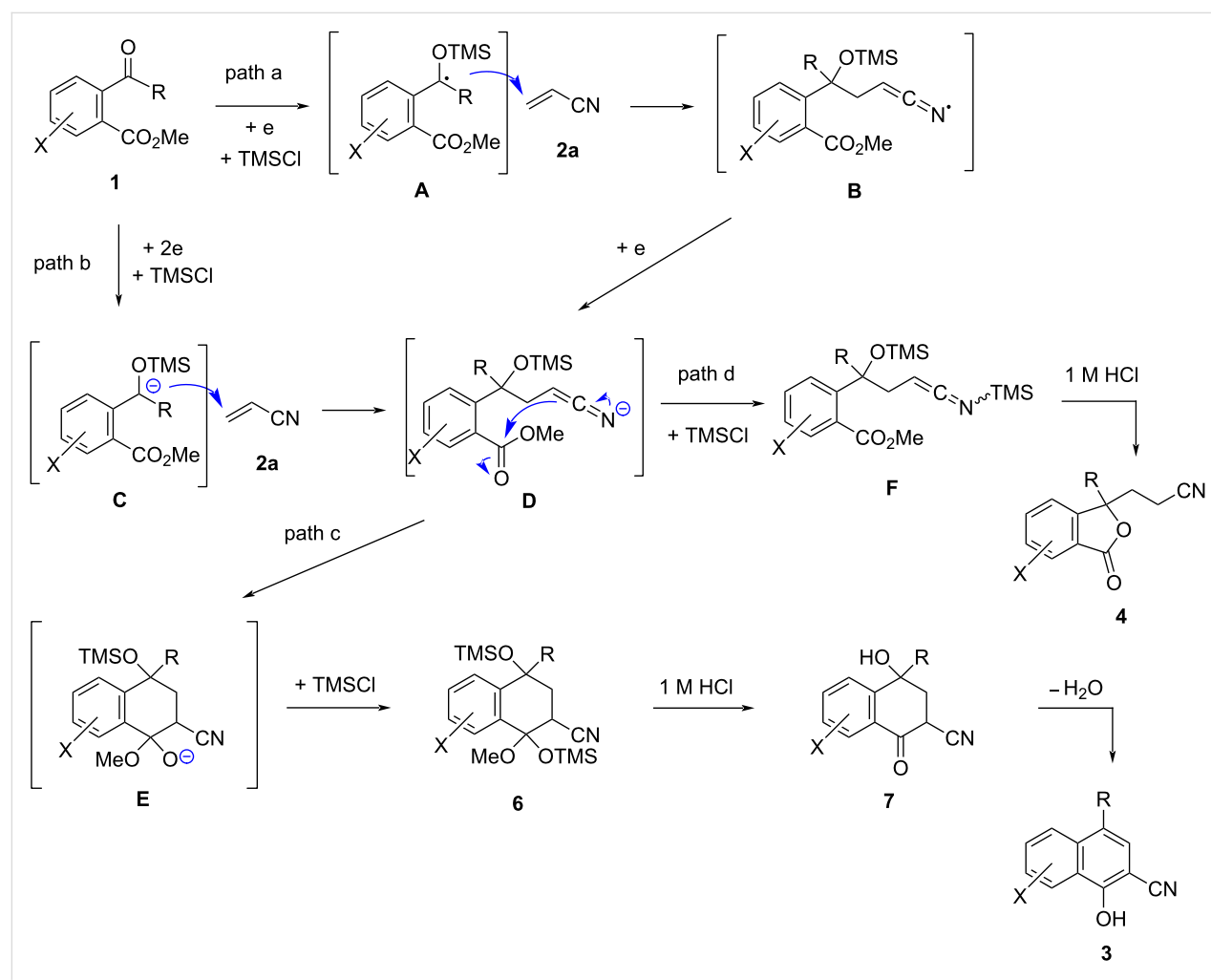
ry (Table 3) and acceptors **2** revealed no reduction peaks from 0 to -2.00 V vs SCE [5,6]. Therefore, this electroreductive coupling is initiated by the reduction of compounds **1**. There are two possible reaction mechanisms for the reductive coupling of **1** with **2a** as illustrated in Scheme 5. The first one is a radical addition of *O*-trimethylsilyl radical **A**, which is formed by a one-electron reduction of **1** and subsequent *O*-trimethylsilylation, to **2a** and a following one-electron reduction of the resultant radical **B** to give enolate anion **D** (path a). The second one is an anionic addition of an *O*-trimethylsilyl anion **C**, which is formed by a two-electron reduction of substrate **1** and *O*-trimethylsilylation, to **2a** (path b). Unlike the two reactions previously reported by us that are presumed to proceed with the addition of an anion species (Scheme 1 and Scheme 2) [5,6], methyl acrylate (**2c**) is much less reactive as an acceptor in this reaction as shown in Scheme 6. The main product in this case was the same dimeric phthalide **9** as the product without the acceptor. These results suggest that this reaction proceeds with the radical addition of **A** to form anion **D** (path a). Next, the

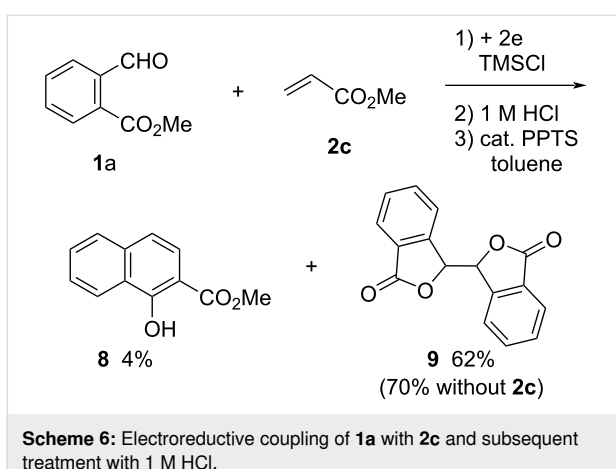
intramolecular addition of the anion **D** and subsequent *O*-trimethylsilylation of the resultant **E** produces intermediate **6** (path c). Desilylation of **6** with 1 M HCl and following dehydration of **7** affords product **3**. On the other hand, *O*-trimethylsilylation of anion **D** forms *N*-(trimethylsilyl)ethenimine **F** and subsequent treatment with 1 M HCl produces phthalide **4** through desilylation and following lactonization of **F** (path d).

Table 3: E_p values of **1a–h** derived from CV.

1	E_p ^a	1	E_p ^a
1a	-1.74	1e	-1.90
1b	-1.86	1f	-1.86
1c	-1.74	1g	-1.96
1d	-1.92	1h	-1.92

^aFirst reduction peak (volts vs SCE) in CV of a 3 mM solution in 0.03 M TBAP/DMF at a Pt cathode at 0.1 V/s and 25 °C.

Scheme 5: Presumed reaction mechanism of electroreductive coupling of **1** with **2a** and subsequent transformation to products **3** and **4**.

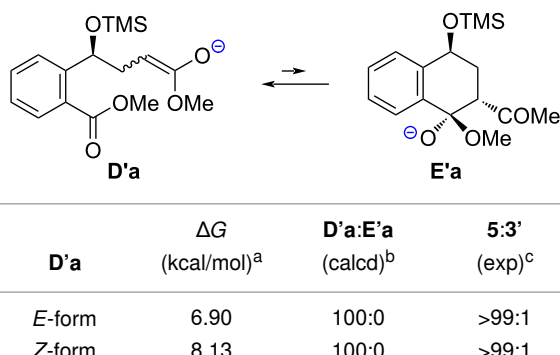


As can be seen from Scheme 5, the cyclization of **D** to **E** is the key step for the formation of compound **6**. Therefore, we calculated the intermediates (**D** and **E**) and transition states (**D-E TS**) for this step using the DFT method at the B3LYP/6-311+(2d,p)/IEFPCM(THF) level of theory (Supporting Information File 1). From the calculation results for the reactions of **1a-h** with **2a** summarized in Table 4, it was found that the ratio of **D:E** calculated from the free energy difference between **D** and **E** (ΔG) and the product ratio of **4:3** from the experimental results (Table 1, entries 1–6) were in good agreement. Therefore, it is presumed that whether the cyclization from **D** to **E** proceeds is thermodynamically controlled. Namely, when ΔG is large and negative, product **3** is selectively formed (Table 4, entries 1–3), and conversely, when ΔG is large and positive, product **4** is selectively produced (Table 4, entries 5 and 6). On the other

hand, when ΔG is close to zero, both products **3** and **4** are generated simultaneously (Table 4, entry 4). These results suggest that the substitution of the methoxy group at the 6-position tends to suppress the cyclization of **D** to **E** (Table 4, entries 4–6), since its electron-donating property reduces the electrophilicity of the ester carbonyl group. In contrast, the substitution of the methoxy group at the 5-position tends to promote the cyclization of **D**, owing to its electron-withdrawing property (Table 4, entries 2 and 3).

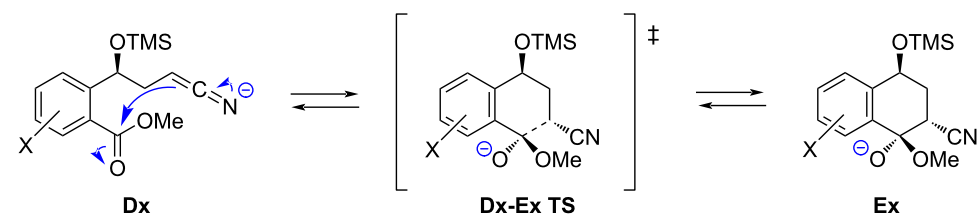
From the calculation results for the reaction of **1a** with **2b** (Table 5), it is understood that the cyclization from **D'a** to **E'a** hardly occurs because it shows a relatively large positive ΔG .

Table 5: Calculations of ΔG from **D'a** to **E'a**.



^aCalculated at the B3LYP/6-311+G(2d,p)/IEFPCM(THF) level of theory at 25 °C. ^bCalculated from ΔG on the basis of the Maxwell–Boltzmann distribution law at 25 °C. ^cData from entry 1 in Table 2.

Table 4: Calculations of activation energies (ΔG^\ddagger) and energy differences (ΔG) from **Dx** to **Ex**.



Entry	Dx	ΔG^\ddagger (kcal/mol) ^a	ΔG (kcal/mol) ^a	D:E (calcd) ^b	4:3 (exp) ^c
1	Da	6.73	-1.22	11:89	<1:99
2	Db	5.86	-2.38	2:98	<1:99
3	Dc	4.94	-2.17	3:97	<1:99
4	Dd	7.82	0.33	36:64	42:58
5	De	9.16	1.37	91:9	>99:1
6	Df	9.13	2.55	99:1	>99:1

^aCalculated at the B3LYP/6-311+G(2d,p)/IEFPCM(THF) level of theory at 25 °C. ^bCalculated from ΔG on the basis of the Maxwell–Boltzmann distribution law at 25 °C. ^cData from entries 1–6 in Table 1.

Conclusion

The electroreduction of *o*-acylbenzoates **1** with acrylonitrile (**2a**) in the presence of TMSCl and subsequent treatment with 1 M HCl gave 2-cyanonaphthalen-1-ols **3** and 3-(3-cyanoethyl)phthalides **4**. Which product was preferentially produced is determined by the position of the methoxy group on the aromatic ring of the substrate **1**. Using the same method, 3-(3-oxobutyl)phthalides **5** were produced as the sole products by the reaction of **1** with methyl vinyl ketone (**2b**). It was found by DFT calculations for the cyclization step of the intermediate enolate anions that the product selectivity was in good agreement with the free energy differences (ΔG) in the cyclization step.

Experimental

General information. The ^1H NMR (500 MHz) and ^{13}C NMR (125 MHz) spectra were measured on a JEOL GMX-500 spectrometer with tetramethylsilane (TMS) or the residual signals of protonated solvents as an internal standard: CDCl_3 ($\delta = 77.0$ in ^{13}C NMR). IR spectra were recorded on a Shimadzu IRAF-affinity-1 infrared spectrometer. HRMS were measured on a Thermo Scientific Exactive FTMS spectrometer. Melting points were uncorrected. Column chromatography was performed on silica gel 60. THF was distilled from sodium benzophenone ketyl radical. TMSCl, TEA, and DMF were distilled from CaH_2 .

Starting materials. Methyl 2-formylbenzoate (**1a**) and methyl 2-benzoylbenzoate (**1h**) were purchased from Tokyo Chemical Industry Corporation. Methyl 2-acetylbenzoate (**1g**) [17] was prepared from commercially available 2-acetylbenzoic acids (Tokyo Chemical Industry Corporation) by usual esterification using MeI , K_2CO_3 /acetone at 25 °C for 12 h. Methoxy-substituted 2-formylbenzoates **1b** [18], **1c** [19], **1d** [20], **1e** [21], and **1f** [22] were prepared according to the reported methods.

Typical procedures for electroreduction in the presence of TMSCl (Table 1, entry 1). A 0.3 M solution of Bu_4NClO_4 in THF (15 mL) was placed in the cathodic chamber of a divided cell (40 mL beaker, 3 cm diameter, 6 cm height) equipped with a platinum cathode ($5 \times 5 \text{ cm}^2$), a platinum anode ($2 \times 1 \text{ cm}^2$), and a ceramic cylindrical diaphragm (1.5 cm diameter). A 0.3 M solution of Bu_4NClO_4 in DMF (4 mL) was placed in the anodic chamber (inside the diaphragm). Methyl 2-formylbenzoate (**1a**, 161 mg, 1.0 mmol), acrylonitrile (**2a**, 258 mg, 2.5 mmol), TMSCl (0.64 mL, 5 mmol), and TEA (0.14 mL, 1 mmol) were added to the cathodic chamber. After 250 C of electricity (2.5 F/mol) have passed at a constant current of 100 mA at room temperature under a nitrogen atmosphere (42 min), the catholyte was evaporated in vacuo. The residue was dissolved in diethyl ether (20 mL) and insoluble solid was

filtered off. After removal of the solvent in vacuo, the residue was dissolved in 1 M HCl (5 mL)/1,4-dioxane (5 mL) and the solution was stirred at 30 °C for 1 h. The mixture was diluted with sat. aqueous NaCl solution (20 mL) and water (20 mL), and then extracted with ethyl acetate (3×20 mL). The organic layer was washed with sat. aqueous NaCl solution, dried over MgSO_4 , and filtered. After removal of the solvent in vacuo, the residue was purified by column chromatography on silica gel (hexanes/EtOAc) to give 146 mg of **7a** [23] (78% yield) as a mixture of two diastereomers (78:22 dr). A solution of **7a** (146 mg) and PPTS (10 mg) in toluene (10 mL) was refluxed using the Dean–Stark apparatus under nitrogen atmosphere for 1 h. After removal of the solvent in vacuo, the residue was purified by column chromatography on silica gel (hexanes/EtOAc) to give 95 mg of **3a** [8,23] (56% yield in two steps).

Supporting Information

Supporting Information File 1

Characterization data for compounds, copies of ^1H and ^{13}C NMR spectra, X-ray crystallographic data (ORTEP) of **3b**, CV data of compounds **1a–h**, and DFT calculation data for cyclization of enolate anions.

[<https://www.beilstein-journals.org/bjoc/content/supplementary/1860-5397-18-95-S1.pdf>]

Supporting Information File 2

Cif for **3b**.

[<https://www.beilstein-journals.org/bjoc/content/supplementary/1860-5397-18-95-S2.cif>]

Acknowledgements

For this research work we used the supercomputer of ACCMS, Kyoto University.

ORCID® IDs

Naoki Kise - <https://orcid.org/0000-0002-2366-3953>

Toshihiko Sakurai - <https://orcid.org/0000-0001-7181-9791>

Preprint

A non-peer-reviewed version of this article has been previously published as a preprint: <https://doi.org/10.3762/bxiv.2022.38.v1>

References

1. Little, R. D. *J. Org. Chem.* **2020**, *85*, 13375–13390. doi:10.1021/acs.joc.0c01408
2. Waldvogel, S. R.; Lips, S.; Selt, M.; Riehl, B.; Kampf, C. *J. Chem. Rev.* **2018**, *118*, 6706–6765. doi:10.1021/acs.chemrev.8b00233

3. Jiang, Y.; Xu, K.; Zeng, C. *Chem. Rev.* **2018**, *118*, 4485–4540. doi:10.1021/acs.chemrev.7b00271
4. Yan, M.; Kawamata, Y.; Baran, P. S. *Chem. Rev.* **2017**, *117*, 13230–13319. doi:10.1021/acs.chemrev.7b00397
5. Kise, N.; Yamamoto, S.; Sakurai, T. *J. Org. Chem.* **2020**, *85*, 13973–13982. doi:10.1021/acs.joc.0c02000
6. Kise, N.; Manto, T.; Sakurai, T. *J. Org. Chem.* **2021**, *86*, 18232–18246. doi:10.1021/acs.joc.1c02512
7. He, M.-X.; Mo, Z.-Y.; Wang, Z.-Q.; Cheng, S.-Y.; Xie, R.-R.; Tang, H.-T.; Pan, Y.-M. *Org. Lett.* **2020**, *22*, 724–728. doi:10.1021/acs.orglett.9b04549
8. Zhang, W.; Li, T.; Wang, Q.; Zhao, W. *Adv. Synth. Catal.* **2019**, *361*, 4914–4918. doi:10.1002/adsc.201900813
9. Zhou, C.; Fang, F.; Cheng, Y.; Li, Y.; Liu, H.; Zhou, Y. *Adv. Synth. Catal.* **2018**, *360*, 2546–2551. doi:10.1002/adsc.201800362
10. Beck, J. J.; Chou, S.-C. *J. Nat. Prod.* **2007**, *70*, 891–900. doi:10.1021/np0605586
11. Karmakar, R.; Pahari, P.; Mal, D. *Chem. Rev.* **2014**, *114*, 6213–6284. doi:10.1021/cr400524q
12. Li, S.; Su, M.; Sun, J.; Hu, K.; Jin, J. *Org. Lett.* **2021**, *23*, 5842–5847. doi:10.1021/acs.orglett.1c01984
13. Jia, B.; Yang, Y.; Jin, X.; Mao, G.; Wang, C. *Org. Lett.* **2019**, *21*, 6259–6263. doi:10.1021/acs.orglett.9b02142
14. Anselmo, M.; Bassi, A.; Protti, S.; Ravelli, D. *ACS Catal.* **2019**, *9*, 2493–2500. doi:10.1021/acscatal.8b03875
15. Miura, H.; Terajima, S.; Shishido, T. *ACS Catal.* **2018**, *8*, 6246–6254. doi:10.1021/acscatal.8b00680
16. Zhang, S.; Li, L.; Wang, H.; Li, Q.; Liu, W.; Xu, K.; Zeng, C. *Org. Lett.* **2018**, *20*, 252–255. doi:10.1021/acs.orglett.7b03617
17. Greszler, S. N.; Johnson, J. S. *Angew. Chem., Int. Ed.* **2009**, *48*, 3689–3691. doi:10.1002/anie.200900215
18. Zhang, H.; Zhang, S.; Liu, L.; Luo, G.; Duan, W.; Wang, W. *J. Org. Chem.* **2010**, *75*, 368–374. doi:10.1021/jo902118x
19. Che, C.; Xiang, J.; Wang, G.-X.; Fathi, R.; Quan, J.-M.; Yang, Z. *J. Comb. Chem.* **2007**, *9*, 982–989. doi:10.1021/cc070058a
20. Bisai, V.; Suneja, A.; Singh, V. K. *Angew. Chem., Int. Ed.* **2014**, *53*, 10737–10741. doi:10.1002/anie.201405074
21. He, Y.; Cheng, C.; Chen, B.; Duan, K.; Zhuang, Y.; Yuan, B.; Zhang, M.; Zhou, Y.; Zhou, Z.; Su, Y.-J.; Cao, R.; Qiu, L. *Org. Lett.* **2014**, *16*, 6366–6369. doi:10.1021/o15031603
22. Betterley, N. M.; Kerdphon, S.; Chaturonrutsamee, S.; Kongsriprapan, S.; Surawatanawong, P.; Soorukram, D.; Pohmakotr, M.; Andersson, P. G.; Reutrakul, V.; Kuhakarn, C. *Asian J. Org. Chem.* **2018**, *7*, 1642–1647. doi:10.1002/ajoc.201800313
23. Broom, N. J. P.; Sammes, P. G. *J. Chem. Soc., Perkin Trans. 1* **1981**, 465–470. doi:10.1039/p19810000465

License and Terms

This is an open access article licensed under the terms of the Beilstein-Institut Open Access License Agreement (<https://www.beilstein-journals.org/bjoc/terms>), which is identical to the Creative Commons Attribution 4.0

International License

(<https://creativecommons.org/licenses/by/4.0>). The reuse of material under this license requires that the author(s), source and license are credited. Third-party material in this article could be subject to other licenses (typically indicated in the credit line), and in this case, users are required to obtain permission from the license holder to reuse the material.

The definitive version of this article is the electronic one which can be found at:

<https://doi.org/10.3762/bjoc.18.95>



Electrochemical and spectroscopic properties of twisted dibenzo[*g,p*]chrysene derivatives

Tomoya Imai¹, Ryuhei Akasaka², Naruhiro Yoshida², Toru Amaya^{*1}
and Tetsuo Iwasawa^{*2}

Full Research Paper

Open Access

Address:

¹Department of Information and Basic Science, Graduate School of Science, Nagoya City University, 1, Yamanohata, Mizuho-cho, Mizuho-ku, Nagoya, Aichi 467-8501, Japan and ²Department of Materials Chemistry, Ryukoku University, Seta, Otsu, Shiga, 520-2194, Japan

Email:

Toru Amaya^{*} - amaya@nsc.nagoya-cu.ac.jp; Tetsuo Iwasawa^{*} - iwasawa@rins.ryukoku.ac.jp

* Corresponding author

Keywords:

DFT calculation; dibenzo[*g,p*]chrysenes; fluorescent compounds; oxidation; polycyclic aromatic hydrocarbon (PAH); twisted acenes

Beilstein J. Org. Chem. **2022**, *18*, 963–971.

<https://doi.org/10.3762/bjoc.18.96>

Received: 04 June 2022

Accepted: 20 July 2022

Published: 03 August 2022

This article is part of the thematic issue "Molecular and macromolecular electrochemistry: synthesis, mechanism, and redox properties".

Guest Editor: S. Inagi

© 2022 Imai et al.; licensee Beilstein-Institut.

License and terms: see end of document.

Abstract

Dibenzo[*g,p*]chrysene (DBC), which consists of a twisted naphthalene core with four fused benzene rings, is a promising framework for organic electronic materials. Therefore, the research for structure–property relationships is important for the design of DBC-based materials. Here, the electrochemical and spectroscopic properties of DBC derivatives were investigated, and the effects of substituents and torsion of the naphthalene moiety were examined based on density functional theory (DFT) calculations. All the substituted DBC derivatives showed higher oxidation potentials than that for **DBC-H**, even for compounds that contained an electron-donating group such as **DBC-Me** and **DBC-SMe**. DFT calculations clearly indicate that these higher oxidation potentials are due to the ineffective conjugation of the MeO group, which is oriented perpendicular to the benzene ring because of the steric repulsion of substituents on both sides. More specifically, the inductive effect of the MeO group is dominant rather than the mesomeric effect when the substituent is located at both sides of the MeO group. Concerning the torsion of the naphthalene moiety, the twisting results in a slight increase in the HOMO and a slight lowering of the LUMO. The twisting effect is much smaller than the conjugation effect of the MeO group. Absorption spectra of all the substituted DBC derivatives also showed a red-shift as compared to that for **DBC-H**. Concerning the luminescence, a strong photoluminescence was observed for **DBC-H** and **DBC-Si**.

Introduction

Polycyclic aromatic hydrocarbons (PAHs) have attracted interest as potential electronic and optoelectronic materials [1–12]. Non-planar PAHs have been extensively investigated

from the viewpoint of their synthetic challenge and/or for the development of functional organic materials [13–22]. Among such PAHs, twisted acenes are an interesting class

of compounds due to their characteristic structures and conjugation systems [23–25]. Dibenzo[*g,p*]chrysene (DBC), which consists of a twisted naphthalene core with four fused benzene rings (Figure 1a) [26], is a promising framework for serving as organic semiconductors, dyes, liquid crystals, and light-emitting materials. A number of substituted DBCs have been reported in this context [27–46]. To develop charge-transport materials, Rathore et al. reported on the stability of radical cations of DBCs with MeO groups located at X and/or Y (MeO-DBC-1, MeO-DBC-2, and MeO-DBC-3, Figure 1b) [43]. The first oxidation potential ($E_{\text{ox}1}$) of **MeO-DBC-1** was reported to be 0.40 V (based on Fc/Fc^+), which is 0.48 V lower than that of **DBC**. In contrast, when a MeO group is introduced at the X position (**MeO-DBC-2**), the $E_{\text{ox}1}$ is lower by only 0.15 V than that of **DBC**. It has also been reported that the oxidation potential of **MeO-DBC-3**, in which the MeO groups are attached at both X and Y, is 0.06 V higher than that for **MeO-DBC-1**. These remarkable substituent effects are an interesting and important finding for molecular design, but the effects of X and Z substituents and the twisting of the naphthalene moiety have not been reported.

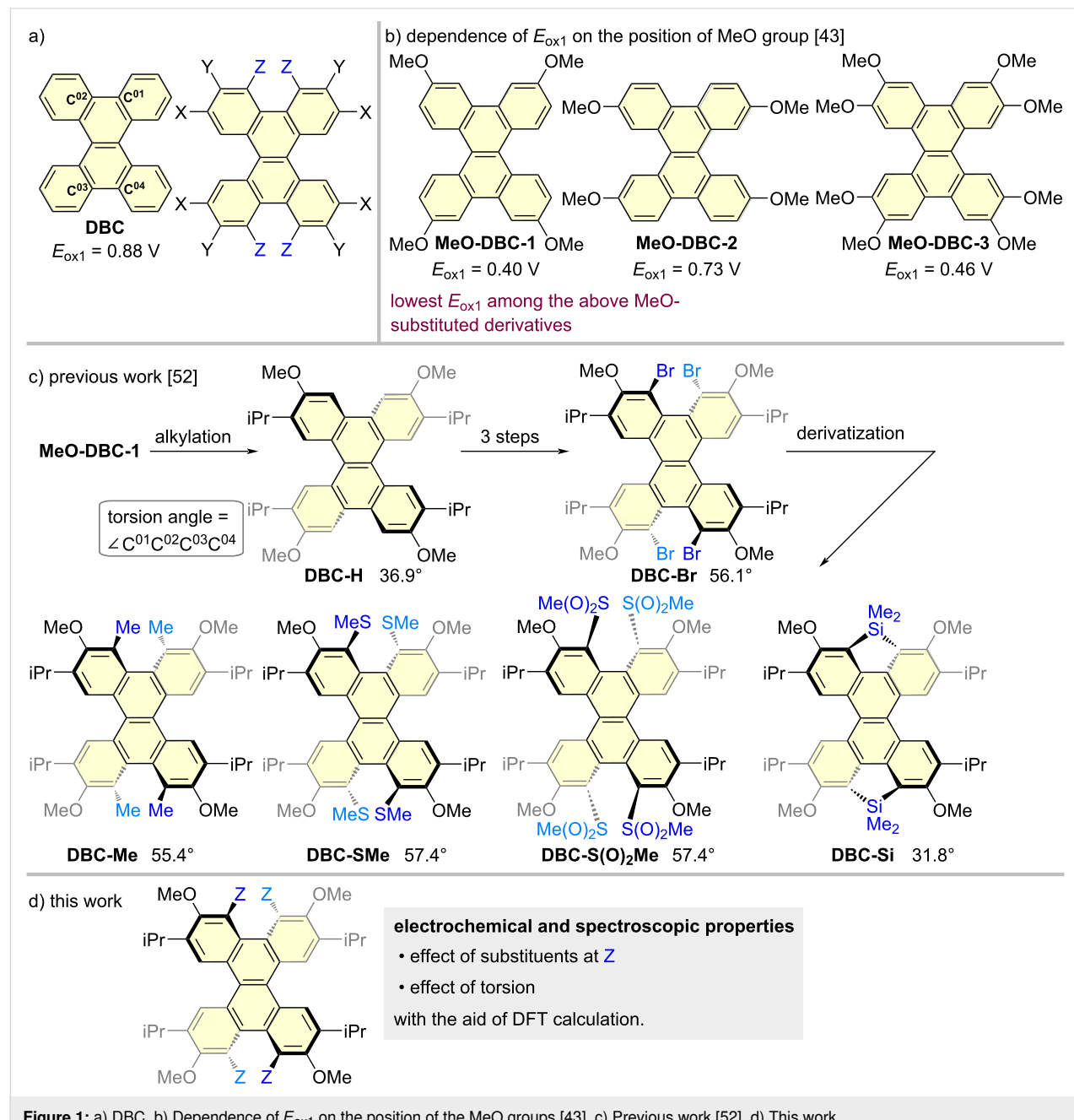


Figure 1: a) DBC. b) Dependence of $E_{\text{ox}1}$ on the position of the MeO groups [43]. c) Previous work [52]. d) This work.

We previously studied the synthesis of solution-processable DBC derivatives with various substituents attached [47–51]. We also recently reported on a synthetic strategy for preparing DBC derivatives using **DBC-H** with four isopropyl groups at X as a key template for the derivatization (Figure 1c). Based on this strategy, various substituents were introduced at Z to produce **DBC-Br**, **DBC-Me**, **DBC-SMe**, **DBC-S(O)₂Me**, and **DBC-Si** (Figure 1c) [52]. The structures of all these derivatives were determined by X-ray crystallographic analysis, in which torsion angles were varied in a range from 31.8° (**DBC-Si**) to 57.4° (**DBC-S(O)₂Me**) [52]. These DBC derivatives have four methoxy moieties at the Y position, which aroused our interest concerning the stability of those oxidation states.

Herein, we report on the electrochemical and spectroscopic properties of the DBC derivatives, where the effects of substitu-

ents and torsion were examined with the aid of DFT calculations. Consequently, the findings revealed that the substitution at the Z position induces a change in the conformation of the MeO groups, making the conjugation of the MeO groups ineffective, thus resulting in the lowering of both HOMO and LUMO energy levels. Concerning the twisting, the effect to the HOMO and LUMO energy levels was found to be small. We anticipate that the impact of diverse substituents and torsion angles on the chemical properties would be beneficial in terms of creating DBC-based materials.

Results and Discussion

Electrochemical properties

Cyclic voltammograms (CVs) and square-wave voltammograms (SWVs) were measured for **DBC-H**, **DBC-Me**, **DBC-SMe**, **DBC-Br**, **DBC-S(O)₂Me**, and **DBC-Si** (Figure 2)

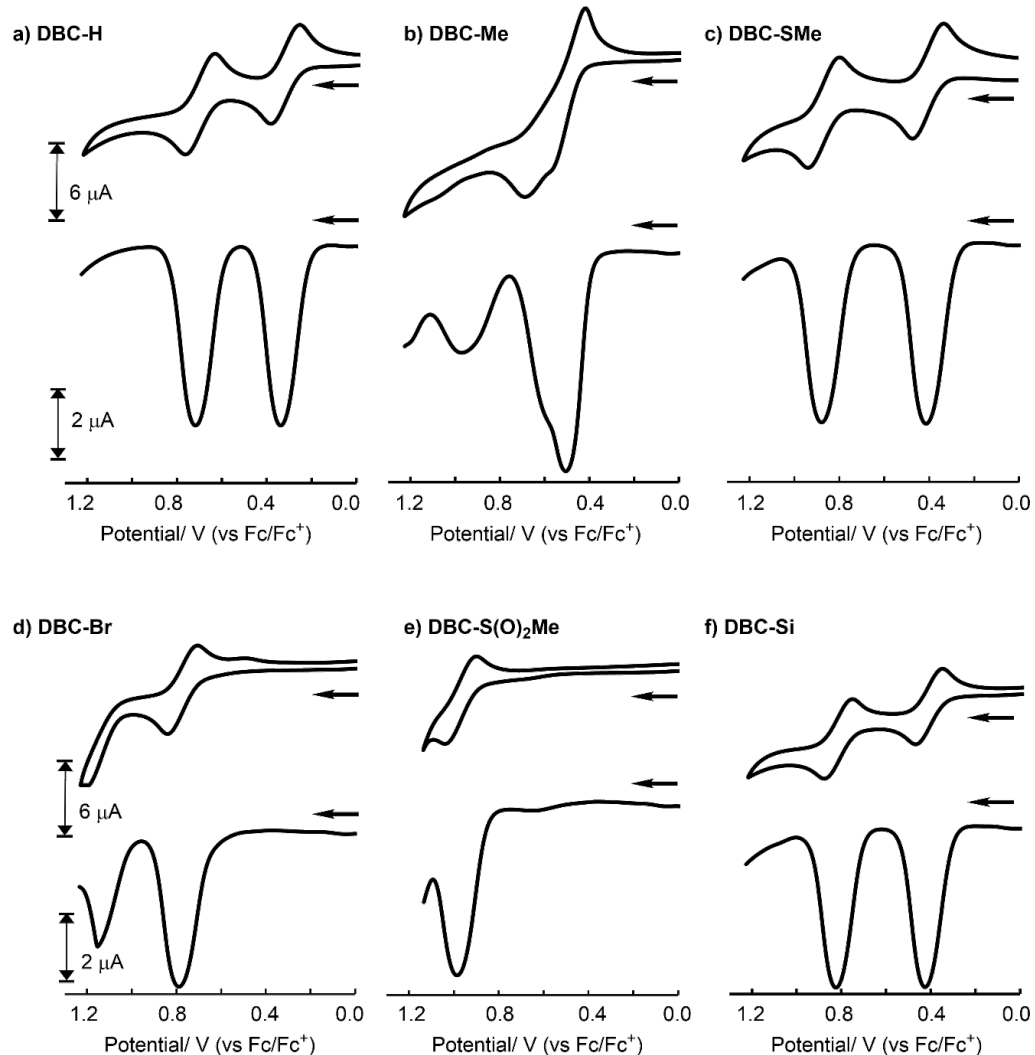


Figure 2: CVs and SWVs of DBC derivatives in CH_2Cl_2 ($\approx 1.0 \times 10^{-3}$ M, see Supporting Information File 1 for details) including 5.0×10^{-2} M NBu_4BF_4 as a supporting electrolyte under Ar at 298 K (working electrode: Pt, scan rate: 100 mV/s and 40 mV/s for CV and SWV measurements, respectively).

[53]. Table 1 summarizes the first and second oxidation potentials based on Fc/Fc^+ ($E_{\text{ox}1}$ and $E_{\text{ox}2}$) determined from the SWVs, together with the torsion angles determined from the X-ray crystal structures [52], the HOMO and LUMO levels determined from DFT calculations [52,54] and estimated based on $E_{\text{ox}1}$. The voltammogram of **DBC-H** exhibited a reversible, two-step, two-electron redox process, with $E_{\text{ox}1}$ and $E_{\text{ox}2}$ values of 0.34 V and 0.72 V, respectively (Figure 2a). The value of $E_{\text{ox}1}$ is 0.06 V lower than that of **MeO-DBC-1** which does not contain isopropyl groups. This is in contrast to **MeO-DBC-3**, in which four MeO groups are introduced in place of the isopropyl groups, which has a 0.06 V higher oxidation potential than that of **MeO-DBC-1**. This indicates that alkyl substituents in the X position are effective in stabilizing the radical cation, thus making it more susceptible to oxidation. Unlike **DBC-H**, an irreversible voltammogram was observed in case of **DBC-Me** (Figure 2b). The first oxidation potential obtained from the SWV was 0.51 V, which is 0.17 V higher than that of **DBC-H**. This higher oxidation potential is somewhat surprising, which is discussed in the next paragraph based on DFT calculations. The CV of **DBC-SMe** showed a reversible two-electron redox process, with $E_{\text{ox}1}$ and $E_{\text{ox}2}$ values of 0.41 V and 0.88 V, respectively (Figure 2c) [53]. It is interesting to note that **DBC-SMe** exhibited a higher oxidation potential than **DBC-H** despite the electron-donating nature due to mesomeric effects based on lone pairs of sulfur atoms. In the CV of **DBC-Br**, a one-electron redox was observed as a reversible process, but a second redox process was not observed (Figure 2d). On the other hand, both the first and second oxidation processes were observed in the SWV of **DBC-Br** ($E_{\text{ox}1}$ and $E_{\text{ox}2}$ are 0.79 V and 1.15 V, respectively). **DBC-S(O)₂Me** with the electron-withdrawing substituents resulted in a reversible oxidation wave, but only a one-electron redox process could be observed due to the limitations of the solvent (Figure 2e). The potential of 0.98 V is the highest among the compounds measured in this study. To investigate the reduction behaviour, **DBC-S(O)₂Me**

was measured in the low potential region. A peak, which appeared to be the one-electron reduction peak, was observed at -2.25 V (see Figure S1 in Supporting Information File 1). Finally, the CV of the silole-fused **DBC-Si** was investigated and the results indicated a reversible two-electron redox process ($E_{\text{ox}1}$ and $E_{\text{ox}2}$ are 0.43 V and 0.82 V, respectively, Figure 2f). These values for $E_{\text{ox}1}$ and $E_{\text{ox}2}$ for **DBC-Si** are slightly higher than those of **DBC-H**. The obtained electrochemical data were nearly consistent with the trend of the values for HOMO obtained based on DFT calculations.

Theoretical calculations

DFT calculations were performed to clarify the reasons for the oxidation potentials [52,54,56]. To investigate the effects of the torsion of the naphthalene moiety and the conformation of the MeO group on the oxidation potential of these materials, hypothetical compounds **DBC-H(56°)-1** and **DBC-H(56°)-2** were created, respectively. In **DBC-H(56°)-1**, the atoms are fixed except for the Me group of **DBC-Me** (torsion angle = 56.5°), and the Me group is changed to H. **DBC-H(56°)-2** is the same structure as **DBC-H(56°)-1** except for the MeO group conformation. Optimizations of **DBC-H(56°)-1** and **DBC-H(56°)-2** based on DFT calculations were performed by fixing the atoms, as described above [56]. The conformations of the MeO group in **DBC-H(56°)-1** and **DBC-H(56°)-2** are nearly perpendicular (98.3°) to and parallel (179.8°) to the benzene ring, respectively (Figure 3 and Table 2). The results were compared to those for **DBC-H** and **DBC-Me** (Figure 3). To examine the torsional effect, **DBC-H** (torsion angle = 39.0°) and **DBC-H(56°)-2** (torsion angle = 56.5°) were compared. The HOMO level of the highly twisted **DBC-H(56°)-2** was 0.09 eV higher than that of the less twisted **DBC-H**. Conversely, the LUMO level of the highly twisted **DBC-H(56°)-2** was 0.05 eV lower than the less twisted **DBC-H**. As a result, the HOMO–LUMO gap of **DBC-H(56°)-2** becomes smaller than that of **DBC-H**. This is consistent with the trend reported for twisted acenes [57]. The

Table 1: Electrochemical data, torsion angles determined from the X-ray crystal structures, and HOMO and LUMO levels for DBC derivatives^a.

compounds	$E_{\text{ox}1}$ [V] ^b	$E_{\text{ox}2}$ [V] ^b	torsion angle [°] ^c	HOMO [eV] ^d (the estimated values based on experimental data in parentheses) ^e	LUMO [eV] ^d
DBC-H	0.34	0.72	36.9	-4.64 (-5.4)	-0.87
DBC-Me	0.51	0.96	55.4	-4.81 (-5.6)	-1.22
DBC-SMe	0.41	0.88	57.4	-5.00 (-5.5)	-1.42
DBC-Br	0.79	1.15	56.1	-5.24 (-5.9)	-1.71
DBC-S(O)₂Me	0.98	–	57.4	-5.56 (-6.1)	-2.00
DBC-Si	0.43	0.82	31.8	-4.80 (-5.5)	-1.09

^aConcentration: Around 1.0×10^{-3} M in CH_2Cl_2 (for detailed values, see Supporting Information File 1) containing 5.0×10^{-2} M NBu_4BF_4 as a supporting electrolyte. SWVs were recorded at a platinum electrode at 298 K under Ar. ^bBased on Fc/Fc^+ . ^cThe values obtained from X-ray crystallographic analyses [52]. ^dThe values obtained from DFT calculations at B3LYP6-31G(d,p) [52,54]. ^eThe energy values of HOMO were estimated based on the following equation $E_{\text{HOMO}} = -(E_{\text{ox}1} \text{ vs } \text{Fc}^+/\text{Fc} + 5.1)$ [55].

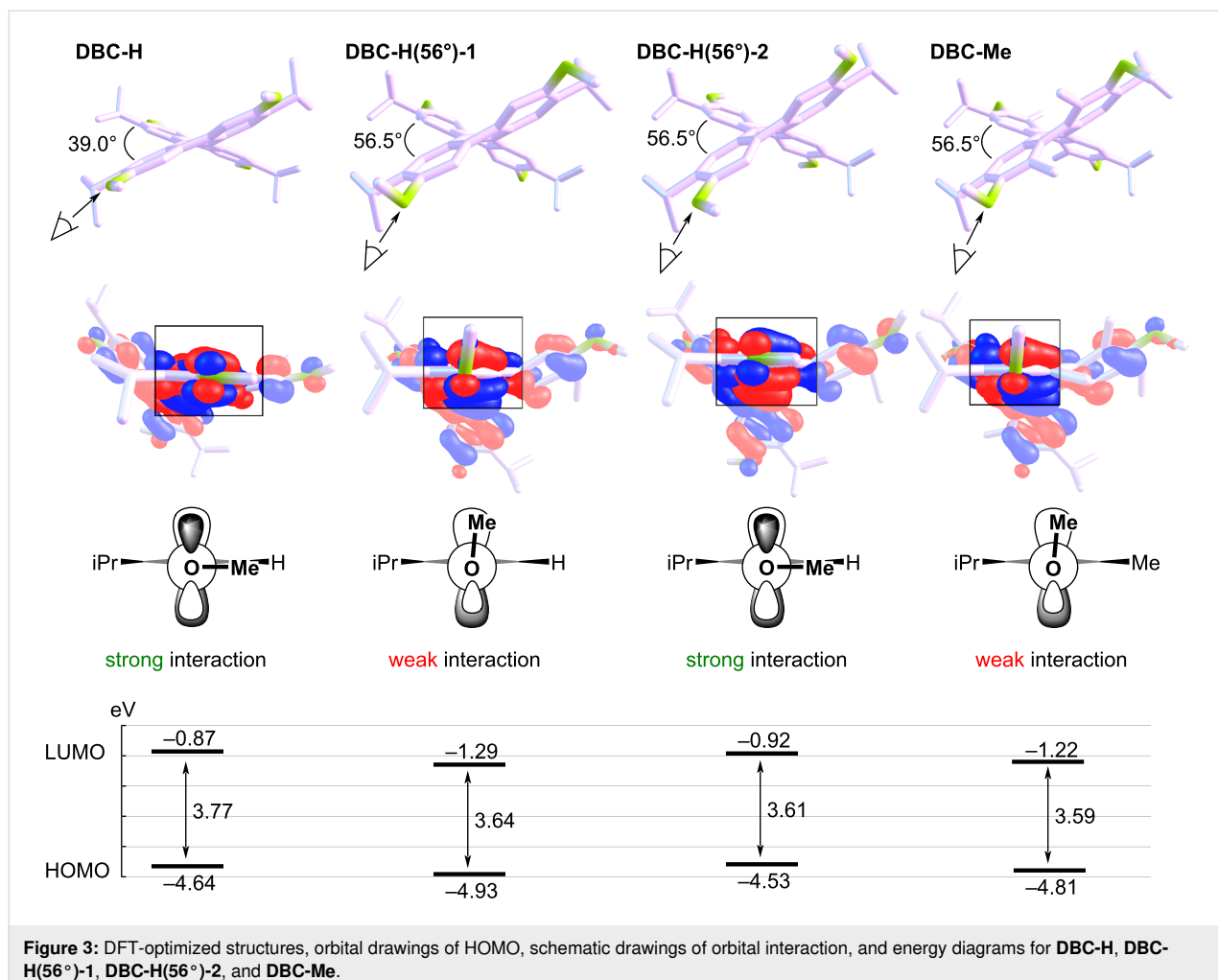
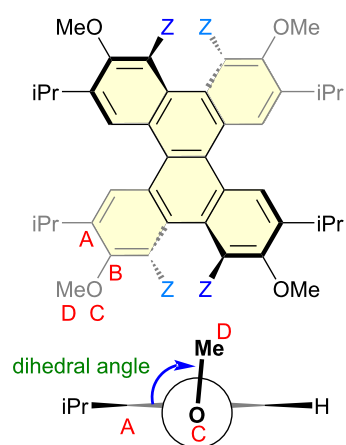


Table 2: Dihedral angles for the DFT-optimized structures of DBC derivatives [B3LYP6-31G(d,p)].

compounds	substituent Z	dihedral angle of ABCD [°]
DBC-H	H	179.6
DBC-H(56°)-1	H	98.3
DBC-H(56°)-2	H	179.8
DBC-Me	Me	98.3
DBC-SMe	SMe	105.7
DBC-Br	Br	111.1
DBC-S(O)₂Me	S(O) ₂ Me	97.8
DBC-Si	-SiMe ₂ -	156.6



conformational effect of the MeO group was investigated by comparison of **DBC-H(56°)-1** (perpendicular to the benzene ring, 98.3°) with **DBC-H(56°)-2** (parallel to the benzene ring,

179.8°). Consequently, both the HOMO and LUMO levels of **DBC-H(56°)-2** are higher than those of **DBC-H(56°)-1** by -0.40 eV and -0.37 eV, respectively. This is likely attributed by

the effect of conjugation for the orbital of an oxygen atom as shown in the schematic drawing in Figure 3. When the conformation of the MeO group is almost parallel to the benzene ring, the strong orbital interaction between the orbitals on the oxygen and adjacent carbon atoms is possible in HOMO (the orbital drawings are also shown in Figure S2 in Supporting Information File 1). In this case, the mesomeric effect of an oxygen atom is dominant. On the other hand, when the conformation of the MeO group is almost perpendicular to the benzene ring, the interaction between orbitals on the oxygen and adjacent carbon atoms becomes weak in the case of HOMO. In this case, the inductive effect of an oxygen atom can be dominant. Thus, the substituents at the Z position allow the MeO group to be oriented perpendicular to the benzene ring, which results in the lowering of both the HOMO and LUMO (Figure 3). In **DBC-Me**, the lowering of the HOMO based on the inductive effect offsets the increase in HOMO due to the electron-donating nature of the Me group. This can account for the observed higher E_{ox1} for **DBC-Me** than that for **DBC-H**.

Other derivatives were also examined. The dihedral angles are summarized in Table 2. The MeS group is an electron-donating group and may increase the HOMO, but the HOMO level of **DBC-SMe** is lower than that of **DBC-H**, as shown in the electrochemical study and by DFT calculations (Table 1). This is considered to be due to the contribution of the inductive effect of the MeO group by ineffective conjugation. In **DBC-Br** and **DBC-S(O)₂Me**, both the HOMO and LUMO are lower, which can be attributed to the combined effects of their electron-withdrawing by Br and S(O)₂Me groups and ineffective conjugation of the MeO group. In the case of **DBC-Si**, where the dihedral angle of the MeO group is 156.6°, both the HOMO and

LUMO are lower than those for **DBC-H**. Although it is not perpendicular, the lower energy levels for HOMO and LUMO can be accounted for by the ineffective conjugation of the MeO group.

Spectroscopic properties

Absorption and photoluminescence spectra and the simulations of absorption based on TD-DFT calculations [58] are shown in Figure 4 (see Figure S3 in Supporting Information File 1 for excited spectra). The spectral data are summarized in Table 3. The TD-DFT calculations reproduce the absorption spectra quite well. The longest absorption peak is attributed to the transition from HOMO to LUMO and HOMO-1 to LUMO+1 (see Tables S1–S6 in Supporting Information File 1). The trend for the order of optical band gap is roughly consistent with that of the HOMO–LUMO gap obtained from DFT calculation [52].

In the photoluminescence spectra, the luminescence of **DBC-Br** was very weak. On the other hand, **DBC-H**, **DBC-Me**, and **DBC-Si** showed relatively strong photoluminescences with quantum yields of 28%, 21%, and 11%, respectively (Table 3). The photoluminescence wavelengths were shifted toward longer wavelengths in the order of **DBC-Si**, **DBC-H**, **DBC-Me**, **DBC-SMe**, and **DBC-S(O)₂Me**. Of these, the Stokes shift for **DBC-S(O)₂Me** was the largest, which is due to the electron-withdrawing nature of the S(O)₂Me group.

Conclusion

The electrochemical and spectroscopic properties of DBC derivatives were investigated, and the effects of substituents and torsion of the naphthalene moiety were discussed based on DFT calculations. It was also found that introducing a substituent at

Table 3: Absorption and photoluminescence spectral data of DBC derivatives in CH₂Cl₂.

compounds	absorption λ_{max} [nm] molar absorption coefficient ϵ [M ⁻¹ ·cm ⁻¹] in parentheses	optical band gap ^a [eV]	photoluminescence λ_{max} [nm]	quantum yield [%] ^b
DBC-H	363 (16200)	2.95	416	28
DBC-Me	381 (20300)	2.91	427	21
DBC-SMe	384 (16500)	2.88	433	3
DBC-Br	386 (16100)	2.86	— ^c	— ^c
DBC-S(O)₂Me	380 (12900)	2.82	455	6
DBC-Si	368 (9500)	2.97	413	11

^aEstimated from the absorption edge. ^bMeasured based on the absolute quantum yield method using an integrating sphere. ^cToo weak photoluminescence to measure.

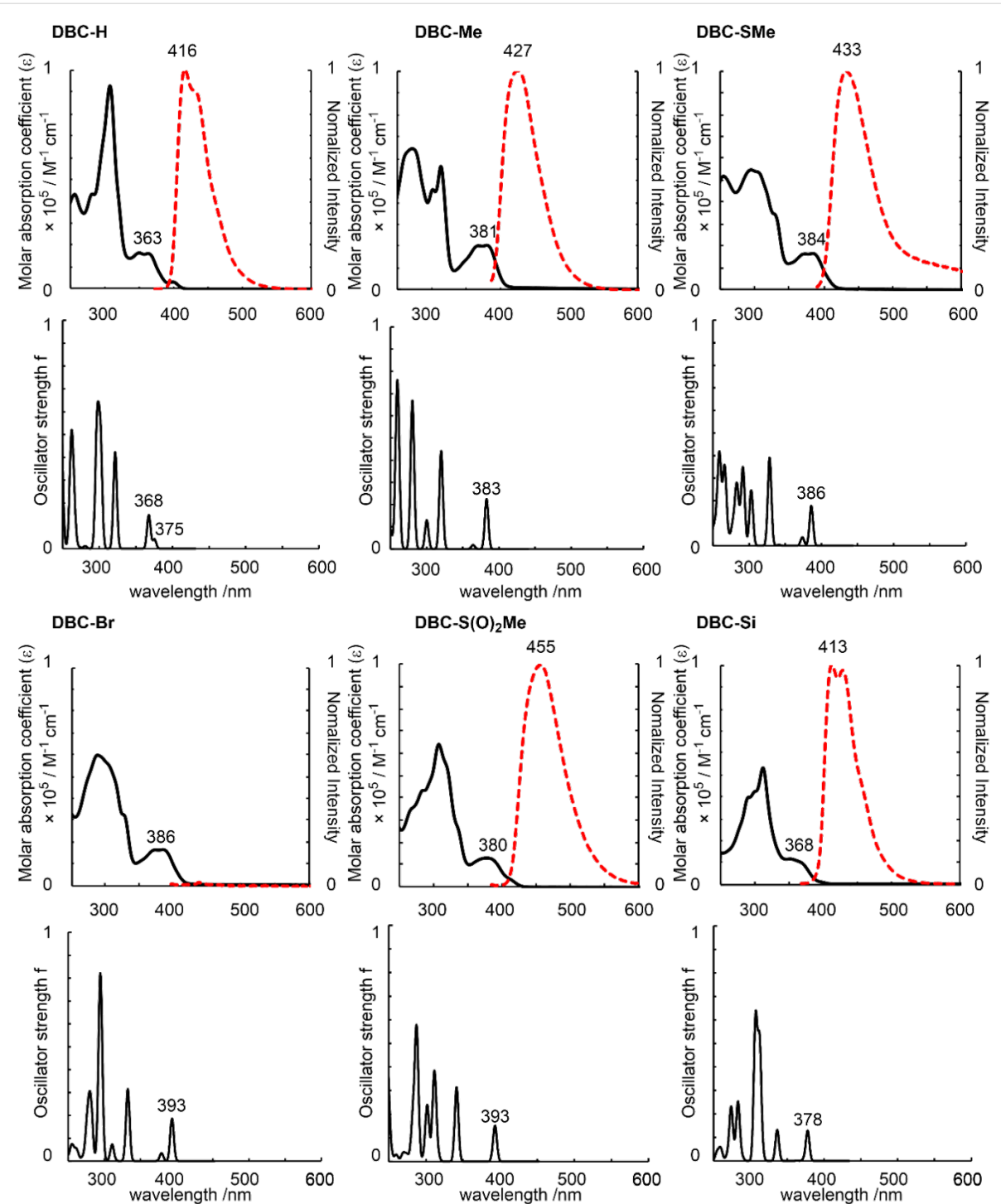


Figure 4: Absorption (solid line) and photoluminescence (dotted red line) spectra (upper graphs) in CH_2Cl_2 and simulations of absorption based on TD-DFT calculations [TD-B3LYP-D3/6-31G(d,p)//B3LYP/6-31G(d,p)] for DBC derivatives.

Z position resulted in a higher oxidation potential than that for **DBC-H**, even for compounds that contained electron-donating groups, such as **DBC-Me** and **DBC-SMe**. DFT calculations clearly indicate that this is due to the ineffective conjugation of the MeO group which is oriented perpendicular to the aromatic

ring because of the steric repulsion of substituents on both sides. More specifically, the inductive effect of the MeO group is dominant rather than the mesomeric effect when the substituent is present at the Z position. Concerning the torsion of the naphthalene moiety, the twisting caused a slight increase in the

HOMO and a slight lowering of the LUMO. The twisting effect is much smaller than the conjugation effect of the MeO group. Absorption spectra of all the substituted DBC derivatives also showed a red-shift as compared to that for **DBC-H**. Concerning photoluminescence, a strong photoluminescence was observed for **DBC-H** and **DBC-Si**. The findings reported in this study will be useful for the molecular design of such materials, and could lead to electronic material applications in the future.

Supporting Information

Supporting Information File 1

Figures S1–S3, Tables S1–S6, general, experimental procedure, and cartesian coordinates of optimized structures obtained based on the theoretical calculation. [https://www.beilstein-journals.org/bjoc/content/supplementary/1860-5397-18-96-S1.pdf]

Acknowledgements

The computation was performed using Research Center for Computational Science, Okazaki, Japan (Project: 21-IMS-C190, 22-IMS-C174). We thank Prof. Shinobu Aoyagi at Graduate School of Science, Nagoya City University for the use of a voltammetry analyser.

Funding

Tetsuo Iwasawa is grateful to JSPS Grant-in-Aid for Scientific Research (C) (22K05086) and 2022 the Joint Research Center for Science and Technology of Ryukoku University.

ORCID® IDs

Toru Amaya - <https://orcid.org/0000-0002-7716-0630>

Tetsuo Iwasawa - <https://orcid.org/0000-0002-1068-2733>

References

- Clar, E. *Polycyclic hydrocarbons*; Academic Press: London, UK, 1964; Vol. I.II.
- Harvey, R. G. *Polycyclic Aromatic Hydrocarbons*; Wiley-VCH: New York, NY, USA, 1997.
- Fetzer, J. C. *Large Polycyclic Aromatic Hydrocarbons*, 1st ed.; *Chemistry and Analysis*, Vol. 158; John Wiley & Sons: Hoboken, NJ, USA, 2000.
- Anthony, J. E. *Chem. Rev.* **2006**, *106*, 5028–5048. doi:10.1021/cr050966z
- Sergeyev, S.; Pisula, W.; Geerts, Y. H. *Chem. Soc. Rev.* **2007**, *36*, 1902–1929. doi:10.1039/b417320c
- Anthony, J. E. *Angew. Chem., Int. Ed.* **2008**, *47*, 452–483. doi:10.1002/anie.200604045
- Pisula, W.; Feng, X.; Müllen, K. *Chem. Mater.* **2011**, *23*, 554–567. doi:10.1021/cm102252w
- Wang, C.; Dong, H.; Hu, W.; Liu, Y.; Zhu, D. *Chem. Rev.* **2012**, *112*, 2208–2267. doi:10.1021/cr100380z
- Sun, Z.; Ye, Q.; Chi, C.; Wu, J. *Chem. Soc. Rev.* **2012**, *41*, 7857–7889. doi:10.1039/c2cs35211g
- Zhang, D.; Duan, L. *J. Phys. Chem. Lett.* **2019**, *10*, 2528–2537. doi:10.1021/acs.jpclett.9b00526
- Tian, D.; Chen, Y. *Adv. Opt. Mater.* **2021**, *9*, 2002264. doi:10.1002/adom.202002264
- Li, Q.; Zhang, Y.; Xie, Z.; Zhen, Y.; Hu, W.; Dong, H. *J. Mater. Chem. C* **2022**, *10*, 2411–2430. doi:10.1039/d1tc04866j
- Yao, T.; Yu, H.; Vermeij, R. J.; Bodwell, G. *J. Pure Appl. Chem.* **2008**, *80*, 533–546. doi:10.1351/pac200880030533
- Petrukhina, M. A.; Scott, L. T., Eds. *Fragments of Fullerenes and Carbon Nanotubes*; John Wiley & Sons: Hoboken, NJ, USA, 2011. doi:10.1002/9781118011263
- Wu, Y.-T.; Siegel, J. S. *Chem. Rev.* **2006**, *106*, 4843–4867. doi:10.1021/cr050554q
- Tsefrikas, V. M.; Scott, L. T. *Chem. Rev.* **2006**, *106*, 4868–4884. doi:10.1021/cr050553y
- Gingras, M. *Chem. Soc. Rev.* **2013**, *42*, 968–1006. doi:10.1039/c2cs35154d
- Amaya, T.; Hirao, T. *Chem. Rec.* **2015**, *15*, 310–321. doi:10.1002/tcr.201402078
- Ball, M.; Zhong, Y.; Wu, Y.; Schenck, C.; Ng, F.; Steigerwald, M.; Xiao, S.; Nuckolls, C. *Acc. Chem. Res.* **2015**, *48*, 267–276. doi:10.1021/ar500355d
- Segawa, Y.; Ito, H.; Itami, K. *Nat. Rev. Mater.* **2016**, *1*, 15002. doi:10.1038/natrevmats.2015.2
- Chen, C.-F.; Shen, Y. *Helicene Chemistry*; Springer: Berlin, Heidelberg, 2017. doi:10.1007/978-3-662-53168-6
- Saito, M.; Shinokubo, H.; Sakurai, H. *Mater. Chem. Front.* **2018**, *2*, 635–661. doi:10.1039/c7qm00593h
- Pascal, R. A., Jr. *Chem. Rev.* **2006**, *106*, 4809–4819. doi:10.1021/cr050550l
- Rickhaus, M.; Mayor, M.; Juríček, M. *Chem. Soc. Rev.* **2016**, *45*, 1542–1556. doi:10.1039/c5cs00620a
- Ma, S.; Gu, J.; Lin, C.; Luo, Z.; Zhu, Y.; Wang, J. *J. Am. Chem. Soc.* **2020**, *142*, 16887–16893. doi:10.1021/jacs.0c08555 and references cited therein.
- Herbstein, F. H. *Acta Crystallogr., Sect. B: Struct. Crystallogr. Cryst. Chem.* **1979**, *35*, 1661–1670. doi:10.1107/s0567740879007354
- Tokito, S.; Noda, K.; Fujikawa, H.; Taga, Y.; Kimura, M.; Shimada, K.; Sawaki, Y. *Appl. Phys. Lett.* **2000**, *77*, 160–162. doi:10.1063/1.126910
- Yamaguchi, S.; Swager, T. M. *J. Am. Chem. Soc.* **2001**, *123*, 12087–12088. doi:10.1021/ja016692o
- Kumar, S.; Varshney, S. K. *Mol. Cryst. Liq. Cryst. Sci. Technol., Sect. A* **2002**, *378*, 59–64. doi:10.1080/713738586
- Li, C.-W.; Wang, C.-I.; Liao, H.-Y.; Chaudhuri, R.; Liu, R.-S. *J. Org. Chem.* **2007**, *72*, 9203–9207. doi:10.1021/jo701504m
- Chaudhuri, R.; Hsu, M.-Y.; Li, C.-W.; Wang, C.-I.; Chen, C.-J.; Lai, C. K.; Chen, L.-Y.; Liu, S.-H.; Wu, C.-C.; Liu, R.-S. *Org. Lett.* **2008**, *10*, 3053–3056. doi:10.1021/o1801029x
- Shimizu, M.; Nagao, I.; Tomioka, Y.; Hiyama, T. *Angew. Chem., Int. Ed.* **2008**, *47*, 8096–8099. doi:10.1002/anie.200803213
- Navale, T. S.; Zhai, L.; Lindeman, S. V.; Rathore, R. *Chem. Commun.* **2009**, 2857–2859. doi:10.1039/b903133b
- Mori, T.; Fujita, K.; Kimura, M. *J. Photopolym. Sci. Technol.* **2010**, *23*, 317–322. doi:10.2494/photopolymer.23.317

35. Tsuji, H.; Ueda, Y.; Ilies, L.; Nakamura, E. *J. Am. Chem. Soc.* **2010**, *132*, 11854–11855. doi:10.1021/ja1059119

36. Navale, T. S.; Thakur, K.; Rathore, R. *Org. Lett.* **2011**, *13*, 1634–1637. doi:10.1021/ol200069c

37. Mochida, K.; Kawasumi, K.; Segawa, Y.; Itami, K. *J. Am. Chem. Soc.* **2011**, *133*, 10716–10719. doi:10.1021/ja202975w

38. Ueda, Y.; Tsuji, H.; Tanaka, H.; Nakamura, E. *Chem. – Asian J.* **2014**, *9*, 1623–1628. doi:10.1002/asia.201402102

39. Hashimoto, S.; Ikuta, T.; Shiren, K.; Nakatsuka, S.; Ni, J.; Nakamura, M.; Hatakeyama, T. *Chem. Mater.* **2014**, *26*, 6265–6271. doi:10.1021/cm503102d

40. Suzuki, N.; Fujita, T.; Ichikawa, J. *Org. Lett.* **2015**, *17*, 4984–4987. doi:10.1021/acs.orglett.5b02426

41. Liu, X.-Y.; Tang, X.; Zhao, Y.; Zhao, D.; Fan, J.; Liao, L.-S. *Dyes Pigm.* **2017**, *146*, 234–239. doi:10.1016/j.dyepig.2017.06.036

42. Song, S.; Huang, G.; Kojima, T.; Nakae, T.; Uno, H.; Sakaguchi, H. *Chem. Lett.* **2017**, *46*, 1525–1527. doi:10.1246/cl.170614

43. Ivanov, M. V.; Talipov, M. R.; Navale, T. S.; Rathore, R. *J. Phys. Chem. C* **2018**, *122*, 2539–2545. doi:10.1021/acs.jpcc.7b11232

44. Wang, S.; Yang, P.; Chang, K.; Lv, W.; Mi, B.; Song, J.; Zhao, X.; Gao, Z. *Org. Electron.* **2019**, *74*, 269–275. doi:10.1016/j.orgel.2019.07.022

45. Kogashi, K.; Matsuno, T.; Sato, S.; Isobe, H. *Angew. Chem., Int. Ed.* **2019**, *58*, 7385–7389. doi:10.1002/anie.201902893

46. Suzuki, Y.; Tohnai, N.; Saeki, A.; Hisaki, I. *Chem. Commun.* **2020**, *56*, 13369–13372. doi:10.1039/d0cc06081j

47. Yoshida, N.; Kamiguchi, S.; Sakao, K.; Akasaka, R.; Fujii, Y.; Maruyama, T.; Iwasawa, T. *Tetrahedron Lett.* **2020**, *61*, 152033. doi:10.1016/j.tetlet.2020.152033

48. Yoshida, N.; Kamiguchi, S.; Fujii, Y.; Sakao, K.; Maruyama, T.; Tokai, S.; Matsumoto, Y.; Taguchi, Y.; Akasaka, R.; Iwasawa, T. *Tetrahedron Lett.* **2020**, *61*, 152406. doi:10.1016/j.tetlet.2020.152406

49. Fujii, Y.; Maruyama, T.; Akasaka, R.; Sakao, K.; Tokai, S.; Taguchi, Y.; Matsumoto, Y.; Kamiguchi, S.; Yoshida, N.; Iwasawa, T. *Tetrahedron Lett.* **2021**, *65*, 152758. doi:10.1016/j.tetlet.2020.152758

50. Fujii, Y.; Taguchi, Y.; Tokai, S.; Matsumoto, Y.; Yoshida, N.; Iwasawa, T. *Tetrahedron* **2021**, *95*, 132353. doi:10.1016/j.tet.2021.132353

51. Yoshida, N.; Akasaka, R.; Awakura, Y.; Amaya, T.; Iwasawa, T. *Eur. J. Org. Chem.* **2021**, 5343–5347. doi:10.1002/ejoc.202100869

52. Kamiguchi, S.; Akasaka, R.; Yoshida, N.; Imai, T.; Yamaoka, Y.; Amaya, T.; Iwasawa, T. *Tetrahedron Lett.* **2022**, *92*, 153664. doi:10.1016/j.tetlet.2022.153664

53. The voltammograms including the low potential region for **DBC-SMe** and **DBC-S(O)₂Me** are shown in Figure S1 (Supporting Information File 1). Other DBC derivatives did not show any peaks in the low potential region.

54. The HOMO and LUMO energy levels for **DBC-H**, **DBC-Me**, **DBC-SMe**, **DBC-Br**, **DBC-S(O)₂Me**, and **DBC-Si** based on DFT calculations were reported in a previous paper together with the optimized structure and HOMO and LUMO orbital drawings (Supporting Information File 1 in reference [52]).

55. Cardona, C. M.; Li, W.; Kaifer, A. E.; Stockdale, D.; Bazan, G. C. *Adv. Mater. (Weinheim, Ger.)* **2011**, *23*, 2367–2371. doi:10.1002/adma.201004554

56. DFT calculations for **DBC-H(56°)-1** and **DBC-H(56°)-2** were performed in this study.

57. Bedi, A.; Gidron, O. *Acc. Chem. Res.* **2019**, *52*, 2482–2490. doi:10.1021/acs.accounts.9b00271

58. TD-DFT calculations for **DBC-H**, **DBC-Me**, **DBC-SMe**, **DBC-Br**, **DBC-S(O)₂Me**, and **DBC-Si** were performed in this study. Tables S1–S6 in Supporting Information File 1 show the wavelengths and oscillator strengths for the DBC derivatives.

License and Terms

This is an open access article licensed under the terms of the Beilstein-Institut Open Access License Agreement (<https://www.beilstein-journals.org/bjoc/terms>), which is identical to the Creative Commons Attribution 4.0 International License

(<https://creativecommons.org/licenses/by/4.0>). The reuse of material under this license requires that the author(s), source and license are credited. Third-party material in this article could be subject to other licenses (typically indicated in the credit line), and in this case, users are required to obtain permission from the license holder to reuse the material.

The definitive version of this article is the electronic one which can be found at:

<https://doi.org/10.3762/bjoc.18.96>



First example of organocatalysis by cathodic N-heterocyclic carbene generation and accumulation using a divided electrochemical flow cell

Daniele Rocco^{*,†1}, Ana A. Folgueiras-Amador^{‡2}, Richard C. D. Brown^{‡2}
and Marta Feroci^{*,‡3}

Full Research Paper

Open Access

Address:

¹Department of Ingegneria Meccanica ed Aerospaziale, Sapienza University, via Eudossiana, 18, 00184, Rome, Italy, ²School of Chemistry, University of Southampton, Southampton SO17 1BJ, UK and ³Department of Scienze di Base e Applicate per l'Ingegneria, Sapienza University, via del Castro Laurenziano, 7, 00161, Rome, Italy

Email:

Daniele Rocco^{*} - daniele.rocco@uniroma1.it; Marta Feroci^{*} - marta.feroci@uniroma1.it

* Corresponding author † Equal contributors

Keywords:

Breslow intermediate; cathodic reduction; flow electrochemistry; N-heterocyclic carbene; oxidative esterification

Beilstein J. Org. Chem. **2022**, *18*, 979–990.
<https://doi.org/10.3762/bjoc.18.98>

Received: 03 June 2022

Accepted: 29 July 2022

Published: 05 August 2022

This article is part of the thematic issue "Molecular and macromolecular electrochemistry: synthesis, mechanism, and redox properties".

Guest Editor: S. Inagi

© 2022 Rocco et al.; licensee Beilstein-Institut.
License and terms: see end of document.

Abstract

In this paper we present the first electrochemical generation of NHC carried out in a divided flow cell. The flow cell operated in the recycle mode. The need for a divided cell derived from the anodic electroactivity of the electrogenerated carbene. In order to have NHC accumulation in the catholyte, the Nafion membrane (cell separator) was pretreated with an alkaline solution. The formation of NHC was quantified as its reaction product with elemental sulfur. The NHC was successfully used as organocatalyst in two classical umpolung reactions of cinnamaldehyde: its cyclodimerization and its oxidative esterification.

Introduction

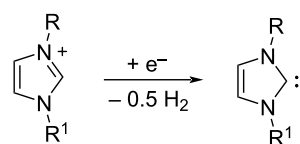
Ionic liquids (ILs) are well known salts, at present used in a wide variety of chemical fields. The first definition of ionic liquids was given by Paul Walden in 1914: "they are materials composed of cations and anions, that melt around 100 °C or below as an arbitrary temperature limit" [1]. ILs are salts formed by non or weakly coordinated cations and anions,

usually bulky organic cations and inorganic or organic anions such as ${}^-\text{BF}_4$, ${}^-\text{PF}_6$, ${}^-\text{N}(\text{CF}_3\text{SO}_2)_2$, etc. [2,3].

The physicochemical properties of RTILs (room temperature ionic liquids) are reported in the literature and include very low vapor pressure, and thus the possibility to recycle them, good

stability, low flammability, good solubility ability for many molecules, salts and gases, the possibility to use them as reagents and/or solvents, large electrochemical window, good electrical conductivity, their ionic nature sometimes increases the reactivity and the selectivity of reactions and usually the product separation is easy [4,5]. Among ILs, imidazolium derivatives are the most studied, in part due to their ease of synthesis, low cost and diverse applications from solvents and reagents in synthesis, to supporting electrolytes in electrochemistry [6].

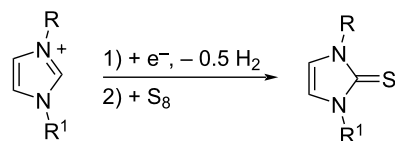
The imidazolium cation can be modified by the presence of a base or by a single electron cathodic reduction of the C–H between nitrogen atoms of the imidazolium ring (Scheme 1), inducing the formation of a N-heterocyclic carbene (NHC) [7,8]. In recent years, NHCs have achieved great success: they have been frequently used as ligands in organometallic catalysts [9] and as versatile organocatalysts [10] in a very wide range of organic reactions such as classical benzoin condensation, transesterification, acylation, Knoevenagel reaction, Claisen condensation etc.



Scheme 1: Electrochemical generation of NHC.

The electrochemical generation of carbenes from ILs avoids the use of strong bases and the formation of byproducts (dimers of carbenes and nitrogen dealkylation products), where the IL acts as NHC precursor, solvent, and supporting electrolyte, needing no additional chemicals in the electrolytic cell [11]. An added attraction of this approach is that unstable NHCs are generated *in situ*, where they may be used as basic or nucleophilic species. Due to the difficulty isolating highly reactive NHCs, the concentration of the obtained NHC solution can be determined indirectly by addition of elemental sulfur after the electrolysis,

which realizes quantitative conversion to the corresponding thione (Scheme 2) [12].

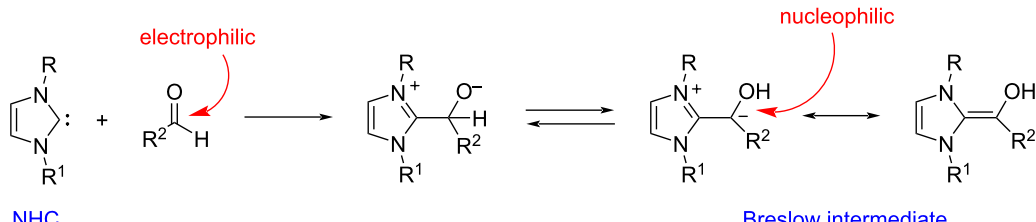


Scheme 2: Transformation of electrochemically generated NHC into the corresponding thione by its reaction with elemental sulfur.

NHCs are used as organocatalysts in many reactions of aldehydes (mainly aromatic) [13,14]. In fact, the reaction of NHCs with aldehydes can lead to the formation of the “Breslow intermediate” [15], in which the reactive character of the carbonyl carbon atom is reversed (umpolung) from electrophilic to nucleophilic (Scheme 3).

This approach can be exploited in many organic reactions, such as: the benzoin condensation [16,17], esterification and amidation of benzaldehydes and cinnamaldehydes [18,19], synthesis of γ -butyrolactones [20], synthesis of 1,3-diketones [21], etc.

Electrosynthesis is considered as a more sustainable approach to perform chemical reactions, and an interesting alternative to conventional synthetic methods both in laboratory and industry processes. In fact, the electron may be considered to be a clean reagent, which replaces toxic chemical redox reagents and dangerous procedures [22–25]. At present, electrosynthesis in batch is more widely used and reported in literature, but some disadvantages can be encountered: the need for high concentrations of supporting electrolyte, poor performance for synthesis such as slow rates of conversion, low selectivity and reproducibility [26]. As a matter of fact, these problems can be addressed by using flow electrochemistry, usually achieving higher rates of conversion of reagents to products [27]. Moreover, electrochemical flow cells can have a very small gap between the electrodes so that lower concentrations of supporting electrolytes are needed to provide sufficient conductivity



Scheme 3: Umpolung of the aldehyde carbonyl carbon atom. Formation of the Breslow intermediate using NHCs.

[28]. Applications of flow electrochemistry reported in the literature are mainly devoted to anodic oxidations, carried out in undivided cells, in which the counter electrode reaction at the cathode is usually H_2 evolution [29]. The use of divided cells is less common in organic electrosynthesis, mainly due to complications inherent with membranes. Useful cathodic processes are less exploited in organic electrochemistry. In the context of NHC organocatalysis in flow electrochemistry, NHC instability (and anodic electroactivity) prevented its cathodic generation and subsequent use as catalyst or reagent. Instead, the NHC was generated by chemical deprotonation using a strong base (DBU) and then applied in anodic esterification [30–32], and amidation of aromatic aldehydes [33]. Flow electrochemistry was applied to oxidize the Breslow intermediate to the corresponding electrophilic acylthiazolium intermediate, which then functioned as an acyl-transfer reagent, reacting with alcohols or amines. To the best of our knowledge, only one research group reported the cathodic reduction of an imidazolium cation to NHC, in an undivided cell under flow conditions, coupled with the anodic generation of Cu(I) from a sacrificial anode to yield the corresponding N-heterocyclic carbene complex [34,35]. In this case, irreversible capture of the NHC by the metallic cation prevented NHC oxidation/degradation.

In this paper we describe the cathodic generation and accumulation of NHC in a divided flow cell and its subsequent use as organocatalyst in the self-annulation of cinnamaldehyde and in the esterification of cinnamaldehyde.

Results and Discussion

Cathodic NHC generation and accumulation using a divided flow electrochemical cell.

Quantification of NHC in IL solution

The flow cell used in this work was previously described [36]. It is based on two electrode plates separated by a spacer/gasket fabricated from an PTFE sheet with its center cut away to form the electrolyte flow chamber (Figure 1). The requirement for a divided cell (a more complicated device than the undivided configuration) arises from the need to protect electrogenerated NHC from its anodic oxidation in the absence of a consumable anode.

To ensure good sealing of the electrolysis cell, the sandwich-type arrangement of cell components was compressed between two end plates using a series of bolts. This design incorporated a solution inlet and a solution outlet for the chamber to allow uniform flow over the surface of the electrodes. In the present work, where a divided cell configuration was required, a proton-permeable membrane (Nafion® 438) was inserted to

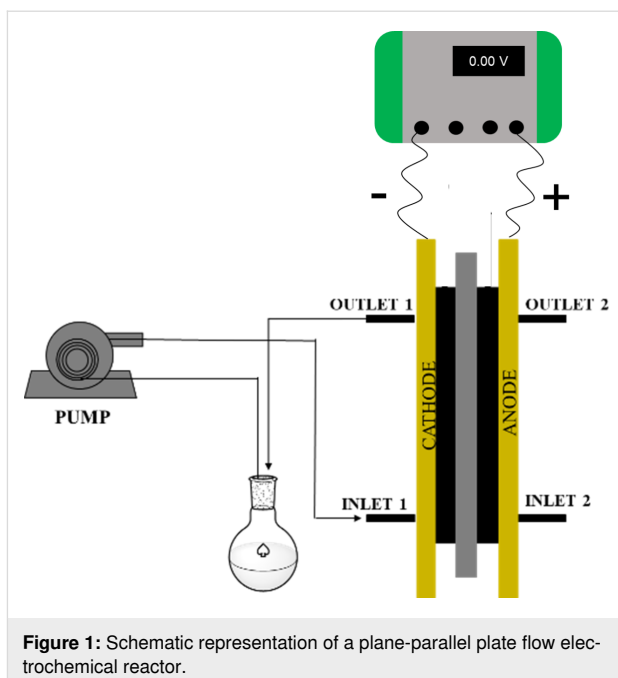


Figure 1: Schematic representation of a plane-parallel plate flow electrochemical reactor.

separate the cathode and anode chambers, and a spacer was used on each compartment [36].

The initial goal of this work was to demonstrate the possibility to achieve NHC formation starting from 1-butyl-3-methylimidazolium tetrafluoroborate (BMImBF₄), by cathodic reduction in a divided cell using flow electrochemistry technique, and to compare the results with the corresponding batch process. Once established, the flow electrochemistry NHC synthesis would be combined with applications as an organocatalyst in some organic transformations of cinnamaldehyde.

Firstly, the conditions for electrogeneration of the carbene in flow were optimized, quantifying the amount of NHC by means of its reaction with elemental sulfur. All the experiments were carried out using a 0.1 M solution of BMImBF₄ in acetonitrile as catholyte in a divided cell using Nafion® 438 membrane, under N₂ atmosphere, at room temperature, under galvanostatic conditions ($I = 134$ mA) with continuous flow rate of 36 mL/min, studying the effect of cathode material, anode solution and number of Faradays per mole of IL supplied (Table 1). At the end of the electrolysis, excess elemental sulfur was added to the catholyte and the mixture was left under ultrasound irradiation for 30 minutes. The solvent was removed under reduced pressure and the residue was purified by column chromatography on silica gel.

The first experiment (Table 1, entry 1) was carried out using stainless steel as cathode and a carbon-filled polyvinylidene fluoride (C/PVDF) plate as anode. BMImBF₄ 0.1 M in aceto-

nitrile was the catholyte, while the anolyte was a solution of tetraethylammonium tetrafluoroborate (Et_4NBF_4) in acetonitrile; after only 12 minutes of electrolysis the current flow stopped. Moreover, a consumption of anode was observed (Figure 2). It is possible that, in the absence of a suitable counter electrode process, the tetrafluoroborate anion was itself oxidized [7] leading to erosion of the anode with the formation of fluorocarbons.

In order to avoid anode consumption/passivation, an alternative to oxidation of BF_4^- was required as the counter electrode reaction, and 10% of methanol was added to the anolyte solution. In this case (Table 1, entry 2) 13% of thione was obtained and the electrode did not show any signs of consumption. The same yield (13%) was obtained using nickel as cathode material (Table 1, entry 4). However, using a silver electrode the corresponding thione was not observed (Table 1, entry 3) [37]. In view of the acidic character of the perfluorosulfonic acid Nafion® membrane, and possible NHC protonation to form the imidazolium cation, the Nafion® membrane was pretreated with an alkaline solution for 24 hours. Using stainless steel as cathode and a lower amount of methanol at the anode the quantity of thione increased to 21% (Table 1, entry 5). Under the same conditions, but using dry acetonitrile, the best yield was obtained (32%, Table 1, entry 6); in this case a small amount of imidazolone **1b** (<5%), probably due to the reaction with adven-

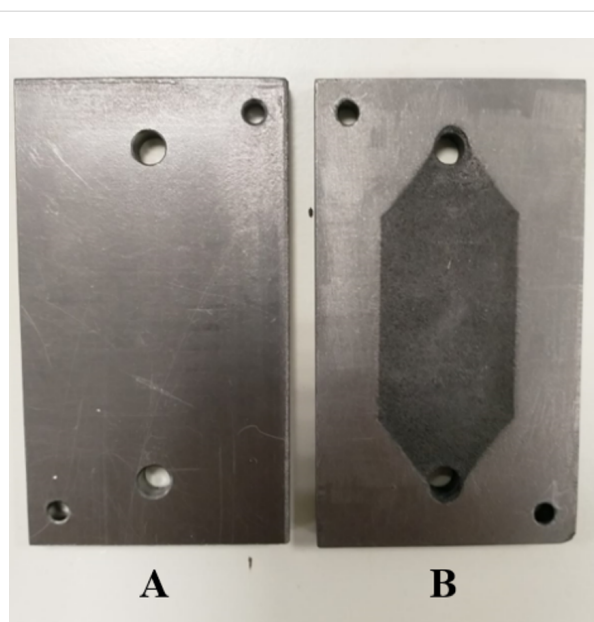


Figure 2: C/PVDF anode before (A) and after (B) the first experiment (Table 1, entry 1).

titious oxygen, was observed from the NMR spectrum. It should be underlined that in these electrolyses BMImBF_4 acts as both electroactive species and supporting electrolyte, and although the cathodic reduction of the imidazolium cation is a monoelec-

Table 1: Electrochemical reduction of BMImBF_4 ,^a followed by the addition of elemental sulfur^b. Flow cell, in recycling mode.

Entry	Cathode material	Anolyte	Q (F)	Time (min)	Yield 1a ^c	Notes	
						1a	1b
1	SS ^d	$\text{MeCN}/\text{Et}_4\text{NBF}_4$ 0.05 M, 25 mL	0.5	12	<5%	anode erosion	
2	SS ^d	$\text{MeCN}-\text{MeOH}$ (9:1)/ Et_4NBF_4 0.05 M, 25 mL	1.0	24	13%	–	
3	Ag	$\text{MeCN}-\text{MeOH}$ (9:1)/ Et_4NBF_4 0.05 M, 25 mL	1.0	24	–	–	
4	Ni	$\text{MeCN}-\text{MeOH}$ (9:1)/ Et_4NBF_4 0.05 M, 25 mL	1.0	24	13%	–	
5	SS ^d	$\text{MeCN}-\text{MeOH}$ (9.5:0.5)/ Et_4NBF_4 0.1 M, 20 mL	1.0	24	21%	Nafion® alkaline pretreatment	
6	SS ^d	Dry $\text{MeCN}-\text{MeOH}$ (9.5:0.5)/ Et_4NBF_4 0.1 M, 20 mL	1.0	24	32% (1b <5%)	Nafion® alkaline pretreatment	

^aDivided cell, carbon-filled polyvinylidene fluoride (C/PVDF) anode material, Nafion® 438 membrane separator, room temperature, N_2 atmosphere, galvanostatic conditions (134 mA), catholyte: $\text{BMImBF}_4/\text{MeCN}$ 0.1 M, 20 mL (2 mmol BMImBF_4); flow rate: 36 mL/min. ^bExcess S_8 (2 mmol) added at the end of the electrolysis to the catholyte. Then energy was supplied to the catholyte (ultrasound irradiation, 35 W) for 30 minutes. ^cIsolated yields, based on starting IL (BMImBF_4). ^dStainless steel.

tronic process, in a similar process carried out in batch the current yield usually does not exceed 50%, thus rendering necessary an excess of current [38]. The yields reported in Table 1 (entries 2 to 6) are obtained using a stoichiometric amount of electricity (1 electron per imidazolium cation). Therefore, the 32% chemical yield (with respect to starting IL) is comparable with the yield of the batch process.

Electrogenerated NHC organocatalysis. Dimerization of *trans*-cinnamaldehyde: synthesis of 4-phenyl-5-styryldihydrofuran- 2(3*H*)-one

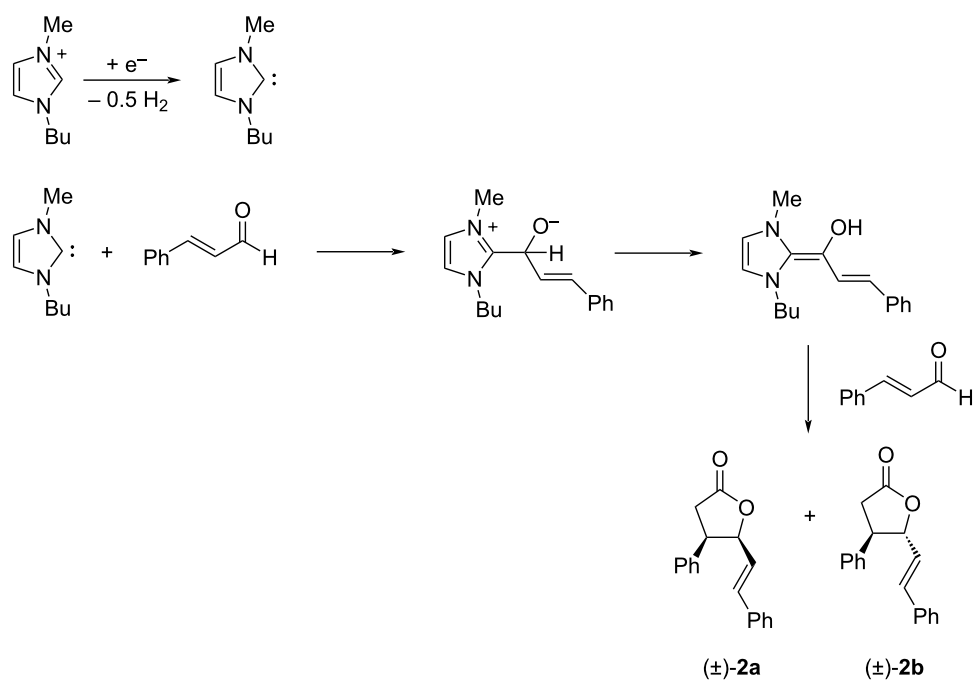
Having demonstrated that NHCs could be generated and accumulated in a continuous flow electrochemical process, the flow methodology was applied to the self-annulation of cinnamaldehyde, a classical NHC-catalyzed reaction (Scheme 4).

All the experiments were carried out using a solution of 0.1 M BMImBF₄ in acetonitrile (20 mL) as catholyte, stainless steel as cathode, C/PVDF as anode, in a divided cell, under N₂ atmosphere, at room temperature, under galvanostatic conditions ($I = 134$ mA) with a flow rate of 36 mL/min, changing anode solution and number of Faradays per mole supplied (Table 2). Following the experimental results previously obtained, the Nafion® membrane was always pretreated with an alkaline solution. At the end of the electrolysis, 1 mmol of cinnamaldehyde was added to the catholyte and the mixture was left under

stirring for two hours at room temperature. Workup and column chromatography yielded a diastereomeric mixture of γ -butyrolactones **2a** and **2b**.

Table 2 reports the results obtained by changing the anolyte composition and the amount of applied electricity. In all cases, with regards to the *trans/cis* diastereomeric ratio, we observed that the *cis* isomer **2a** was predominantly formed. The diastereoselectivity was not high; however, *trans* and *cis* γ -butyrolactones were easily separated by column chromatography. Increasing the applied charge from 0.5 F (Table 2, entry 1) to 1.0 F (Table 2, entry 2) improved the yield of both *cis* (**2a**) and *trans* (**2b**) lactones by approximately three fold. Instead, with a charge of 2.0 F the yield of **2a** improved by 10%, but the yield of **2b** increased only 2% (Table 2, entry 3). However, in these experiments methyl ester **3a** was isolated (24% yield) as byproduct derived from methanol, which passed through the membrane, reacting with the Breslow intermediate through a redox neutral process (Scheme 5) [19].

We decided to use 1 F/mol and a lower amount of methanol at the anode, in order to minimize the formation of byproduct **3a**; the same amount of **2a** was obtained, but the yield of the *trans* diastereoisomer increased from 24% to 32% (Table 2, entry 2 vs entry 4). Finally, changing methanol with DMSO in the anolyte, a lower amount of both diastereoisomers was observed (Table 2, entries 5 and 6). Thus the best yield (79%, 67:33 *cis/trans* ratio) was obtained using a charge of 2.0 F and a solu-

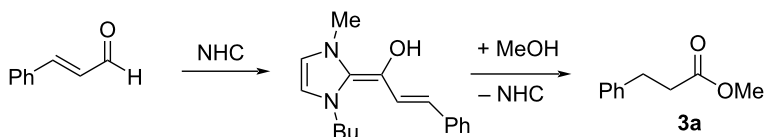


Scheme 4: Electrogenerated NHC-catalyzed self-annulation of cinnamaldehyde.

Table 2: Electrochemical synthesis of γ -butyrolactones **2a** and **2b** by conjugate umpolung reaction.^a

Entry	Anolyte	Q (F) ^b	Time (min)	Yield ^c	
				2a	2b
1	MeCN–MeOH (95:5)/Et ₄ NBF ₄ (0.1 M), 20 mL	0.50	6	15%	8%
2	MeCN–MeOH (95:5)/Et ₄ NBF ₄ (0.1 M), 20 mL	1.00	12	43%	24%
3	MeCN–MeOH (95:5)/Et ₄ NBF ₄ (0.1 M), 20 mL	2.00	24	53%	26%
4	MeCN–MeOH (98:2)/Et ₄ NBF ₄ (0.1 M), 20 mL	1.00	12	42%	32%
5	MeCN–DMSO (95:5)/Et ₄ NBF ₄ (0.1 M), 20 mL	0.50	6	7%	<5%
6	MeCN–DMSO (95:5)/Et ₄ NBF ₄ (0.1 M), 20 mL	1.00	12	20%	12%

^aDivided cell, carbon-filled polyvinylidene fluoride (C/PVDF) anode, stainless steel cathode, alkaline pretreated Nafion® 438 membrane as compartments separator, room temperature, N₂ atmosphere, galvanostatic conditions (134 mA), catholyte: BMImBF₄/MeCN 0.1 M, 20 mL (2 mmol BMImBF₄); flow rate: 36 mL/min; 1 mmol of cinnamaldehyde added at the end of the electrolysis to the catholyte. ^bWith respect to the starting BMImBF₄. ^cIsolated yields, based on starting cinnamaldehyde.

**Scheme 5:** Byproduct obtained from the reaction between methanol and the Breslow intermediate.

tion of MeCN–MeOH (9.5:0.5)/Et₄NBF₄ (0.1 M) as anolyte (Table 2, entry 3).

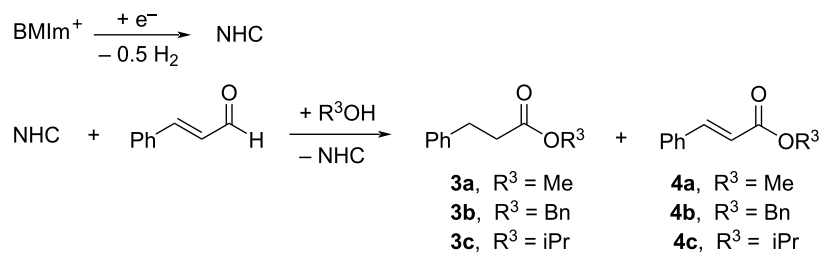
Electrogenerated NHC organocatalysis. Esterification of *trans* cinnamaldehyde

Once the possibility of obtaining the Breslow intermediate was demonstrated, another typical reaction of N-heterocyclic carbenes was tested: the oxidative esterification of cinnamaldehyde in the presence of alcohols. To carry out these experiments three different alcohols (methyl, isopropyl and benzyl alcohols) were used and the results are shown in Table 3.

All the experiments were carried out using a solution of 0.1 M of BMImBF₄ in acetonitrile (20 mL) as catholyte, stainless steel as cathode, C/PVDF as anode, in a divided cell, under N₂ atmo-

sphere, at room temperature, under galvanostatic conditions (*I* = 134 mA, *t*_{electrolysis} = 12 min) with a flow rate of 36 mL/min, anode solution as in Table 3, and with 1.0 Faraday per mole of aldehyde. At the end of the electrolysis, 1 mmol of cinnamaldehyde was added to the catholyte and the mixture was left under stirring for five minutes and then the corresponding alcohol was added and the reaction was stirred for two hours at room temperature. Workup and column chromatography yielded esters **3a–c** and unsaturated esters **4a,b** as byproducts.

Good yields were obtained using benzyl and methyl alcohols (73% and 68%, respectively), while with the isopropyl alcohol the formation of the ester was only 37%, probably due to steric hindrance. In two cases (Table 3, entries 1 and 2) oxidation byproducts (esters **4a** and **4b**) were obtained, where the olefinic

Table 3: Electrochemical synthesis of esters **3a–c** from cinnamaldehyde and an alcohol.^a

Entry	ROH	Anolyte	$Q (\text{F})^b$	Yield ^c
1	$\text{R}^3 = \text{Me}$	MeCN–MeOH (98:2)/ Et_4NBF_4 0.1 M, 20 mL	0.5	3a 68% 4a 11%
2	$\text{R}^3 = \text{Bn}$	MeCN–:BnOH (98:2)/ Et_4NBF_4 0.1 M, 20 mL	0.5	3b 73% 4b 13%
3	$\text{R}^3 = \text{iPr}$	MeCN–iPrOH (98:2)/ Et_4NBF_4 0.1 M, 20 mL	0.5	3c 37% 4c –

^aDivided cell, carbon-filled polyvinylidene fluoride (C/PVDF) anode, stainless steel cathode, alkaline pretreated Nafion® 438 membrane separator, room temperature, N_2 atmosphere, galvanostatic conditions (134 mA), catholyte: BMImBF₄/MeCN 0.1 M, 20 mL (2 mmol BMImBF₄); flow rate: 36 mL/min; 1 mmol of cinnamaldehyde added at the end of the electrolysis to the catholyte and, after 5 minutes 2 mmol of the corresponding alcohol were added. ^bWith respect to the starting BMImBF₄, $t_{\text{electrolysis}} = 12$ min. ^cIsolated yields, based on starting cinnamaldehyde.

double bond is preserved. In contrast to the internal redox reactions of cinnamaldehyde giving esters **3a–c**, formation of enoate byproducts **4a** and **4b** invoke the involvement of an external chemical oxidant species as cinnamaldehyde is added to the cathode chamber after the electrolysis has been stopped. The presence of byproducts **4a** and **4b** is most likely accounted for by the presence of molecular oxygen, or electrochemically generated superoxide (cathodic reduction of O_2), which oxidize the Breslow intermediate [30,39]. In fact, the presence of some reactive oxygen species in the reaction environment was previously demonstrated by the formation of compound **1b** (see Table 1).

IL Recycling

To investigate the possibility to recycle BMImBF₄, the experiment reported in Table 3, entry 1, was replicated, using the same reagents and conditions. Exploiting the low vapor pressure of BMImBF₄, (and of ILs in general), the organic solvent was removed under reduced pressure, and after the extractive workup, the recycled BMImBF₄ was resubjected to cathodic reduction (thus reused in different reactions). Although this procedure led to decreased yields of esterification products **3a**, **4a** (10% and 12%, respectively) and diastereoisomeric 4-phenyl-5-styryldihydrofuran-2(3H)-ones **2a,b** (35%, 45:55 *cis/trans* mixture), the potential of the recycled BMImBF₄ to function as a N-heterocyclic carbene precursor was demonstrated. Interestingly, the reaction selectivity is completely lost using the recovered IL, and experiments are undergoing in order to understand the cause of this selectivity loss.

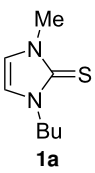
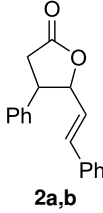
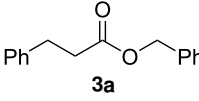
Batch vs flow electrolysis

At this point, the preliminary results from flow electrochemistry may be compared with those reported in the literature for NHC formation using batch electrolysis. The comparison between these two techniques is not straightforward. In fact, in batch electrosynthesis, the ionic liquid is normally used as solvent, but in this work the IL was present as a 0.1 M solution in MeCN.

In regard to the results obtained in the synthesis of thione **1a** (the only reaction for which a reasonable comparison is possible), we compared the current efficiencies, the current being the limiting factor (Table 4). Although the current yield (49%) for the batch electrolysis in pure IL is higher than in flow, the yields for 0.1 M solutions are comparable between batch (29%) and flow (32%). In this case, the rate of production of the NHC in the electrolysis step was higher in the flow reactor (1.60 mmol/h) than in batch using pure IL (0.37 mmol/h). However, other factors should also be highlighted, including the 8× larger electrode area in the flow reactor, which enables a higher current to be passed while maintaining the same current density (15 mA/cm²).

In the case of the NHC organocatalysis, we compared chemical yields of products (Table 4), although in different solvents. As far as the literature allows comparison of the two methodologies, the data in Table 4 show that, although further optimization of the flow electrochemistry conditions is required, it provides a valid alternative to batch technique. Again, produc-

Table 4: Comparison between electrosynthesis in batch and flow electrochemistry.

Product	Solvent	Batch electrochemistry yield (current density)	Flow electrochemistry yield (current density)
	BMImBF ₄	49% ^a (15 mA/cm ²)	–
1a	solvent/BMImBF ₄	29% ^b (15 mA/cm ²)	32% ^c (15 mA/cm ²)
	MeCN/BMImBF ₄	–	79% ^d (15 mA/cm ²)
2a,b			
	BMImBF ₄	91% ^e (20 mA/cm ²)	–
3a	MeCN/BMImBF ₄	–	73% ^f (15 mA/cm ²)

^aCurrent yield. $Q = 193$ C. Theoretical current for a mono-electron process: 96.5 C for 1.0 mmol substrate/product. Current yield: (experimental yield/theoretical yield) $\times 100$. [38]. ^bCurrent yield (see note a). DMF as solvent. [12]. ^cCurrent yield (see note a). MeCN as solvent; flow rate: 36 mL/min.

^dChemical yield, with respect to starting cinnamaldehyde. 2.0 F/mol cinnamaldehyde; flow rate: 36 mL/min. ^eChemical yield, with respect to starting cinnamaldehyde. 0.7 F/mol cinnamaldehyde. 0.97 mmol/h [40]. ^fChemical yield, with respect to starting cinnamaldehyde. 3.65 mmol/h. 1.0 F/mol cinnamaldehyde; flow rate: 36 mL/min.

tivity for the esterification is four-fold higher (3.65 mmol/h, 0.1 M solution) in flow than in batch (0.97 mmol/h, pure IL), and in flow the reaction volume could simply be increased to allow scale-up, obviously in a longer time.

Conclusion

The results reported in this work demonstrate for the first time the possibility to synthesize and accumulate N-heterocyclic carbene starting from BMImBF₄ in a divided electrochemical flow cell. Although not fully optimized, the production of NHC was confirmed indirectly by isolation of its reaction product with elemental sulfur. A solution of the electrogenerated carbene was used to promote dimerization and oxidative esterification reactions of cinnamaldehyde. Under the flow conditions investigated, a higher rate of NHC production was achieved, compared to previously reported batch reactions, which is an important consideration for scale up. In the case of the flow procedure, a 0.1 M solution of the IL is employed, which may be more convenient than using pure ILs. Further investigations of electrogeneration of NHCs and applications in organic synthesis are underway.

Experimental Materials and methods

Chemicals were purchased from Sigma-Aldrich and Alfa Aesar and used as received. All air/moisture sensitive reactions were

carried out under an inert atmosphere, in oven-dried or flame-dried glassware. TLC was performed on aluminium plates precoated with silica gel 60 with an F₂₅₄ indicator; visualized under UV light (254 nm) and/or by staining with potassium permanganate. Flash column chromatography was performed using high purity silica gel, pore size 60 Å, 230–400 mesh particle size, purchased from Merck. ¹H NMR and ¹³C NMR spectra were recorded in CDCl₃ (purchased from Cambridge Isotope Laboratories) at 298 K using a Bruker DPX400 (400 and 101 MHz, respectively) spectrometer. Chemical shifts are reported on the δ scale in ppm and were referenced to residual solvent (CDCl₃: 7.27 ppm for ¹H NMR spectra and 77.0 ppm for ¹³C NMR spectra). Coupling constants (J) were given in Hz and matched where possible. The following abbreviations for the multiplicity of the peaks are used: s (singlet), d (doublet), t (triplet), q (quartet) and m (multiplet).

Parallel plate divided flow cell

See Figure 3 for an expanded view of the electrochemical cell components. The details about the dimensions of each cell component are reported elsewhere [36].

General procedure for the synthesis of 1-butyl-3-methyl-1H-imidazole-2(3H)-thione

Constant current electrolyses ($I = 134$ mA) were carried out using a parallel plate divided cell. Anolyte (25 mL) and

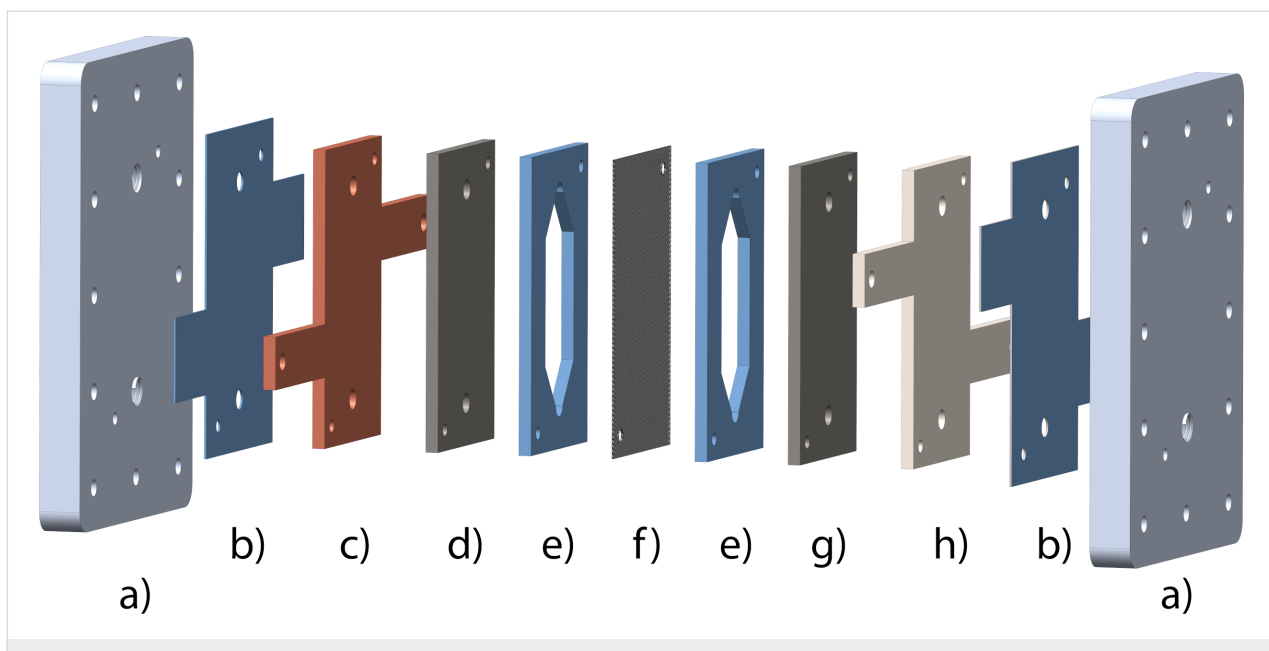


Figure 3: Expanded view of the electrochemical cell components: (a) Aluminium end plates; (b) insulating PTFE foil, (c) copper plate for electrical contact; (d) carbon electrode; (e) PTFE gasket (reaction channel and sealing); (f) Nafion® membrane; (g) stainless steel electrode; (h) stainless-steel plate/electrode for electrical contact. Figure 3 was adapted from [36] with permission from The Royal Society of Chemistry. This content is not subject to CC BY 4.0.

catholyte (20 mL) were separated through a Nafion® 438 membrane. The anode material was carbon-filled polyvinylidene fluoride (C/PVDF) and the cathode material is described in Table 1. Electrolyses were carried out at room temperature, under nitrogen atmosphere, using a solution of 0.1 M of BMImBF₄ in acetonitrile as catholyte. Anolyte solution is given in Table 1. Electrolyte solutions were continuously passed (recycling method) through their respective compartments at a flow rate of 36 mL/min. After consumption of the requisite amount of charge (Faradays per mol of BMImBF₄ reported in Table 1), the current was switched off, the flow stopped, and elemental sulfur (2.0 mmol) was added to the catholyte. The mixture was left under ultrasound irradiation for 30 minutes. The solvent was removed under reduced pressure and the residue was purified by column chromatography on silica gel (petroleum ether/ethyl acetate 7:3), affording the corresponding pure **1a** as an off-white solid.

1-Butyl-3-methyl-1*H*-imidazole-2(3*H*)-thione (1a): Spectral data are consistent with those reported in the literature [38]. ¹H NMR (CDCl₃) δ 6.64 (s, 2H), 3.99 (t, *J* = 7.4 Hz, 2H), 3.57 (s, 3H), 1.79–1.64 (m, 2H), 1.39–1.28 (m, 2H), 0.92 (t, *J* = 7.3 Hz, 3H) ppm; ¹³C NMR (CDCl₃) δ 162.3, 117.5, 116.4, 47.8, 35.0, 30.9, 19.7, 13.6 ppm.

1-Butyl-3-methyl-1*H*-imidazol-2(3*H*)-one (1b): Spectral data are consistent with those reported in the literature [40]. ¹H NMR (CDCl₃) δ 6.19 (d, AB, $\Delta\nu/J = 2.5$, $\Delta\nu = 7.1$ Hz, *J* =

2.8 Hz, 1H), 6.17 (d, AB, $\Delta\nu/J = 2.5$, $\Delta\nu = 7.1$ Hz, *J* = 2.8 Hz, 1H), 3.59 (t, *J* = 7.2 Hz, 2H), 3.24 (s, 3H), 1.70–1.59 (m, 2H), 1.42–1.24 (m, 2H), 0.92 (t, *J* = 7.2 Hz, 3H) ppm; ¹³C NMR (CDCl₃) δ 153.1, 111.3, 110.2, 43.5, 31.1, 30.5, 19.9, 13.6 ppm.

General procedure for dimerization of *trans* cinnamaldehyde

Constant current electrolyses (*I* = 134 mA) were carried out using a parallel plate divided cell. Anolyte (20 mL) and catholyte (20 mL) were separated through a Nafion® 438 membrane. The anode material was carbon-filled polyvinylidene fluoride C/PVDF and stainless steel for the cathode material. Electrolyses were carried out at room temperature, under nitrogen atmosphere, using a solution 0.1 M of BMImBF₄ in acetonitrile as catholyte and for anolyte solution see Table 2, which were passed (recycling method) in their compartments with a flow rate of 36 mL/min. After the consumption of the number of Faradays per mol of BMImBF₄ reported in Table 2, the current was switched off, the flow stopped and cinnamaldehyde (1.0 mmol) was added to the catholyte. The mixture was stirred for 2 h. The solvent was removed under reduced pressure and the residue was extracted with Et₂O (15 mL × 3) and then purified by column chromatography on silica gel (petroleum ether/ethyl acetate 9:1), affording the corresponding pure products **2a** and **2b**.

(±) *cis*-4-Phenyl-5-((E)-styryl)dihydrofuran-2(3*H*)-one (2a): Spectral data are consistent with those reported in the literature

[41]. ^1H NMR (CDCl_3) δ 7.38–7.25 (m, 3H), 7.29–7.24 (m, 3H), 7.23–7.15 (m, 4H), 6.63 (d, J = 15.9 Hz, 1H), 5.65 (dd, J = 15.9 Hz, 6.5 Hz, 1H), 5.42–5.38 (m, 1H), 3.99–3.93 (m, 1H), 2.98 (dd, J = 17.4 Hz, 8.1 Hz, 1H), 2.91 (dd, J = 17.4 Hz, 7.4 Hz, 1H) ppm; ^{13}C NMR (CDCl_3) δ 176.3, 136.9, 135.8, 133.4, 128.9, 128.6, 128.2, 127.9, 127.8, 126.6, 123.8, 83.5, 45.6, 34.3 ppm.

(\pm) **trans-4-Phenyl-5-((E)-styryl)dihydrofuran-2(3H)-one (2b):** Spectral data are consistent with those reported in the literature [41]. ^1H NMR (CDCl_3) δ 7.39–7.27 (m, 10H), 6.60 (d, J = 15.9 Hz, 1H), 6.23 (dd, J = 15.9 Hz, 6.7 Hz, 1H), 5.06–5.02 (m, 1H), 3.57–3.50 (m, 1H), 3.04 (dd, J = 17.5 Hz, 8.6 Hz, 1H), 2.87 (dd, J = 17.5 Hz, 10.5 Hz, 1H) ppm; ^{13}C NMR (CDCl_3) δ 175.2, 138.0, 135.6, 133.8, 129.2, 128.7, 128.4, 127.9, 127.3, 126.8, 124.7, 86.7, 48.4, 36.7 ppm.

General procedure for the esterification of *trans*-cinnamaldehyde

Constant current electrolyses (I = 134 mA) were carried out using a parallel plates divided cell. Anolyte (20 mL) and catholyte (20 mL) were separated through a Nafion® 438 membrane. The anode material was C/PVDF and stainless steel for the cathode material. Electrolyses were carried out at room temperature, under nitrogen atmosphere, using a solution 0.1 M of BMImBF₄ in acetonitrile as catholyte. Anolyte solution is given in Table 3. Electrolyte solutions were continuously passed (recycling method) through their respective compartments at a flow rate of 36 mL/min. After the consumption of 0.5 F/mol of BMImBF₄ (12 min, 96 C), the current was switched off, the flow stopped and cinnamaldehyde (1.0 mmol) was added to the catholyte. The mixture was left under stirring for 5 minutes and then the corresponding alcohol (2.0 mmol) was added and the reaction was stirred for 2 hours at room temperature. The solvent was removed under reduced pressure and the residue was extracted with of Et₂O (15 mL \times 3) and purified by column chromatography on silica gel (petroleum ether/ethyl acetate 9.5:0.5), affording the corresponding pure esters **3a–c** and **4a,b**.

BMImBF₄ Recycling procedure

After extraction of product **3a** from the solution, the catholyte was placed under vacuum at room temperature for 30 min to remove diethyl ether residues, then it was used as catholyte for a new electrolysis (see the general procedure for the esterification of *trans*-cinnamaldehyde to repeat the same procedure).

Methyl 3-phenylpropanoate (3a): Spectral data are consistent with those reported in the literature [42]. ^1H NMR (CDCl_3) δ 7.32–7.23 (m, 2H), 7.22–7.14 (m, 3H), 3.65 (s, 3H), 2.94 (t, J = 7.9 Hz, 2H), 2.62 (dd, J = 8.4 Hz, 7.3 Hz, 2H) ppm; ^{13}C NMR

(CDCl_3) δ 173.3, 140.5, 128.5, 128.3, 126.3, 51.6, 35.7, 30.9 ppm.

Benzyl 3-phenylpropanoate (3b): Spectral data are consistent with those reported in the literature [43]. ^1H NMR (CDCl_3) δ 7.19–7.39 (m, 10H), 5.13 (s, 2H), 2.99 (t, J = 7.0 Hz, 2H), 2.70 (t, J = 7.0 Hz, 2H) ppm; ^{13}C NMR (CDCl_3) δ 172.7, 140.4, 136.0, 128.6, 128.5, 128.3, 128.2, 126.3, 66.3, 35.9, 31.0 ppm.

Isopropyl 3-phenylpropanoate (3c): Spectral data are consistent with those reported in the literature [44]. ^1H NMR (CDCl_3) δ 7.28–7.36 (m, 2H), 7.19–7.27 (m, 3H), 4.99–5.11 (m, 1H), 2.99 (t, J = 7.5 Hz, 2H), 1.24 (d, J = 6.3 Hz, 6H) ppm; ^{13}C NMR (75 MHz, CDCl_3) δ 172.5, 140.6, 128.5, 128.4, 126.2, 67.8, 36.3, 31.1, 21.8 ppm.

Methyl cinnamate (4a): Spectral data are consistent with those reported in the literature [45]. ^1H NMR (CDCl_3) δ 7.69 (d, J = 16.0 Hz, 1H), 7.58–7.45 (m, 2H), 7.41–7.32 (m, 3H), 6.43 (d, J = 16.0 Hz, 1H), 3.78 (s, 3H) ppm; ^{13}C NMR (CDCl_3) δ 167.4, 144.8, 134.4, 130.3, 128.9, 128.1, 117.8, 51.7 ppm.

Benzyl cinnamate (4b): Spectral data are consistent with those reported in the literature [46]. ^1H NMR (CDCl_3) δ 7.73 (d, J = 16.0 Hz, 1H), 7.56–7.49 (m, 2H), 7.45–7.31 (m, 8H), 6.49 (d, J = 16.0 Hz, 1H), 5.26 (s, 2H) ppm; ^{13}C NMR (CDCl_3) δ 166.8, 145.2, 136.1, 136.0, 134.3, 130.4, 128.9, 128.6, 128.29, 128.26, 128.1, 117.9, 66.4 ppm.

Acknowledgements

The authors thank Professor Derek Pletcher for the stimulating discussions and helpful tips.

Funding

D.R. thanks the Sapienza University for a Ph.D. grant. The authors acknowledge financial support from EPSRC (Photo-Electro Programme Grant EP/P013341/1).

ORCID® iDs

Ana A. Folgueiras-Amador - <https://orcid.org/0000-0002-0728-4902>
Richard C. D. Brown - <https://orcid.org/0000-0003-0156-7087>
Marta Feroci - <https://orcid.org/0000-0002-3673-6509>

Preprint

A non-peer-reviewed version of this article has been previously published as a preprint: <https://doi.org/10.3762/bxiv.2022.43.v1>

References

- Walden, P. *Bull. Acad. Imp. Sci. St.-Petersbourg* **1914**, 1800.
- Hayes, R.; Warr, G. G.; Atkin, R. *Chem. Rev.* **2015**, *115*, 6357–6426. doi:10.1021/cr500411q

3. Pandolfi, F.; Bortolami, M.; Feroci, M.; Fornari, A.; Scarano, V.; Rocco, D. *Materials* **2022**, *15*, 866. doi:10.3390/ma15030866
4. Wasserscheid, P.; Welton, T., Eds. *Ionic liquids in synthesis*, 2nd ed.; Wiley-VCH: Weinheim, Germany, 2008; Vol. 1. doi:10.1002/9783527621194
5. Feroci, M.; Orsini, M.; Inesi, A. Room Temperature Ionic Liquids (RTILs) Versus Volatile Organic Compounds (VOCs) in Organic Electrosynthesis: The Requirement of a Careful Comparison. *Green Solvents II*; Springer: Dordrecht, Netherlands, 2012; pp 435–471. doi:10.1007/978-94-007-2891-2_16
6. Green, M. D.; Long, T. E. *Polym. Rev. (Philadelphia, PA, U. S.)* **2009**, *49*, 291–314. doi:10.1080/15583720903288914
7. Xiao, L.; Johnson, K. E. *J. Electrochem. Soc.* **2003**, *150*, E307. doi:10.1149/1.1568740
8. Feroci, M.; Chiarotto, I.; Inesi, A. *Curr. Org. Chem.* **2013**, *17*, 204–219. doi:10.2174/1385272811317030003
9. Schuster, O.; Yang, L.; Raubenheimer, H. G.; Albrecht, M. *Chem. Rev.* **2009**, *109*, 3445–3478. doi:10.1021/cr8005087
10. Bugaut, X.; Glorius, F. *Chem. Soc. Rev.* **2012**, *41*, 3511–3522. doi:10.1039/c2cs1533e
11. Bourissou, D.; Guerret, O.; Gabbaï, F. P.; Bertrand, G. *Chem. Rev.* **2000**, *100*, 39–92. doi:10.1021/cr940472u
12. Rocco, D.; Chiarotto, I.; D'Anna, F.; Mattiello, L.; Pandolfi, F.; Rizzo, C.; Feroci, M. *ChemElectroChem* **2019**, *6*, 4275–4283. doi:10.1002/celc.201900099
13. Enders, D.; Niemeier, O.; Henseler, A. *Chem. Rev.* **2007**, *107*, 5606–5655. doi:10.1021/cr068372z
14. Marion, N.; Díez-González, S.; Nolan, S. P. *Angew. Chem., Int. Ed.* **2007**, *46*, 2988–3000. doi:10.1002/anie.200603380
15. Breslow, R. J. *Am. Chem. Soc.* **1958**, *80*, 3719–3726. doi:10.1021/ja01547a064
16. Xu, L.-W.; Gao, Y.; Yin, J.-J.; Li, L.; Xia, C.-G. *Tetrahedron Lett.* **2005**, *46*, 5317–5320. doi:10.1016/j.tetlet.2005.06.015
17. Chiarotto, I.; Feroci, M.; Orsini, M.; Feeney, M. M. M.; Inesi, A. *Adv. Synth. Catal.* **2010**, *352*, 3287–3292. doi:10.1002/adsc.201000555
18. Vora, H. U.; Wheeler, P.; Rovis, T. *Adv. Synth. Catal.* **2012**, *354*, 1617–1639. doi:10.1002/adsc.201200031
19. Forte, G.; Chiarotto, I.; Inesi, A.; Loreto, M. A.; Feroci, M. *Adv. Synth. Catal.* **2014**, *356*, 1773–1781. doi:10.1002/adsc.201400163
20. Murauski, K. J. R.; Jaworski, A. A.; Scheidt, K. A. *Chem. Soc. Rev.* **2018**, *47*, 1773–1782. doi:10.1039/c7cs00386b
21. Singh, S.; Singh, P.; Rai, V. K.; Kapoor, R.; Yadav, L. D. S. *Tetrahedron Lett.* **2011**, *52*, 125–128. doi:10.1016/j.tetlet.2010.10.175
22. Wiebe, A.; Gieshoff, T.; Möhle, S.; Rodrigo, E.; Zirbes, M.; Waldvogel, S. R. *Angew. Chem., Int. Ed.* **2018**, *57*, 5594–5619. doi:10.1002/anie.201711060
23. Yoshida, J.-i.; Kataoka, K.; Horcajada, R.; Nagaki, A. *Chem. Rev.* **2008**, *108*, 2265–2299. doi:10.1021/cr0680843
24. Frontana-Uribe, B. A.; Little, R. D.; Ibanez, J. G.; Palma, A.; Vasquez-Medrano, R. *Green Chem.* **2010**, *12*, 2099–2119. doi:10.1039/c0gc00382d
25. Pandolfi, F.; Chiarotto, I.; Rocco, D.; Feroci, M. *Electrochim. Acta* **2017**, *254*, 358–367. doi:10.1016/j.electacta.2017.09.135
26. Atobe, M.; Tateno, H.; Matsumura, Y. *Chem. Rev.* **2018**, *118*, 4541–4572. doi:10.1021/acs.chemrev.7b00353
27. Pletcher, D.; Green, R. A.; Brown, R. C. D. *Chem. Rev.* **2018**, *118*, 4573–4591. doi:10.1021/acs.chemrev.7b00360
28. Folgueiras-Amador, A. A.; Wirth, T. J. *Flow Chem.* **2017**, *7*, 94–95. doi:10.1556/1846.2017.00020
29. Luis, S. V.; García-Verdugo, E. *Flow Chemistry: Integrated Approaches for Practical Applications*; Royal Society of Chemistry: Cambridge, UK, 2019. doi:10.1039/9781788016094
30. Green, R. A.; Pletcher, D.; Leach, S. G.; Brown, R. C. D. *Org. Lett.* **2015**, *17*, 3290–3293. doi:10.1021/acs.orglett.5b01459
31. Finney, E. E.; Ogawa, K. A.; Boydston, A. J. *J. Am. Chem. Soc.* **2012**, *134*, 12374–12377. doi:10.1021/ja304716r
32. Ogawa, K. A.; Boydston, A. J. *Org. Lett.* **2014**, *16*, 1928–1931. doi:10.1021/ol500459x
33. Green, R. A.; Brown, R. C. D.; Pletcher, D.; Harji, B. *Electrochim. Commun.* **2016**, *73*, 63–66. doi:10.1016/j.elecom.2016.11.004
34. Chapman, M. R.; Shafi, Y. M.; Kapur, N.; Nguyen, B. N.; Willans, C. E. *Chem. Commun.* **2015**, *51*, 1282–1284. doi:10.1039/c4cc08874c
35. Schotten, C.; Bourne, R. A.; Kapur, N.; Nguyen, B. N.; Willans, C. E. *Adv. Synth. Catal.* **2021**, *363*, 3189–3200. doi:10.1002/adsc.202100264
36. Folgueiras-Amador, A. A.; Teuten, A. E.; Pletcher, D.; Brown, R. C. D. *React. Chem. Eng.* **2020**, *5*, 712–718. doi:10.1039/d0re00019a
37. Gurjar, S.; Sharma, S. K.; Sharma, A.; Ratnani, S. *Appl. Surf. Sci. Adv.* **2021**, *6*, 100170. doi:10.1016/j.apsadv.2021.100170
We do not have a conclusive answer for this behavior. As the reaction of electro-generated NHC with the elemental sulfur was carried out “ex-cell” we can exclude the formation of silver sulfide. It is possible however, that either the over potential for hydrogen evolution from the imidazolium is higher at the silver cathode, or that some electrode passivation takes place on the silver electrode. While we do not have direct evidence to support the latter proposal, imidazolium species are well-known as anti-corrosion additives (usually for steel) and electrochemically generated NHCs may form a stable layer on silver.
38. Feroci, M.; Orsini, M.; Inesi, A. *Adv. Synth. Catal.* **2009**, *351*, 2067–2070. doi:10.1002/adsc.200900359
39. De Sarkar, S.; Biswas, A.; Samanta, R. C.; Studer, A. *Chem. – Eur. J.* **2013**, *19*, 4664–4678. doi:10.1002/chem.201203707
40. AlNashef, I. M.; Hashim, M. A.; Mjalli, F. S.; Ali, M. Q. A.-h.; Hayyan, M. *Tetrahedron Lett.* **2010**, *51*, 1976–1978. doi:10.1016/j.tetlet.2010.02.030
41. Sohn, S. S.; Rosen, E. L.; Bode, J. W. *J. Am. Chem. Soc.* **2004**, *126*, 14370–14371. doi:10.1021/ja044714b
42. Ficker, M.; Svenningsen, S. W.; Larriebeau, T.; Christensen, J. B. *Tetrahedron Lett.* **2018**, *59*, 1125–1129. doi:10.1016/j.tetlet.2018.02.026
43. Feroci, M.; Chiarotto, I.; Orsini, M.; Pelagalli, R.; Inesi, A. *Chem. Commun.* **2012**, *48*, 5361–5363. doi:10.1039/c2cc30371j
44. Salomé, C.; Kohn, H. *Tetrahedron* **2009**, *65*, 456–460. doi:10.1016/j.tet.2008.10.062
45. Dahiya, A.; Das, B.; Sahoo, A. K.; Patel, B. K. *Adv. Synth. Catal.* **2022**, *364*, 966–973. doi:10.1002/adsc.202101431
46. Sato, H.; Hosokawa, S. *Synthesis* **2018**, *50*, 1343–1349. doi:10.1055/s-0036-1589162

License and Terms

This is an open access article licensed under the terms of the Beilstein-Institut Open Access License Agreement (<https://www.beilstein-journals.org/bjoc/terms>), which is identical to the Creative Commons Attribution 4.0 International License (<https://creativecommons.org/licenses/by/4.0>). The reuse of material under this license requires that the author(s), source and license are credited. Third-party material in this article could be subject to other licenses (typically indicated in the credit line), and in this case, users are required to obtain permission from the license holder to reuse the material.

The definitive version of this article is the electronic one which can be found at:

<https://doi.org/10.3762/bjoc.18.98>



Electrochemical vicinal oxyazidation of α -arylvinylic acetates

Yi-Lun Li¹, Zhaojiang Shi¹, Tao Shen^{*2} and Ke-Yin Ye^{*1}

Letter

Open Access

Address:

¹Institute of Pharmaceutical Science and Technology, College of Chemistry, Fuzhou University, Fuzhou 350108, China and ²Frontiers Science Center for Transformative Molecules, School of Chemistry and Chemical Engineering, Shanghai Jiao Tong University, Shanghai 200240, China

Email:

Tao Shen* - shentao199102@aliyun.com; Ke-Yin Ye* - kyee@fzu.edu.cn

* Corresponding author

Keywords:

azide; azidoketone; electrosynthesis; enol acetate; radical

Beilstein J. Org. Chem. **2022**, *18*, 1026–1031.

<https://doi.org/10.3762/bjoc.18.103>

Received: 29 May 2022

Accepted: 01 August 2022

Published: 12 August 2022

This article is part of the thematic issue "Molecular and macromolecular electrochemistry: synthesis, mechanism, and redox properties".

Guest Editor: S. Inagi

© 2022 Li et al.; licensee Beilstein-Institut.

License and terms: see end of document.

Abstract

α -Azidoketones are valuable and versatile building blocks in the synthesis of various bioactive small molecules. Herein, we describe an environmentally friendly and efficient electrochemical vicinal oxyazidation protocol of α -arylvinylic acetates to afford diverse α -azidoketones in good yields without the use of a stoichiometric amount of chemical oxidant. A range of functionality is shown to be compatible with this transformation, and further applications are demonstrated.

Introduction

Organooazides play important roles in pharmaceutical, bio-orthogonal chemistry, and many other interdisciplinary research areas [1-3]. Among them, azidoketones are also very versatile building blocks in organic synthesis, pharmaceutical, and materials science [4-6]. Therefore, the development of a green, efficient, and sustainable protocol for the synthesis of azidoketones is of great significance [7-9].

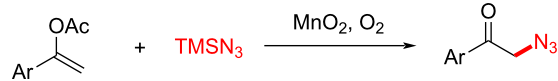
Retrosynthetically, the nucleophilic substitution of α -bromoketones by sodium azide [10] and oxidation of the azido alcohols [11] are among the most straightforward methods to generate azidoketones. Remarkably, photoredox [12] and electrochemical [13] oxyazidation of vinylarenes are also becoming

competent synthetic approaches. Besides vinylarenes, vinyl acetates are potentially versatile precursors for the anticipated vicinal oxyazidation.

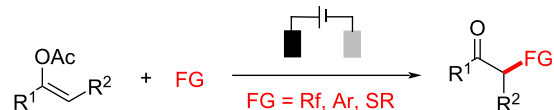
For instance, Singh and co-workers have reported a manganese dioxide-catalyzed radical azidation of enol acetates to afford the corresponding azidoketones using dioxygen as the oxidant (Scheme 1A) [14]. The adoption of electrosynthesis in green and sustainable redox transformations has been experiencing a dynamic renaissance [15-22] not only because it employs the passage of charge instead of chemical oxidants or reductants but also offers opportunities for the precise control of reactivity by "dialing-in" the specific potential on demand [23-25].

Results and Discussion

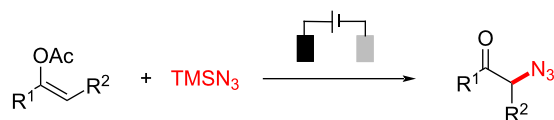
(A) MnO_2 -catalyzed azidation of enol acetates (previous work)



(B) electrochemical oxyfunctionalization of enol acetates (previous work)



(C) electrochemical oxyazidation of enol acetates (this work)



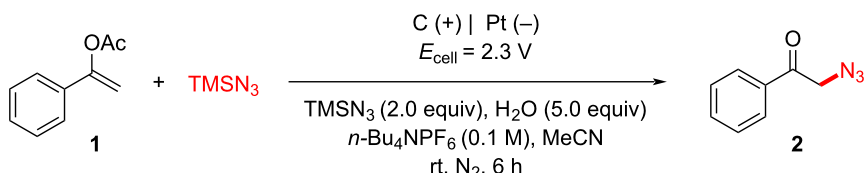
Scheme 1: From vinyl acetates to α -azidoketones.

Specifically, the electrochemical oxyfunctionalization of vinyl acetates has been developed to afford the corresponding α -fluorinated [26], -arylated [27], and -sulfonylated [28] ketones (Scheme 1B). In addition, electrochemical azidation [29–33] has also become a robust and reliable synthetic tool to incorporate azido functionality [34,35] into diverse organic frameworks. Herein, we report that the electrochemical oxyfunctionalization strategy could be well applied to the synthesis of α -azidoketone using readily available α -arylvinylic acetates, and azidotrimethylsilane (Scheme 1C).

The constant cell potential electrolysis ($E_{\text{cell}} = 2.3$ V, carbon cloth anode, and Pt cathode) of 1-phenylvinyl acetate (**1**) with azidotrimethylsilane was performed and the desired α -azidoketone (**2**) was obtained in 68% yield (Table 1, entry 1, for details of the reaction optimization see Supporting Information File 1). The cyclic voltammetry studies showed while there was no obvious oxidation peak for TMSN_3 , 1-phenylvinyl acetate (**1**) exhibits two oxidation peaks. The first peak ($E_{\text{p/2}} = 1.51$ V vs Fc^{+}/F^-) was assigned to be the oxidation of the vinyl acetate moiety. The control experiment demonstrated that there was no conversion without an electric current (Table 1, entry 2). In addition, in the absence of the electrolyte only a low yield of the desired product was obtained (Table 1, entry 3). The use of $n\text{-Bu}_4\text{NPF}_6$ was crucial because lower yields were generally obtained with other electrolytes, such as $n\text{-Bu}_4\text{NOAc}$ or $n\text{-Bu}_4\text{NBF}_4$ (Table 1, entries 4 and 5). Note that the yield decreased without the addition of water suggesting water may facilitate the formation of the azidoketone (Table 1, entry 6). Interestingly, the H_2^{18}O labeling experiment confirmed that there was no ^{18}O incorporation in the obtained α -azidoketone (**2**, for details see Supporting Information File 1). Therefore, the oxygen source of the newly formed carbonyl moiety may originate directly from the vinyl acetate. This conclusion is also consistent with the fact that even in the absence of water, the desired α -azidoketone was still obtained.

Under the optimal conditions, the substrate scope of this electrochemical oxyazidation reaction was investigated (Scheme 2). Enol acetates derived from various alkyl-substituted phenylace-

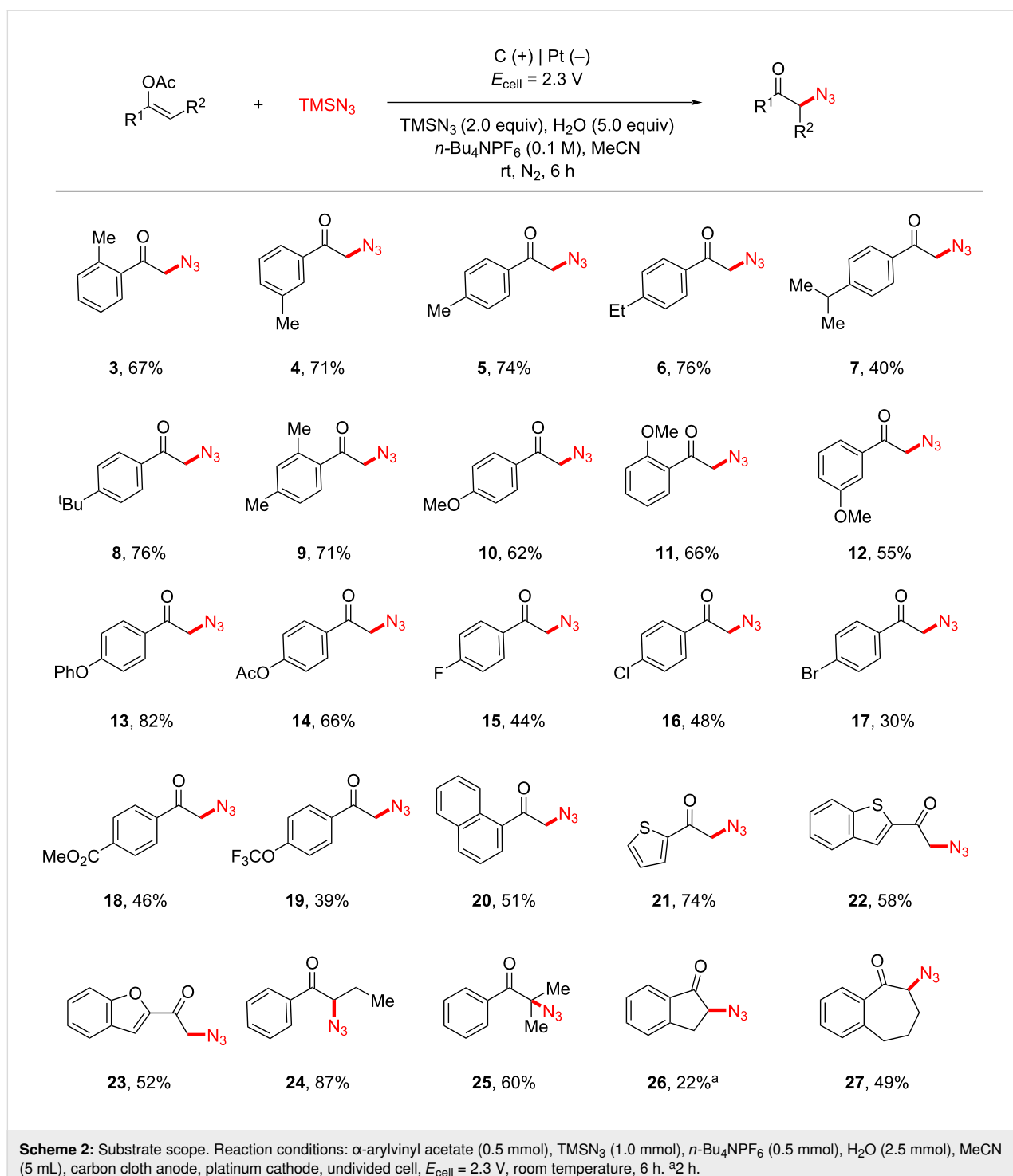
Table 1: Optimization of reaction conditions.^a



Entry	Variation from the standard reaction conditions	Yield (%)
1	none	65 (68) ^b
2	no current	n.d.
3	without electrolyte	9
4	$n\text{-Bu}_4\text{NOAc}$ instead of $n\text{-Bu}_4\text{NPF}_6$	12
5	$n\text{-Bu}_4\text{NBF}_4$ instead of $n\text{-Bu}_4\text{NPF}_6$	35
6	without H_2O	34

^aReaction conditions: **1** (0.5 mmol), TMSN_3 (1.0 mmol), $n\text{-Bu}_4\text{NPF}_6$ (0.5 mmol), H_2O (2.5 mmol), MeCN (5 mL), carbon cloth anode, platinum cathode, undivided cell, $E_{\text{cell}} = 2.3$ V, room temperature, 6 h, yields were determined using ^1H NMR with dibromomethane as the internal standard.

^bIsolated yield.



tones were generally well tolerated (**3–9**, 40–76% yields). The relatively low yield of the isopropyl-substituted one (**7**) was attributed to the competing oxidation of the isopropylbenzene moiety [31,36], which was consistent with its relative low oxidation potential ($E_{\text{onset}} = 1.68$ V vs Fc^{+0}). Other electron-donating substituents, such as the OMe (**10–12**), OPh (**13**), and OAc (**14**) were also well tolerated.

However, halogenated substrates, including fluoro (**15**), chloro (**16**), and bromo (**17**), proceeded with the anticipated reactivity less efficiently (30–48% yields). The presence of other electron-withdrawing groups, such as CO_2Me (**18**) and OCF_3 (**19**), exhibited similar negative effects on the reaction yields. Naphthalene (**20**), thiophene (**21**), benzothiophene (**22**), and benzofuran (**23**) were all amenable in this transformation. In addition,

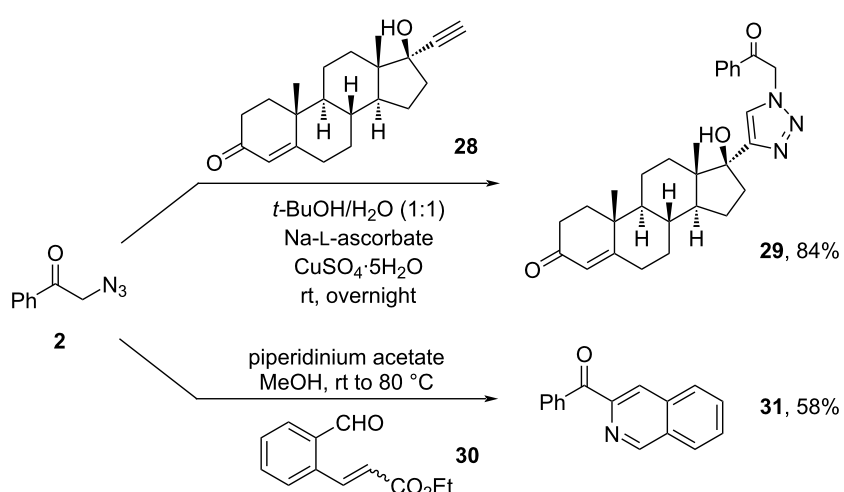
various linear- (**24**, **25**) and cyclic enol acetates (**26**, **27**) also readily underwent the anticipated oxyazidation. Unfortunately, the current protocol was not applicable to the oxyazidation of enol acetate deriving from aliphatic ketones, such as cyclohexanone (see Supporting Information File 1 for details). As illustrated in Scheme 3, the synthetic utility of α -azidoketone was further evaluated [37,38]. Click reaction between 2-azido-1-phenylethan-1-one (**2**) and ethisterone (**28**) [39–41] readily afforded the target triazole product (**29**) in 84% yield. Upon treatment with piperidinium acetate and ethyl 3-(2-formylphenyl)acrylate (**30**), α -azidoketone (**2**) was transformed into isoquinoline product (**31**) in 58% yield [42].

Based on our reaction results and the known literature [13,14], a possible mechanism is proposed (Scheme 4). The enol acetate **A**

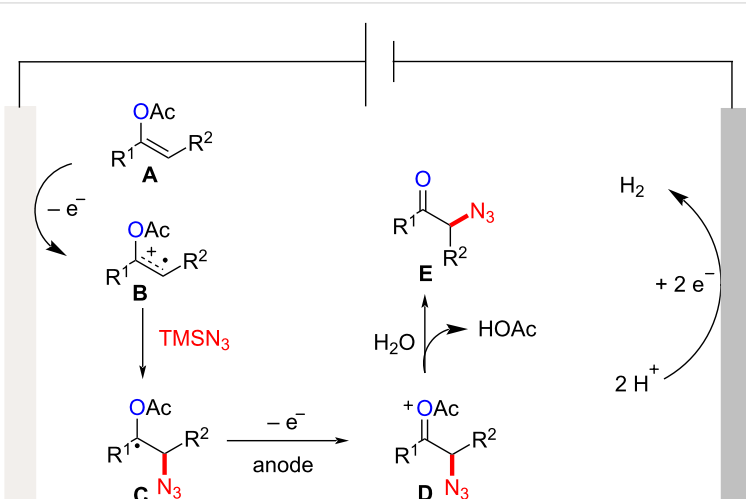
first undergoes anodic oxidation to form a radical cation intermediate **B**, which is then intercepted by azidotrimethylsilane to afford the benzyl radical **C**. Subsequently, this radical is further anodically oxidized to its oxocarbenium ion intermediate **D**, which finally reacts with water to form the desired product **E**. According to our ^{18}O labeling experiment, the oxygen source of the newly installed carbonyl group probably originates from the vinyl acetate, not from H_2O .

Conclusion

In summary, we have developed an environmentally friendly and efficient electrochemical oxyazidation of α -arylvinyl acetates to access diverse vicinal α -azidoketones. The protocol employs the experimentally simple undivided electrochemical cell and tolerates a broad substrate scope. The obtained



Scheme 3: Derivatization of α -azidoketone **2**.



Scheme 4: Proposed mechanism.

α -azidoketones have been shown to be versatile building blocks for the preparation of biologically relevant heterocycles.

Supporting Information

Supporting Information File 1

Experimental procedures, characterization data, copies of ^1H and ^{13}C NMR spectra.

[<https://www.beilstein-journals.org/bjoc/content/supplementary/1860-5397-18-103-S1.pdf>]

Funding

Financial support from the National Natural Science Foundation of China (22071025, 21901041), State Key Laboratory of Physical Chemistry of Solid Surfaces, Xiamen University (202008), Hundred-Talent Project of Fujian (50012742), and Fuzhou University (510841) is gratefully acknowledged.

ORCID® iDs

Ke-Yin Ye - <https://orcid.org/0000-0003-3955-7079>

References

1. Sletten, E. M.; Bertozzi, C. R. *Acc. Chem. Res.* **2011**, *44*, 666–676. doi:10.1021/ar200148z
2. Li, J.; Chen, P. R. *Nat. Chem. Biol.* **2016**, *12*, 129–137. doi:10.1038/nchembio.2024
3. Prescher, J. A.; Bertozzi, C. R. *Nat. Chem. Biol.* **2005**, *1*, 13–21. doi:10.1038/nchembio0605-13
4. Kádár, Z.; Frank, É.; Schneider, G.; Molnár, J.; Zupkó, I.; Kóti, J.; Schönecker, B.; Wölfling, J. *ARKIVOC* **2012**, No. 3, 279–296. doi:10.3998/ark.5550190.0013.320
5. Brusis, T.; Grofe, H. J.; Förster, D.; Weuta, H. *Infection (Munich, Ger.)* **1977**, *5*, 26–31. doi:10.1007/bf01639106
6. Zhao, R.; Chen, B.-C.; Bednarz, M. S.; Wang, B.; Skoumbourdis, A. P.; Sundeen, J. E.; Dhar, T. G. M.; Iwanowicz, E. J.; Balasubramanian, B.; Barrish, J. C. *ARKIVOC* **2007**, No. 12, 36–42. doi:10.3998/ark.5550190.0008.c03
7. Erythropel, H. C.; Zimmerman, J. B.; de Winter, T. M.; Petitjean, L.; Melnikov, F.; Lam, C. H.; Lounsbury, A. W.; Mellor, K. E.; Janković, N. Z.; Tu, Q.; Pincus, L. N.; Falinski, M. M.; Shi, W.; Coish, P.; Plata, D. L.; Anastas, P. T. *Green Chem.* **2018**, *20*, 1929–1961. doi:10.1039/c8gc00482j
8. Frontana-Uribe, B. A.; Little, R. D.; Ibanez, J. G.; Palma, A.; Vasquez-Medrano, R. *Green Chem.* **2010**, *12*, 2099–2119. doi:10.1039/c0gc00382d
9. Kim, Y.; Li, C.-J. *Green Synth. Catal.* **2020**, *1*, 1–11. doi:10.1016/j.gresc.2020.06.002
10. Patonay, T.; Hoffman, R. V. *J. Org. Chem.* **1994**, *59*, 2902–2905. doi:10.1021/jo00089a043
11. Yang, B.; Lu, Z. *ACS Catal.* **2017**, *7*, 8362–8365. doi:10.1021/acscatal.7b02892
12. Hossain, A.; Vidyasagar, A.; Eichinger, C.; Lankes, C.; Phan, J.; Rehbein, J.; Reiser, O. *Angew. Chem., Int. Ed.* **2018**, *57*, 8288–8292. doi:10.1002/anie.201801678
13. Ye, Z.; Zhu, R.; Wang, F.; Jiang, H.; Zhang, F. *Org. Lett.* **2021**, *23*, 8240–8245. doi:10.1021/acs.orglett.1c02991
14. Panday, P.; Garg, P.; Singh, A. *Asian J. Org. Chem.* **2018**, *7*, 111–115. doi:10.1002/ajoc.201700508
15. Yan, M.; Kawamata, Y.; Baran, P. S. *Chem. Rev.* **2017**, *117*, 13230–13319. doi:10.1021/acs.chemrev.7b00397
16. Kingston, C.; Palkowitz, M. D.; Takahira, Y.; Vantourout, J. C.; Peters, B. K.; Kawamata, Y.; Baran, P. S. *Acc. Chem. Res.* **2020**, *53*, 72–83. doi:10.1021/acs.accounts.9b00539
17. Francke, R.; Little, R. D. *Chem. Soc. Rev.* **2014**, *43*, 2492–2521. doi:10.1039/c3cs60464k
18. Yoshida, J.-i.; Shimizu, A.; Hayashi, R. *Chem. Rev.* **2018**, *118*, 4702–4730. doi:10.1021/acs.chemrev.7b00475
19. Xiong, P.; Xu, H.-C. *Acc. Chem. Res.* **2019**, *52*, 3339–3350. doi:10.1021/acs.accounts.9b00472
20. Jiao, K.-J.; Xing, Y.-K.; Yang, Q.-L.; Qiu, H.; Mei, T.-S. *Acc. Chem. Res.* **2020**, *53*, 300–310. doi:10.1021/acs.accounts.9b00603
21. Novaes, L. F. T.; Liu, J.; Shen, Y.; Lu, L.; Meinhardt, J. M.; Lin, S. *Chem. Soc. Rev.* **2021**, *50*, 7941–8002. doi:10.1039/d1cs00223f
22. Shi, S.-H.; Liang, Y.; Jiao, N. *Chem. Rev.* **2021**, *121*, 485–505. doi:10.1021/acs.chemrev.0c00335
23. Aoyama, M.; Fukuhara, T.; Hara, S. *J. Org. Chem.* **2008**, *73*, 4186–4189. doi:10.1021/jo8004759
24. Lam, K.; Markó, I. E. *Org. Lett.* **2009**, *11*, 2752–2755. doi:10.1021/ol900828x
25. Yu, Y.; Jiang, Y.; Wu, S.; Shi, Z.; Wu, J.; Yuan, Y.; Ye, K. *Chin. Chem. Lett.* **2022**, *33*, 2009–2014. doi:10.1016/j.cclet.2021.10.016
26. Vil', V. A.; Merkulova, V. M.; Illovaisky, A. I.; Paveliev, S. A.; Nikishin, G. I.; Terent'ev, A. O. *Org. Lett.* **2021**, *23*, 5107–5112. doi:10.1021/acs.orglett.1c01643
27. de Souza, A. A. N.; Bartolomeu, A. d. A.; Brocksom, T. J.; Noël, T.; de Oliveira, K. T. *J. Org. Chem.* **2022**, *87*, 5856–5865. doi:10.1021/acs.joc.2c00147
28. Zhou, P.; Liu, Y.; Xu, Y.; Wang, D. *Org. Chem. Front.* **2022**, *9*, 2215–2219. doi:10.1039/d1qo01765a
29. Wu, J.; Dou, Y.; Guillot, R.; Kouklovsky, C.; Vincent, G. *J. Am. Chem. Soc.* **2019**, *141*, 2832–2837. doi:10.1021/jacs.8b13371
30. Meyer, T. H.; Samanta, R. C.; Del Vecchio, A.; Ackermann, L. *Chem. Sci.* **2021**, *12*, 2890–2897. doi:10.1039/d0sc05924b
31. Niu, L.; Jiang, C.; Liang, Y.; Liu, D.; Bu, F.; Shi, R.; Chen, H.; Chowdhury, A. D.; Lei, A. *J. Am. Chem. Soc.* **2020**, *142*, 17693–17702. doi:10.1021/jacs.0c08437
32. Siu, J. C.; Parry, J. B.; Lin, S. *J. Am. Chem. Soc.* **2019**, *141*, 2825–2831. doi:10.1021/jacs.8b13192
33. Fu, N.; Sauer, G. S.; Saha, A.; Loo, A.; Lin, S. *Science* **2017**, *357*, 575–579. doi:10.1126/science.aan6206
34. Wu, K.; Liang, Y.; Jiao, N. *Molecules* **2016**, *21*, 352. doi:10.3390/molecules21030352
35. Ge, L.; Chiou, M.-F.; Li, Y.; Bao, H. *Green Synth. Catal.* **2020**, *1*, 86–120. doi:10.1016/j.gresc.2020.07.001
36. Sharma, A.; Hartwig, J. F. *Nature* **2015**, *517*, 600–604. doi:10.1038/nature14127
37. Bangalore, P. K.; Vagolu, S. K.; Bollikonda, R. K.; Veeragoni, D. K.; Choudante, P. C.; Misra, S.; Sriram, D.; Sridhar, B.; Kantevari, S. *J. Nat. Prod.* **2020**, *83*, 26–35. doi:10.1021/acs.jnatprod.9b00475

38. Lv, G.; Qiu, L.; Li, K.; Liu, Q.; Li, X.; Peng, Y.; Wang, S.; Lin, J. *New J. Chem.* **2019**, *43*, 3419–3427. doi:10.1039/c8nj04159h
39. Buil, M. L.; Esteruelas, M. A.; Garcés, K.; Oñate, E. *Organometallics* **2009**, *28*, 5691–5696. doi:10.1021/om900647a
40. Levine, P. M.; Lee, E.; Greenfield, A.; Bonneau, R.; Logan, S. K.; Garabedian, M. J.; Kirshenbaum, K. *ACS Chem. Biol.* **2012**, *7*, 1693–1701. doi:10.1021/cb300332w
41. Levine, P. M.; Imberg, K.; Garabedian, M. J.; Kirshenbaum, K. *J. Am. Chem. Soc.* **2012**, *134*, 6912–6915. doi:10.1021/ja300170n
42. Prasad, B.; Phanindrudu, M.; Tiwari, D. K.; Kamal, A. *J. Org. Chem.* **2019**, *84*, 12334–12343. doi:10.1021/acs.joc.9b01534

License and Terms

This is an open access article licensed under the terms of the Beilstein-Institut Open Access License Agreement (<https://www.beilstein-journals.org/bjoc/terms>), which is identical to the Creative Commons Attribution 4.0 International License

(<https://creativecommons.org/licenses/by/4.0>). The reuse of material under this license requires that the author(s), source and license are credited. Third-party material in this article could be subject to other licenses (typically indicated in the credit line), and in this case, users are required to obtain permission from the license holder to reuse the material.

The definitive version of this article is the electronic one which can be found at:

<https://doi.org/10.3762/bjoc.18.103>



Electrochemical Friedel–Crafts-type amidomethylation of arenes by a novel electrochemical oxidation system using a quasi-divided cell and trialkylammonium tetrafluoroborate

Hisanori Senboku^{*1,2}, Mizuki Hayama² and Hidetoshi Matsuno²

Letter

Open Access

Address:

¹Division of Applied Chemistry, Faculty of Engineering, Hokkaido University, Kita 13 Nishi 8, Kita-ku, Sapporo, Hokkaido 060-8628, Japan and ²Graduate School of Chemical Sciences and Engineering, Hokkaido University, Kita 13 Nishi 8, Kita-ku, Sapporo, Hokkaido 060-8628, Japan

Email:

Hisanori Senboku^{*} - senboku@eng.hokudai.ac.jp

^{*} Corresponding author

Keywords:

electrochemical oxidation; Friedel–Crafts type amidomethylation; *N*-acyliminium ion; quasi-divided cell; trialkylammonium salt

Beilstein J. Org. Chem. **2022**, *18*, 1040–1046.

<https://doi.org/10.3762/bjoc.18.105>

Received: 01 June 2022

Accepted: 03 August 2022

Published: 18 August 2022

This article is part of the thematic issue "Molecular and macromolecular electrochemistry: synthesis, mechanism, and redox properties".

Guest Editor: S. Inagi

© 2022 Senboku et al.; licensee Beilstein-Institut.

License and terms: see end of document.

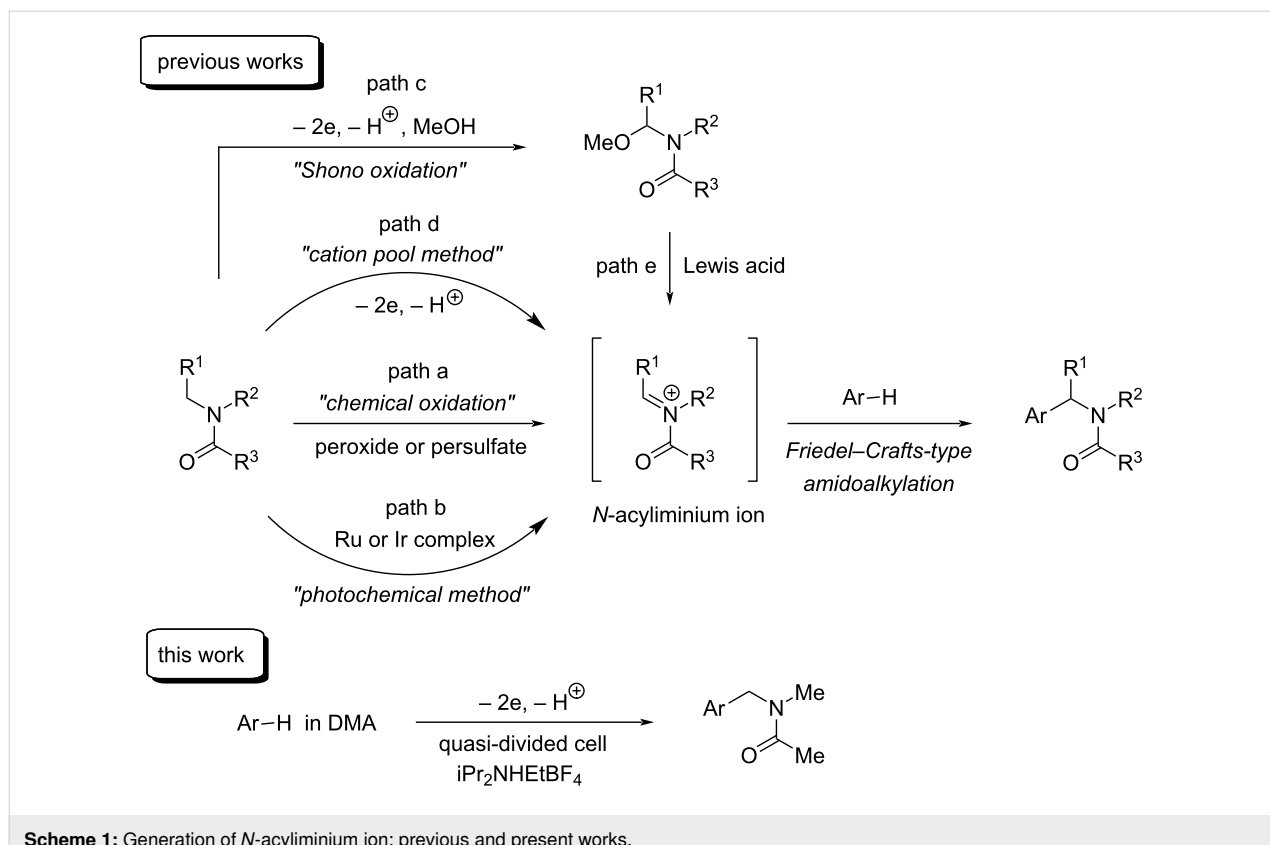
Abstract

Electrochemical Friedel–Crafts-type amidomethylation was successfully carried out by a novel electrochemical oxidation system using a quasi-divided cell and trialkylammonium tetrafluoroborates, such as $i\text{Pr}_2\text{NHEtBF}_4$. Constant current electrolysis of 1,3,5-trimethoxybenzene or indoles in DMA containing 0.1 M $i\text{Pr}_2\text{NHEtBF}_4$ using an undivided cell equipped with a Pt plate cathode and a Pt wire anode (a quasi-divided cell) resulted in selective formation of *N*-acyliminium ions of DMA at the anode, which reacted with arenes to give the corresponding amidomethylated products in good to high yields.

Introduction

Oxidation of amides generates useful intermediates, *N*-acyliminium ions, which have been widely used in organic synthesis [1–4]. For example, Friedel–Crafts-type amidomethylation [5–15] proceeds efficiently by the reaction of *N*-acyliminium ions with electron-rich arenes to give the corresponding amidomethylated products in good yields. Since amides are important intermediates in organic synthesis and sometimes appear in biologically active compounds, pharmaceuticals, agrochemicals and functional molecules, amidomethylation induced by *N*-acyliminium ions is a helpful and valuable protocol

for direct introduction of an amide function into organic molecules. Generation of *N*-acyliminium ions in chemical methods has been generally accomplished by the reaction of amides with chemical oxidants, such as peroxides and persulfates at high temperature (path a in Scheme 1) [10–13]. A metal catalyst or a photocatalyst consisting of metals, such as ruthenium or iridium, is also necessary in some cases (path b in Scheme 1) [14,15]. On the other hand, *N*-acyliminium ions can easily be generated by electrochemical oxidation without those reagents. Electrochemical oxidation of amides/carbamates yielding



Scheme 1: Generation of *N*-acyliminium ion: previous and present works.

N-acyliminium ions is well known as Shono oxidation (path c in Scheme 1) [16] and has also been applied to organic synthesis [17–20]. However, when electrochemical oxidation of amides/carbamates in the presence of nucleophiles, such as electron-rich arenes or silyl enol ethers, is carried out for Friedel–Crafts-type amidomethylation, electrochemical oxidation of electron-rich arenes or silyl enol ethers preferentially takes place at the anode due to their, in general, more positive oxidation potentials than those of amides/carbamates. Therefore, Friedel–Crafts-type amidomethylation by using Shono oxidation is successfully carried out as a two-step process: electrochemical oxidation of amides/carbamates yielding α -methoxyated amides/carbamates (Shono oxidation, path c in Scheme 1) followed by the reaction of the isolated α -methoxyated amides/carbamates with arenes in the presence of a Lewis acid catalyst (path e in Scheme 1) [16]. Although the use of CH_2Cl_2 as a solvent and a divided cell with a low temperature ($-78\text{ }^\circ\text{C}$) and a relatively high concentration of the supporting electrolyte are necessary, the cation pool method [21] developed by Yoshida and Suga was effective for electrochemical oxidation-induced Friedel–Crafts-type amidomethylation (path d in Scheme 1) [22,23]. We also succeeded in generating *N*-acyliminium ions from *N,N*-dimethylformamide (DMF) used as a solvent in the electrochemical carboxylation of benzyl bromides. Electrolysis of benzyl bromides in DMF containing 0.1 M Bu_4NBF_4 and

iPr_2NEt (1 equiv) using an undivided cell equipped with a Pt plate cathode and a Pt wire anode (a quasi-divided cell) [24–28] in the presence of carbon dioxide resulted in reductive carboxylation at the cathode and selective formation of *N*-acyliminium ions of DMF at the anode to produce coupling products, *N*-phenylacetoxymethyl-*N*-methylformamides, in good yields [29]. In this reaction system, the use of a quasi-divided cell enabled DMF to be oxidized with high selectivity at the anode even in the presence of carboxylate and bromide ions, which would generally be oxidized more easily than DMF. Accordingly, we tried this electrolysis system using a quasi-divided cell to apply electrochemical Friedel–Crafts-type amidomethylation of arenes, and we found that the use of $\text{iPr}_2\text{NHEtBF}_4$ in electrolysis using a quasi-divided cell was highly effective for electrochemical Friedel–Crafts-type amidomethylation of electron-rich arenes, such as 1,3,5-trimethoxybenzene and indoles (this work in Scheme 1). To the best of our knowledge, this is the first example of the use of trialkylammonium salts, such as $\text{iPr}_2\text{NHEtBF}_4$, in electroorganic synthesis, especially with the electrochemical oxidation system as a supporting electrolyte as well as a proton source for the cathodic reduction producing hydrogen gas. We report electrochemical Friedel–Crafts-type amidomethylation of electron-rich arenes by a novel electrochemical oxidation system using a quasi-divided cell and $\text{iPr}_2\text{NHEtBF}_4$.

Results and Discussion

We chose 1,3,5-trimethoxybenzene (**1**) as a model substrate for electrochemical Friedel–Crafts-type amidomethylation. For electrolysis, a test tube-like undivided cell equipped with a Pt plate cathode ($2 \times 2 \text{ cm}^2$) and a Pt wire anode (2 cm \times 1 mm Ø) was used. Electrolysis of an *N,N*-dimethylacetamide (DMA) solution of **1** containing 0.1 M Bu_4NBF_4 as a supporting electrolyte, trifluoroacetic acid (TFA, 1 equiv) as a proton source for the cathodic reduction, and iPr_2NEt (1 equiv) as a base for the formation of *N*-acyliminium ions of DMA at the anode was carried out under constant current conditions (20 mA/cm^2) with 3 F/mol of electricity at 0 °C. It was found that 66% of **1** remained unchanged and mono-amidomethylation product **2** was formed in 16% yield along with 6% of di-substituted product **3** by analysis of the ^1H NMR spectrum of the crude product mixture using 1,4-dinitrobenzene as an internal standard (Table 1, entry 1). These results indicate that anodic oxidation of not the substrate **1** but DMA successfully proceeded at the anode. In other words, *N*-acyliminium ions of DMA would be expectedly formed. We speculated that the reason for the lower product yields of **2** and **3** was a side reaction of the produced *N*-acyliminium ions with other nucleophiles in the reaction medium. The most likely nucleophile in this reaction medium was the trifluoroacetate ion, which was produced by electrochemical reduction of TFA at the cathode, although we could not detect the coupling product of trifluoroacetate and the corresponding *N*-acyliminium ion due to the high solubility in water. In addition to TFA, iPr_2NEt was also included in this reaction medium, and they probably formed the corresponding ammonium trifluoroacetate in the reaction medium. The thus-generated trifluoroacetate ion could also react with *N*-acyliminium ions of DMA. Therefore, to avoid the reaction of the cathodic product with *N*-acyliminium ions, a proton source for which the conjugate base has no nucleophilicity would be necessary in the cathodic reduction. After several attempts, we finally reached

$\text{HBF}_4\text{-OEt}_2$ as a proton source for cathodic reduction and the result is shown in entry 2 of Table 1. Strong increases of conversion of **1** and yield of **2** were observed. These results indicate that DMA was selectively oxidized at the anode to generate the corresponding *N*-acyliminium ions, which were trapped by trifluoroacetate ions preventing the desired amidomethylation in the presence of TFA. The exchange of the proton source from TFA to $\text{HBF}_4\text{-OEt}$, for which the conjugate base has no nucleophilicity, improved the yield of **2** and the conversion of **1**.

Incidentally, this reaction medium includes a base, iPr_2NEt , that would accelerate the deprotonation step in the formation of *N*-acyliminium ions from DMA at the anode. TFA and $\text{HBF}_4\text{-OEt}_2$ will react with iPr_2NEt in the reaction medium to form the corresponding ammonium salt. We thought that if trialkylammonium tetrafluoroborate, R_3NHBF_4 , would be usable not only as a proton source for cathodic reduction but also as a supporting electrolyte, a novel and innovative electrochemical oxidation system could be developed. The use of R_3NHBF_4 in the electrochemical reaction as a supporting electrolyte and a proton source was investigated and the results are summarized in Table 2.

When electrolysis of **1** in DMA was carried out in the presence of 0.1 M Bu_3NHBF_4 without any other supporting electrolyte using a quasi-divided cell, the desired amidomethylation took place efficiently to give **2** in 62% ^1H NMR yield along with **3** (Table 2, entry 1). The use of Et_3NHBF_4 instead of Bu_3NHBF_4 gave a similar result (Table 2, entry 2). A slight increase in the yield of **2** was observed when electrolysis of **1** was carried out using Et_3NHBF_4 at –10 °C (Table 2, entry 3). Instead of Et_3NHBF_4 , sterically more hindered $\text{iPr}_2\text{NHEtBF}_4$ was effective for the electrochemical synthesis to give the desired compound **2** in the highest yield, 72% by ^1H NMR (Table 2, entry

Table 1: Effect of the proton source in electrochemical amidomethylation.

Entry	Proton source	Conversion of 1 [%] ^a	Yield of 2 [%] ^a	Yield of 3 [%] ^a
1	$\text{CF}_3\text{CO}_2\text{H}$	34	16	6
2	$\text{HBF}_4\text{-OEt}_2$	80	63	12

^aDetermined by ^1H NMR using 1,4-dinitrobenzene as an internal standard.

Table 2: Effect of trialkylammonium salt in electrochemical amidomethylation.

Entry	R_3NHBf_4	Temperature [°C]	Conversion of 1 [%] ^a		
			Yield of 2 [%] ^a	Yield of 3 [%] ^a	
1	Bu_3NHBf_4	0	83	62	12
2	Et_3NHBf_4	0	83	61	17
3	Et_3NHBf_4	-10	79	65	14
4	$iPr_2NHEtBF_4$	-10	82	72	6

^aDetermined by 1H NMR using 1,4-dinitrobenzene as an internal standard.

4). These results strongly indicate that trialkylammonium salts, R_3NHBf_4 , can play roles not only as a proton source but also as supporting electrolyte in the electrochemical oxidation system using a quasi-divided cell. With these results in hand, we moved to screening of electrolysis conditions and the results are summarized in Table 3.

Electrochemical Friedel–Crafts-type amidoalkylation also took place efficiently with a lower concentration (0.05 M) of the supporting electrolyte $iPr_2NHEtBF_4$, to give **2** in good yields under various electrolysis conditions (Table 3, entries 1–6). After several attempts in screening of current density (Table 3, entries

1–3), electricity (Table 3, entries 2 and 4–6), and the effect of concentration of the supporting electrolyte, the best result was obtained by a constant current electrolysis of **1** in DMA containing 0.05 or 0.1 M $iPr_2NHEtBF_4$ with 4 F/mol of electricity at -10 °C to yield amidomethylation product **2** in 79% 1H NMR yield (Table 3, entries 4 and 8) and 71% isolated yield (Table 3, entry 8). The use of a Pt plate ($2 \times 2 \text{ cm}^2$) instead of a Pt wire as the anode resulted in a drastic decrease in the yield of **2** (Table 3, entry 9). These results indicate that a Pt wire anode plays an important role and that the use of a Pt wire as an anode is critical and essential in the present electrochemical amidomethylation.

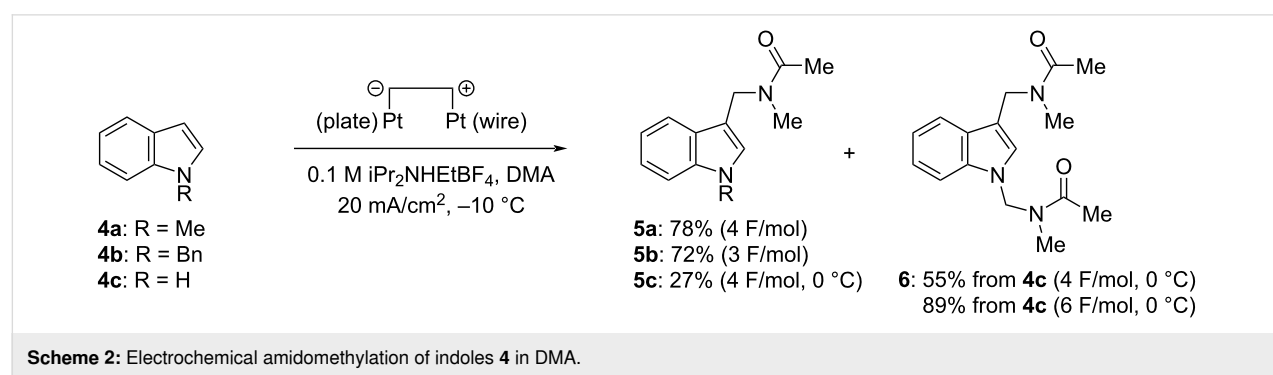
Table 3: Screening of reaction conditions in electrochemical amidomethylation.

Entry	Concentration of $iPr_2NHEtBF_4$ [M]	Current density [mA/cm^2]	Electricity [F/mol]	Conversion of 1 [%] ^a		
				Yield of 2 [%] ^a	Yield of 3 [%] ^a	
1	0.05	10	3	77	70	6
2	0.05	20	3	81	73	8
3	0.05	30	3	77	68	9
4	0.05	20	4	89	79	10
5	0.05	20	2	58	53	4
6	0.05	20	5	93	74	15
7	0.10	20	3	82	72	6
8	0.10	20	4	95	79 (71) ^b	15
9 ^c	0.10	20	4	76	38	trace

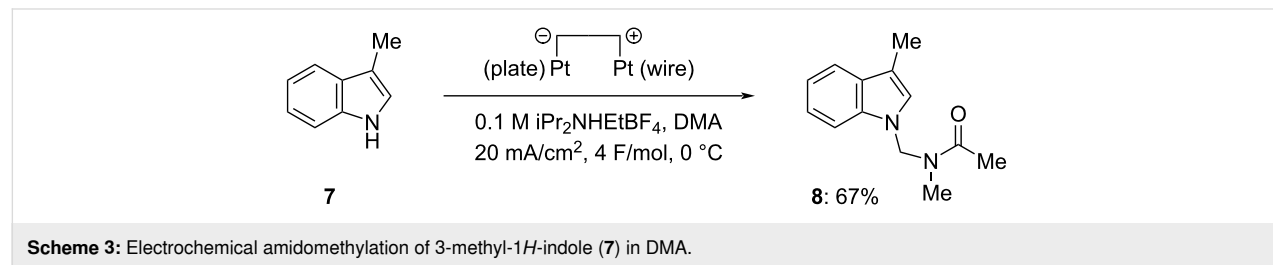
^aDetermined by 1H NMR using 1,4-dinitrobenzene as an internal standard; ^bIsolated yield; ^cA Pt plate ($2 \times 2 \text{ cm}^2$) was used as an anode.

When other substituted benzenes such as anisole, 1,2- and 1,4-dimethoxybenzenes, 1,2,3-trimethoxybenzene, and 1,3,5-trimethylbenzene were used as substrates in the electrochemical Friedel–Crafts-type amidalkylation, the desired products were not obtained/detected by ^1H NMR. In contrast, it was reported that anisole [9,11,23] and 1,3,5-trimethylbenzene [23] could react with acylium ions generated by the chemical [9,11] or cation pool method [23] to produce amidomethylated products. These results indicate that the present electrochemical amidomethylation seems to be relatively less reactive than other chemical methods and the cation pool method. On the other hand, similar electrolysis of 1,3-dimethoxybenzene gave a mixture of products including regioisomeric mono-amidomethylation products together with diamidomethylation products, and it was difficult to analyze them exactly. Although *N*-acetylindole was also ineffective, several indoles were found to be applicable to the present amidomethylation reaction and the results are summarized in Scheme 2. When *N*-methylindole (**4a**) was electrolyzed using a quasi-divided cell under the conditions shown in Scheme 1, electrochemical amidomethylation took place efficiently at the C3 position of **4a** to yield **5a** in 78% isolated yield. Similar electrolysis of *N*-benzylindole (**4b**) also induced amidomethylation at its C3 position to give **5b** in 72% isolated yield. To our surprise, we found that electrolysis of *N*-benzylindole (**4b**) at $-10\text{ }^\circ\text{C}$ under the conditions of 20 mA/cm^2 of current density and a lower concentration (0.05 M) of $\text{iPr}_2\text{NHEtBF}_4$ in DMA with 3–6 F/mol of electricity resulted in removal of the benzyl group followed by amidomethylation at the nitrogen atom of **4b** to yield *N*,*3*-diamidomethylated indole **6** in 4–34% (^1H NMR yield), al-

though similar electrolysis with 2 F/mol of electricity gave only **5b** in 66% yield with 68% conversion. It is thought that supplying an excess amount of electricity under the conditions of a lower concentration of the proton source (supporting electrolyte), $\text{iPr}_2\text{NHEtBF}_4$, caused competitive electrochemical reduction of a proton and the *N*-benzyl group of **5b** at the cathode. We also carried out electrochemical amidomethylation of indole (**4c**) and found that a mixture of 3-amidomethylated indole **5c** and *N*,*3*-diamidomethylated indole **6** was produced. However, *N*-amidomethylated indole was not observed in the ^1H NMR spectra of the crude products. These results indicate that amidomethylation firstly occurs at the C3 position of **4c** and then the second amidomethylation takes place on the indole nitrogen atom of **5c**. Despite our efforts, selective formation of **5c** could not be achieved under various electrolysis conditions. Electrolysis of **4c** supplying 4 F/mol of electricity at $0\text{ }^\circ\text{C}$ afforded 3-amidomethylated **5c** and *N*,*3*-diamidomethylated **6** in 27% and 55% isolated yields, respectively. Fortunately, electrolysis with 6 F/mol of electricity could predominantly produce diamidomethylated **6** in 89% isolated yield. Similar amidomethylation of indole (**4c**) using chemical methods has already been reported by Shirakawa [12] and Doan [11]. However, mono-amidomethylation at the C3 position of indole **4c** only took place to yield **5c** predominantly and no *N*-amidomethylated product was obtained. We investigated electrochemical amidomethylation of 3-methylindole (**7**) and found that amidomethylation similarly proceeded at the nitrogen atom of **7** to yield *N*-amidomethylated **8** in 67% isolated yield (Scheme 3). These results indicate that the present electrochemical amidomethylation has quite different reactivity from that of the



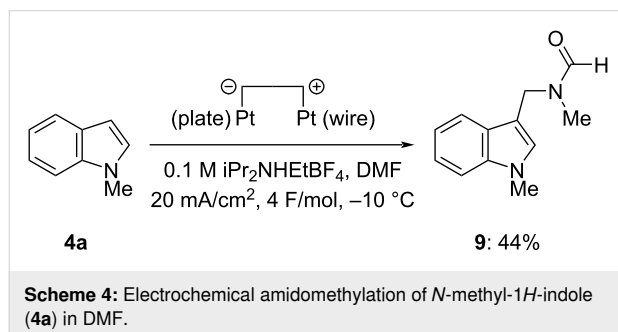
Scheme 2: Electrochemical amidomethylation of indoles **4** in DMA.



Scheme 3: Electrochemical amidomethylation of 3-methyl-1*H*-indole (**7**) in DMA.

reported chemical ones, although the exact reason is not clear at the present.

It was found that DMF instead of DMA was also applicable to the present electrochemical amidomethylation. Similar electrolysis of **4a** in DMF containing 0.1 M $i\text{Pr}_2\text{NHEtBF}_4$ using a quasi-divided cell gave 3-amidomethylated *N*-methylindole **9** in 47% ^1H NMR yield and 44% isolated yield at full conversion (Scheme 4). The moderate yield of **9** is thought to be due to its high solubility in water.

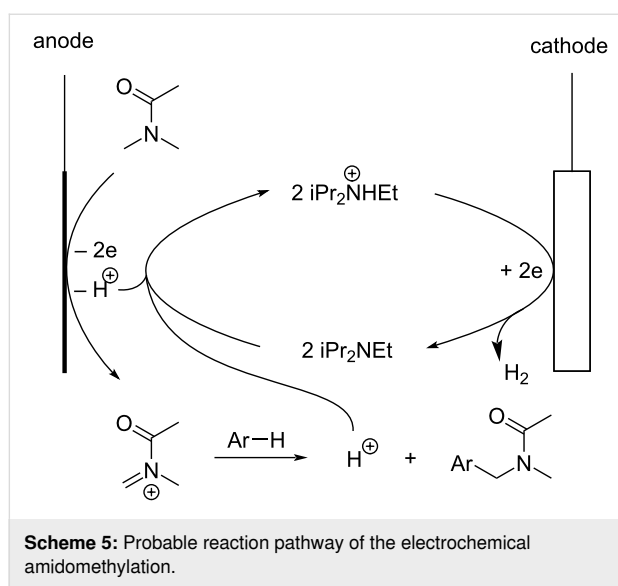


A probable reaction pathway is shown in Scheme 5. The present amidomethylation is induced by electrolysis using a quasi-divided cell equipped with a Pt plate cathode ($2 \times 2 \text{ cm}^2$) and a Pt wire anode ($2 \text{ cm} \times 1 \text{ mm } \varnothing$) in DMA containing 0.1 M $i\text{Pr}_2\text{NHEtBF}_4$. At the cathode, electrochemical reduction of a proton in $i\text{Pr}_2\text{NHEt}^+$ takes place to generate hydrogen gas and $i\text{Pr}_2\text{NEt}$. Evolution of a gas at the cathode can be observed visually. It is well known that electrochemical reduction can generate the intermediates/products which play as bases. Thus-generated bases are called electrogenerated bases (EGBs) and have widely been used in electroorganic synthesis [30–35]. At

the anode, electrochemical one-electron oxidation of the solvent, DMA, takes place selectively. Deprotonation, probably supported by $i\text{Pr}_2\text{NEt}$ generated at the cathode, followed by further one-electron oxidation generates the corresponding *N*-acyliminium ion of DMA. Deprotonation supported by $i\text{Pr}_2\text{NEt}$ produces $i\text{Pr}_2\text{NHEt}^+$, which is used again as a proton source and a supporting electrolyte. In a quasi-divided cell, two electrodes have largely different surface areas. Current density, 20 mA/cm^2 , is realized at a Pt plate cathode. On the other hand, the anode is a Pt wire, which has a significantly smaller surface area, and a much higher current density is realized. At the anode with a much higher current density, the concentrations of the starting material, $i\text{Pr}_2\text{NEt}$, and the products, which seem to be more easily oxidized, are relatively low and there is insufficient mass transfer at the anode that results in selective oxidation of the solvent, DMA, which is the substance with the largest amount at the anode [28,29].

Conclusion

We have developed a novel electrochemical oxidation system using a quasi-divided cell and trialkylammonium tetrafluoroborates, especially $i\text{Pr}_2\text{NHEtBF}_4$, both as a supporting electrolyte and as a proton source for the cathodic reduction. The system was successfully applied to Friedel–Crafts-type electrochemical amidoalkylation of arenes, such as 1,3,5-trimethoxybenzene and indoles, to yield the corresponding amidomethylated products in good to high yields. The novel electrochemical oxidation system will be promising as a powerful tool for electroorganic synthesis using anodic oxidation. In addition, trialkylammonium salts have high potential both as novel supporting electrolytes and proton sources for cathodic reduction in the anodic oxidation process.



Supporting Information

Supporting Information File 1

General experimental information, preparation of trialkylammonium salts, general procedure for electrolysis, spectral data information including ^1H and ^{13}C NMR spectra of new compounds.

[<https://www.beilstein-journals.org/bjoc/content/supplementary/1860-5397-18-105-S1.pdf>]

Acknowledgements

We would like to thank Professor Tomoki Yoneda, Hokkaido University, for his helpful discussion and support for NMR measurement at $150 \text{ }^\circ\text{C}$. ^1H and ^{13}C NMR spectra were measured at Instrumental Analysis Support Office, the Frontier Chemistry Center, Faculty of Engineering, Hokkaido University.

sity. ESI mass spectra were measured at the Instrumental Analysis Division, Global Facility Center, Creative Research Institution, Hokkaido University. The authors would like to express their gratitude to the staff.

Funding

This work was partly supported by Grant-in-Aid for Scientific Research(C) (JSPS KAKENHI Grant Number 22K0518202).

ORCID® IDs

Hisanori Senboku - <https://orcid.org/0000-0003-2205-626X>

References

- Wu, P.; Nielsen, T. E. *Chem. Rev.* **2017**, *117*, 7811–7856. doi:10.1021/acs.chemrev.6b00806
- Yazici, A.; Pyne, S. G. *Synthesis* **2009**, 339–368. doi:10.1055/s-0028-1083325
- Yazici, A.; Pyne, S. G. *Synthesis* **2009**, 513–541. doi:10.1055/s-0028-1083346
- Maryanoff, B. E.; Zhang, H.-C.; Cohen, J. H.; Turchi, I. J.; Maryanoff, C. A. *Chem. Rev.* **2004**, *104*, 1431–1628. doi:10.1021/cr0306182
- Mazurkiewicz, R.; Październiok-Holewa, A.; Adamek, J.; Zielińska, K. α -Amidoalkylating Agents: Structure, Synthesis, Reactivity and Application. In *Advances in Heterocyclic Chemistry*; Katritzky, A. R., Ed.; Elsevier: San Diego, CA, USA, 2014; Vol. 111, pp 43–94. doi:10.1016/b978-0-12-420160-6.00002-1
- Graham, T. J. A.; Shields, J. D.; Doyle, A. G. *Chem. Sci.* **2011**, *2*, 980–984. doi:10.1039/c1sc00026h
- Boiaryna, L.; El Mkaddem, M. K.; Taillier, C.; Dalla, V.; Othman, M. *Chem. – Eur. J.* **2012**, *18*, 14192–14200. doi:10.1002/chem.201202225
- Ryder, G. M.; Wille, U.; Willis, A. C.; Pyne, S. G. *Org. Biomol. Chem.* **2019**, *17*, 7025–7035. doi:10.1039/c9ob01363f
- Ikeda, K.; Morimoto, T.; Sekiya, M. *Chem. Pharm. Bull.* **1980**, *28*, 1178–1182. doi:10.1248/cpb.28.1178
- Nakamura, K.; Togo, H. *Eur. J. Org. Chem.* **2020**, 4713–4722. doi:10.1002/ejoc.202000680
- Doan, S. H.; Nguyen, K. D.; Huynh, P. T.; Nguyen, T. T.; Phan, N. T. S. *J. Mol. Catal. A: Chem.* **2016**, *423*, 433–440. doi:10.1016/j.molcata.2016.07.042
- Shirakawa, E.; Uchiyama, N.; Hayashi, T. *J. Org. Chem.* **2011**, *76*, 25–34. doi:10.1021/jo102217m
- Zhang, Y.; Teuscher, K. B.; Ji, H. *Chem. Sci.* **2016**, *7*, 2111–2118. doi:10.1039/c5sc03640b
- Dai, C.; Meschini, F.; Narayanan, J. M. R.; Stephenson, C. R. J. *J. Org. Chem.* **2012**, *77*, 4425–4431. doi:10.1021/jo300162c
- Kaur, J.; Shahin, A.; Barham, J. P. *Org. Lett.* **2021**, *23*, 2002–2006. doi:10.1021/acs.orglett.1c00132
- Shono, T.; Matsumura, Y.; Tsubata, K. *J. Am. Chem. Soc.* **1981**, *103*, 1172–1176. doi:10.1021/ja00395a029
- Jones, A. M.; Banks, C. E. *Beilstein J. Org. Chem.* **2014**, *10*, 3056–3072. doi:10.3762/bjoc.10.323
- Jones, A. M. *Chem. Rec.* **2021**, *21*, 2120–2129. doi:10.1002/tcr.202000116
- Yamamoto, K.; Kuriyama, M.; Onomura, O. *Chem. Rec.* **2021**, *21*, 2239–2253. doi:10.1002/tcr.202100031
- Geske, L.; Sato, E.; Opatz, T. *Synthesis* **2020**, *52*, 2781–2794. doi:10.1055/s-0040-1707154
- Yoshida, J.-i.; Shimizu, A.; Hayashi, R. *Chem. Rev.* **2018**, *118*, 4702–4730. doi:10.1021/acs.chemrev.7b00475
- Suga, S.; Nagaki, A.; Yoshida, J.-i. *Chem. Commun.* **2003**, 354–355. doi:10.1039/b211433j
- Nagaki, A.; Togai, M.; Suga, S.; Aoki, N.; Mae, K.; Yoshida, J.-i. *J. Am. Chem. Soc.* **2005**, *127*, 11666–11675. doi:10.1021/ja0527424
- Werdecker, B.; Beck, F. *Electrochim. Acta* **1985**, *30*, 1491–1500. doi:10.1016/0013-4686(85)80011-6
- Danielmeier, K.; Schierle, K.; Steckhan, E. *Tetrahedron* **1996**, *52*, 9743–9754. doi:10.1016/0040-4020(96)00506-6
- Hilt, G. *Angew. Chem., Int. Ed.* **2003**, *42*, 1720–1721. doi:10.1002/anie.2003050892
- Gong, M.; Huang, J.-M. *Chem. – Eur. J.* **2016**, *22*, 14293–14296. doi:10.1002/chem.201602454
- Hilt, G. *ChemElectroChem* **2020**, *7*, 395–405. doi:10.1002/celc.201901799
- Senboku, H.; Nagakura, K.; Fukuura, T.; Hara, S. *Tetrahedron* **2015**, *71*, 3850–3856. doi:10.1016/j.tet.2015.04.020
- Utley, J. H. P.; Nielsen, M. F. Electrogenerated Bases. In *Organic Electrochemistry*; Lund, H.; Hammerich, O., Eds.; Marcel Dekker: New York, NY, USA, 2001; pp 1227–1257.
- Torii, S. Electrogenerated Base-assisted Conversion. *Electroorganic Reduction Synthesis*; Kodansha: Tokyo, Japan, 2006; pp 635–702.
- Kashimura, S.; Matsumoto, K. Electrogenerated Base. In *Encyclopedia of Applied Electrochemistry*; Kreysa, G.; Ota, K.; Savinell, R. F., Eds.; Springer: New York, NY, USA, 2014; pp 706–713. doi:10.1007/978-1-4419-6996-5_354
- Frontana-Uribe, B. A.; Little, R. D.; Ibanez, J. G.; Palma, A.; Vasquez-Medrano, R. *Green Chem.* **2010**, *12*, 2099–2119. doi:10.1039/c0gc00382d
- Kashimura, S. *J. Synth. Org. Chem., Jpn.* **1985**, *43*, 549–556. doi:10.5059/yukigoseikyokaishi.43.549
- Uneyama, K.; Itano, N. *Denki Kagaku oyobi Kogyo Butsuri Kagaku* **1994**, *62*, 1151–1153. doi:10.5796/electrochemistry.62.1151

License and Terms

This is an open access article licensed under the terms of the Beilstein-Institut Open Access License Agreement (<https://www.beilstein-journals.org/bjoc/terms>), which is identical to the Creative Commons Attribution 4.0 International License (<https://creativecommons.org/licenses/by/4.0/>). The reuse of material under this license requires that the author(s), source and license are credited. Third-party material in this article could be subject to other licenses (typically indicated in the credit line), and in this case, users are required to obtain permission from the license holder to reuse the material.

The definitive version of this article is the electronic one which can be found at:

<https://doi.org/10.3762/bjoc.18.105>



Synthesis, optical and electrochemical properties of (D- π)₂-type and (D- π)₂Ph-type fluorescent dyes

Kosuke Takemura, Kazuki Ohira, Taiki Higashino, Keiichi Imato and Yousuke Ooyama^{*}

Full Research Paper

Open Access

Address:

Applied Chemistry Program, Graduate School of Advanced Science and Engineering, Hiroshima University, 1-4-1 Kagamiyama, Higashi-Hiroshima 739-8527, Japan

Beilstein J. Org. Chem. **2022**, *18*, 1047–1054.

<https://doi.org/10.3762/bjoc.18.106>

Email:

Yousuke Ooyama^{*} - yooyama@hiroshima-u.ac.jp

Received: 26 May 2022

Accepted: 12 August 2022

Published: 18 August 2022

* Corresponding author

This article is part of the thematic issue "Molecular and macromolecular electrochemistry: synthesis, mechanism, and redox properties".

Keywords:

(D- π)₂ structure; fluorescence; fluorescent dyes; photoabsorption; redox properties

Guest Editor: S. Inagi

© 2022 Takemura et al.; licensee Beilstein-Institut.

License and terms: see end of document.

Abstract

The (D- π)₂-type fluorescent dye **OTT-2** with two (diphenylamino)carbazole-thiophene units as D (electron-donating group)- π (π -conjugated bridge) moiety and the (D- π)₂Ph-type fluorescent dye **OTK-2** with the two D- π moieties connected through a phenyl ring were derived by oxidative homocoupling of a stannyli D- π unit and Stille coupling of a stannyli D- π unit with 1,3-diiodobenzene, respectively. Their optical and electrochemical properties were investigated by photoabsorption and fluorescence spectroscopy, time-resolved fluorescence spectroscopy, cyclic voltammetry (CV) and molecular orbital (MO) calculations. In toluene the photoabsorption and fluorescence maximum wavelengths ($\lambda_{\text{max,abs}}$ and $\lambda_{\text{max,fl}}$) of **OTT-2** appear in a longer wavelength region than those of **OTK-2**. The fluorescence quantum yield (Φ_{fl}) of **OTT-2** is 0.41, which is higher than that ($\Phi_{\text{fl}} = 0.36$) of **OTK-2**. In the solid state **OTT-2** shows relatively intense fluorescence properties ($\Phi_{\text{fl-solid}} = 0.24$ nm), compared with **OTK-2** ($\Phi_{\text{fl-solid}} = 0.15$ nm). CV results demonstrated that **OTT-2** and **OTK-2** exhibit a reversible oxidation wave. Based on photoabsorption, fluorescence spectroscopy and CV for the two dyes, it was found that the lowest unoccupied molecular orbital (LUMO) energy level of **OTT-2** is lower than that of **OTK-2**, but **OTT-2** and **OTK-2** have comparable highest occupied molecular orbital (HOMO) energy levels. Consequently, this work reveals that compared to the (D- π)₂Ph-type structure, the (D- π)₂-type structure exhibits not only a bathochromic shift of the photoabsorption band, but also intense fluorescence emission both in solution and the solid state.

Introduction

The design and development of a new type of organic fluorescent dyes have been of considerable scientific and practical concern with the objective of not only fundamental studies

[1–13] in synthetic chemistry, electrochemistry and photochemistry, but also their potential applications to emitters for optoelectronic devices, such as organic light-emitting diodes

(OLEDs) [14–22], as well as fluorescent probes [23–28] for bioimaging and fluorescent sensors for specific target species [29–32]. Among many kinds of organic fluorescent dyes, much efforts have been made on the development of donor– π –acceptor (D– π –A)-type fluorescent dyes constructed of an electron-donating moiety (D) and an electron-withdrawing moiety (A), linked by a π -conjugated unit thanks to their intense photoabsorption and fluorescence emission characteristics originating from the intramolecular charge transfer (ICT) excitation from the D to the A moiety [4–9,18–20,25,26]. Furthermore, the (D– π)₂A-type fluorescent dyes with two D– π moieties have recently been stimulating intensive research efforts because of their high molar extinction coefficients and fluorescence quantum yields, compared to those of D– π –A-type fluorescent dyes [10–13,21,22,27,28,32].

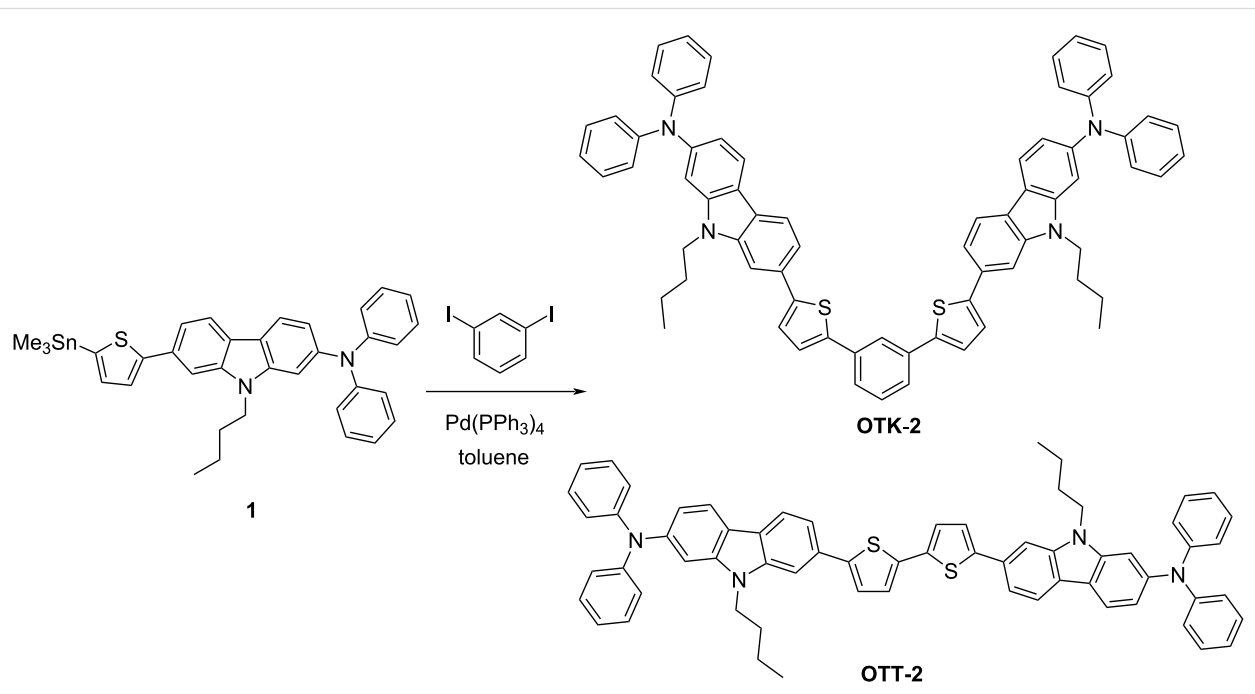
In our previous work [33], we have reported the synthesis, optical and electrochemical properties of the (D– π)₂Ph-type fluorescent dye **OTK-2** with two (diphenylamino)carbazole-thiophene units as D– π moiety connected through a phenyl ring (Scheme 1). The ICT-based photoabsorption and fluorescence bands of **OTK-2** appear in a shorter wavelength region than those of the corresponding (D– π)₂A-type fluorescent dye having an azine ring (pyridine, pyrazine or triazine ring) as a substitute for the phenyl ring. However, the molar extinction coefficient (ϵ_{max}) and fluorescence quantum yield (Φ_{fl}) of **OTK-2** are comparable to those of the (D– π)₂A-type fluorescent dyes. More recently, we found that the (D– π)₂-type fluo-

rescent dye **OTT-2** consisting of two D– π moieties is derived by oxidative homocoupling of a stannyli D– π unit. There is an obvious structural difference between the two dyes: **OTK-2** has a cross-conjugated system due to the involvement of the 1,3-phenylene unit as an additional linker, but **OTT-2** has a conjugated system. Therefore, it is interesting to reveal the optical and electrochemical properties of (D– π)₂-type fluorescent dyes, making a comparison with (D– π)₂Ph-type fluorescent dyes. Herein, we report the syntheses of (D– π)₂-type and (D– π)₂Ph-type fluorescent dyes and their optical and electrochemical properties based on photoabsorption and fluorescence spectroscopy, time-resolved fluorescence spectroscopy, cyclic voltammetry (CV) and molecular orbital (MO) calculations.

Results and Discussion

Using a toluene solution containing 1,3-diiodobenzene and (diphenylamino)carbazole-thiophenestannane derivative **1** [33] in the presence of $\text{Pd}(\text{PPh}_3)_4$, the (D– π)₂-type and (D– π)₂Ph-type fluorescent dyes **OTK-2** [33] and **OTT-2** were obtained by Stille coupling of **1** with 1,3-diiodobenzene and oxidative homocoupling of **1**, respectively (Scheme 1).

The photoabsorption and fluorescence spectra of **OTK-2** and **OTT-2** in toluene are shown in Figure 1a,b, and their optical data are summarized in Table 1. As shown in insets of Figure 1a,b, the toluene solutions of **OTK-2** and **OTT-2** are nearly-colorless and greenish-yellow, and show blue and green fluorescent colors, respectively. The photoabsorption spectra



Scheme 1: Synthesis of **OTK-2** and **OTT-2**.

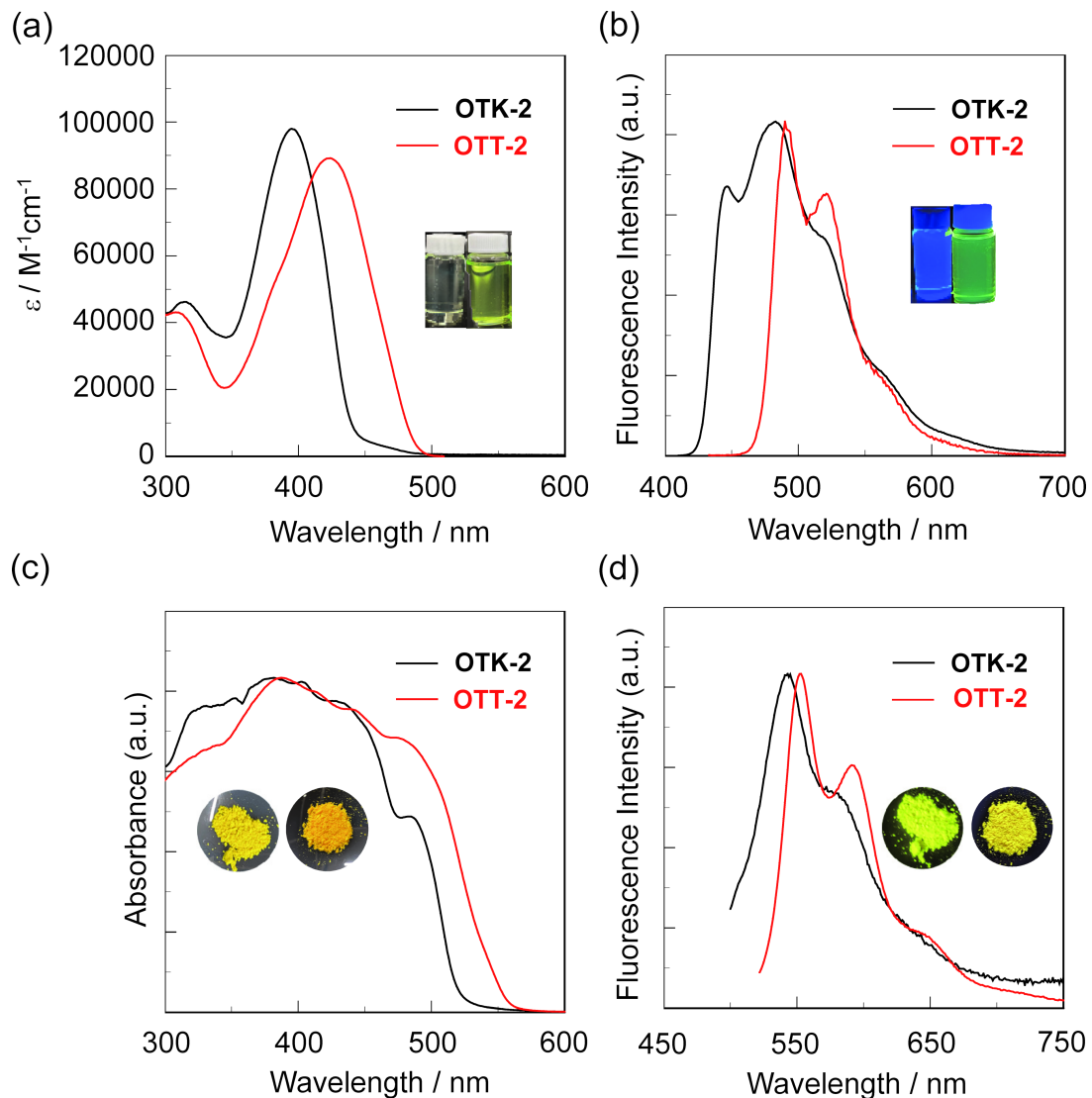


Figure 1: (a) Photoabsorption and (b) fluorescence ($\lambda_{\text{ex}} = \lambda_{\text{max,abs}}$) spectra of **OTK-2** [33] and **OTT-2** in toluene. (c) Solid-state UV–vis diffuse reflection–absorption and (b) and (d) fluorescence spectra ($\lambda_{\text{ex}} = 484$ nm for **OTK-2** [33] and 512 nm for **OTT-2**) of **OTK-2** and **OTT-2** in the solid state. Insets in (a) and (b): color and fluorescence images of **OTK-2** (left) and **OTT-2** (right) in toluene. Insets in (c) and (d): color and fluorescence images of **OTK-2** (left) and **OTT-2** (right) in the solid state. The photos depicted as insets in Figure 1a–d were reproduced from [33] (“Mechanofluorochromism of (D–π–)2A-type azine-based fluorescent dyes, © 2022 K. Takemura et al., published by the Royal Society of Chemistry, distributed under the terms of the Creative Commons Attribution 3.0 Unported License, <https://creativecommons.org/licenses/by/3.0/>”).

Table 1: Optical data of **OTK-2** [33] and **OTT-2** in toluene.

Dye	$\lambda_{\text{max,abs}}$ [nm] (ϵ [$\text{M}^{-1}\text{cm}^{-1}$])	$\lambda_{\text{max,fl}}$ [nm] (Φ_{fl}) ^a	SS [cm^{-1}] ^b	τ_{fl} [ns] ^c	k_{r} [s^{-1}] ^d	k_{nr} [s^{-1}] ^e	$k_{\text{nr}}/k_{\text{r}}$
OTK-2	395 (98 000)	447 (0.36)	2945	0.62	5.8×10^8	1.0×10^9	1.7
OTT-2	424 (89 200)	490 (0.41)	3177	0.66	6.2×10^8	8.9×10^8	1.4

^aFluorescence quantum yields (Φ_{fl}) were determined by using a calibrated integrating sphere system ($\lambda_{\text{ex}} = \lambda_{\text{max,abs}}$); ^bStokes shift; ^cfluorescence lifetime; ^dradiative rate constant ($k_{\text{r}} = \Phi_{\text{fl}}/\tau_{\text{fl}}$); ^enonradiative rate constant ($k_{\text{nr}} = (1 - \Phi_{\text{fl}})/\tau_{\text{fl}}$).

demonstrate that the photoabsorption maximum wavelength ($\lambda_{\text{max,abs}} = 424$ nm) of **OTT-2** occurs at a by 29 nm longer wavelength than that ($\lambda_{\text{max,abs}} = 395$ nm) of **OTK-2**. The ϵ_{max} value for the $\lambda_{\text{max,abs}}$ of **OTT-2** is $89\,200\,\text{M}^{-1}\,\text{cm}^{-1}$, which is comparable to that ($\epsilon_{\text{max}} = 98\,000\,\text{M}^{-1}\,\text{cm}^{-1}$) of **OTK-2**. In the corresponding fluorescence spectra, as in the case of **OTK-2**, **OTT-2** exhibited a vibronically-structured fluorescence band. The fluorescence maximum ($\lambda_{\text{max,fl}}$) of **OTT-2** appeared at 490 nm, which is a by 43 nm longer wavelength than that ($\lambda_{\text{max,fl}} = 447$ nm) of **OTK-2**. The Stokes shift (SS) value of **OTT-2** is estimated to be $3177\,\text{cm}^{-1}$, which is higher than that ($2945\,\text{cm}^{-1}$) of **OTK-2**. In addition, the Φ_{fl} of **OTT-2** is 0.41, which is higher than that ($\Phi_{\text{fl}} = 0.36$) of **OTK-2**. Time-resolved fluorescence spectroscopy of the two dyes revealed that the fluorescence lifetimes (τ_{fl}) are 0.62 ns for **OTK-2** and 0.66 ns for **OTT-2**, indicating that there is a little difference in the τ_{fl} values of the two dyes. The radiative rate constant ($k_{\text{r}} = 6.2 \times 10^8\,\text{s}^{-1}$) for **OTT-2** is slightly larger than that ($5.8 \times 10^8\,\text{s}^{-1}$) for **OTK-2**. However, the nonradiative rate constant ($k_{\text{nr}} = 8.9 \times 10^8\,\text{s}^{-1}$) of **OTT-2** is smaller than that ($1.0 \times 10^9\,\text{s}^{-1}$) for **OTK-2**. As the result, the ratio of nonradiative constant to radiative constant ($k_{\text{nr}}/k_{\text{r}} = 1.4$) for **OTT-2** is smaller than that (1.7) for **OTK-2**, suggesting that the higher Φ_{fl} value of **OTT-2** is mainly attributed to the smaller k_{nr} value compared with that of **OTK-2**.

The solid-state optical properties of **OTK-2** and **OTT-2** were investigated by solid-state UV–vis diffuse reflection–photoabsorption and fluorescence spectral measurements, and time-resolved fluorescence spectroscopy for the solids (Figure 1c,d). As shown in insets of Figure 1c,d, in the solid state, the colors are yellowish orange for **OTK-2** and orange for **OTT-2**, and the fluorescent colors are greenish yellow for **OTK-2** and yellow for **OTT-2**. The photoabsorption bands of **OTK-2** and **OTT-2** in the solid state are broadened in a longer wavelength region with an onset of ca. 520–550 nm, and the $\lambda_{\text{max,abs-solid}}$ of **OTK-2** and **OTT-2** appeared at around 480 nm, which showed bathochromic shifts by 85 nm and 56 nm, respectively, compared with those in toluene (Table 2). The corresponding solid-state fluorescence spectra demonstrated that as in the case of

toluene solutions, **OTK-2** and **OTT-2** in the solid state exhibited a vibronically-structured fluorescence band. The $\lambda_{\text{max,fl-solid}}$ of **OTK-2** and **OTT-2** occur at 543 nm and 552 nm, which exhibited significant bathochromic shifts of 96 nm and 62 nm, respectively, compared with those in toluene. The $\Phi_{\text{fl-solid}}$ (0.24) of **OTT-2** is higher than that ($\Phi_{\text{fl-solid}} = 0.15$) of **OTK-2**, while the $\Phi_{\text{fl-solid}}$ of **OTK-2** and **OTT-2** are lower than those in toluene. Although single crystals of **OTK-2** and **OTT-2** with sufficient size for X-ray structural analysis were not obtained, the intermolecular π – π interactions between the fluorophores leading to delocalization of excitons or excimers in the solid state would be responsible for the bathochromic shifts of $\lambda_{\text{max,abs}}$ and $\lambda_{\text{max,fl}}$ and lowering of Φ_{fl} with change of state from solution to solid [34–36]. The $\tau_{\text{fl-solid}}$ values of **OTK-2** and **OTT-2** are longer than those in toluene, however, the $\tau_{\text{fl-solid}}$ value (1.03 ns) of **OTT-2** is comparable to that ($\tau_{\text{fl-solid}} = 0.93$ ns) of **OTK-2**. Whereas the $k_{\text{r-solid}}$ value ($2.3 \times 10^8\,\text{s}^{-1}$) for **OTT-2** is larger than that ($1.6 \times 10^8\,\text{s}^{-1}$) for **OTK-2**, the $k_{\text{nr-solid}}$ value ($7.4 \times 10^8\,\text{s}^{-1}$) for **OTT-2** is slightly smaller than that ($9.4 \times 10^8\,\text{s}^{-1}$) for **OTK-2**. Consequently, the $k_{\text{nr-solid}}/k_{\text{r-solid}}$ values for **OTK-2** and **OTT-2** in the solid state are 5.7 and 3.2, respectively, which are larger than those (1.7 and 1.4, respectively) in toluene, indicating that the nonradiative decay in the solid state is accelerated. However, the $k_{\text{nr-solid}}/k_{\text{r-solid}}$ value (3.2) of **OTT-2** is smaller than that (5.7) of **OTK-2**, suggesting that the higher $\Phi_{\text{fl-solid}}$ value of **OTT-2** is due to the larger k_{r} value compared with that of **OTK-2**. Therefore, it was found that the (D– π)₂-type structure exhibits not only the bathochromic shift of photoabsorption band but also intense fluorescence emission both in solution and the solid state, compared to the (D– π)₂Ph-type structure.

The electrochemical properties of **OTK-2** and **OTT-2** (0.1 mM) were evaluated using CV in DMF containing 0.1 M tetrabutylammonium perchlorate (Bu_4NClO_4), in which the potentials were internally referenced to ferrocene/ferrocenium (Fc/Fc^+). The electrochemical data are summarized in Table 3. The cyclic voltammograms of the two dyes show a reversible oxidation wave with the anodic peak potential ($E_{\text{pa}}^{\text{ox}}$) at 0.32 V for **OTK-2** and 0.40 V for **OTT-2** (Figure 2), while any obvious

Table 2: Optical data of **OTK-2** [33] and **OTT-2** in the solid-state.

Dye	$\lambda_{\text{max,abs-solid}}$ [nm]	$\lambda_{\text{max,fl-solid}}$ [nm] ($\Phi_{\text{fl-solid}}$) ^a	$\tau_{\text{fl-solid}}$ [ns] ^b	$k_{\text{r-solid}}$ [s^{-1}] ^c	$k_{\text{nr-solid}}$ [s^{-1}] ^d	$k_{\text{nr-solid}}/k_{\text{r-solid}}$
OTK-2	480 shoulder	543 (0.15)	0.93	1.6×10^8	9.1×10^8	5.7
OTT-2	480 shoulder	552 (0.24)	1.03	2.3×10^8	7.4×10^8	3.2

^aFluorescence quantum yields ($\Phi_{\text{fl-solid}}$) were determined by using a calibrated integrating sphere system (484 nm for **OTK-2** and $\lambda_{\text{ex}} = 512$ nm for **OTT-2**, respectively); ^bfluorescence lifetime; ^cradiative rate constant ($k_{\text{r-solid}} = \Phi_{\text{fl-solid}}/\tau_{\text{fl-solid}}$); ^dnonradiative rate constant ($k_{\text{nr-solid}} = (1 - \Phi_{\text{fl-solid}})/\tau_{\text{fl-solid}}$).

Table 3: Electrochemical data, and HOMO and LUMO energy levels of **OTK-2** and **OTT-2**.

Dye	E_{pa}^{ox} [V] ^a	E_{pc}^{ox} [V] ^a	$E_{1/2}^{ox}$ [V] ^a	HOMO [eV] ^b	LUMO [eV] ^c	E_{0-0} [eV] ^d
OTK-2	0.32	0.24	0.28	-5.08	-2.29	2.79 eV
OTT-2	0.40	0.30	0.35	-5.15	-2.54	2.61 eV

^aThe anodic peak (E_{pa}^{ox}), the cathodic peak (E_{pc}^{ox}) and the half-wave ($E_{1/2}^{ox}$) potentials for oxidation vs Fc/Fc⁺ were recorded in DMF/Bu₄NClO₄ (0.1 M) solution; ^b[- $E_{1/2}^{ox}$ + 4.8] eV; ^c[HOMO + E_{0-0}] eV; ^d444 nm for **OTK-2** and 475 nm for **OTT-2**.

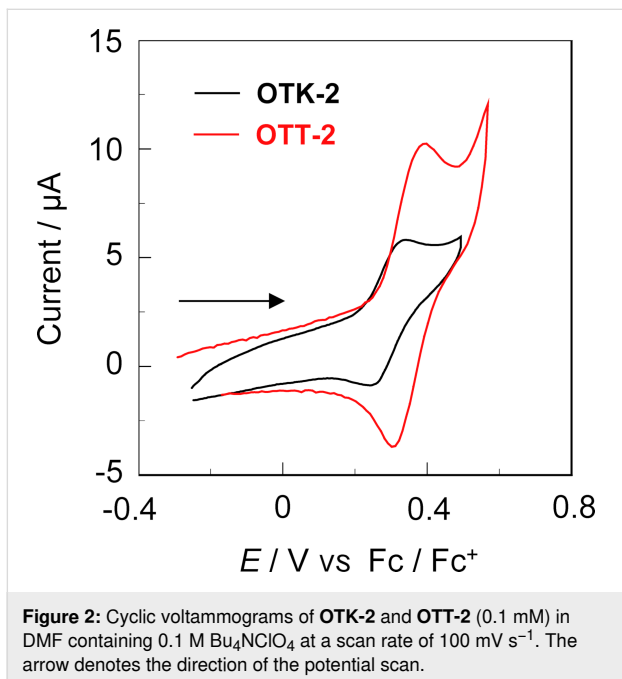


Figure 2: Cyclic voltammograms of **OTK-2** and **OTT-2** (0.1 mM) in DMF containing 0.1 M Bu₄NClO₄ at a scan rate of 100 mV s⁻¹. The arrow denotes the direction of the potential scan.

reduction waves and another oxidation waves did not appear within the potential window (Figure 3a and Figure S2a, Supporting Information File 1). The corresponding cathodic peak potential (E_{pc}^{ox}) appeared at 0.24 V for **OTK-2** and 0.30 V for **OTT-2**, and thus the peak separations between the E_{pa}^{ox} and E_{pc}^{ox} waves are ca. 80–100 mV. This result may indicate that the two dyes undergo an electrochemically stable one-electron oxidation–reduction process, but further studies are necessary to exactly determine the number of electrons in the oxidation–reduction process. The half-wave potential ($E_{1/2}^{ox}$) was evaluated to be 0.28 V for **OTK-2** and 0.35 V for **OTT-2**. Therefore, the $E_{1/2}^{ox}$ for **OTK-2** with the (D– π)₂Ph-type structure is cathodically shifted by 0.07 V, compared with that for **OTT-2** with the (D– π)₂-type structure. Furthermore, we investigated the diffusion-controlled process form CV at different scan rates (50, 100, 200, 400, 600 and 1000 mV s⁻¹) and reversibility of the oxidation process by repeated potential cycling (20 cycles). For both **OTK-2** and **OTT-2**, the E_{pa}^{ox} remained steady at different scan rates while the anodic peak current (I_{pa}) increased with the increase in scan rate. The I_{pa} showed a negligible change during 20 cycles at a scan rate of 100 mV s⁻¹, in-

dicating diffusion control and good reversibility of the oxidation process (Figures S2b,c and S3b,c, Supporting Information File 1). The highest occupied molecular orbital (HOMO) energy level versus vacuum level was estimated from the $E_{1/2}^{ox}$, that is, $-[E_{1/2}^{ox} + 4.8]$ eV. On the other hand, the lowest unoccupied molecular orbital (LUMO) energy level versus the vacuum level was estimated by using [HOMO + E_{0-0}] eV from the $E_{1/2}^{ox}$ and intersections (optical energy gap: E_{0-0} = 2.79 eV for **OTK-2** and 2.61 eV for **OTT-2**) of the photoabsorption and fluorescence spectra in toluene. It was found that the HOMO energy level (−5.15 eV) of **OTT-2** is slightly lower than that (−5.08 eV) of **OTK-2**, indicating that the two dyes have comparable HOMO energy levels. On the other hand, the LUMO energy level (−2.54 eV) of **OTT-2** is significantly lower than that (−2.29 eV) of **OTK-2**. Semi-empirical MO calculations (PM5, INDO/S method) revealed that for **OTK-2** both the HOMO and LUMO were mostly localized on the two (diphenylamino)carbazole-thiophene moieties. On the other hand, for **OTT-2** both the HOMO and LUMO are delocalized over the whole molecule through the thiophene units (Figure 3). Consequently, the fact reveals that compared to the (D– π)₂Ph-type structure, the (D– π)₂-type structure can cause not only the stabilization of the LUMO energy level but also the delocalization of the HOMO and LUMO over the whole molecule, leading to a narrower HOMO–LUMO band gap of **OTT-2** than **OTK-2**, that is, the bathochromic shift of the photoabsorption band from **OTT-2** to **OTK-2**.

Conclusion

We have developed the (D– π)₂-type fluorescent dye **OTT-2** and the (D– π)₂Ph-type fluorescent dye **OTK-2** and evaluated their optical and electrochemical properties. Both in solution and the solid state, the photoabsorption and fluorescence maximum wavelengths of **OTT-2** appear in a longer wavelength region than those of **OTK-2**, and the fluorescence quantum yields of **OTT-2** are higher than those of **OTK-2**. The cyclic voltammograms demonstrated that **OTT-2** and **OTK-2** exhibit a reversible oxidation wave, indicating that the two dyes undergo an electrochemically stable oxidation–reduction process. It was found that the LUMO energy level of **OTT-2** is lower than that of **OTK-2**, while **OTT-2** and **OTK-2** have comparable HOMO energy levels. Semi-empirical MO calculations showed that for

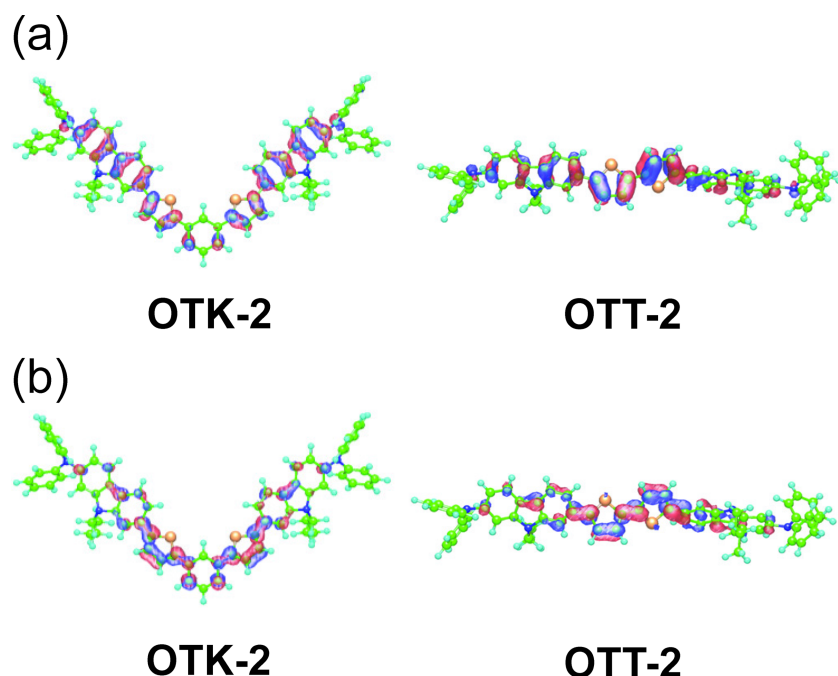


Figure 3: (a) HOMO and (b) LUMO of **OTK-2** [33] and **OTT-2** derived from MO calculations (PM5, INDO/S method). The red and blue lobes denote the positive and negative signs of the coefficients of the molecular orbitals. The size of each lobe is proportional to the MO coefficient.

OTK-2 both the HOMO and LUMO were mostly localized on the two D– π moieties, whereas for **OTT-2** both the HOMO and LUMO are delocalized over the whole molecule through the thiophene units. Consequently, this work reveals that compared to the (D– π)₂Ph-type structure, the (D– π)₂-type structure not only has intense fluorescence emission properties both in solution and the solid state, but also can cause delocalization of the HOMO and the LUMO over the whole molecule as well as the stabilization of the LUMO energy level, leading to a narrower HOMO–LUMO band gap of **OTT-2** than **OTK-2**, that is, the bathochromic shift of photoabsorption band from **OTT-2** to **OTK-2**.

Experimental

General methods

Melting points were measured with an AS ONE ATM-02 apparatus. IR spectra were recorded on a SHIMADZU IRTtracer-100 spectrometer by ATR method. ¹H NMR and ¹³C NMR spectra were recorded on a Varian-500 FT NMR spectrometer. High-resolution mass spectral data by APCI were acquired on a Thermo Fisher Scientific LTQ Orbitrap XL apparatus. Photoabsorption spectra of solutions were observed with a Shimadzu UV-3600 plus spectrophotometer. Photoabsorption spectra of solids were recorded by a Shimadzu UV-3600 plus spectrophotometer with a calibrated integrating sphere system. Fluorescence spectra of solutions and solids were measured with a HORIBA FluoroMax-4 spectrofluorometer. Fluorescence quan-

tum yields in solution and in the solid state were determined using a HORIBA FluoroMax-4 spectrofluorometer with a calibrated integrating sphere system. Fluorescence decay measurements were performed on a HORIBA DeltaFlex modular fluorescence lifetime system using a Nano LED pulsed diode excitation source (451 nm). Cyclic voltammetry (CV) curves were recorded in DMF/Bu₄NClO₄ (0.1 M) solution with a three-electrode system consisting of Ag/Ag⁺ as the reference electrode, a Pt plate as the working electrode and a Pt wire as the counter electrode using an Electrochemical Measurement System HZ-7000 (HOKUTO DENKO). Semi-empirical molecular orbital calculations were carried out with the WinMOPAC Ver. 3.9 package (Fujitsu, Chiba, Japan), where geometry calculations of the compounds in the ground state were made using the PM5 method. Dipole moments and HOMO and LUMO energy levels of the compounds were also evaluated from INDO/S calculations.

Synthesis

7,7'-(1,3-Phenylenebis(thiophene-5,2-diyl))bis(9-butyl-N,N-diphenyl-9H-carbazol-2-amine) (OTK-2) and 7,7'-(1,2,2'-bithiophene]-5,5'-diyl)bis(9-butyl-N,N-diphenyl-9H-carbazol-2-amine) (OTT-2): A solution of **1** (87 mg, 0.137 mmol), 1,3-diiodobenzene (14 mg, 0.041 mmol), and Pd(PPh₃)₄ (2 mg, 0.001 mmol) in toluene (1 mL) was stirred for 29 h at 110 °C under an argon atmosphere. The reaction mixture was diluted with water, and then, the solution was extracted

with dichloromethane. The dichloromethane extract was dried over anhydrous MgSO_4 , filtrated, and concentrated. The residue was chromatographed on silica gel (ethyl acetate/hexane 1:4) to give **OTK-2** (19 mg, yield 27%) and **OTT-2** (9 mg, yield 14%) as a light yellow solid and an orange solid, respectively; the characterization data for **OTK-2** are in agreement with those reported in the literature [33]; **OTT-2**: mp >300 °C; FTIR (ATR) \bar{v} : 1591, 1491, 1460 cm^{-1} ; ^1H NMR (500 MHz, CD_2Cl_2) δ 0.76–1.02 (m, 6H), 1.23–1.38 (m, 4H), 1.71–1.81 (m, 4H), 4.12–4.21 (m, 4H), 6.95 (dd, J = 1.8 and 8.4 Hz, 2H), 7.01–7.05 (m, 4H), 7.10–7.16 (m, 10H), 7.24–7.31 (m, 10H), 7.39 (d, J = 3.8 Hz, 2H), 7.50 (dd, J = 1.4 and 8.0 Hz, 2H), 7.59 (d, J = 1.2 Hz, 2H), 7.93 (d, J = 8.3 Hz, 2H), 7.99 (d, J = 8.0 Hz, 2H) ppm; ^{13}C NMR (125 MHz, CD_2Cl_2) δ 14.04, 20.85, 31.44, 43.04, 105.37, 105.84, 117.54, 117.56, 118.73, 120.46, 121.16, 122.94, 122.96, 124.02, 124.36, 124.84, 129.55, 131.14, 136.68, 141.67, 142.73, 144.74, 146.92, 148.61 ppm; HRMS (APCI) m/z (%): [M + H^+] calcd. for $\text{C}_{64}\text{H}_{55}\text{N}_4\text{S}_2$, 943.38627; found, 943.38635.

Supporting Information

Supporting Information File 1

^1H and ^{13}C NMR spectra of **OTT-2**.

[<https://www.beilstein-journals.org/bjoc/content/supplementary/1860-5397-18-106-S1.pdf>]

Funding

This work was supported by the Grant-in-Aids for Scientific Research on Innovative Areas “Soft Crystals” (No. 2903) (JSPS KAKENHI Grant No. 18H04520) and the Suga Weathering Technology Foundation.

ORCID® iDs

Keiichi Imato - <https://orcid.org/0000-0002-6305-6453>

Yousuke Ooyama - <https://orcid.org/0000-0002-0257-6930>

References

1. Kubo, Y.; Nozawa, T.; Maeda, K.; Hashimoto, Y. *Mater. Adv.* **2021**, *2*, 1059–1071. doi:10.1039/d0ma00910e
2. Dai, J.; Yao, L.; Wang, C.; Wang, Y.; Liu, F.; Yan, X.; Sun, P.; Zhang, H.; Wang, Y.; Zhou, J.; Lu, G. *J. Phys. Chem. Lett.* **2022**, *13*, 4754–4761. doi:10.1021/acs.jpclett.2c01226
3. Walęsa-Chorab, M.; Muras, K.; Filiault, H. L.; Skene, W. G. *J. Mater. Chem. C* **2022**, *10*, 3691–3703. doi:10.1039/d1tc03388c
4. Ooyama, Y.; Ito, G.; Kushimoto, K.; Komaguchi, K.; Imae, I.; Harima, Y. *Org. Biomol. Chem.* **2010**, *8*, 2756–2770. doi:10.1039/c003526b
5. Ooyama, Y.; Harima, Y. *J. Mater. Chem.* **2011**, *21*, 8372–8380. doi:10.1039/c0jm03601c
6. Josse, P.; Allain, M.; Calupitan, J. P.; Jiang, Y.; Cabanetos, C.; Roncali, J. *Adv. Opt. Mater.* **2020**, *8*, 2000420. doi:10.1002/adom.202000420
7. Feng, X.; Chen, Y.; Lei, Y.; Zhou, Y.; Gao, W.; Liu, M.; Huang, X.; Wu, H. *Chem. Commun.* **2020**, *56*, 13638–13641. doi:10.1039/d0cc05538g
8. Zhang, X.; Ma, Z.; Yang, Y.; Zhang, X.; Jia, X.; Wei, Y. *J. Mater. Chem. C* **2014**, *2*, 8932–8938. doi:10.1039/c4tc01457j
9. Liu, J.; Cui, Y.; Pan, Y.; Chen, Z.; Jia, T.; Li, C.; Wang, Y. *Angew. Chem., Int. Ed.* **2022**, *61*, e202117087. doi:10.1002/anie.202117087
10. Narayanaswamy, K.; Venkateswararao, A.; Gupta, V.; Chand, S.; Singh, S. P. *Chem. Commun.* **2016**, *52*, 210–213. doi:10.1039/c5cc07435e
11. Roy, S.; Nandi, S. K.; Halder, D.; Pal, B. *J. Mater. Chem. C* **2022**, *10*, 8767–8775. doi:10.1039/d2tc00951j
12. Yu, L.; Xi, J.; Chan, H. T.; Su, T.; Antrobus, L. J.; Tong, B.; Dong, Y.; Chan, W. K.; Phillips, D. L. *J. Phys. Chem. C* **2013**, *117*, 2041–2052. doi:10.1021/jp3113182
13. Enoki, T.; Ohshita, J.; Ooyama, Y. *Bull. Chem. Soc. Jpn.* **2018**, *91*, 1704–1709. doi:10.1246/bcsj.20180210
14. Yagi, S. Luminous Materials for Organic Light-Emitting Diodes. In *Progress in the Science of Functional Dyes*; Ooyama, Y.; Yagi, S., Eds.; Springer Nature: Singapore, 2021; pp 561–601. doi:10.1007/978-981-33-4392-4_16
15. Gregory, P. Functional Dyes. In *Industrial Dyes*; Hunger, K., Ed.; Wiley-VCH: Weinheim, Germany, 2003; pp 543–584. doi:10.1002/3527602011.ch6
16. Zollinger, H. Photo-, Thermo-, and Electrochemical Reactions of Colorants. Wiley-VCH: Weinheim, Germany, 2003; pp 429–504.
17. Rao, J.; Yang, L.; Li, X.; Zhao, L.; Wang, S.; Tian, H.; Ding, J.; Wang, L. *Angew. Chem., Int. Ed.* **2021**, *60*, 9635–9641. doi:10.1002/anie.202016428
18. Tagare, J.; Vaidyanathan, S. *J. Mater. Chem. C* **2018**, *6*, 10138–10173. doi:10.1039/c8tc03689f
19. Shi, J.; Ding, Q.; Xu, L.; Lv, X.; Liu, Z.; Sun, Q.; Pan, Y.; Xue, S.; Yang, W. *J. Mater. Chem. C* **2018**, *6*, 11063–11070. doi:10.1039/c8tc03777a
20. Qiu, X.; Ying, S.; Wang, C.; Hanif, M.; Xu, Y.; Li, Y.; Zhao, R.; Hu, D.; Ma, D.; Ma, Y. *J. Mater. Chem. C* **2019**, *7*, 592–600. doi:10.1039/c8tc05469j
21. Cai, X.; Li, X.; Xie, G.; He, Z.; Gao, K.; Liu, K.; Chen, D.; Cao, Y.; Su, S.-J. *Chem. Sci.* **2016**, *7*, 4264–4275. doi:10.1039/c6sc00542j
22. Ji, S.-C.; Jiang, S.; Zhao, T.; Meng, L.; Chen, X.-L.; Lu, C.-Z. *New J. Chem.* **2022**, *46*, 8991–8998. doi:10.1039/d2nj01072k
23. Kundu, S.; Chowdhury, A.; Nandi, S.; Bhattacharyya, K.; Patra, A. *Chem. Sci.* **2021**, *12*, 5874–5882. doi:10.1039/d0sc07050e
24. Liu, X.-Y.; Wang, X.-J.; Shi, L.; Liu, Y.-H.; Wang, L.; Li, K.; Bu, Q.; Cen, X.-B.; Yu, X.-Q. *Anal. Chem. (Washington, DC, U. S.)* **2022**, *94*, 7665–7673. doi:10.1021/acs.analchem.2c01046
25. Xu, C.; Li, Y.; Wu, X.; Li, X.; Li, L.; Kong, F.; Tang, B. *Chem. Commun.* **2022**, *58*, 5976–5979. doi:10.1039/d2cc01607a
26. Liu, Z.; Wang, Q.; Qiu, W.; Lyu, Y.; Zhu, Z.; Zhao, X.; Zhu, W.-H. *Chem. Sci.* **2022**, *13*, 3599–3608. doi:10.1039/d2sc00067a
27. Dai, X.; Dong, B.; Ren, M.; Lin, W. *J. Mater. Chem. B* **2018**, *6*, 381–385. doi:10.1039/c7tb02414b
28. Li, Y.; Wang, K.; Zhou, K.; Guo, W.; Dai, B.; Liang, Y.; Dai, J.; Cui, M. *Chem. Commun.* **2018**, *54*, 8717–8720. doi:10.1039/c8cc05259j

29. Jacob, F. Fluorescent Molecular Sensors of Ions and Molecules. In *Molecular Fluorescence*; Valeur, B., Ed.; Wiley-VCH: Weinheim, Germany, 2002; pp 273–350. doi:10.1002/3527600248.ch10
30. Ooyama, Y. Fluorescent Sensors for Water. In *Sustainable and Functional Redox Chemistry*; Inagi, S., Ed.; Royal Society of Chemistry: Cambridge, UK, 2022; pp 300–330. doi:10.1039/9781839164828-00300
31. Sarkar, B.; Prasad, E.; Gardas, R. L. *Mater. Adv.* **2022**, *3*, 2871–2883. doi:10.1039/d1ma01162f
32. Tsumura, S.; Enoki, T.; Ooyama, Y. *Chem. Commun.* **2018**, *54*, 10144–10147. doi:10.1039/c8cc06257a
33. Takemura, K.; Imato, K.; Ooyama, Y. *RSC Adv.* **2022**, *12*, 13797–13809. doi:10.1039/d2ra02431d
34. Ooyama, Y.; Okamoto, T.; Yamaguchi, T.; Suzuki, T.; Hayashi, A.; Yoshida, K. *Chem. – Eur. J.* **2006**, *12*, 7827–7838. doi:10.1002/chem.200600094
35. Langhals, H.; Potrawa, T.; Nöth, H.; Linti, G. *Angew. Chem., Int. Ed. Engl.* **1989**, *28*, 478–480. doi:10.1002/anie.198904781
36. Yeh, H.-C.; Wu, W.-C.; Wen, Y.-S.; Dai, D.-C.; Wang, J.-K.; Chen, C.-T. *J. Org. Chem.* **2004**, *69*, 6455–6462. doi:10.1021/jo049512c

License and Terms

This is an open access article licensed under the terms of the Beilstein-Institut Open Access License Agreement (<https://www.beilstein-journals.org/bjoc/terms>), which is identical to the Creative Commons Attribution 4.0 International License (<https://creativecommons.org/licenses/by/4.0>). The reuse of material under this license requires that the author(s), source and license are credited. Third-party material in this article could be subject to other licenses (typically indicated in the credit line), and in this case, users are required to obtain permission from the license holder to reuse the material.

The definitive version of this article is the electronic one which can be found at:

<https://doi.org/10.3762/bjoc.18.106>



Electrochemical hydrogenation of enones using a proton-exchange membrane reactor: selectivity and utility

Koichi Mitsudo, Haruka Inoue, Yuta Niki, Eisuke Sato and Seiji Suga^{*}

Full Research Paper

Open Access

Address:

Division of Applied Chemistry, Graduate School of Natural Science and Technology, Okayama University, 3-1-1 Tsushima-naka, Kita-ku, Okayama 700-8530, Japan

Email:

Seiji Suga^{*} - suga@cc.okayama-u.ac.jp

^{*} Corresponding author

Keywords:

enone; hydrogenation; iridium; palladium; PEM reactor

Beilstein J. Org. Chem. **2022**, *18*, 1055–1061.

<https://doi.org/10.3762/bjoc.18.107>

Received: 01 June 2022

Accepted: 11 August 2022

Published: 19 August 2022

This article is part of the thematic issue "Molecular and macromolecular electrochemistry: synthesis, mechanism, and redox properties".

Guest Editor: S. Inagi

© 2022 Mitsudo et al.; licensee Beilstein-Institut.

License and terms: see end of document.

Abstract

Electrochemical hydrogenation of enones using a proton-exchange membrane reactor is described. The reduction of enones proceeded smoothly under mild conditions to afford ketones or alcohols. The reaction occurred chemoselectively with the use of different cathode catalysts (Pd/C or Ir/C).

Introduction

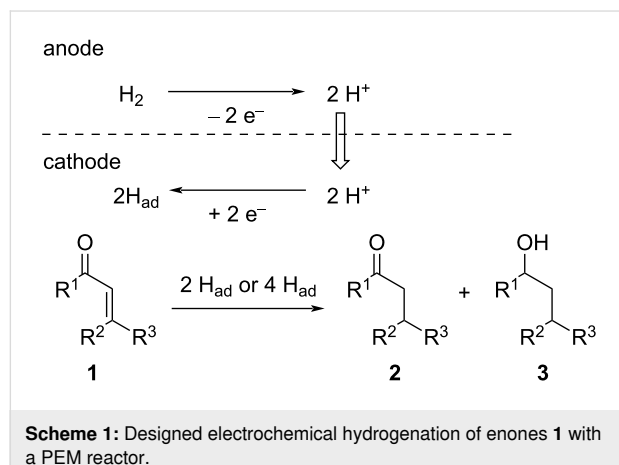
Catalytic hydrogenation of α,β -enones is a significant transformation in organic synthesis [1]. Hydrogenation of enones can give ketones, allyl alcohols, and saturated alcohols, and the control of the chemoselectivity is important. Therefore, there have been numerous studies on the hydrogenation of enones using homogeneous and heterogeneous catalysts.

Meanwhile, electrochemical systems using a proton-exchange membrane (PEM) reactor have been shown to be powerful tools for electrochemical hydrogenation [2–21]. A PEM reactor consists of a membrane called a membrane electrode assembly (MEA), which can act as supporting electrolyte, electrode, and heterogeneous catalyst. Therefore, the further addition of a supporting electrolyte is not necessary for the electrochemical reactions using a PEM reactor, which offers clean and environmen-

tally benign organic transformations. Despite these advantages, the utility of PEM reactors in precise organic synthesis has long been unclear. Recently, however, Atobe and co-workers showed that PEM reactors can be used as a powerful and novel tool for precise organic synthesis [22–26]. For instance, they recently reported a stereoselective reduction of alkynes to Z-alkenes using a PEM reactor. The use of a Pd/C cathode catalyst and the appropriate cathode potential realize the selective synthesis of Z-alkenes [22–24]. They also reported the stereoselective hydrogenation of α,β -unsaturated acids [25] and the reduction of benzoic acids [26].

We have been interested in electrochemical transformations for a long time [27–31] and are paying the most attention to the utility of PEM reactors for organic syntheses, especially chemo-

selective transformations. In our research, we examined the hydrogenation of enones using a PEM reactor. The designed process is illustrated in Scheme 1. Humidified hydrogen gas is passed through the anodic chamber and substrate is passed through the cathodic chamber. The hydrogen molecules are anodically oxidized to two protons. Then, they move to the cathodic chamber and are reduced by the catalyst of the MEA to monoatomic hydrogen species (adsorbed hydrogen, H_{ad}) [22]. Thus generated H_{ad} reduces enones **1** to give the corresponding hydrogenated products (ketones **2** and alcohols **3**). The expected advantage of PEM reactors is that the reactivity of H_{ad} should be controllable by the cathode catalyst and electrochemical parameters. Fortunately, we found that chemoselective reduction of enones **1** can be carried out using different cathode catalysts (Pd/C or Ir/C).



Results and Discussion

Electroreduction of enones to ketones

First, we chose cyclohex-2-en-1-one (**1a**) as a model compound, and the electroreduction of **1a** was carried out using a PEM reactor (Figure 1a, a single path). Pd/C was used as a cathode catalyst. Without electricity, trace amounts of cyclohexanone

(**2a**) and cyclohexanol (**3a**) were obtained (Table 1, entry 1). With a current of $2.5 \text{ mA}\cdot\text{cm}^{-2}$, **2a** and **3a** were obtained in a yield of 3% (current efficiency 66%) and 0.57% (current efficiency 5.7%), respectively (Table 1, entry 2). While **2a** was obtained with moderate current efficiency, the yield was far from satisfactory. Therefore, electroreduction with a higher current density was examined (Table 1, entries 3–7). The yield of **2a** increased with an increase in the current density (22% yield, $50 \text{ mA}\cdot\text{cm}^{-2}$).

To improve the conversion, we designed a circulating system for the PEM reactor (Figure 1b) and used it for the electroreduction of **1a** (Table 2). First, we carried out the electroreduction of **1a** with a current of $12.5 \text{ mA}\cdot\text{cm}^{-2}$. As expected, **1a** was almost entirely consumed after the passage of $2.0 \text{ F}\cdot\text{mol}^{-1}$, and **2a** was obtained in 67% yield as a major product (Table 2, entry 1). The yield of **2a** and **3a** was almost the same with a current of $25 \text{ mA}\cdot\text{cm}^{-2}$ (Table 2, entry 2). Further, the conversion of **1a** decreased to 82% with a current of $50 \text{ mA}\cdot\text{cm}^{-2}$, but **2a** was obtained in 64% yield with a similar current efficiency (64%). When the reaction was performed in cyclopentyl methyl ether (CPME) as a solvent, the yield of **2a** decreased to 54%, and **3a** was obtained in 11% yield (Table 2, entry 4).

Next, the effect of cathode catalysts was investigated (Table 3). With Ru catalyst, further reduction of the carbonyl group proceeded, and both **2a** (32% yield) and **3a** (14% yield) were obtained (Table 3, entry 2). With Rh catalyst, the conversion was up to 81%, while the yield of **2a** was similar to that with Ru catalyst (Table 3, entry 3). Similarly, both **2a** and **3a** were obtained with Ir and Pt catalyst (Table 3, entries 4 and 5). In particular, **3a** was obtained preferentially with the Ir catalyst. These results revealed that the cathode catalysts strongly affected the selectivity between **2a** and **3a**. Pd was the best catalyst for the selective synthesis of **2a**, and Ir catalyst should be suitable for the formation of **3a**, regarding the current efficiency and selectivity (Table 3, entry 4).

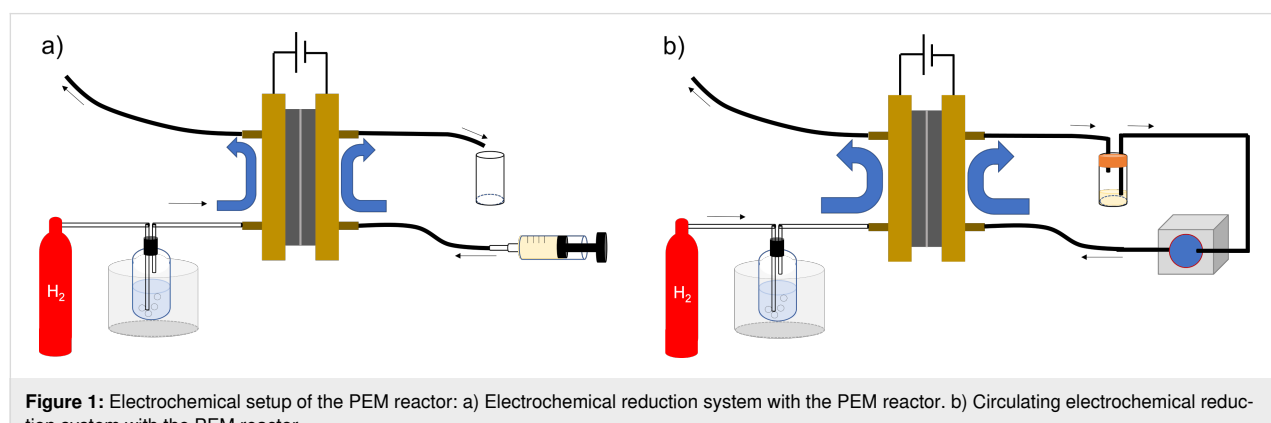


Table 1: Effect of the current density on the electrochemical hydrogenation of **1a** with a PEM reactor (a single path).^a

entry	current density (mA·cm ⁻²)	conversion (%)	yield (efficiency, %) ^b		selectivity of 2a (%)
			2a	3a	
1	0	8	2	0.43	84
2	2.5	<5	3 (66)	0.57 (5.7)	85
3	5	<5	4 (43)	0.52 (2.6)	89
4	10	10	6 (29)	0.52 (1.3)	92
5	12.5	15	7 (27)	0.50 (1.0)	93
6	25	19	12 (23)	0.46 (0.5)	96
7	50	28	22 (23)	0.50 (0.3)	98

^aReaction conditions: anode catalyst Pt/C, cathode catalyst Pd/C, concentration of **1a** 1.0 M, solvent dichloromethane, flow rate of the solution of **1a** 0.25 mL·min⁻¹, flow rate of H₂ gas 500 mL·min⁻¹, reaction temperature room temperature. ^bDetermined by GC analysis using *n*-dodecane as an internal standard. Values in parentheses are the current efficiency.

Table 2: Effect of the current density and solvent on the electrochemical hydrogenation of **1a** with a circulating PEM reactor.^a

entry	current density (mA·cm ⁻²)	conversion (%)	yield (efficiency, %) ^b		selectivity of 2a (%)
			2a	3a	
1	12.5	99	67 (67)	5 (11)	93
2	25	96	63 (63)	3 (5)	95
3	50	82	64 (64)	2 (4)	97
4 ^c	50	82	54 (54)	11 (22)	83

^aReaction conditions: anode catalyst Pt/C, concentration of **1a** 1.0 M, solvent dichloromethane, flow rate of the solution of **1a** 0.25 mL·min⁻¹, flow rate of H₂ gas, 100 mL·min⁻¹, reaction temperature room temperature, current density 50 mA·cm⁻². The solution was circulated until the passage of 2.0 F·mol⁻¹. ^bDetermined by GC analysis using *n*-dodecane as an internal standard. Values in parentheses show the current efficiency. ^cPerformed in CPME instead of dichloromethane.

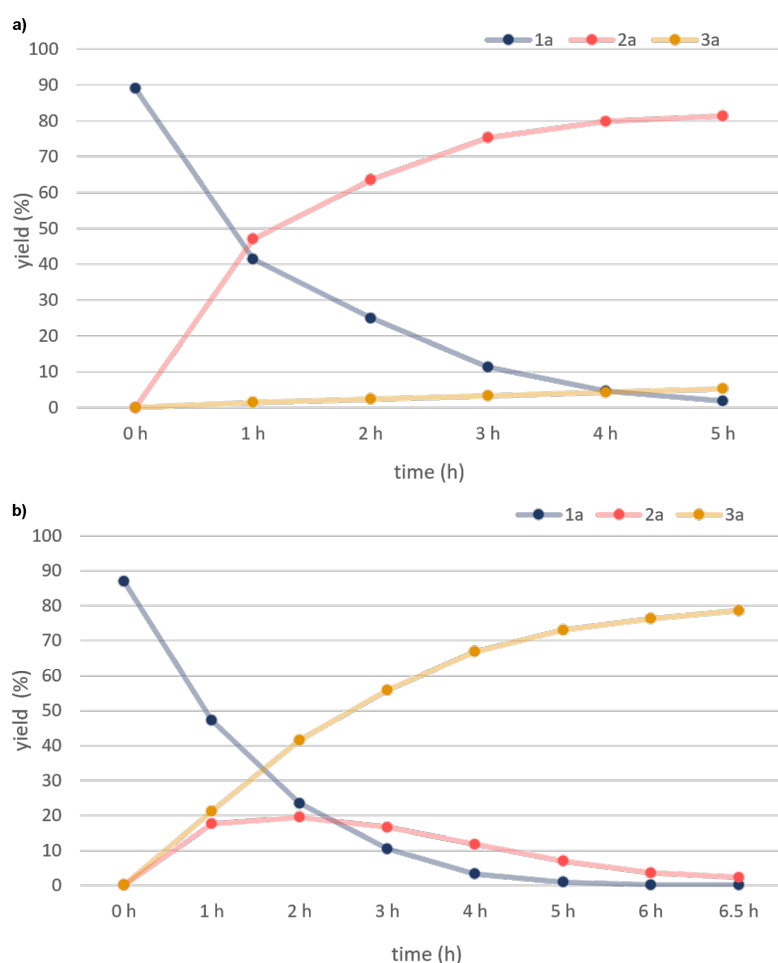
We also observed reaction profiles of the hydrogenation of **1a** with the use of a Pd/C and Ir/C cathode catalyst, respectively (Figure 2). When a Pd/C catalyst was used, **1a** was hydrogenated to **2a** selectively, and further reduction to **3a** was almost completely suppressed (Figure 2a). In contrast, the use of an Ir/C catalyst afforded both **2a** and **3a**, and generated **2a** was smoothly reduced to **3a** by further electrolysis (Figure 2b).

As mentioned above, ketone **2a** was obtained selectively with the use of a Pd/C catalyst for the cathode (Table 3, entry 1). To clarify the scope of the reaction, we carried out the electrochemical reduction of several enones **1** using Pd/C cathode catalyst (Scheme 2). After current was passed to the circulating system until **1a** was consumed, the ketone **2a**, obtained by the exclusive reduction of the C=C moiety, was obtained in 81% yield

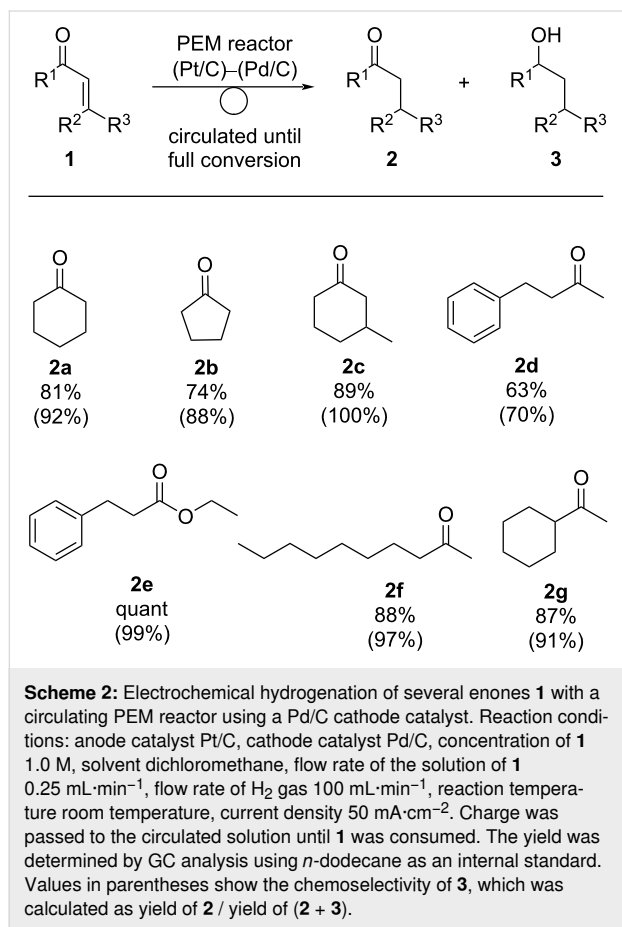
Table 3: Effect of catalysts on the electrochemical hydrogenation of **1a** with a circulating PEM reactor.^a

entry	cathode catalyst	conversion (%)	yield (efficiency, %) ^b		selectivity of 2a (%)
			2a	3a	
1	Pd/C	82	64 (64)	2 (4)	97
2	Ru/C	59	32 (32)	14 (28)	70
3	Rh/C	81	37 (37)	19 (39)	66
4	Ir/C	65	24 (24)	26 (52)	48
5	Pt/C	52	11 (12)	27 (56)	29

^aReaction conditions: anode catalyst Pt/C, concentration of **1a** 1.0 M, solvent dichloromethane, flow rate of the solution of **1a** 0.25 mL·min⁻¹, flow rate of H₂ gas 100 mL·min⁻¹, reaction temperature room temperature, current density 50 mA·cm⁻². The solution was circulated until the passage of 2.0 F·mol⁻¹. ^bDetermined by GC analysis using *n*-dodecane as an internal standard. Values in parentheses show the current efficiency.

**Figure 2:** Reaction profile of the electrochemical hydrogenation of **1a** with a PEM reactor using a) Pd/C and b) Ir/C cathode catalyst. The yield of **2a** and **3a** and the recovery of **1a** are shown in red, brown, and blue, respectively.

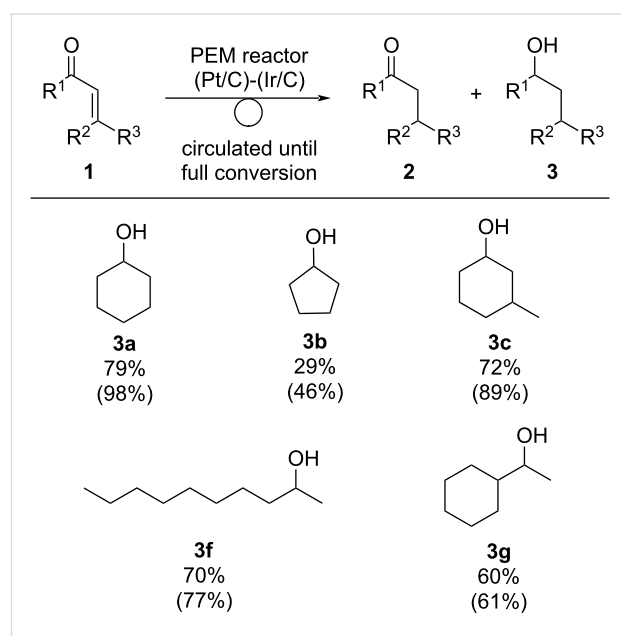
with a chemoselectivity of 92%. Similarly, cyclopentanone **2b** was obtained from the corresponding enone **1b** in 74% yield (88% selectivity). Substituted cyclohexanone such as 3-methylcyclohex-2-en-1-one (**1c**) gave the desired product **2c** selectively in 89% yield (100% selectivity). A benzene-conjugated ketone **1d** and an ester **1e** could also be subjected to electroreduction to afford the corresponding ketones **2d** and **2e** in 63% and quantitative yield, respectively. Linear enone **1f** gave the desired ketone **2f** in high yield (88%, 97% selectivity). Reduction with the PEM reactor also proceeded smoothly with enone **1g**, which has a cyclohexene moiety, to give the corresponding ketone **2g** in 87% yield (91% selectivity). As shown so far, several kinds of enones **1** could be subjected to electroreduction using the PEM reactor to afford ketones in high yield and selectivity.



Electroreduction of enones to saturated alcohols

We next examined the electrochemical reduction of several enones **1** to saturated alcohols **3** using an Ir/C catalyst for the cathode (Scheme 3). Full conversion of **1a** under the indicated conditions gave **3a** in 79% yield with 98% selectivity. In contrast, electroreduction of cyclopent-2-en-1-one (**1b**) gave

cyclopentanol **3b** in 29% yield (46% selectivity), but the reason has not been elaborated yet. With 3-methyl-2-cyclohexen-1-one (**1c**), alcohol **3c** was obtained 72% yield with good selectivity (89%). Both **1f** and **1g** could be used in this reactions, and the corresponding alcohols **3f** and **3g** were obtained as major products.



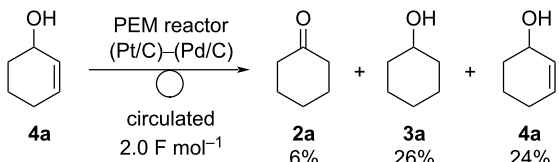
Scheme 3: Electrochemical hydrogenation of several enones **1** with a circulating PEM reactor using an Ir/C cathode catalyst. Reaction conditions: anode catalyst Pt/C, cathode catalyst Ir/C, concentration of **1** 1.0 M, solvent dichloromethane, flow rate of the solution of **1** 0.25 mL·min⁻¹, flow rate of H₂ gas 100 mL·min⁻¹, reaction temperature room temperature, current density 50 mA·cm⁻². Charge was passed to the circulated solution until **1** was consumed. The yield was determined by GC analysis using *n*-dodecane as an internal standard. Values in parentheses show the chemoselectivity of **3**, which was calculated as yield of **3** / yield of (**2** + **3**).

Mechanistic studies

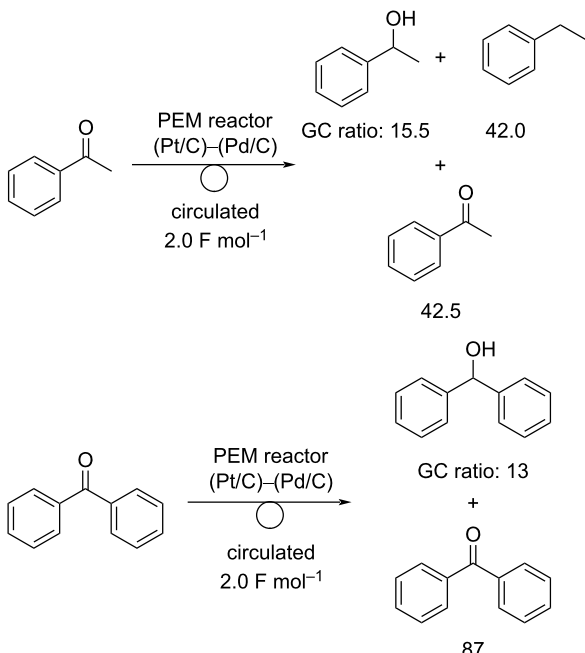
To gain further insight into the reaction mechanism of the chemoselectivity of a Pd/C cathode system, some additional reactions were carried out (Scheme 4). Electroreduction of **4a** as a starting material was carried out using the circulating PEM reactor equipped with a Pd/C cathode. Compound **4a** has not been observed under the standard reaction conditions performed so far. The reduction of **4a** did not proceed efficiently. Compound **3a** was obtained as a major product (26% yield) and **2a** was obtained in 6% yield (Scheme 4a). Hydrogenation of the alkene moiety of **4a** would proceed selectively, and **2a** would be generated via a transfer hydrogenation reaction from **3a** as a hydrogen donor [32–35]. These results suggest that electroreduction of **1a** would afford **2a** directly and not via **4a**. Electroreduction of acetophenone did not proceed efficiently, and 42.5% (GC ratio) of acetophenone was recovered with ethylbenzene as a major reduced product (Scheme 4b). We assumed that the

reduction would proceed via an enol or enolate intermediate. The reduction of benzophenone also did not proceed smoothly, and only 13% of benzophenone was converted. These results suggest that a Pd/C cathode significantly targets an alkene moiety over a carbonyl group, predominantly leading to the reduction of the C=C moiety.

a) electroreduction of **4a** with the circulated PEM reactor



b) electroreduction acetophenone and benzophenone

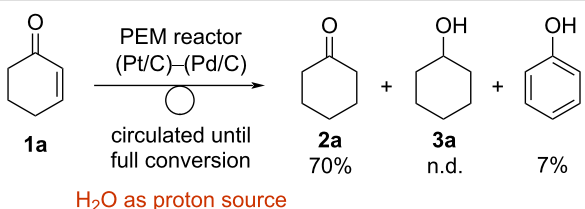


Scheme 4: Mechanistic studies.

Finally, the electroreduction of **1a** was carried out with the use of H₂O as a proton source by the PEM reactor with a Pd/C cathode catalyst (Scheme 5). Similar to the reaction with H₂, the electroreduction proceeded with high chemoselectivity, and the desired ketone **2a** was obtained in 70% yield, whereas alcohol **3a** was not observed. Interestingly, the generation of phenol was observed (7% yield), probably because **1a** could serve as a hydrogen donor due to the low concentration of hydrogen [32].

Conclusion

In conclusion, we have developed a system for the electroreduction of enones using a PEM reactor. The reactions proceeded under mild conditions, and highly chemoselective reductions were achieved with the use of appropriate cathode catalysts.



Scheme 5: Electrocatalytic reduction of **1a** with the circulated PEM reactor using H₂O as a proton source.

The use of a Pd/C cathode gave carbonyl compounds selectively. In contrast, saturated alcohols were obtained selectively with an Ir/C cathode. The reaction with H₂O as a proton source was also achieved. With this reaction system, chemoselective reduction can be performed using only electricity and water, and the product can be easily obtained by simply concentrating the solution coming out of the outlet of the flow system. We are currently trying to reduce various functional groups using this system and shall report the results at a later time.

Supporting Information

Supporting Information File 1

Experimental details.

[<https://www.beilstein-journals.org/bjoc/content/supplementary/1860-5397-18-107-S1.pdf>]

Acknowledgements

The authors thank Prof. Mahito Atobe (Yokohama National University) and his group members for fruitful discussions and suggestions. The authors also thank Prof. Yuta Nishina (Okayama University) and his group members for the help with making the MEA. We also thank Mr. Atsushi Ohsaki in our group for his help.

Funding

This work was supported in part by JST CREST Grant No. JP65R1204400, Japan, JSPS KAKENHI Grant Number JP19K05477, JP19K05478, and JP22H02122.

ORCID® iDs

Koichi Mitsudo - <https://orcid.org/0000-0002-6744-7136>

References

- Baba, A.; Yasuda, M.; Nishimoto, Y. Partial Reduction of Enones, Styrenes, and Related Systems. In *Partial reduction of enones, styrenes, and related systems*; Molander, G. A.; Knochel, P., Eds.; Elsevier: Amsterdam, Netherlands, 2014; Vol. 8, pp 673–740.
doi:10.1016/b978-0-08-097742-3.00822-3

2. Hicks, M. T.; Fedkiw, P. S. *J. Electrochem. Soc.* **1998**, *145*, 3728–3734. doi:10.1149/1.1838866
3. Pintauro, P. N.; Gil, M. P.; Warner, K.; List, G.; Neff, W. *Ind. Eng. Chem. Res.* **2005**, *44*, 6188–6195. doi:10.1021/ie0490738
4. Sedighi, S.; Gardner, C. L. *Electrochim. Acta* **2010**, *55*, 1701–1708. doi:10.1016/j.electacta.2009.10.053
5. Zhang, R.; Weidner, J. W. *ECS Trans.* **2010**, *28* (26), 51–63. doi:10.1149/1.3501095
6. Foncho, R.; Gardner, C. L.; Ternan, M. *Electrochim. Acta* **2012**, *75*, 171–178. doi:10.1016/j.electacta.2012.04.116
7. Green, S. K.; Tompsett, G. A.; Kim, H. J.; Kim, W. B.; Huber, G. W. *ChemSusChem* **2012**, *5*, 2410–2420. doi:10.1002/cssc.201200416
8. Ehteshami, S. M. M.; Zhou, W. J.; Chan, S. H. *Int. J. Hydrogen Energy* **2013**, *38*, 188–196. doi:10.1016/j.ijhydene.2012.10.043
9. Stuve, E. M.; Spies, K. A. *ECS Trans.* **2013**, *58* (1), 1723–1731. doi:10.1149/05801.1723ecst
10. Stuve, E. M.; Spies, K. *ECS Trans.* **2013**, *53* (9), 21–28. doi:10.1149/05309.0021ecst
11. Ehteshami, S. M. M.; Vignesh, S.; Rasheed, R. K. A.; Chan, S. H. *Appl. Energy* **2016**, *170*, 388–393. doi:10.1016/j.apenergy.2016.03.001
12. Ogihara, H.; Maezuru, T.; Ogishima, Y.; Yamanaka, I. *ChemistrySelect* **2016**, *1*, 5533–5537. doi:10.1002/slct.201601082
13. Ogihara, H.; Maezuru, T.; Ogishima, Y.; Yamanaka, I. *Electrocatalysis* **2018**, *9*, 220–225. doi:10.1007/s12678-017-0419-1
14. Caravaca, A.; Garcia-Lorefice, W. E.; Gil, S.; de Lucas-Consuegra, A.; Vernoux, P. *Electrochim. Commun.* **2019**, *100*, 43–47. doi:10.1016/j.elecom.2019.01.016
15. Carl, S.; Waldrop, K.; Pintauro, P.; Thompson, L. T.; Tarpeh, W. A. *ChemElectroChem* **2019**, *6*, 5563–5570. doi:10.1002/celc.201901314
16. Sato, M.; Ogihara, H.; Yamanaka, I. *ISIJ Int.* **2019**, *59*, 623–627. doi:10.2355/isijinternational.isijint-2018-551
17. Takano, K.; Tateno, H.; Matsumura, Y.; Fukazawa, A.; Kashiwagi, T.; Nakabayashi, K.; Nagasawa, K.; Mitsushima, S.; Atobe, M. *Chem. Lett.* **2016**, *45*, 1437–1439. doi:10.1246/cl.160766
18. Takano, K.; Tateno, H.; Matsumura, Y.; Fukazawa, A.; Kashiwagi, T.; Nakabayashi, K.; Nagasawa, K.; Mitsushima, S.; Atobe, M. *Bull. Chem. Soc. Jpn.* **2016**, *89*, 1178–1183. doi:10.1246/bcsj.20160165
19. Fukazawa, A.; Takano, K.; Matsumura, Y.; Nagasawa, K.; Mitsushima, S.; Atobe, M. *Bull. Chem. Soc. Jpn.* **2018**, *91*, 897–899. doi:10.1246/bcsj.20180021
20. Egbert, J. D.; Thomsen, E. C.; O'Neill-Slawecki, S. A.; Mans, D. M.; Leitch, D. C.; Edwards, L. J.; Wade, C. E.; Weber, R. S. *Org. Process Res. Dev.* **2019**, *23*, 1803–1812. doi:10.1021/acs.oprd.8b00379
21. Liu, J.; Chen, R.; Zhu, X.; Liao, Q.; Ye, D.; Zhang, B.; Liu, M.; Chen, G.; Wang, K. *RSC Adv.* **2019**, *9*, 23560–23569. doi:10.1039/c9ra02648g
22. Fukazawa, A.; Minoshima, J.; Tanaka, K.; Hashimoto, Y.; Kobori, Y.; Sato, Y.; Atobe, M. *ACS Sustainable Chem. Eng.* **2019**, *7*, 11050–11055. doi:10.1021/acssuschemeng.9b01882
23. Nogami, S.; Nagasawa, K.; Fukazawa, A.; Tanaka, K.; Mitsushima, S.; Atobe, M. *J. Electrochem. Soc.* **2020**, *167*, 155506. doi:10.1149/1945-7111/abaae7
24. Nogami, S.; Shida, N.; Iguchi, S.; Nagasawa, K.; Inoue, H.; Yamanaka, I.; Mitsushima, S.; Atobe, M. *ACS Catal.* **2022**, *12*, 5430–5440. doi:10.1021/acscatal.2c01594
25. Fukazawa, A.; Tanaka, K.; Hashimoto, Y.; Sato, Y.; Atobe, M. *Electrochim. Commun.* **2020**, *115*, 106734. doi:10.1016/j.elecom.2020.106734
26. Fukazawa, A.; Shimizu, Y.; Shida, N.; Atobe, M. *Org. Biomol. Chem.* **2021**, *19*, 7363–7368. doi:10.1039/d1ob01197a
27. Yoshida, J.-i.; Suga, S.; Suzuki, S.; Kinomura, N.; Yamamoto, A.; Fujiwara, K. *J. Am. Chem. Soc.* **1999**, *121*, 9546–9549. doi:10.1021/ja9920112
28. Suga, S.; Suzuki, S.; Yamamoto, A.; Yoshida, J.-i. *J. Am. Chem. Soc.* **2000**, *122*, 10244–10245. doi:10.1021/ja002123p
29. Mitsudo, K.; Yamamoto, J.; Akagi, T.; Yamashita, A.; Haisa, M.; Yoshioka, K.; Mandai, H.; Ueoka, K.; Hempel, C.; Yoshida, J.-i.; Suga, S. *Beilstein J. Org. Chem.* **2018**, *14*, 1192–1202. doi:10.3762/bjoc.14.100
30. Mitsudo, K.; Matsuo, R.; Yonezawa, T.; Inoue, H.; Mandai, H.; Suga, S. *Angew. Chem., Int. Ed.* **2020**, *59*, 7803–7807. doi:10.1002/anie.202001149
31. Kurimoto, Y.; Yamashita, J.; Mitsudo, K.; Sato, E.; Suga, S. *Org. Lett.* **2021**, *23*, 3120–3124. doi:10.1021/acs.orglett.1c00807
32. Brieger, G.; Nestrick, T. *J. Chem. Rev.* **1974**, *74*, 567–580. doi:10.1021/cr60291a003
33. Bagnell, L.; Strauss, C. R. *Chem. Commun.* **1999**, 287–288. doi:10.1039/a808977i
34. Albrecht, M.; Crabtree, R. H.; Mata, J.; Peris, E. *Chem. Commun.* **2002**, 32–33. doi:10.1039/b109491b
35. Hillier, A. C.; Lee, H. M.; Stevens, E. D.; Nolan, S. P. *Organometallics* **2001**, *20*, 4246–4252. doi:10.1021/om0103456

License and Terms

This is an open access article licensed under the terms of the Beilstein-Institut Open Access License Agreement (<https://www.beilstein-journals.org/bjoc/terms>), which is identical to the Creative Commons Attribution 4.0

International License

(<https://creativecommons.org/licenses/by/4.0>). The reuse of material under this license requires that the author(s), source and license are credited. Third-party material in this article could be subject to other licenses (typically indicated in the credit line), and in this case, users are required to obtain permission from the license holder to reuse the material.

The definitive version of this article is the electronic one which can be found at:

<https://doi.org/10.3762/bjoc.18.107>



Electrochemical formal homocoupling of *sec*-alcohols

Kosuke Yamamoto, Kazuhisa Arita, Masashi Shiota, Masami Kuriyama
and Osamu Onomura*

Letter

Open Access

Address:
Graduate School of Biomedical Sciences, Nagasaki University, 1-14
Bunkyo-machi, Nagasaki 852-8521, Japan

Beilstein J. Org. Chem. **2022**, *18*, 1062–1069.
<https://doi.org/10.3762/bjoc.18.108>

Email:
Osamu Onomura* - onomura@nagasaki-u.ac.jp

Received: 31 May 2022
Accepted: 09 August 2022
Published: 22 August 2022

* Corresponding author

Keywords:
alcohols; dimerization; electrooxidation; electroreduction; paired
electrolysis

This article is part of the thematic issue "Molecular and macromolecular
electrochemistry: synthesis, mechanism, and redox properties" and is
dedicated to the late Professor Tatsuya Shono for his great contributions
to electroorganic chemistry.

Guest Editor: S. Inagi

© 2022 Yamamoto et al.; licensee Beilstein-Institut.
License and terms: see end of document.

Abstract

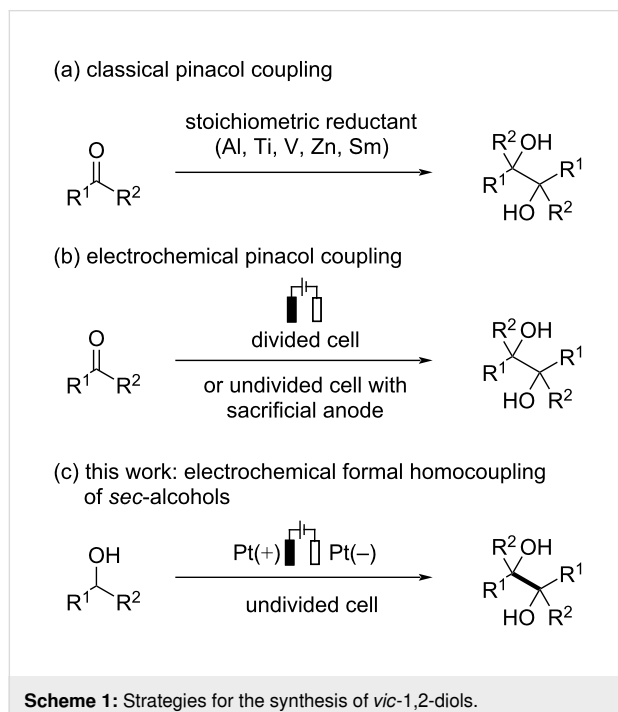
Electrochemical pinacol coupling of carbonyl compounds in an undivided cell with a sacrificial anode would be a promising approach toward synthetically valuable *vic*-1,2-diol scaffolds without using low-valent metal reductants. However, sacrificial anodes produce an equimolar amount of metal waste, which may be a major issue in terms of sustainable chemistry. Herein, we report a sacrificial anode-free electrochemical protocol for the synthesis of pinacol-type *vic*-1,2-diols from *sec*-alcohols, namely benzyl alcohol derivatives and ethyl lactate. The corresponding *vic*-1,2-diols are obtained in moderate to good yields, and good to high levels of stereoselectivity are observed for *sec*-benzyl alcohol derivatives. The present transformations smoothly proceed in a simple undivided cell under constant current conditions without the use of external chemical oxidants/reductants, and transition-metal catalysts.

Introduction

Carbon–carbon bond formation is one of the most fundamental and important reactions in synthetic organic chemistry. Reductive coupling of carbonyl compounds known as pinacol coupling would be a powerful method to construct *vic*-1,2-diol scaffolds through C–C bond formation [1,2]. Such scaffolds are widely utilized as versatile building blocks in the synthesis of biologically active compounds [3–7], chiral auxiliaries [8,9],

and chiral ligands [10–13]. Traditional pinacol coupling reactions are performed with a stoichiometric or even excess amount of low-valent metal reductants, such as Al, Ti, V, Zn, and Sm (Scheme 1a). Although these protocols have proven to be a reliable strategy to access *vic*-1,2-diols, producing a large amount of metal waste may be a major drawback especially in a large-scale synthesis. Thus, the improved procedures using a

catalytic amount of transition-metal reductants have been developed, but stoichiometric silicon electrophiles and co-reductants such as Zn were commonly required to complete the catalytic cycle [14]. More recently, visible light-mediated pinacol coupling reactions have been disclosed by several groups [15–18]. In addition to the reductive coupling of carbonyl compounds, oxidative homocoupling reactions of benzyl alcohols under transition metal- or semiconductor-based photoredox catalysis have been demonstrated as attractive approaches to access *vic*-1,2-diols [19–23].



Scheme 1: Strategies for the synthesis of *vic*-1,2-diols.

Electroorganic chemistry has been recognized as an environmentally benign and powerful strategy to promote redox reactions using electricity as a traceless oxidant or reductant [24–28]. Electrochemical pinacol coupling would be a promising alternative to avoid the use of low-valent metal reductants. The reported methods commonly carried out in a divided cell [29–34] or an undivided cell with sacrificial anodes [35], such as Al, Mg, and Sn, to prevent undesired oxidative reactions (Scheme 1b) [36–39]. While sacrificial anodes enable the reactions to be performed with a simple and user-friendly undivided cell set-up, consuming the anode material with generating stoichiometric metal waste may be a serious issue in terms of green and sustainable chemistry. Thus, the development of a sacrificial anode-free process such as paired electrolysis would be highly desirable [40–44]. The group of Wang recently reported the sacrificial anode-free electroreduction of benzophenone derivatives to afford *vic*-1,2-diols using over-stoichiometric NaN_3 under acidic conditions, but appropriate precau-

tions should be taken for in situ-generated explosive and toxic HN_3 [45]. Kim et al. reported the formation of *vic*-1,2-diols in the sacrificial anode-free electrocarboxylation of 1-phenylethanol and benzyl alcohol which involves tetramethylpiperidine-1-oxyl-mediated alcohol oxidation as an anodic event [46]. However, *vic*-1,2-diols were obtained only as minor products and formal homocoupling of benzhydrol did not occur under Kim's reaction conditions. Thus, the development of an environmentally benign and efficient electrochemical protocol to access *vic*-1,2-diols would be still highly desirable. Herein, we report the sacrificial anode-free electrochemical synthesis of *vic*-1,2-diols through the formal homocoupling of *sec*-alcohols using platinum electrodes in an undivided cell (Scheme 1c).

Results and Discussion

We commenced the optimization study for the electrochemical formal homocoupling of *sec*-alcohols by using 1-phenylethanol (**1a**) as a model substrate. The results are summarized in Table 1. The electrolysis was carried out using an undivided cell in the presence of Et_4NBr as an electrolyte with a mixed solvent of MeCN and H_2O under air atmosphere. When 4 F/mol of electricity was passed through the reaction mixture using two platinum electrodes at 0 °C, the corresponding pinacol-type product **2a** was obtained in 58% yield with an 89:11 ratio of *dl* and *meso* isomers (Table 1, entry 1). Acetophenone (**3a**) was also formed in 32% yield under the reaction conditions described in entry 1. Using different electrode materials such as Ni, Zn, and graphite as cathode did not improve the yield of **2a** (Table 1, entries 2–4). The present reaction proceeded in the presence of quaternary ammonium salts with different counter anions including the BF_4^- anion, and Et_4NBr was found to be the preferable electrolyte among them (Table 1, entry 1 vs entries 5–7). Next, we examined the effect of acidic and basic additives on the reaction outcome. While the use of $\text{Mg}(\text{OTf})_2$, HCO_2H , or 2,6-lutidine resulted in reduced reaction efficiency, imidazole exhibited the positive effect on the product yield, providing **2a** in 72% yield (Table 1, entries 8–11). Addition of H_2O was crucial to obtain **2a** in a high yield, and we chose 125 μL of H_2O as the optimal volume for the present transformation (Table 1, entries 11–13). The reaction under inert atmosphere did not improve the yield of **2a** (Table 1, entry 14).

With the optimized conditions in hand, the substrate scope of the present transformation was investigated as shown in Scheme 2. Various 1-arylethanol derivatives were firstly examined. Substrates bearing *p*-methyl (**1b**) or *p*-*tert*-butyl (**1c**) groups afforded the desired products **2b** and **2c** in moderate yields. Halogen substituents such as fluorine (**1d**) and chlorine (**1e**) atoms were tolerated under the present reaction conditions providing **2d** and **2e** in 70% and 57% yields, respectively, with high diastereoselectivities. Substrates having electron-with-

Table 1: Optimization of reaction conditions.^a

entry	(+)-(-)	electrolyte	additive	yield (%) ^b		<i>dl</i> : <i>meso</i> for 2a ^c
				2a	3a	
1	Pt-Pt	Et ₄ NBr	–	58	32	89:11
2	Pt-Ni	Et ₄ NBr	–	5	49	90:10
3	Pt-Zn	Et ₄ NBr	–	24	20	89:11
4	Pt-C	Et ₄ NBr	–	28	40	89:11
5	Pt-Pt	Et ₄ NCl	–	39	30	90:10
6	Pt-Pt	Et ₄ NI	–	10	5	90:10
7	Pt-Pt	Et ₄ NBF ₄	–	46	32	90:10
8	Pt-Pt	Et ₄ NBr	Mg(OTf) ₂	26	64	90:10
9	Pt-Pt	Et ₄ NBr	HCO ₂ H	39	33	89:11
10	Pt-Pt	Et ₄ NBr	2,6-lutidine	24	41	89:11
11	Pt-Pt	Et ₄ NBr	imidazole	72	24	90:10
12^d	Pt-Pt	Et₄NBr	imidazole	78 (78)	8	90:10
13 ^e	Pt-Pt	Et ₄ NBr	imidazole	39	11	77:23
14 ^{d,f}	Pt-Pt	Et ₄ NBr	imidazole	77	12	90:10

^aReaction conditions: **1a** (1.0 mmol), electrolyte (0.1 equiv), additive (0.05 equiv), MeCN (5 mL), H₂O (250 µL), 50 mA constant current (cc), 4 F/mol, 0 °C, under air. ^bDetermined by ¹H NMR using 1,3,5-trimethoxybenzene as an internal standard. The number in parentheses refers to the isolated yield. ^cDetermined by ¹H NMR analysis. ^dH₂O (125 µL). ^eWithout H₂O. ^fUnder Ar.

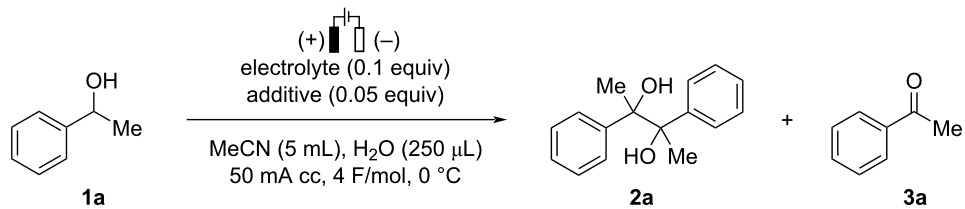
drawing groups such as ester (**1f**) and trifluoromethyl (**1g**) on the *para*-position of the aryl moiety afforded the desired products in good yields (**2f** and **2g**). On the other hand, the reaction of 1-(4-cyanophenyl)ethanol (**1h**) resulted in a decrease in both the yield and the *dl*:*meso* ratio. While steric hindrance of substituents on the *meta*-position of the aryl moiety did not impede the present transformation (**2i** and **2j**), the *ortho*-substituted substrate **1k** gave **2k** in a less satisfactory yield but with good diastereoselectivity. 1-Phenyl-1-propanol (**1l**) was successfully transformed into the desired product **2l** in a moderate yield. In addition, ethyl lactate (**1m**) provided the corresponding *vic*-1,2-diol **2m** in 60% yield but with low diastereoselectivity [47]. Benzhydrol derivatives (**1n–p**) were found to be good substrates for the present reaction, affording the corresponding benzopinacols (**2n–p**) in good yields after the passage of 8 F/mol in a mixed solvent of MeCN/MeOH.

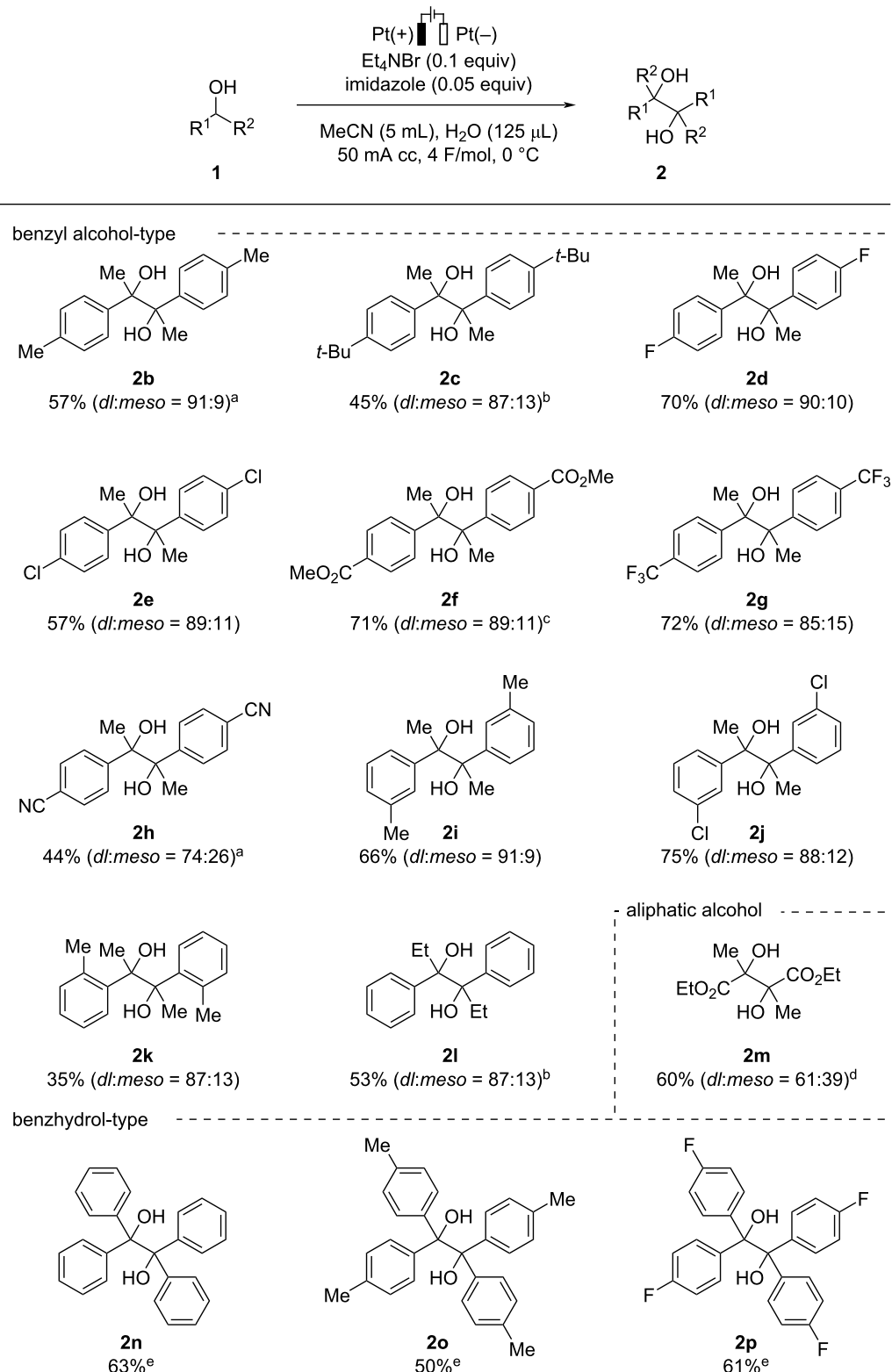
Next, we examined the possibility to extend the present process to the cross-coupling reaction of two different benzyl alcohols (Scheme 3). Pleasingly, the reaction using a 1:1 mixture of **1a**

and **1f** under the standard reaction conditions provided the cross-coupling product **2af** (dr = 94:6) together with the homocoupling products **2a** and **2f**.

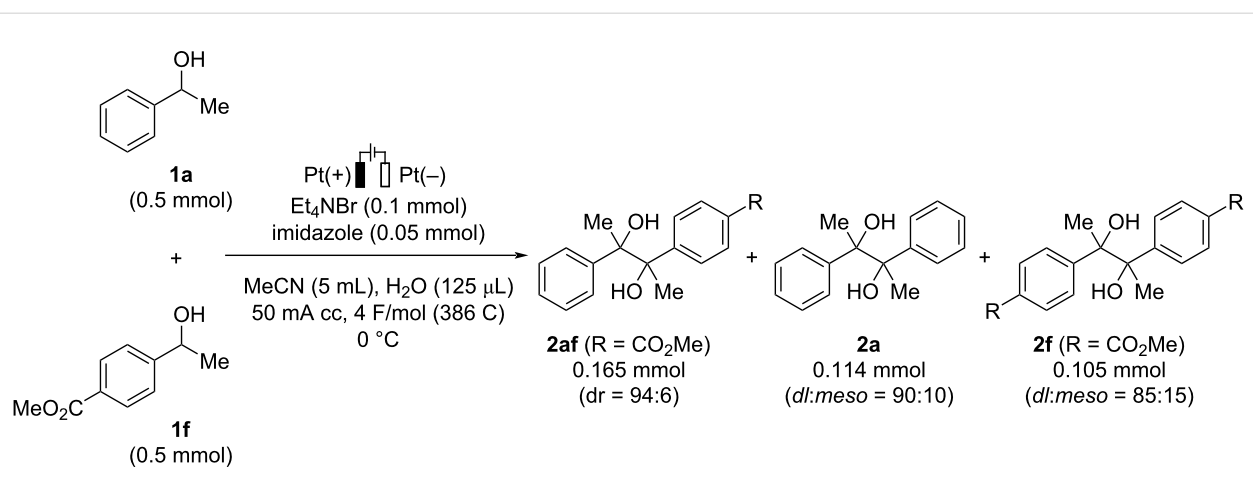
To demonstrate the scalability of the present electrochemical transformation, a large-scale experiment was performed as shown in Scheme 4. The formal homocoupling of **1a** smoothly proceeded on a 10 mmol scale to provide the desired product in 72% yield under slightly modified reaction conditions.

In order to gain insight into the present reaction, several control experiments were conducted as shown in Scheme 5. When acetophenone (**3a**) was used as a starting material under the standard reaction conditions, *vic*-1,2-diol **2a** and **3a** were obtained in 39% and 52% yields, respectively, and 1-phenylethanol (**1a**) was not observed in this reaction (Scheme 5a). The *dl*:*meso* ratio of **2a** was identical compared with that observed in the reaction using **1a** as the starting material. This observation indicated that ketone **3a** would be the intermediate in the present transformation. The reaction in the absence of imida-

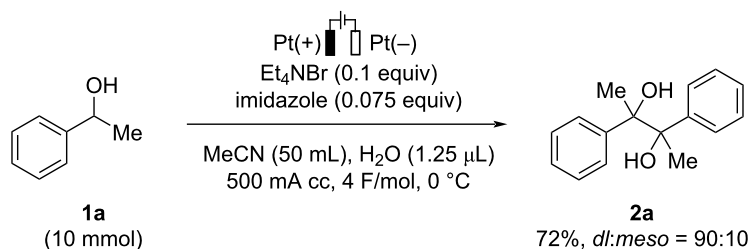




Scheme 2: Substrate scope. Reaction conditions: **1** (1.0 mmol), Et₄NBr (0.1 equiv), imidazole (0.05 equiv), MeCN (5 mL), H₂O (125 μL), 50 mA cc, 4 F/mol, 0 °C, under air. ^a100 mA cc. ^b6 F/mol, imidazole (0.075 equiv). ^c6 F/mol, imidazole (0.1 equiv). ^d8 F/mol, imidazole (0.1 equiv). ^e8 F/mol, MeCN/MeOH (4:1, 5 mL) without H₂O.



Scheme 3: Investigation of cross-coupling reaction.



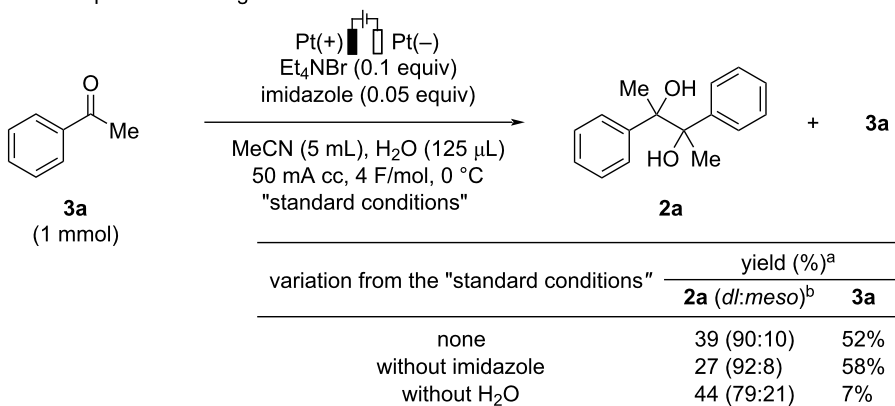
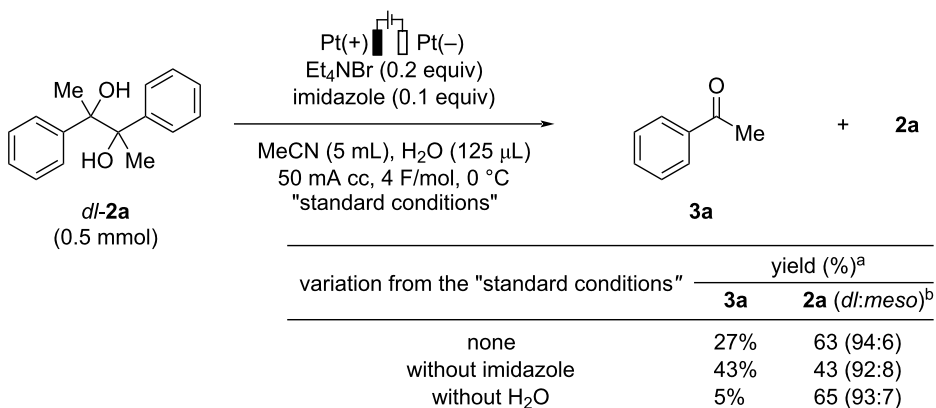
Scheme 4: Large-scale experiment.

zole also proceeded to afford **2a** in a somewhat lower yield with a high diastereoselectivity. In both cases, the reaction proceeded with the good mass balance of **2a** and **3a**. On the other hand, the reaction without adding water resulted in a decrease in the *dl:meso* ratio of **2a**, and ketone **3a** was transformed into unidentified byproducts. When *dl*-**2a** was subjected to the present reaction conditions, oxidative C–C bond cleavage of *dl*-**2a** proceeded to give the corresponding ketone **3a** (Scheme 5b) [48]. Recovered **2a** was found to be a mixture of *dl* and *meso* isomers, indicating that homocoupling of *in situ*-generated ketone **3a** occurred under the reaction conditions. While ketone **3a** was obtained in a higher yield when the reaction was performed in the absence of imidazole, a lower yield of **3a** and a poor mass balance were observed in the reaction without adding water. These results indicate that imidazole may suppress the formation of the ketone from the corresponding *vic*-1,2-diol. Water may play a role as a proton source to facilitate the formation of the protonated ketyl radical through a concerted proton–electron transfer toward the ketone or smooth protonation of the radical anion species, which readily dimerize to *vic*-1,2-diol **2a** [46,49]. The addition of water may be also important to achieve high diastereoselectivity in the present reaction.

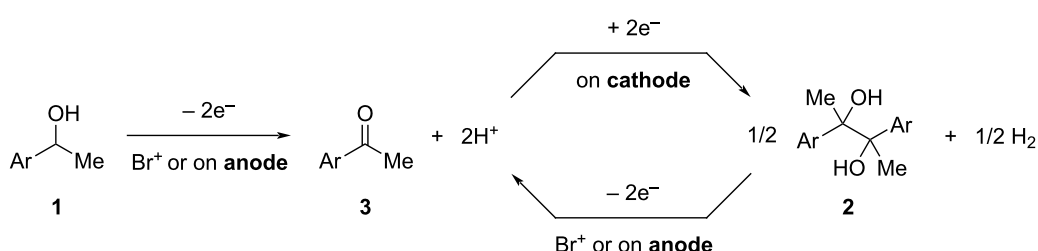
On the basis of the results of the control experiments, a plausible reaction mechanism is depicted in Scheme 6. Initially, *sec*-alcohol **1** is oxidized by an anodically generated Br^+ species to provide the corresponding ketone **3**. Then, ketone **3** undergoes electrochemical pinacol coupling to form *vic*-1,2-diol **2**. Overoxidation of compound **2** could proceed under the reaction conditions to reproduce ketone **3**, which could be transformed again into **2**. Initial screening of electrolytes indicated that direct oxidation of *sec*-alcohol **1** to ketone **3** could also proceed under the present reaction conditions.

Conclusion

In conclusion, we have developed the sacrificial anode-free electrochemical protocol for the synthesis of *vic*-1,2-diols from *sec*-alcohols without external chemical oxidants or reductants. The present reaction smoothly proceeded in a simple undivided cell with platinum electrodes under constant current conditions, affording pinacol-type products in moderate to good yields with good to high diastereoselectivities. The successful large-scale experiment showed the potential synthetic utility of this transformation. Further investigations of the reaction mechanism are currently underway in our laboratory.

(a) control experiments using **3a**(b) control experiments using *dl*-**2a**

Scheme 5: Control experiments. ^aDetermined by ¹H NMR using 1,3,5-trimethoxybenzene as an internal standard. ^bDetermined by ¹H NMR analysis.



Scheme 6: Proposed mechanism.

Supporting Information

Supporting Information File 1

Experimental procedure, characterization data, and copies of NMR spectra of the products.

[<https://www.beilstein-journals.org/bjoc/content/supplementary/1860-5397-18-108-S1.pdf>]

Funding

This work was supported by the Japan Society of Promotion for the Sciences (JSPS) Grant-in-Aid for Scientific Research (19K05459, 19K16317, and 18K06582). The spectral data were collected with the research equipment shared in the MEXT Project for promoting public utilization of advanced research infrastructure (Program for supporting introduction of the new sharing system JPMXS0422500320).

ORCID® iDs

Kosuke Yamamoto - <https://orcid.org/0000-0002-8189-7141>
 Masami Kuriyama - <https://orcid.org/0000-0002-4871-6273>
 Osamu Onomura - <https://orcid.org/0000-0003-3703-1401>

References

1. Suzuki, K.; Tamiya, M. Pinacol Coupling Reactions. In *Comprehensive Organic Synthesis*, 2nd ed.; Knochel, P.; Molander, G. A., Eds.; Elsevier: Amsterdam, Netherlands, 2014; Vol. 3, pp 580–620. doi:10.1016/b978-0-08-097742-3.00316-5
2. Chatterjee, A.; Joshi, N. N. *Tetrahedron* **2006**, *62*, 12137–12158. doi:10.1016/j.tet.2006.09.002
3. Ogata, M.; Matsumoto, H.; Takahashi, K.; Shimizu, S.; Kida, S.; Murabayashi, A.; Shiro, M.; Tawara, K. *J. Med. Chem.* **1987**, *30*, 1054–1068. doi:10.1021/jm00389a016
4. Nicolaou, K. C.; Yang, Z.; Liu, J. J.; Ueno, H.; Nantermet, P. G.; Guy, R. K.; Claiborne, C. F.; Renaud, J.; Couladouros, E. A.; Paulvannan, K.; Sorensen, E. J. *Nature* **1994**, *367*, 630–634. doi:10.1038/367630a0
5. Mateo, C.; Álvarez, R.; Pérez-Melero, C.; Peláez, R.; Medarde, M. *Bioorg. Med. Chem. Lett.* **2007**, *17*, 6316–6320. doi:10.1016/j.bmcl.2007.08.075
6. Singh, P.; Mittal, A.; Kaur, S.; Holzer, W.; Kumar, S. *Org. Biomol. Chem.* **2008**, *6*, 2706–2712. doi:10.1039/b803608j
7. Werner, B.; Kalesse, M. *Org. Lett.* **2017**, *19*, 1524–1526. doi:10.1021/acs.orglett.7b00288
8. Alexakis, A.; Mangeney, P. *Tetrahedron: Asymmetry* **1990**, *1*, 477–511. doi:10.1016/s0957-4166(00)80536-4
9. Fujioka, H.; Kita, Y. Asymmetric Synthesis Using Chiral Acetals from C_2 -Symmetric Diols and Its Application to Natural Product Synthesis. In *Studies in Natural Products Chemistry*; Atta-ur-Rahman, Ed.; Elsevier: Amsterdam, Netherlands, 1994; Vol. 14, pp 469–516. doi:10.1016/b978-0-444-81780-8.50018-1
10. Fleischer, R.; Braun, M. *Synlett* **1998**, 1441–1443. doi:10.1055/s-1998-1953
11. Stodulski, M.; Jaźwiński, J.; Mlynarski, J. *Eur. J. Org. Chem.* **2008**, 5553–5562. doi:10.1002/ejoc.200800726
12. Hashimoto, T.; Gálvez, A. O.; Maruoka, K. *J. Am. Chem. Soc.* **2013**, *135*, 17667–17670. doi:10.1021/ja407764u
13. Gök, Y.; Karayığit, İ. Ü.; Gök, H. Z. *J. Organomet. Chem.* **2017**, *846*, 44–50. doi:10.1016/j.jorgchem.2017.05.059
14. Hirao, T. Catalytic Reductive Coupling of Carbonyl Compounds – The Pinacol Coupling Reaction and Beyond. In *Metal Catalyzed Reductive C–C Bond Formation*; Krische, M. J., Ed.; Topics in Current Chemistry, Vol. 279; Springer: Berlin, Germany, 2007; pp 53–75. doi:10.1007/128_2007_120
15. Nakajima, M.; Fava, E.; Loescher, S.; Jiang, Z.; Rueping, M. *Angew. Chem., Int. Ed.* **2015**, *54*, 8828–8832. doi:10.1002/anie.201501556
16. Liu, M.; Tan, L.; Rashid, R. T.; Cen, Y.; Cheng, S.; Botton, G.; Mi, Z.; Li, C.-J. *Chem. Sci.* **2020**, *11*, 7864–7870. doi:10.1039/d0sc02718a
17. Xi, Z.-W.; Yang, L.; Wang, D.-Y.; Feng, C.-W.; Qin, Y.; Shen, Y.-M.; Pu, C.; Peng, X. *J. Org. Chem.* **2021**, *86*, 2474–2488. doi:10.1021/acs.joc.0c02627
18. Wang, H.; Qu, J.-P.; Kang, Y.-B. *Org. Lett.* **2021**, *23*, 2900–2903. doi:10.1021/acs.orglett.1c00537
19. Mitkina, T.; Stanglmaier, C.; Setzer, W.; Gruber, M.; Kisch, H.; König, B. *Org. Biomol. Chem.* **2012**, *10*, 3556–3561. doi:10.1039/c2ob07053g
20. McClelland, K. P.; Weiss, E. A. *ACS Appl. Energy Mater.* **2019**, *2*, 92–96. doi:10.1021/acsaem.8b01652
21. Wang, J.; Feng, Y.-X.; Zhang, M.; Zhang, C.; Li, M.; Li, S.-J.; Zhang, W.; Lu, T.-B. *CCS Chem.* **2020**, *2*, 81–88. doi:10.31635/ccschem.020.201900093
22. Fujita, M.; Kobayashi, F.; Ide, T.; Egami, H.; Hamashima, Y. *Eur. J. Org. Chem.* **2020**, 7151–7155. doi:10.1002/ejoc.202001329
23. Ishida, N.; Son, M.; Kawasaki, T.; Ito, M.; Murakami, M. *Synlett* **2021**, *32*, 2067–2070. doi:10.1055/a-1644-4876
24. Frontana-Uribe, B. A.; Little, R. D.; Ibanez, J. G.; Palma, A.; Vasquez-Medrano, R. *Green Chem.* **2010**, *12*, 2099–2119. doi:10.1039/c0gc00382d
25. Schäfer, H. J. *C. R. Chim.* **2011**, *14*, 745–765. doi:10.1016/j.crci.2011.01.002
26. Meyer, T. H.; Finger, L. H.; Gandeepan, P.; Ackermann, L. *Trends Chem.* **2019**, *1*, 63–76. doi:10.1016/j.trechm.2019.01.011
27. Cembellín, S.; Batanero, B. *Chem. Rec.* **2021**, *21*, 2453–2471. doi:10.1002/tcr.202100128
28. Claraz, A.; Masson, G. *ACS Org. Inorg. Au* **2022**, *2*, 126–147. doi:10.1021/acsorginorgau.1c00037
29. Stocker, J. H.; Jenevein, R. M. *J. Org. Chem.* **1968**, *33*, 294–297. doi:10.1021/jo1265a058
30. Maurice, C.; Schöllhorn, B.; Canet, I.; Mousset, G.; Mousty, C.; Guilbot, J.; Plusquellec, D. *Eur. J. Org. Chem.* **2000**, 813–821. doi:10.1002/(sici)1099-0690(200003)2000:5<813::aid-ejoc813>3.0.co;2-q
31. Lagrost, C.; Hapiot, P.; Vaultier, M. *Green Chem.* **2005**, *7*, 468–474. doi:10.1039/b500839e
32. Kise, N.; Isemoto, S.; Sakurai, T. *Tetrahedron* **2012**, *68*, 8805–8816. doi:10.1016/j.tet.2012.07.094
33. Nakahara, K.; Naba, K.; Saitoh, T.; Sugai, T.; Obata, R.; Nishiyama, S.; Einaga, Y.; Yamamoto, T. *ChemElectroChem* **2019**, *6*, 4153–4157. doi:10.1002/celc.201900202
34. Liu, C.; Li, R.; Zhou, W.; Liang, Y.; Shi, Y.; Li, R.-L.; Ling, Y.; Yu, Y.; Li, J.; Zhang, B. *ACS Catal.* **2021**, *11*, 8958–8967. doi:10.1021/acscatal.1c01382
35. Chaussard, J.; Folest, J.-C.; Nedelec, J.-Y.; Perichon, J.; Sibille, S.; Troupel, M. *Synthesis* **1990**, 369–381. doi:10.1055/s-1990-26880
36. Léonard, E.; Duñach, E.; Péridon, J. *J. Chem. Soc., Chem. Commun.* **1989**, 276–277. doi:10.1039/c39890000276
37. Thomas, H. G.; Littmann, K. *Synlett* **1990**, 757–758. doi:10.1055/s-1990-21241
38. Sahloul, K.; Sun, L.; Requet, A.; Chahine, Y.; Mellah, M. *Chem. – Eur. J.* **2012**, *18*, 11205–11209. doi:10.1002/chem.201201390
39. Kronenwetter, H.; Husek, J.; Etz, B.; Jones, A.; Manchanayakage, R. *Green Chem.* **2014**, *16*, 1489–1495. doi:10.1039/c3gc41641k
40. Hilt, G. *ChemElectroChem* **2020**, *7*, 395–405. doi:10.1002/celc.201901799
41. Sbei, N.; Hardwick, T.; Ahmed, N. *ACS Sustainable Chem. Eng.* **2021**, *9*, 6148–6169. doi:10.1021/acssuschemeng.1c00665
42. Senboku, H.; Nagakura, K.; Fukuhara, T.; Hara, S. *Tetrahedron* **2015**, *71*, 3850–3856. doi:10.1016/j.tet.2015.04.020
43. Matthessen, R.; Fransaer, J.; Binnemans, K.; De Vos, D. E. *ChemElectroChem* **2015**, *2*, 73–76. doi:10.1002/celc.201402299
44. Medvedev, J. J.; Steksova, Y. P.; Medvedeva, X. V.; Pivovarova, Y.; Krivoshapkina, E. F.; Klinkova, A. *J. Electrochem. Soc.* **2020**, *167*, 155521. doi:10.1149/1945-7111/abb839
45. Wang, Y.; Zhao, J.; Qiao, T.; Zhang, J.; Chen, G. *Chin. J. Chem.* **2021**, *39*, 3297–3302. doi:10.1002/cjoc.202100508

46. Muchez, L.; De Vos, D. E.; Kim, M. *ACS Sustainable Chem. Eng.* **2019**, 7, 15860–15864. doi:10.1021/acssuschemeng.9b04612
47. The reaction using 4-phenylbutan-2-ol did not give the corresponding *vic*-1,2-diol, and the starting alcohol and the corresponding ketone were detected in 53% and 1% NMR yields, respectively.
48. Shono, T.; Matsumura, Y.; Hashimoto, T.; Hibino, K.; Hamaguchi, H.; Aoki, T. *J. Am. Chem. Soc.* **1975**, 97, 2546–2548. doi:10.1021/ja00842a044
49. Wang, S.; Singh, P. S.; Evans, D. H. *J. Phys. Chem. C* **2009**, 113, 16686–16693. doi:10.1021/jp904976v

License and Terms

This is an open access article licensed under the terms of the Beilstein-Institut Open Access License Agreement (<https://www.beilstein-journals.org/bjoc/terms>), which is identical to the Creative Commons Attribution 4.0 International License (<https://creativecommons.org/licenses/by/4.0>). The reuse of material under this license requires that the author(s), source and license are credited. Third-party material in this article could be subject to other licenses (typically indicated in the credit line), and in this case, users are required to obtain permission from the license holder to reuse the material.

The definitive version of this article is the electronic one which can be found at:

<https://doi.org/10.3762/bjoc.18.108>



Radical cation Diels–Alder reactions of arylidene cycloalkanes

Kaii Nakayama¹, Hidehiro Kamiya¹ and Yohei Okada^{*2}

Letter

Open Access

Address:

¹Department of Chemical Engineering, Tokyo University of Agriculture and Technology, 2-24-16 Naka-cho, Koganei, Tokyo 184-8588, Japan

and ²Department of Applied Biological Science, Tokyo University of Agriculture and Technology, 3-5-8 Saiwai-cho, Fuchu, Tokyo 183-8509, Japan

Email:

Yohei Okada^{*} - yokada@cc.tuat.ac.jp

* Corresponding author

Keywords:

arylidene cycloalkane; Diels–Alder reaction; radical cation; single-electron transfer; spiro ring system

Beilstein J. Org. Chem. **2022**, *18*, 1100–1106.

<https://doi.org/10.3762/bjoc.18.112>

Received: 29 May 2022

Accepted: 18 August 2022

Published: 25 August 2022

This article is part of the thematic issue "Molecular and macromolecular electrochemistry: synthesis, mechanism, and redox properties".

Guest Editor: S. Inagi

© 2022 Nakayama et al.; licensee Beilstein-Institut.

License and terms: see end of document.

Abstract

TiO₂ photoelectrochemical and electrochemical radical cation Diels–Alder reactions of arylidene cycloalkanes are described, leading to the construction of spiro ring systems. Although the mechanism remains an open question, arylidene cyclobutanes are found to be much more effective in the reaction than other cycloalkanes. Since the reaction is completed with a substoichiometric amount of electricity, a radical cation chain pathway is likely to be involved.

Introduction

Single-electron transfer is one of the simplest modes for small molecule activation, employing a polarity inversion to generate radical ions which have proven to be unique reactive intermediates in the field of synthetic organic chemistry. A radical cation Diels–Alder reaction is a typical example of this activation mode since both the original diene and dienophile are electron-rich and thus not an effective combination of reactants [1–11]. Single-electron transfer makes the construction of six-membered ring systems possible. In general, single-electron oxidation of an electron-rich dienophile generates its radical cation which is then trapped by the diene (Figure 1). Since the forming cyclohexene remains in the radical cation state as well, one electron reduction is required to complete the net redox neutral transformation. Therefore, a chain pathway can be involved, where an electron acts as a catalyst rather than a reagent [12–

18]. In this reaction format, *trans*-anethole is an electron-rich dienophile and has widely been studied as a benchmark for single-electron transfer using photochemical and electrochemical methods [19–32]. A one electron oxidant can also be an initiator for this transformation [33–35]. Overall, the scope of the reaction has been expanding. Starting from *trans*-anethole, several functionalities at the β -position are found to be compatible with the reaction, while those at the aryl ring are somewhat limited (Figure 2). It should be noted that a second substituent at the β -position of *trans*-anethole has a significant impact on the reaction and surprisingly, even an additional methyl group is not acceptable.

We have developed radical cation cycloadditions using (photo)electrochemical single-electron transfer in lithium per-

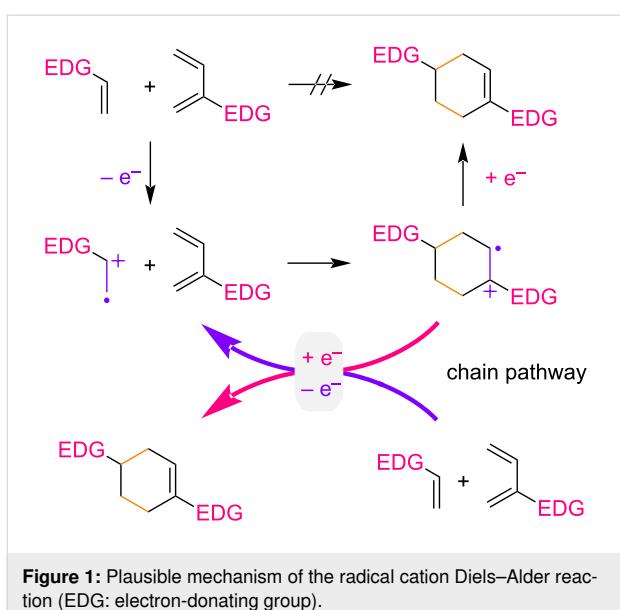
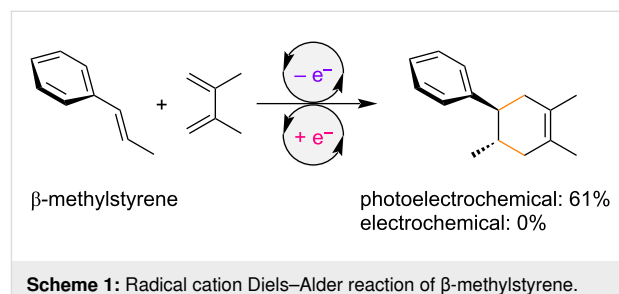


Figure 1: Plausible mechanism of the radical cation Diels–Alder reaction (EDG: electron-donating group).

chlorate (LiClO_4)/nitromethane (CH_3NO_2) solution [36–44]. During the course of our studies, we found that the TiO_2 photoelectrochemical approach was more beneficial than simple electrochemistry in most cases, probably because both single-electron oxidation and reduction are made possible at the same surface [45]. This is especially true for the radical cation Diels–Alder reaction, since non-substituted β -methylstyrene, which was previously reported as an unsuccessful dienophile,

was found to participate under TiO_2 photoelectrochemical conditions (Scheme 1) [46,47]. We questioned whether the scope of the radical cation Diels–Alder reaction could be further expanded, with particular interest on the installation of a second substituent at the β -position. Described herein is our unexpected finding that various spiro ring systems can be constructed by a radical cation Diels–Alder reaction of arylidene cycloalkanes.



Scheme 1: Radical cation Diels–Alder reaction of β -methylstyrene.

Results and Discussion

The present work began with the reaction of β -methylanethole (**1**) with 2,3-dimethyl-1,3-butadiene (**2**) under TiO_2 photoelectrochemical and electrochemical conditions (Scheme 2). The initial attempts using both conditions provided us two small indications that the reaction was not totally inaccessible. The simple electrochemical approach gave a better result than TiO_2 photoelectrochemistry. Furthermore, we confirmed that the ad-

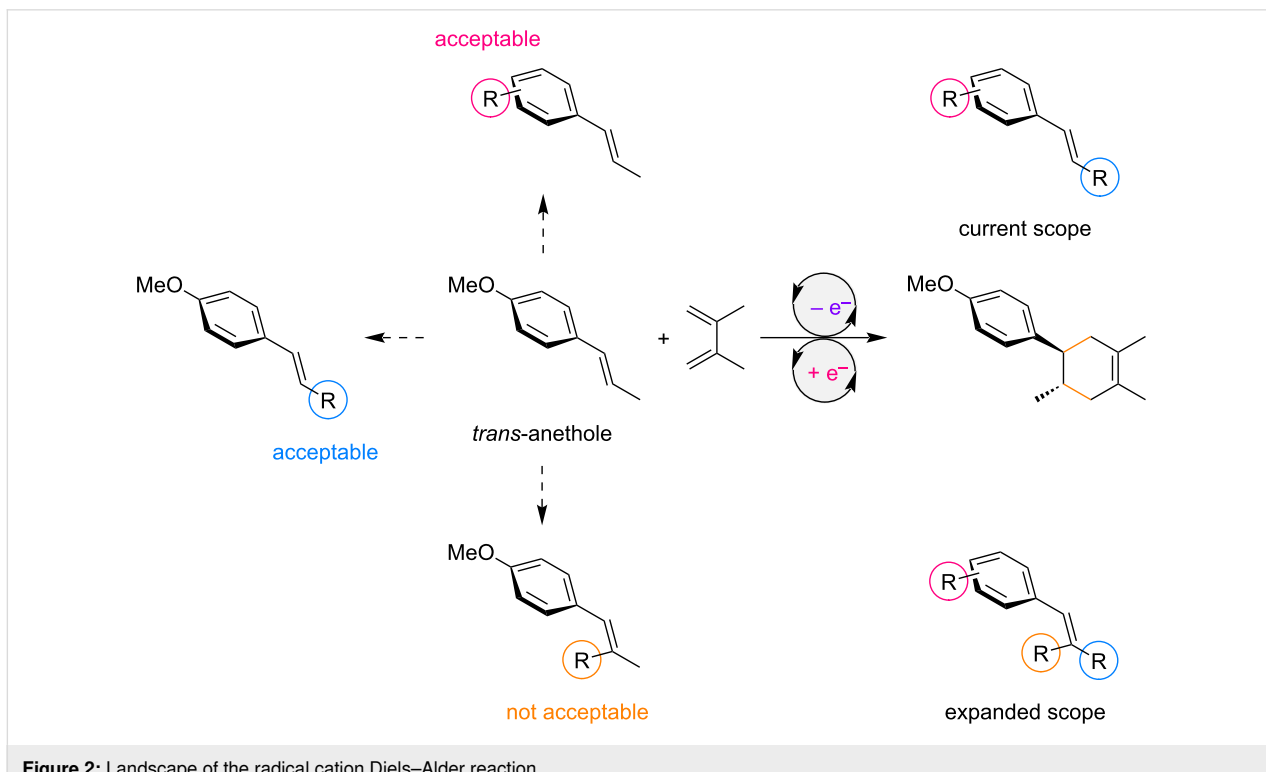
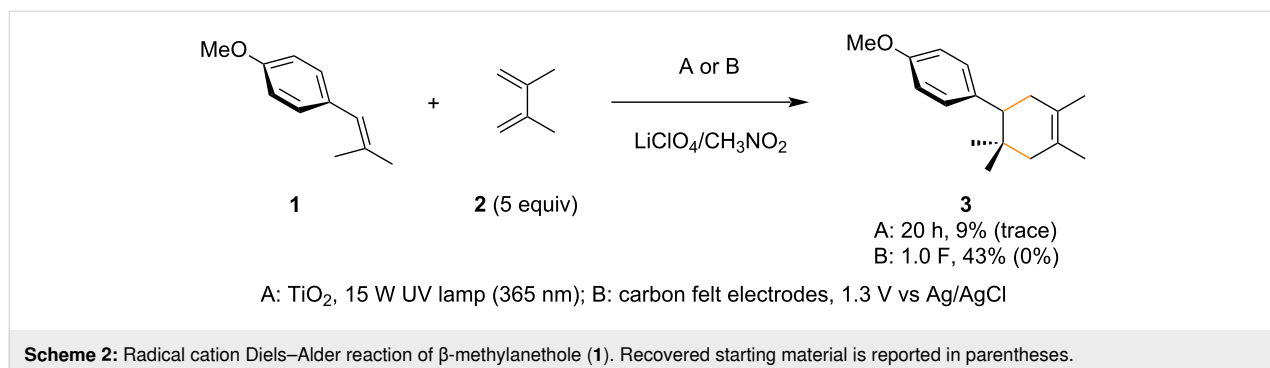


Figure 2: Landscape of the radical cation Diels–Alder reaction.



Scheme 2: Radical cation Diels–Alder reaction of β -methylanethole (**1**). Recovered starting material is reported in parentheses.

ditional methyl group at the β -position had a significant impact on the reaction. In general, tertiary radicals (or cations) are more stable than secondary ones and therefore, the additional methyl group seems to have a strong steric effect (Figure 3). If so, tying up the two methyl groups as a cyclopropane ring may decrease the steric hindrance at the β -position and

improve the reaction. Unfortunately, the arylidene cyclopropane **4** was found to be totally unreactive under both conditions (Scheme 3). However, to our surprise, the arylidene cyclobutane **5** was found to be productive and the corresponding spiro ring compound **9** was obtained in good yield. The arylidene cyclopentane **6** and cyclohexane **7** were found to be less

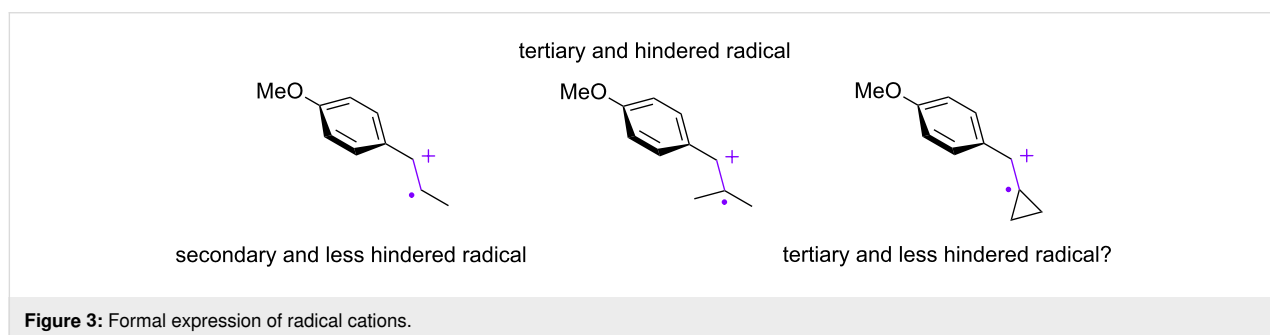
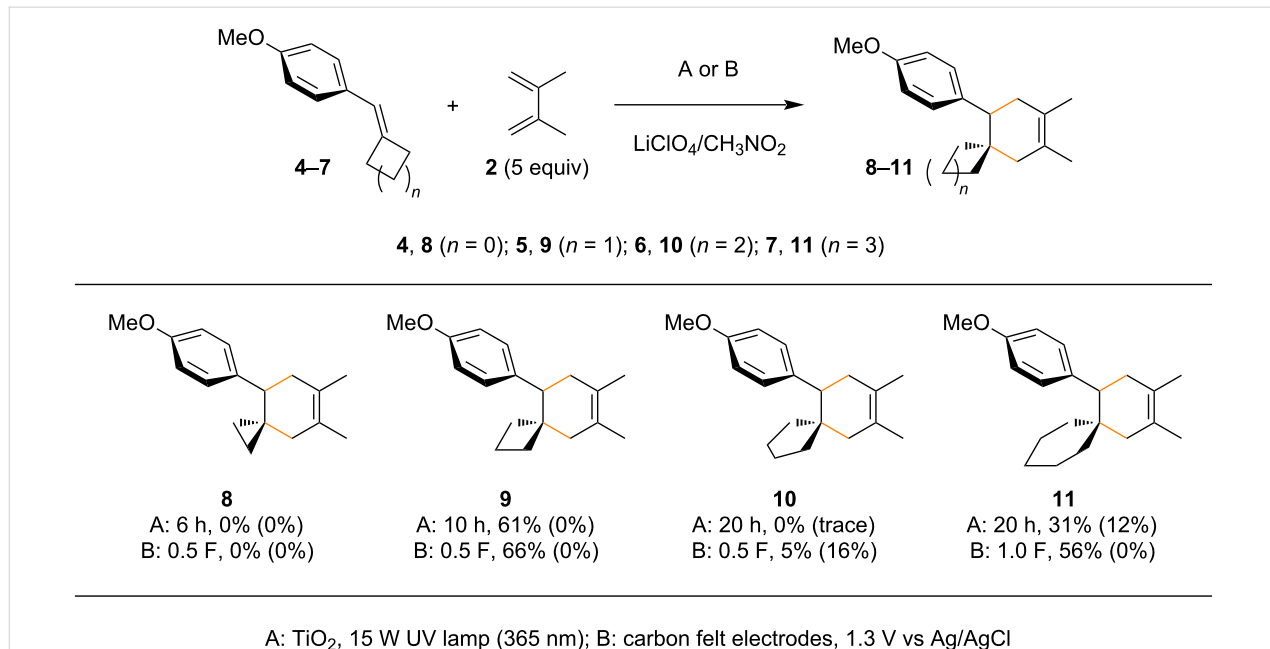


Figure 3: Formal expression of radical cations.



Scheme 3: Radical cation Diels–Alder reactions of the arylidene cycloalkanes (**4–7**). Recovered starting material is reported in parentheses.

effective for the reaction and in particular, the former (**6**) was almost totally unsuccessful. Although the mechanism remains unclear, Knowles and Romanov-Michailidis recently reported that a similar trend is observed in photosensitized [2 + 2] cycloadditions [48]. Since their report was not a [4 + 2] but a [2 + 2] reaction and they proposed an energy transfer mechanism as opposed to an electron transfer pathway, it cannot be directly compared to our results. Even so, it would be fair to say that there is some correlation between these arylidene cycloalkane cycloadditions.

Control studies are summarized in Table 1. LiClO_4 , TiO_2 , and light were crucial for the reaction (Table 1, entries 1–4) and the equivalents of the diene **2** was also key (entries 5 and 6 in Table 1). The reaction was sensitive toward atmosphere; both oxygen and argon had a negative impact (Table 1, entries 7 and 8). In the electrochemical approach, potentiostatic conditions gave better results than galvanostatic conditions and more importantly, it was found that the reaction was completed within 0.5 F/mol (Table 1, entries 9–11). This result clearly suggests that a chain pathway is involved in the reaction.

The scope of the reaction was studied using dimethyl and non-substituted aryl rings in combination with several cycloalkanes (Scheme 4). The TiO_2 photoelectrochemical approach was more beneficial than simple electrochemistry in many cases for these dienophiles, which accords well with our previous reports. The ring size effect of cycloalkanes was also clearly observed and cyclobutane was much more effective than the others. A simi-

lar trend was observed using some heterocycles, which also accorded well with the previous report by Knowles and Romanov-Michailidis.

Conclusion

In conclusion, we have demonstrated that radical cation Diels–Alder reactions of arylidene cycloalkanes are enabled under TiO_2 photoelectrochemical and electrochemical conditions to construct various spiro ring systems. Although further detailed experimental and/or theoretical studies are required to elucidate the complete mechanistic picture, arylidene cyclobutanes were found to be much more effective than others. A similar ring size effect was observed by Knowles and Romanov-Michailidis in photosensitized [2 + 2] cycloadditions of benzylidene cycloalkanes and therefore, the results described herein may support a detailed mechanistic understanding. Further experimental and theoretical studies of radical cation cycloadditions of arylidene cycloalkanes are under investigation in our laboratory.

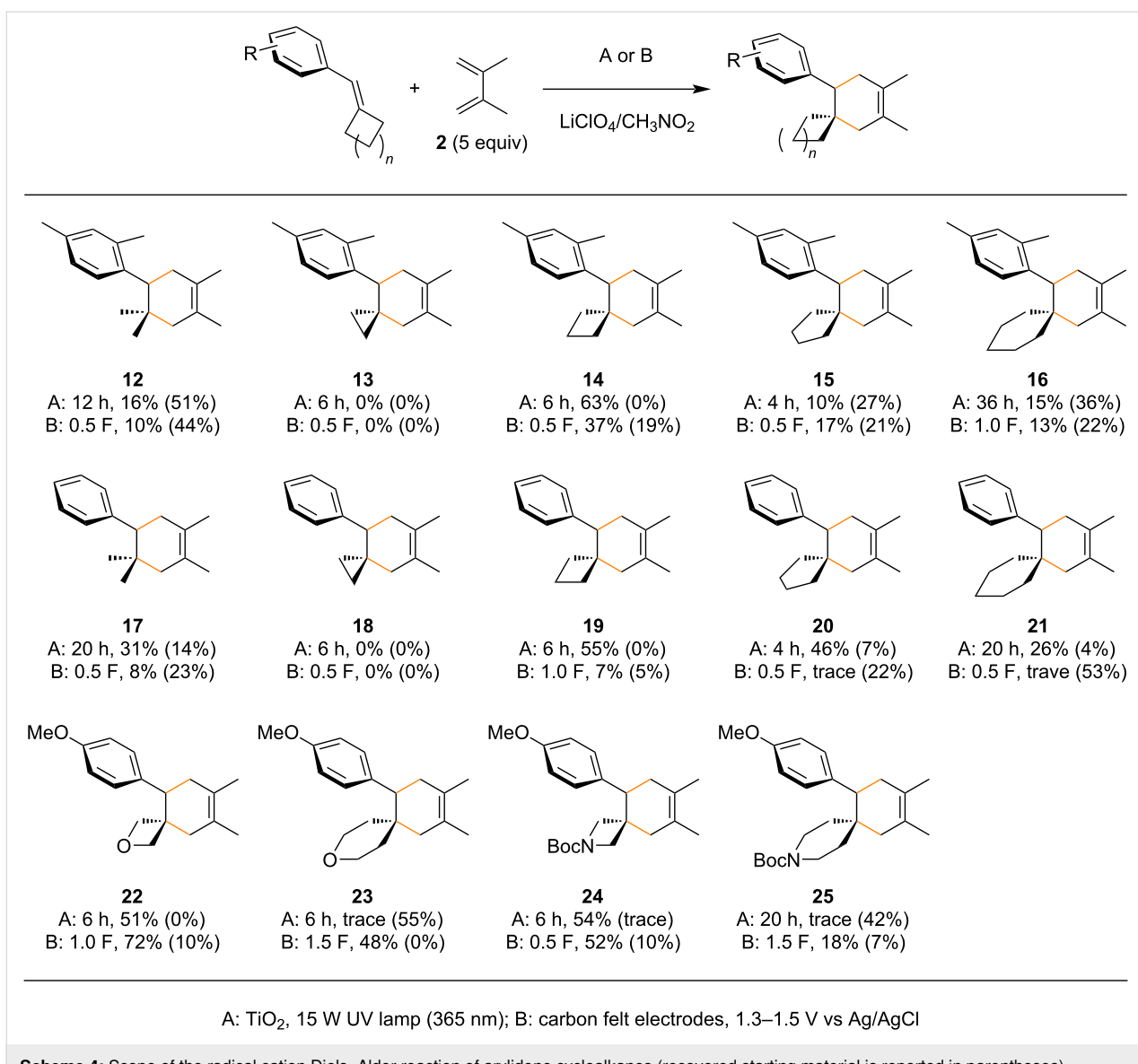
Experimental

Photoelectrochemical: The appropriate arylidene cycloalkane (0.20 mmol), 2,3-dimethyl-1,3-butadiene (**2**, 113 μL , 1.0 mmol), and TiO_2 (100 mg) were added to a solution of $\text{LiClO}_4/\text{CH}_3\text{NO}_2$ (1.0 M, 4.0 mL) while stirring at room temperature. The resulting reaction mixture was stirred at room temperature in front of a 15 W UV lamp (365 nm). Then, the solution was diluted with water and extracted with EtOAc . The combined organic layers were dried over Na_2SO_4 , filtered, and

Table 1: Control studies for the radical cation Diels–Alder reaction of the arylidene cyclobutane **5**.

entry	deviation from the standard conditions	yield (%) ^a
1		61 (0)
2	no LiClO_4	0 (40)
3	no light	0 (83)
4	no TiO_2	15 (32)
5	2 equiv of diene	22 (0)
6	10 equiv of diene	58 (0)
7	under O_2	19 (16)
8	under Ar	21 (0)
9	1.3 V vs. Ag/AgCl , 0.1 F/mol	22 (52)
10	1.3 V vs. Ag/AgCl , 0.5 F/mol	66 (0)
11	1.0 mA, 0.5 F/mol	46 (trace)

^arecovered starting material is reported in parentheses.

**Scheme 4:** Scope of the radical cation Diels–Alder reaction of arylidene cycloalkanes (recovered starting material is reported in parentheses).

concentrated in *vacuo*. Yields were determined by ¹H NMR analysis using dibromomethane as an internal standard. Silica gel column chromatography (hexane/ethyl acetate) gave the corresponding spiro ring compound.

Electrochemical: The appropriate arylidene cycloalkane (0.20 mmol) and 2,3-dimethyl-1,3-butadiene (**2**, 113 μ L, 1.0 mmol) were added to a solution of LiClO₄/CH₃NO₂ (1.0 M, 4.0 mL) while stirring at room temperature. The resulting reaction mixture was electrolyzed at 1.3–1.5 V vs Ag/AgCl using carbon felt electrodes (10 mm \times 10 mm) in an undivided cell with stirring. Then, the solution was diluted with water and extracted with EtOAc. The combined organic layers were dried over Na₂SO₄, filtered, and concentrated in *vacuo*. Yields were determined by ¹H NMR analysis using dibromomethane

as an internal standard. Silica gel column chromatography (hexane/ethyl acetate) gave the corresponding spiro ring compound.

Supporting Information

Supporting Information File 1

General remarks, photocatalyst analysis data, synthesis procedure, additional control studies, electrochemical measurements, and characterization data, including copies of ¹H and ¹³C NMR spectra.

[<https://www.beilstein-journals.org/bjoc/content/supplementary/1860-5397-18-112-S1.pdf>]

Funding

This work was supported in part by JSPS KAKENHI grant Nos. 16H06193, 17K19221, 22K05450 (to Y. O.), 21J12556 (to K. N.), and TEPCO Memorial Foundation (to Y. O.).

ORCID® iDs

Yohei Okada - <https://orcid.org/0000-0002-4353-1595>

References

- Bellville, D. J.; Wirth, D. W.; Bauld, N. L. *J. Am. Chem. Soc.* **1981**, *103*, 718–720. doi:10.1021/ja00393a061
- Bauld, N. L.; Bellville, D. J.; Harirchian, B.; Lorenz, K. T.; Pabon, R. A., Jr.; Reynolds, D. W.; Wirth, D. D.; Chiou, H. S.; Marsh, B. K. *Acc. Chem. Res.* **1987**, *20*, 371–378. doi:10.1021/ar00142a003
- Bauld, N. L. *Tetrahedron* **1989**, *45*, 5307–5363. doi:10.1016/s0040-4020(01)89486-2
- McCoch, J.; Steckhan, E. *Tetrahedron Lett.* **1987**, *28*, 1081–1084. doi:10.1016/s0040-4039(00)95916-1
- Gieseier, A.; Steckhan, E.; Wiest, O.; Knoch, F. *J. Org. Chem.* **1991**, *56*, 1405–1411. doi:10.1021/jo00004a013
- Haberl, U.; Wiest, O.; Steckhan, E. *J. Am. Chem. Soc.* **1999**, *121*, 6730–6736. doi:10.1021/ja983993y
- Valley, N. A.; Wiest, O. *J. Org. Chem.* **2007**, *72*, 559–566. doi:10.1021/jo0620361
- Pérez-Ruiz, R.; Domingo, L. R.; Jiménez, M. C.; Miranda, M. A. *Org. Lett.* **2011**, *13*, 5116–5119. doi:10.1021/ol201984s
- Lim, H. N.; Parker, K. A. *J. Org. Chem.* **2014**, *79*, 919–926. doi:10.1021/jo402082y
- Moore, J. C.; Davies, E. S.; Walsh, D. A.; Sharma, P.; Moses, J. E. *Chem. Commun.* **2014**, *50*, 12523–12525. doi:10.1039/c4cc05906a
- Tan, J. S. J.; Hirvonen, V.; Paton, R. S. *Org. Lett.* **2018**, *20*, 2821–2825. doi:10.1021/acs.orglett.8b00737
- Ischay, M. A.; Yoon, T. P. *Eur. J. Org. Chem.* **2012**, 3359–3372. doi:10.1002/ejoc.201101071
- Studer, A.; Curran, D. P. *Nat. Chem.* **2014**, *6*, 765–773. doi:10.1038/nchem.2031
- Fukuzumi, S.; Ohkubo, K. *Org. Biomol. Chem.* **2014**, *12*, 6059–6071. doi:10.1039/c4ob00843j
- Luca, O. R.; Gustafson, J. L.; Maddox, S. M.; Fenwick, A. Q.; Smith, D. C. *Org. Chem. Front.* **2015**, *2*, 823–848. doi:10.1039/c5qo00075k
- Qiu, G.; Li, Y.; Wu, J. *Org. Chem. Front.* **2016**, *3*, 1011–1027. doi:10.1039/c6qo00103c
- Francke, R.; Little, R. D. *ChemElectroChem* **2019**, *6*, 4373–4382. doi:10.1002/celc.201900432
- Costentin, C.; Savéant, J.-M. *Proc. Natl. Acad. Sci. U. S. A.* **2019**, *116*, 11147–11152. doi:10.1073/pnas.1904439116
- Reynolds, D. W.; Bauld, N. L. *Tetrahedron* **1986**, *42*, 6189–6194. doi:10.1016/s0040-4020(01)88079-0
- Lin, S.; Ischay, M. A.; Fry, C. G.; Yoon, T. P. *J. Am. Chem. Soc.* **2011**, *133*, 19350–19353. doi:10.1021/ja2093579
- Stevenson, S. M.; Shores, M. P.; Ferreira, E. M. *Angew. Chem., Int. Ed.* **2015**, *54*, 6506–6510. doi:10.1002/anie.201501220
- Higgins, R. F.; Fatur, S. M.; Shepard, S. G.; Stevenson, S. M.; Boston, D. J.; Ferreira, E. M.; Damrauer, N. H.; Rappé, A. K.; Shores, M. P. *J. Am. Chem. Soc.* **2016**, *138*, 5451–5464. doi:10.1021/jacs.6b02723
- Alpers, D.; Gallhof, M.; Stark, C. B. W.; Brasholz, M. *Chem. Commun.* **2016**, *52*, 1025–1028. doi:10.1039/c5cc08994h
- Zhao, Y.; Antonietti, M. *Angew. Chem., Int. Ed.* **2017**, *56*, 9336–9340. doi:10.1002/anie.201703438
- Stevenson, S. M.; Higgins, R. F.; Shores, M. P.; Ferreira, E. M. *Chem. Sci.* **2017**, *8*, 654–660. doi:10.1039/c6sc03303b
- Yang, Y.; Liu, Q.; Zhang, L.; Yu, H.; Tang, Z. *Organometallics* **2017**, *36*, 687–698. doi:10.1021/acs.organomet.6b00886
- Shin, J. H.; Seong, E. Y.; Mun, H. J.; Jang, Y. J.; Kang, E. J. *Org. Lett.* **2018**, *20*, 5872–5876. doi:10.1021/acs.orglett.8b02541
- Tanaka, K.; Kishimoto, M.; Sukekawa, M.; Hoshino, Y.; Honda, K. *Tetrahedron Lett.* **2018**, *59*, 3361–3364. doi:10.1016/j.tetlet.2018.07.058
- Farney, E. P.; Chapman, S. J.; Swords, W. B.; Torelli, M. D.; Hamers, R. J.; Yoon, T. P. *J. Am. Chem. Soc.* **2019**, *141*, 6385–6391. doi:10.1021/jacs.9b01885
- Huber, N.; Li, R.; Ferguson, C. T. J.; Gehrig, D. W.; Ramanan, C.; Blom, P. W. M.; Landfester, K.; Zhang, K. A. *Catal. Sci. Technol.* **2020**, *10*, 2092–2099. doi:10.1039/d0cy00016g
- Tanaka, K.; Kishimoto, M.; Tanaka, Y.; Kamiyama, Y.; Asada, Y.; Sukekawa, M.; Ohtsuka, N.; Suzuki, T.; Momiyama, N.; Honda, K.; Hoshino, Y. *J. Org. Chem.* **2022**, *87*, 3319–3328. doi:10.1021/acs.joc.1c02972
- Tang, M.; Cameron, L.; Poland, E. M.; Yu, L.-J.; Moggach, S. A.; Fuller, R. O.; Huang, H.; Sun, J.; Thickett, S. C.; Massi, M.; Coote, M. L.; Ho, C. C.; Bissember, A. C. *Inorg. Chem.* **2022**, *61*, 1888–1898. doi:10.1021/acs.inorgchem.1c02964
- Yu, Y.; Fu, Y.; Zhong, F. *Green Chem.* **2018**, *20*, 1743–1747. doi:10.1039/c8gc00299a
- Horibe, T.; Ohmura, S.; Ishihara, K. *J. Am. Chem. Soc.* **2019**, *141*, 1877–1881. doi:10.1021/jacs.8b12827
- Horibe, T.; Ishihara, K. *Chem. Lett.* **2020**, *49*, 107–113. doi:10.1246/cl.190790
- Okada, Y.; Chiba, K. *Chem. Rev.* **2018**, *118*, 4592–4630. doi:10.1021/acs.chemrev.7b00400
- Okada, Y. *Electrochemistry* **2020**, *88*, 497–506. doi:10.5796/electrochemistry.20-00088
- Shida, N.; Imada, Y.; Okada, Y.; Chiba, K. *Eur. J. Org. Chem.* **2020**, *570*–574. doi:10.1002/ejoc.201901576
- Imada, Y.; Yamaguchi, Y.; Shida, N.; Okada, Y.; Chiba, K. *Chem. Commun.* **2017**, *53*, 3960–3963. doi:10.1039/c7cc00664k
- Okada, Y.; Yamaguchi, Y.; Ozaki, A.; Chiba, K. *Chem. Sci.* **2016**, *7*, 6387–6393. doi:10.1039/c6sc02117d
- Okada, Y.; Maeta, N.; Nakayama, K.; Kamiya, H. *J. Org. Chem.* **2018**, *83*, 4948–4962. doi:10.1021/acs.joc.8b00738
- Okada, Y. *J. Org. Chem.* **2019**, *84*, 1882–1886. doi:10.1021/acs.joc.8b02861
- Okada, Y.; Yamaguchi, Y.; Chiba, K. *ChemElectroChem* **2019**, *6*, 4165–4168. doi:10.1002/celc.201900184
- Maeta, N.; Kamiya, H.; Okada, Y. *Org. Lett.* **2019**, *21*, 8519–8522. doi:10.1021/acs.orglett.9b02808
- Okada, Y. *Chem. Rec.* **2021**, *21*, 2223–2238. doi:10.1002/tcr.202100029
- Nakayama, K.; Maeta, N.; Horiguchi, G.; Kamiya, H.; Okada, Y. *Org. Lett.* **2019**, *21*, 2246–2250. doi:10.1021/acs.orglett.9b00526

47. Nakayama, K.; Kamiya, H.; Okada, Y. *J. Electrochem. Soc.* **2020**, *167*, 155518. doi:10.1149/1945-7111/abb97f
48. Murray, P. R. D.; Bussink, W. M. M.; Davies, G. H. M.; van der Mei, F. W.; Antropow, A. H.; Edwards, J. T.; D'Agostino, L. A.; Ellis, J. M.; Hamann, L. G.; Romanov-Michaillidis, F.; Knowles, R. R. *J. Am. Chem. Soc.* **2021**, *143*, 4055–4063. doi:10.1021/jacs.1c01173

License and Terms

This is an open access article licensed under the terms of the Beilstein-Institut Open Access License Agreement (<https://www.beilstein-journals.org/bjoc/terms>), which is identical to the Creative Commons Attribution 4.0 International License (<https://creativecommons.org/licenses/by/4.0>). The reuse of material under this license requires that the author(s), source and license are credited. Third-party material in this article could be subject to other licenses (typically indicated in the credit line), and in this case, users are required to obtain permission from the license holder to reuse the material.

The definitive version of this article is the electronic one which can be found at:

<https://doi.org/10.3762/bjoc.18.112>



Electrogenerated base-promoted cyclopropanation using alkyl 2-chloroacetates

Kouichi Matsumoto^{*1}, Yuta Hayashi¹, Kengo Hamasaki¹, Mizuki Matsuse¹, Hiyono Suzuki¹, Keiji Nishiwaki² and Norihito Kawashita³

Letter

Open Access

Address:

¹Department of Chemistry, School of Science and Engineering, Kindai University 3-4-1 Kowakae, Higashi-osaka, Osaka 577-8502, Japan,
²Department of Pharmaceutical Sciences, Faculty of Pharmacy, Kindai University 3-4-1 Kowakae, Higashi-osaka, Osaka 577-8502, Japan and ³Department of Life Science, School of Science and Engineering, Kindai University, 3-4-1 Kowakae, Higashi-osaka, Osaka 577-8502, Japan

Email:

Kouichi Matsumoto^{*} - kmatsumo@chem.kindai.ac.jp

* Corresponding author

Keywords:

alkyl 2-chloroacetates; cyclopropane derivatives; divided cell; electro-reduction

Beilstein J. Org. Chem. **2022**, *18*, 1116–1122.

<https://doi.org/10.3762/bjoc.18.114>

Received: 10 February 2022

Accepted: 11 August 2022

Published: 29 August 2022

This article is part of the thematic issue "Molecular and macromolecular electrochemistry: synthesis, mechanism, and redox properties".

Guest Editor: S. Inagi

© 2022 Matsumoto et al.; licensee Beilstein-Institut.

License and terms: see end of document.

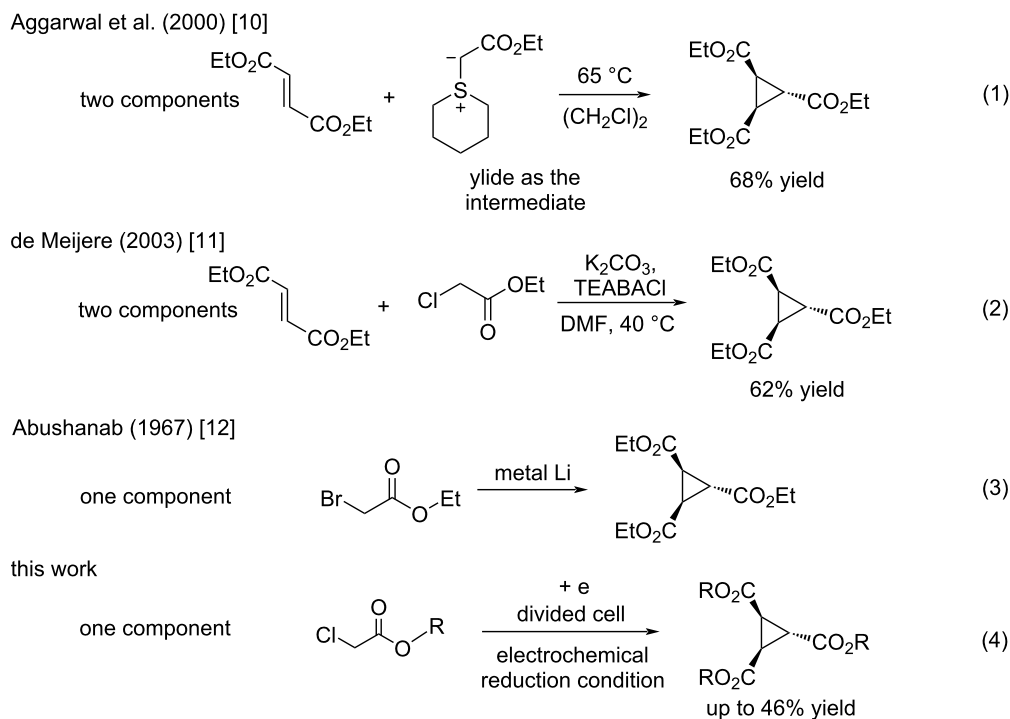
Abstract

The electrochemical reduction conditions of the reaction of alkyl 2-chloroacetates in $\text{Bu}_4\text{NBr}/\text{DMF}$ using a divided cell equipped with Pt electrodes to produce the corresponding cyclopropane derivatives in moderate yields were discovered. The reaction conditions were optimized, the scope and limitations, as well as scale-up reactions were investigated. The presented method for the electrochemical production of cyclopropane derivatives is an environmentally friendly and easy to perform synthetic procedure.

Introduction

In organic chemistry, cyclopropanes and their related compounds have been recognized as important molecules. For example, cyclopropane derivatives are found in both natural products and pharmaceutical products. The cyclopropane skeleton is also found in agrochemicals, especially pyrethroid, as an insecticide, is one important compound. Cyclopropanes also play a significant role in organic synthesis as versatile building blocks [1-5]. In general, some synthetic procedures for cyclopropane derivatives have been discovered, e.g., the Simmons-Smith reaction and the use of metal carbenoids being two of the more prominent and reliable methods [6-9].

Aggarwal and colleagues reported in 2000 that the reaction between a Michael acceptor such as diethyl fumarate and a sulfur ylide, prepared from ethyl 2-diazoacetate and tetrahydro-2*H*-thiopyran in the presence of $\text{Cu}(\text{acac})_2$, yielded triethyl cyclopropane-1,2,3-tricarboxylate in 68% yield (Scheme 1, reaction 1) [10]. The same chemical yield was obtained by using a catalytic amount of tetrahydro-2*H*-thiopyran (0.2 equiv) in the process [10]. Furthermore, de Meijere and colleagues in 2003 demonstrated that the reaction of diethyl fumarate and ethyl 2-chloroacetate in DMF at 40 °C with K_2CO_3 and TEBACl (benzyltriethylammonium chloride) produced triethyl cyclo-



Scheme 1: Formations of 1,2,3-trialkyl cyclopropanetricarboxylates. Previous reports (reactions 1–3) and this work (reaction 4).

propane-1,2,3-tricarboxylate in 62% yield (Scheme 1, reaction 2) [11]. Both procedures are two-component coupling reactions. In contrast, a method involving a one-component reaction using alkyl 2-haloacetate has been developed by Abushanab in 1967, in which a stoichiometric amount of metal lithium was utilized to reduce ethyl 2-bromoacetate to form the corresponding 1,2,3-trisubstituted cyclopropane derivatives (Scheme 1, reaction 3) [12]. The generation of an anionic intermediate was indicated. During our study, we discovered that 1,2,3-trisubstituted cyclopropane derivatives could be formed in moderate yields through the electrochemical reduction [13–21] of alkyl 2-chloroacetates in a divided cell (Scheme 1, reaction 4). The in Abushanab's study utilized metal lithium is one of the rarest and most expensive metals. In addition, the treatment of metal lithium is difficult and occasionally dangerous, and the reaction also produces the corresponding Li salt as waste [22,23]. In contrast, in this work, we use basic electricity to make the corresponding cyclopropane derivatives. Herein, we would like to report the details of our investigation.

Results and Discussion

First, we investigated the reaction conditions for the electrochemical reduction to optimize the reaction outcome. The typical procedure is as follows: the electrochemical reduction was carried out in an H-type divided cell. Both electrodes were made from Pt plates. In the cathodic chamber, **1** (0.5 mmol) was

dissolved in 0.3 M Bu_4NBr in DMF (4.0 mL) and 0.3 M Bu_4NBr in DMF (4.0 mL) was introduced to the anodic chamber. Constant current electrolysis at 12 mA until 1.0 F/mol was consumed in the cathode yielded the corresponding compound **2** in a 46% yield (Table 1, entry 1). Various parameters were varied to increase the chemical yield, as shown in Table 1. For example, the use of carbon felt as the cathode produced **2** in <25% yield (Table 1, entry 2). The small influence of the anodic electrode material was confirmed in the reaction using carbon felt as the anode. In this reaction compound **2** was obtained in 40% yield (Table 1, entry 3). The use of DMSO instead of DMF resulted in <22% yield of **2** (Table 1, entry 4). However, when MeOH was used **2** could not be obtained at all (Table 1, entry 5). Reactions with Bu_4NCl , Bu_4NI , and Bu_4NBF_4 instead of Bu_4NBr produced the corresponding compound **2** in 35%, <21%, and 44% yields, respectively (Table 1, entries 6–8). The amount of the supporting electrolyte Bu_4NBr , such as 0.8 equiv and 4.0 equiv instead of 2.4 equiv, appeared to have no influence, and **2** was produced at 40% and 43% yields, respectively (Table 1, entries 9 and 10). In terms of temperature and current (Table 1, entries 11–14), 6 mA at room temperature yielded the best result of 46% yield (Table 1, entry 14). The reaction did not take place in the absence of electricity (Table 1, entry 15). Based on the above optimizations, we chose the conditions given in entry 1 of Table 1 as the optimized parameters [24].

Table 1: Reaction optimization.

Entry	Variation from standard conditions ^a	% Yield ^b
1	none	46
2	Pt (+) C (–) instead of Pt (+) Pt (–)	<25 ^c
3	C (+) Pt (–) instead of Pt (+) Pt (–)	40
4	DMSO as solvent ^d	<22
5	MeOH as solvent ^d	n.d. ^e
6	Bu ₄ NCl instead of Bu ₄ NBr ^d	35
7	Bu ₄ NI instead of Bu ₄ NBr ^d	<21
8	Bu ₄ NBF ₄ instead of Bu ₄ NBr ^d	44
9	0.8 equiv Bu ₄ NBr instead of 2.4 equiv Bu ₄ NBr ^d	40
10	4.0 equiv Bu ₄ NBr instead of 2.4 equiv Bu ₄ NBr ^d	43
11	0 °C instead of rt	45
12	60 °C instead of rt	<44
13	20 mA instead of 12 mA, 1.0 F/mol	<33
14	6 mA instead of 12 mA, 1.0 F/mol	46
15	no electric current	n.d. ^{c,e}

^aStandard conditions: 1 (0.5 mmol), 0.3 M Bu₄NBr in DMF (4.0 mL × 2), divided cell, 12 mA, rt, 1.0 F/mol of electricity against 0.5 mmol of substrate 1. ^bIsolated yields using preparative GPC separation of the crude materials. ^cObserved from gas chromatography (GC) analysis. ^dIn both anodic and cathodic chambers. ^en.d. = no detection.

Next, we investigated the effect of electricity around 1 F/mol on the yield, as shown in Table 2, using the optimized conditions [25]. The yield of **2** was 46% in the case of 1.0 F/mol (Table 2,

Table 2: Effect of electricity around 1 F/mol and type of electrochemical cell.

Entry	F/mol	% Yield ^a
1	1.0	46 ^b
2	0.90	44
3	1.1	<35
4 ^c	1.0	<5

^aIsolated yields using preparative GPC separation of the crude materials. Compound **2** of entry 3 contained a small amount of impurity.

^bThis yield is from entry 1 of Table 1. ^cAn undivided cell was used instead of a divided cell.

entry 1), as shown in entry 1 of Table 1. The chemical output of **2** was 44% in the case of 0.90 F/mol (Table 2, entry 2). However, using 1.1 F/mol resulted as well in a lower yield of **2** (<35%, Table 2, entry 3). Thus, 0.90 F/mol or 1.0 F/mol of electricity for the current reaction was found to be sufficient to obtain the product in high yield, and we choose 1.0 F/mol of electricity for the next investigations (Table 3). Finally, the electrolysis using the undivided cell shown in entry 4 of Table 2 yielded **2** in <5% yield, indicating that the divided cell is essential for the current reaction. In the undivided cell, the anionic species from the cathode might be consumed on the surface of the anode.

To examine the scope and limitations, we carried out electrochemical reductions of various alkyl 2-haloacetates under the optimized conditions. Table 3 summarizes the results. The reac-

Table 3: Scope and limitations.

Entry	Ester	Product	% Yield ^a
1			28

Table 3: Scope and limitations. (continued)

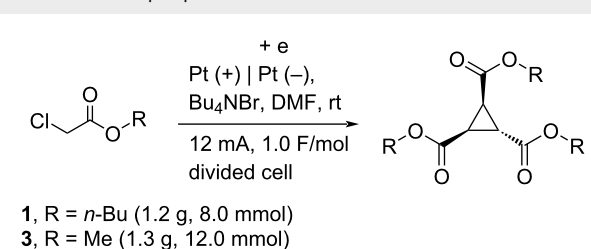
2		5		6	<23 (21)
3		7		6	<24 (19)
4		8		6	<26 (20)
5		9		10	<22 (20)
6		11		12	<31 (28)
7		13		14	n.d. ^b
8		15		16	34
9		17		18	31 ^c

^aIsolated yields using preparative GPC separation of the crude materials. Compound **6** in entries 3 and 4 contained an impurity of non-negligible amount, despite of repeated purification by GPC. Compound **6** in entry 2, **10** in entry 5 and **12** in entry 6 contained a small amount of impurities (see ¹³C NMR spectra of compounds **6**, **10** and **12** in Supporting Information File 1). Values in parentheses in entries 2–6 are estimated yields, calculated from the ratio of isolated compounds and impurities given in the ¹H NMR spectra, because the impurities seem to be the corresponding trialkyl propane-1,2,3-carboxylates (vide infra). ^bn.d. = no detection. ^cIsolated yield after silica-gel column chromatography.

tion of methyl 2-chloroacetate (**3**) afforded the corresponding compound **4** in 28% yield (Table 3, entry 1). The reaction of ethyl 2-chloroacetate (**5**) produced the corresponding compound **6** in a similar <23% yield (Table 3, entry 2). Ethyl 2-bromoacetate (**7**) and ethyl 2-iodoacetate (**8**), in which the leaving groups were changed from Cl to Br and I, showed similar reactivities to produce compound **6** in <24% and <26% yields, respectively (Table 3, entries 3 and 4). *n*-Propyl 2-chloroacetate (**9**), with the longer alkyl chain, and *tert*-butyl 2-chloroacetate (**11**), with the bulky alkyl group, produced **10** and **12** in <22% and <31% yields, respectively (Table 3, entries

5 and **6**). The reaction of **13** with the vinyl group did not occur (Table 3, entry 7), but the reaction of compound **15** with the allyl group formed **16** in 34% yield (Table 3, entry 8). Finally, benzyl 2-chloroacetate (**17**) produced the corresponding compound **18** in 31% yield (Table 3, entry 9).

The current electrolysis reaction can be easily scaled-up with obtaining similar yields of the products. The reaction of **1** (1.2 g, 8.0 mmol) in Bu₄NBr/DMF at room temperature with 12 mA and 1.0 F/mol yielded the corresponding compound **2** in <45% yield (Table 4, entry 1). In addition, the reac-

Table 4: Scale-up experiments.

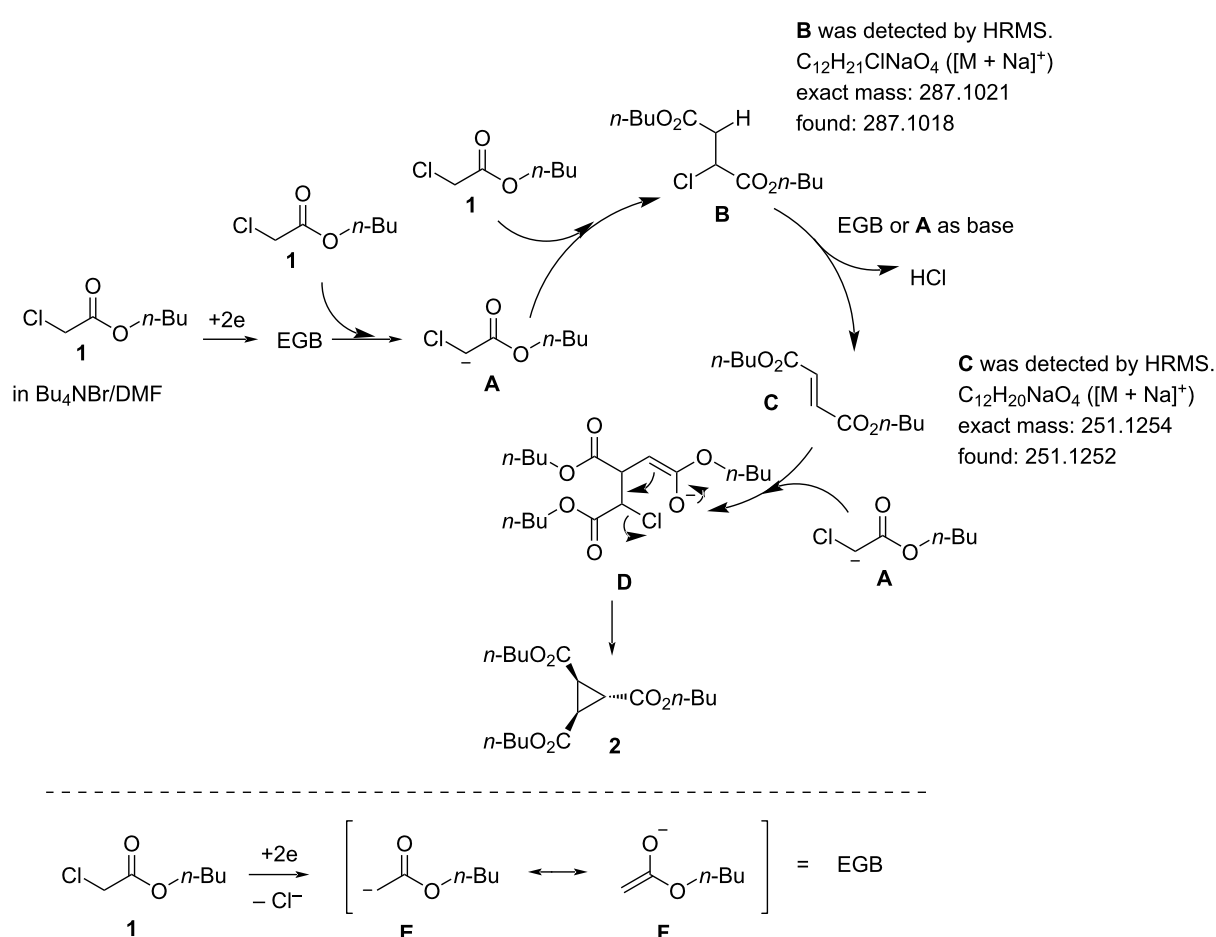
1, R = n-Bu (1.2 g, 8.0 mmol)
3, R = Me (1.3 g, 12.0 mmol)

Entry	Ester	R	Product	% Yield ^a
1	1	n-Bu	2	<45 (38)
2	3	Me	4	32

^aIsolated yields using preparative GPC separation of the crude materials. Compound 2 in entry 1 contained a small amount of impurity. The value in parenthesis in entry 1 is an estimated yield, calculated from the ratio of isolated compound and impurity given in the ¹H NMR spectrum, because the impurity seems to be tri-n-butyl propane-1,2,3-carboxylate (vide infra).

tion of 3 (1.3 g, 12.0 mmol) yielded 4 in 32% yield (Table 4, entry 2).

Scheme 2 depicts a plausible reaction mechanism. We assume that the current reaction follows a similar mechanism as described in Abushanab's report [12]. In addition, the current reaction indicated the generation of an EGB (electrogenerated base) [26–29]. The electrochemical reduction conditions of the solution containing 1 may generate an EGB, which reacts with 1 to produce anionic A. At the stage of the generation of the EGB, the reduction of 1 may generate an enolate ion such as E or F, which might serve as EGB, although other sources of EGBs cannot be denied [30,31]. Intermediate A may combine with 1 to produce B, which may react with the EGB or another molecule A to produce C, releasing HCl. In Abushanab's report [12], C can be coupled with A in a similar manner to yield D [12]. Finally, intramolecular cyclization of D may yield 2. In order to obtain a deeper insight in the reaction, we made an analysis of the crude material, which was prepared by passing

**Scheme 2:** Plausible reaction mechanism. EGB = electrogenerated base.

0.5 F/mol using the standard conditions and the usual work up procedure. Compounds **B** and **C** were confirmed by HRMS analysis shown in Scheme 2, which supported the current mechanism.

In addition, one of the impurities seems to be the trialkyl propane-1,2,3-carboxylates [32], because the HRMS analyses of the isolated compounds, such as **6** (Table 3, entry 2), **10** (Table 3, entry 5), and **12** (Table 3, entry 6), which were not of high purity, showed the existence of the corresponding trialkyl propane-1,2,3-carboxylates, together with the signal of the desired products **6**, **10**, and **12**. The formation of trialkyl propane-1,2,3-carboxylate might be through the Michael addition of the electrogenerated base (**E** in Scheme 2) to **C** or the electrochemical reduction of **2**.

Conclusion

A new electrochemical transformation of alkyl 2-chloroacetates to cyclopropane derivatives has been developed. The reaction has been optimized, the scope and limitations have been investigated. Scale-up reactions were performed and satisfactory yields obtained. The generation of an EGB of the enolate ion from alkyl 2-chloroacetates is indicated. The current method is one of the most environmentally benign and accessible methods for the preparation of 1,2,3-trisubstituted cyclopropane derivatives, notwithstanding the low reaction yields. In our laboratory, further synthetic investigations are in progress.

Supporting Information

Supporting Information File 1

Experimental details, characterization data of new compounds and copies of ^1H NMR and ^{13}C NMR spectra. [<https://www.beilstein-journals.org/bjoc/content/supplementary/1860-5397-18-114-S1.pdf>]

Acknowledgements

We are grateful to the Kindai University Joint Research Center for the use of facilities. We also appreciate the reviewers for fruitful suggestion.

Funding

This work was supported in part by JSPS KAKENHI Grants JP 20K05588 (Grant-in-Aid for Scientific Research (C)). K. M. acknowledges the Tokyo Ohka Foundation for The Promotion of Science and Technology for the financial support. This work was also partially supported by 2021 Kindai University Research Enhancement Grants (KD2106 and KD2104).

ORCID® iDs

Keiji Nishiwaki - <https://orcid.org/0000-0001-5017-244X>
Norihiro Kawashita - <https://orcid.org/0000-0002-1740-7232>

References

- Cohen, Y.; Cohen, A.; Marek, I. *Chem. Rev.* **2021**, *121*, 140–161. doi:10.1021/acs.chemrev.0c00167
- Pirenne, V.; Muriel, B.; Waser, J. *Chem. Rev.* **2021**, *121*, 227–263. doi:10.1021/acs.chemrev.0c00109
- Ebner, C.; Carreira, E. M. *Chem. Rev.* **2017**, *117*, 11651–11679. doi:10.1021/acs.chemrev.6b00798
- Augustin, A. U.; Werz, D. B. *Acc. Chem. Res.* **2021**, *54*, 1528–1541. doi:10.1021/acs.accounts.1c00023
- Pons, A.; Delion, L.; Poisson, T.; Charette, A. B.; Jubault, P. *Acc. Chem. Res.* **2021**, *54*, 2969–2990. doi:10.1021/acs.accounts.1c00261
- Simmons, H. E.; Smith, R. D. *J. Am. Chem. Soc.* **1958**, *80*, 5323–5324. doi:10.1021/ja01552a080
- Ye, T.; McKervey, M. A. *Chem. Rev.* **1994**, *94*, 1091–1160. doi:10.1021/cr00028a010
- Bartoli, G.; Bencivenni, G.; Dalpozzo, R. *Synthesis* **2014**, *46*, 0979–1029. doi:10.1055/s-0033-1340838
- Bos, M.; Poisson, T.; Pannecoucke, X.; Charette, A. B.; Jubault, P. *Chem. – Eur. J.* **2017**, *23*, 4950–4961. doi:10.1002/chem.201604564
- Aggarwal, V. K.; Smith, H. W.; Hynd, G.; Jones, R. V. H.; Fieldhouse, R.; Spey, S. E. *J. Chem. Soc., Perkin Trans. 1* **2000**, 3267–3276. doi:10.1039/b004367m
- Kozhushkov, S. I.; Leonov, A.; de Meijere, A. *Synthesis* **2003**, 956–958. doi:10.1055/s-2003-38687
- Abushanab, E. *Tetrahedron Lett.* **1967**, *8*, 2833–2836. doi:10.1016/s0040-4039(00)90868-2
- Shida, N.; Nakamura, Y.; Atobe, M. *Chem. Rec.* **2021**, *21*, 2164–2177. doi:10.1002/tcr.202100016
- Shimakoshi, H.; Hisaeda, Y. *Chem. Rec.* **2021**, *21*, 2080–2094. doi:10.1002/tcr.202100077
- Shibuya, A.; Nokami, T. *Chem. Rec.* **2021**, *21*, 2389–2396. doi:10.1002/tcr.202100085
- Krueger, R.; Moeller, K. D. *J. Org. Chem.* **2021**, *86*, 15847–15865. doi:10.1021/acs.joc.1c01609
- Nutting, J. E.; Gerken, J. B.; Stamoulis, A. G.; Bruns, D. L.; Stahl, S. S. *J. Org. Chem.* **2021**, *86*, 15875–15885. doi:10.1021/acs.joc.1c01520
- Mitsudo, K.; Kurimoto, Y.; Yoshioka, K.; Suga, S. *Chem. Rev.* **2018**, *118*, 5985–5999. doi:10.1021/acs.chemrev.7b00532
- Yan, M.; Kawamata, Y.; Baran, P. S. *Chem. Rev.* **2017**, *117*, 13230–13319. doi:10.1021/acs.chemrev.7b00397
- Fuchigami, T.; Inagi, S. *Acc. Chem. Res.* **2020**, *53*, 322–334. doi:10.1021/acs.accounts.9b00520
- Senboku, H.; Katayama, A. *Curr. Opin. Green Sustainable Chem.* **2017**, *3*, 50–54. doi:10.1016/j.cogsc.2016.10.003
- Elinson, M. N.; Feducovich, S. K.; Vereshchagin, A. N.; Gorbunov, S. V.; Belyakov, P. A.; Nikishin, G. I. *Tetrahedron Lett.* **2006**, *47*, 9129–9133. doi:10.1016/j.tetlet.2006.10.075
See for a reported electrochemical synthesis of cyclopropanes.
- Tokuda, M.; Hayashi, A.; Suginome, H. *Bull. Chem. Soc. Jpn.* **1991**, *64*, 2590–2592. doi:10.1246/bcsj.64.2590
See for a reported electrochemical synthesis of cyclopropanes.

24. As the possibility for the generation of an EGB, the electrolysis in the presence of *pre*-EGB, such as H₂O (1 mmol) or 2-pyrrolidone (1 mmol), under the optimized conditions gave 12% yield or trace of **2**, respectively, which was estimated by ¹H NMR analysis of the crude materials.

25. We roughly performed the GC-monitoring of the electrochemical reaction until ca. 2 F/mol were consumed, and found that around 1 F/mol seems to be suitable for the best yield of **2** in the reaction.

26. Torii, S.; Hayashi, N.; Kuroboshi, M. *Synlett* **1998**, 599–600.
doi:10.1055/s-1998-1752

27. Strehl, J.; Hilt, G. *Org. Lett.* **2019**, 21, 5259–5263.
doi:10.1021/acs.orglett.9b01866

28. Mirza, B.; Samiei, S. S. *Asian J. Chem.* **2012**, 24, 1101–1103.

29. William, J. M.; Kuriyama, M.; Onomura, O. *Electrochemistry* **2013**, 81, 374–376. doi:10.5796/electrochemistry.81.374

30. Baizer, M. M.; Chruma, J. L. *J. Org. Chem.* **1972**, 37, 1951–1960.
doi:10.1021/jo00977a020

31. Inesi, A.; Zeppa, A.; Zeuli, E. *J. Electroanal. Chem. Interfacial Electrochem.* **1982**, 137, 103–115.
doi:10.1016/0022-0728(82)85070-5

32. Ye, Y.; Ma, G.; Yao, K.; Gong, H. *Synlett* **2021**, 32, 1625–1628.
doi:10.1055/a-1328-0352
See for NMR spectra of triethyl propane-1, 2, 3-carboxylate. By comparison with NMR spectra of *trans*-triethyl cyclopropane-1,2,3-tricarboxylate (**6**) in the Supporting Information, triethyl propane-1,2,3-carboxylate was identified as the impurity.

License and Terms

This is an open access article licensed under the terms of the Beilstein-Institut Open Access License Agreement (<https://www.beilstein-journals.org/bjoc/terms>), which is identical to the Creative Commons Attribution 4.0 International License (<https://creativecommons.org/licenses/by/4.0>). The reuse of material under this license requires that the author(s), source and license are credited. Third-party material in this article could be subject to other licenses (typically indicated in the credit line), and in this case, users are required to obtain permission from the license holder to reuse the material.

The definitive version of this article is the electronic one which can be found at:

<https://doi.org/10.3762/bjoc.18.114>



Synthesis of protected precursors of chitin oligosaccharides by electrochemical polyglycosylation of thioglycosides

Md Azadur Rahman¹, Kana Kuroda¹, Hirofumi Endo¹, Norihiko Sasaki^{1,2}, Tomoaki Hamada³, Hiraku Sakai³ and Toshiki Nokami^{*1,2}

Full Research Paper

Open Access

Address:

¹Department of Chemistry and Biotechnology, Tottori University, 4-101 Koyamacho-minami, Tottori City, 680-8552 Tottori, Japan, ²Center for Research on Green Sustainable Chemistry, Faculty of Engineering, Tottori University, 4-101 Koyamacho-minami, Tottori City, 680-8552 Tottori, Japan and ³Koganei Corporation, 3-11-28 Midorimachi, Koganei City, 184-8533 Tokyo, Japan

Email:

Toshiki Nokami* - tnokami@tottori-u.ac.jp

* Corresponding author

Keywords:

electrochemical glycosylation; glucosamine; oligosaccharide; oxidation potential; polyglycosylation

Beilstein J. Org. Chem. **2022**, *18*, 1133–1139.

<https://doi.org/10.3762/bjoc.18.117>

Received: 04 July 2022

Accepted: 18 August 2022

Published: 30 August 2022

This article is part of the thematic issue "Molecular and macromolecular electrochemistry: synthesis, mechanism, and redox properties".

Guest Editor: S. Inagi

© 2022 Rahman et al.; licensee Beilstein-Institut.

License and terms: see end of document.

Abstract

The synthesis of protected precursors of chitin oligosaccharides by electrochemical polyglycosylation of thioglycosides as monomer is described. Oligosaccharides up to the hexasaccharide were synthesized under optimized reaction conditions. Further, a modified method enabled the synthesis of oligosaccharides up to the octasaccharide by repeating electrolysis with additional monomers. The mechanism of the electrochemical polyglycosylation is also discussed, based on the oxidation potential of the monomer and oligosaccharides.

Introduction

Chitin oligosaccharides are partial structures of chitin, which is an abundant β -1,4-linked polysaccharide composed of *N*-acetyl-glucosamine as repeating unit (Figure 1) [1]. Biological activities of longer oligosaccharides, such as octasaccharide, have been paid much attention for many years. However, it is difficult to obtain pure oligosaccharides by isolation from natural sources or by synthesis via chemical glycosylation [2]. Total syntheses of chitin and chitosan oligosaccharides based on

conventional chemical glycosylation of protected monosaccharides as building blocks have already been reported. Convergent synthesis using oligosaccharide building blocks can reduce the number of steps in the total synthesis. However, it requires manipulation of the anomeric leaving groups and deprotection of the protected hydroxy group at the 4-position prior to glycosylation. Although automated electrochemical assembly, which is a one-pot iterative synthesis of oligosaccharides based on

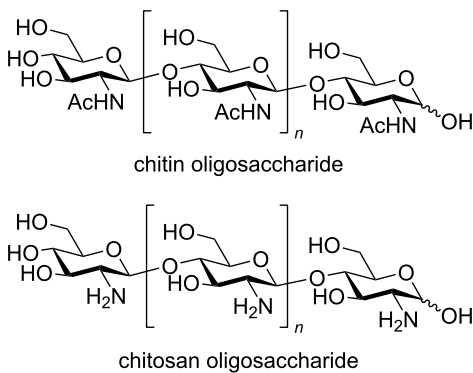


Figure 1: Structures of chitin and chitosan oligosaccharides.

electrochemical preactivation of building blocks, is an alternative method for the synthesis of chitin oligosaccharides [3,4], it is also time-consuming and too sophisticated to prepare oligosaccharides composed of a single repeating structure. Thus, we assume that the electrochemical polyglycosylation via the electrochemical activation of thioglycosides is a practical approach for the preparation of chitin oligosaccharides. Hashimoto and co-workers have already reported the synthesis of protected precursors of chitin oligosaccharides by polyglycosylation of thioglycosides [5]. However, this is one of a few examples of chemical synthesis of chitin oligosaccharides through polyglycosylation of a glucosamine monosaccharide [6]. Recently, we have reported electrochemical polyglycosylation using a glucos-

amine derivative as a monomer [7]. This is another example of polyglycosylation of a glucosamine monosaccharide. However, *N*-acetylglucosamines are linked by α -1,4-glycosidic bonds. Here, we report electrochemical polyglycosylation of thioglycosides to produce protected precursors of chitin oligosaccharides.

Results and Discussion

Optimization of electrochemical polyglycosylation

We initiated our study with the optimization of the arylthio group of thioglycoside **1**, carrying an unprotected 4-OH group, an acetyl-protected 3-OH unit, a benzyl-protected 6-OH group, and a phthaloyl-protected 2-NH₂ unit (Figure 2) [3]. Electrochemical polyglycosylation was performed by a sequential two-step process, which involved anodic oxidation at -80 °C and glycosylation at -50 °C. The crude product of the reaction was purified by gel permeation chromatography (GPC), and the monosaccharides **1a–d** and oligosaccharides **2a–d** ($n = 2$)–**7a–d** ($n = 7$) were isolated. Only thioglycoside **1a** ($\text{Ar} = 4\text{-FC}_6\text{H}_4$, $E_{\text{ox}} = 1.70$ V vs SCE) gave oligosaccharides up to hexasaccharide **6a**, although the yield of pentasaccharide **5a** (3%) and hexasaccharide **6a** (1%) was very low. For thioglycoside **1b** ($\text{Ar} = 4\text{-ClC}_6\text{H}_4$, $E_{\text{ox}} = 1.68$ V vs SCE), the highest conversion (79%) and the highest yield of tetrasaccharide **4b** (14%) were observed. Contrary, thioglycoside **1c** ($\text{Ar} = 4\text{-MeC}_6\text{H}_4$, $E_{\text{ox}} = 1.47$ V vs SCE), which had the lowest oxidation potential, showed the lowest conversion (51%) and the lowest yield of

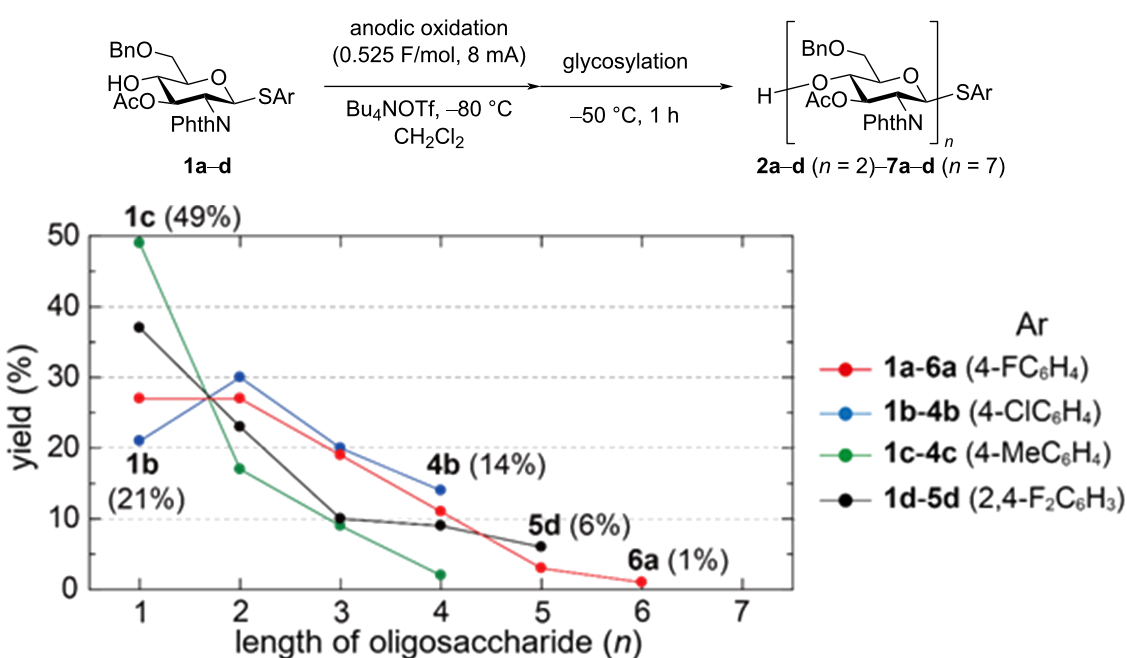


Figure 2: Effect of the anomeric leaving group on the yield of oligosaccharides.

tetrosaccharide **4c** (2%) [8]. This being the case, lower conversion of the building block **1c** and lower yield of oligosaccharides **2c–4c** indicated that thus-generated oligosaccharides **2c–4c**, with a lower oxidation potential, also consumed electricity and converted to the corresponding hydroxy-substituted sugars, as observed by MS analysis. Thioglycoside **1d** ($\text{Ar} = 2,4\text{-F}_2\text{C}_6\text{H}_3$, $E_{\text{ox}} = 1.73$ V vs SCE), which had the highest oxidation potential, also showed low conversion (63%). However, it gave pentasaccharide **5d** in the highest yield (6%) among these four thioglycosides. Based on these results, we optimized the reaction using thioglycoside **1a**, which afforded oligosaccharides **2a–6a** and recovered monosaccharide **1a** in the highest total yield (88%).

Reaction parameters of the electrochemical polyglycosylation, such as amount of electricity and electrolyte, were also optimized using thioglycoside **1a** (see Supporting Information File 1 for details). The complete conversion of monosaccharide **1a** was observed with 0.6 F/mol. However, 0.525 F/mol was chosen as the optimal amount of electricity to prevent formation of byproducts, such as hydroxy-substituted sugars that carry an anomeric hydroxy group instead of the ArS group. Although we tested other ammonium triflates, such as tetraethylammonium triflate and 1-butyl-1-methylpyrrolidinium triflate as electrolytes, both electrolytes gave oligosaccharides in lower yield.

Next, we investigated the influence of the glycosylation temperature (T_2), and it was revealed that glycosylation proceeded even at -80 °C (Figure 3, in pink). Although higher conversion

of thioglycoside **1a** was observed at higher temperature, we did not test a glycosylation temperature above -30 °C because of the low stability of the glycosylation intermediate at an elevated temperature [9]. It is important to note that heptasaccharide **7a**, which was never obtained at -50 °C, was produced at -40 °C (in blue) and -30 °C (in black), although the yield of **7a** was very low (1%). These results indicated that the glycosylation temperature was an important parameter for obtaining longer oligosaccharides, and glycosylation might proceed during the anodic oxidation at -80 °C.

The temperature of anodic oxidation (T_1) was also investigated together with the glycosylation temperature (T_2) because glycosylation must occur during the anodic oxidation at elevated temperature (Figure 4). Indeed, formation of oligosaccharides longer than tetrasaccharide **4a** was increased at elevated temperature. The highest total yield of oligosaccharides **2a–7a** was obtained at $T_1 = -60$ °C and $T_2 = -30$ °C, although heptasaccharide **7a** was not produced. MALDI-TOF MS spectra indicated the formation of byproducts derived from longer oligosaccharides at $T_1 = -30$ °C and $T_2 = -30$ °C (Figure 5). The relative intensity of the molecular ion peaks of hydroxy-substituted sugars of oligosaccharides and/or trehalose pseudo-oligosaccharides, which were major byproducts at the elevated temperature, became stronger in the corresponding peaks of longer oligosaccharides, such as hexasaccharide **6a** and heptasaccharide **7a**. Proposed structures of byproducts of trisaccharide **3a**, including hydroxy-substituted sugar **9** and trehalose product **10**, are shown in Figure 6. These byproducts were obtained as inseparable mixture because of the same molecular weight and simi-

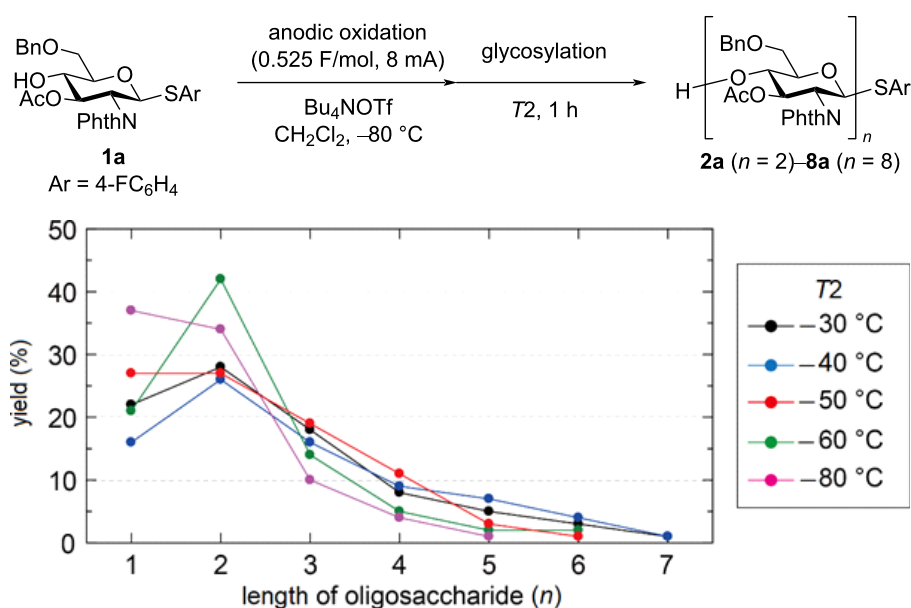


Figure 3: Influence of the glycosylation temperature (T_2) on the yield of oligosaccharides.

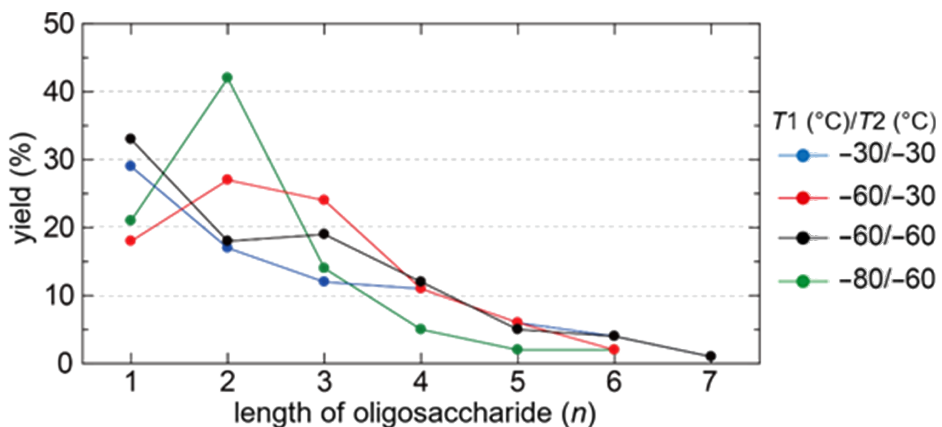
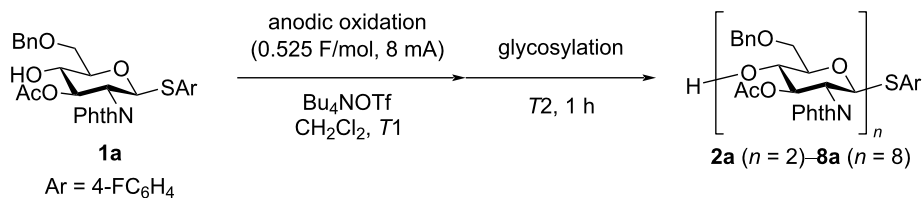


Figure 4: Influence of temperatures of anodic oxidation (T_1) and glycosylation (T_2).

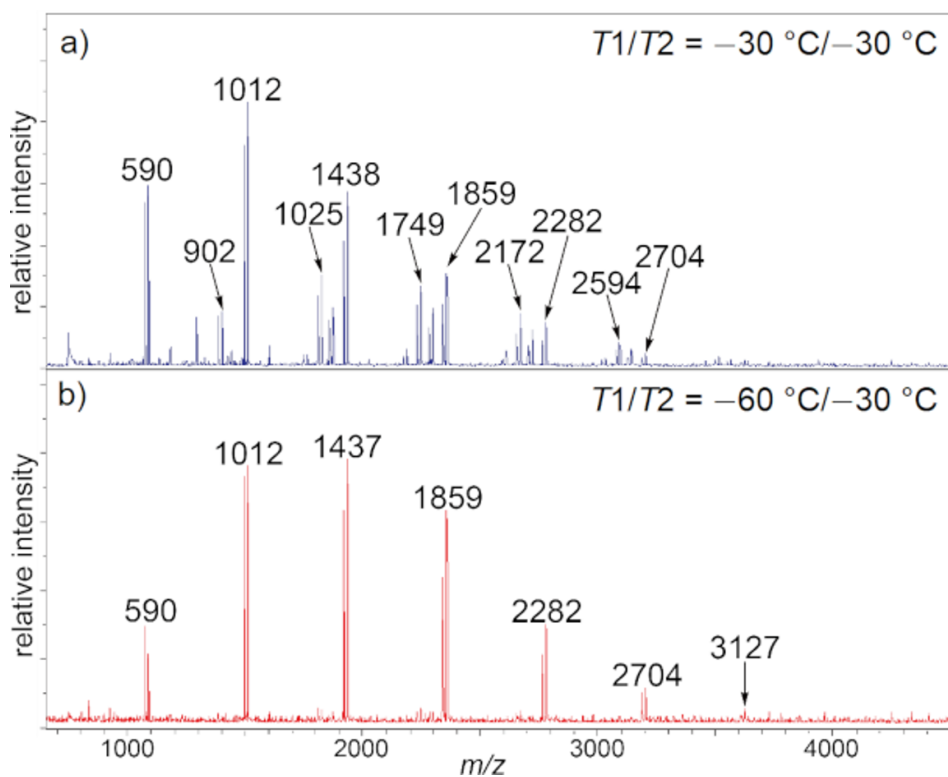


Figure 5: MALDI-TOF MS spectra of oligosaccharides.

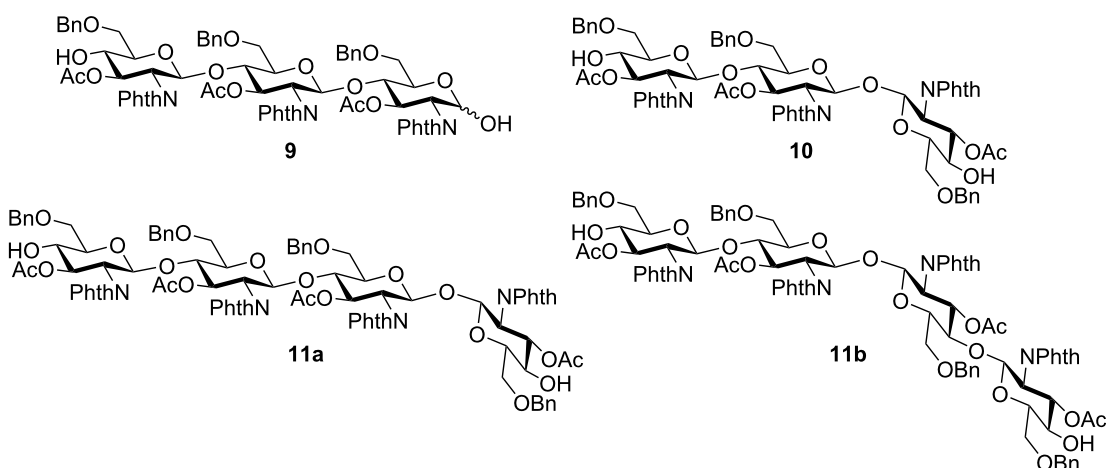


Figure 6: Proposed structures of byproducts of electrochemical polyglycosylation.

lar polarity. Moreover, the trehalose product of longer oligosaccharides has more than two possible structures. For example, there are two pseudo-tetrasaccharide structures **11a** and **11b**, which would be hard to separate by preparative-scale purification techniques.

Reaction mechanism

There are two possible pathways for chain elongation in electrochemical polyglycosylation (Figure 7). In path a, monosaccharide **1a** is converted to the corresponding glycosyl triflate **12**, and 4-OH of oligosaccharides **2a–6a** reacts with **12** [9]. In path b, oligosaccharides **2a–6a** are converted to the corresponding glycosyl triflates **13–17**, and 4-OH of monosaccharide **1a** reacts with **13–17**. It is difficult to exclude the possibility of reactions between oligosaccharides. However, polyglycosylation has been carried out with a slightly excessive amount of electricity (0.525 F/mol), and monosaccharide **1a** has always been recovered in more than 15% [10]. Moreover, longer oligosaccharides might be less reactive on grounds of mass transfer because electrochemical activation occurs at the surface of the anode and the substrates must move to the surface of the electrode.

To confirm the reactivity of oligosaccharides, we measured oxidation potentials of monosaccharide **1a**, disaccharide **2a**, and trisaccharide **3a** using a rotating disk electrode (RDE) made of glassy carbon (Figure 8). The oxidation potential of oligosaccharides **2a** and **3a** ($E_{\text{ox}} = 1.76$ and 1.74 V vs SCE) was higher than that of monosaccharide **1a** ($E_{\text{ox}} = 1.70$ V vs SCE). We also examined electrochemical activation of tetrasaccharide **4a** to obtain octasaccharide **8a** through the dimerization of **4a**. However, a trace amount of **8a** was formed together with byproducts, and the recovered amount of tetrasaccharide **4a** was 64% (Scheme 1). These results strongly suggested that path a in Figure 7 is the most probable mechanism of the reaction.

Modification of electrochemical polyglycosylation protocol

The optimized conditions of the electrochemical polyglycosylation can afford oligosaccharides up to the hexasaccharide **6a**. However, we were also interested in longer oligosaccharides, such as the heptasaccharide **7a** and the octasaccharide **8a** because of the biological activities [11]. Accordingly, the higher reactivity of monosaccharide **1a** compared to the oligosaccha-

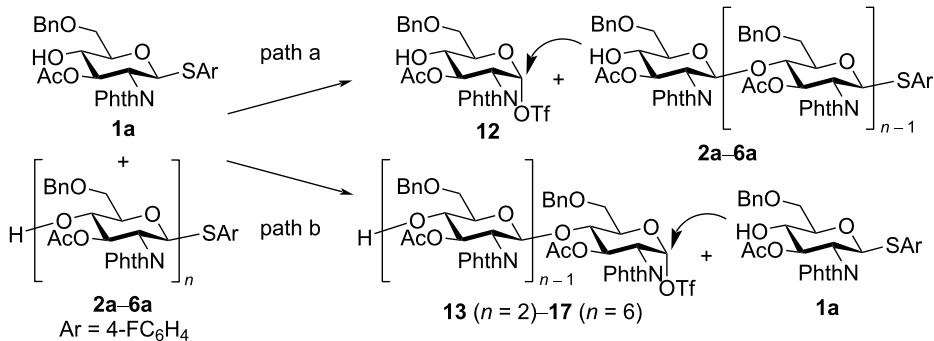


Figure 7: Proposed mechanisms of electrochemical polyglycosylation.

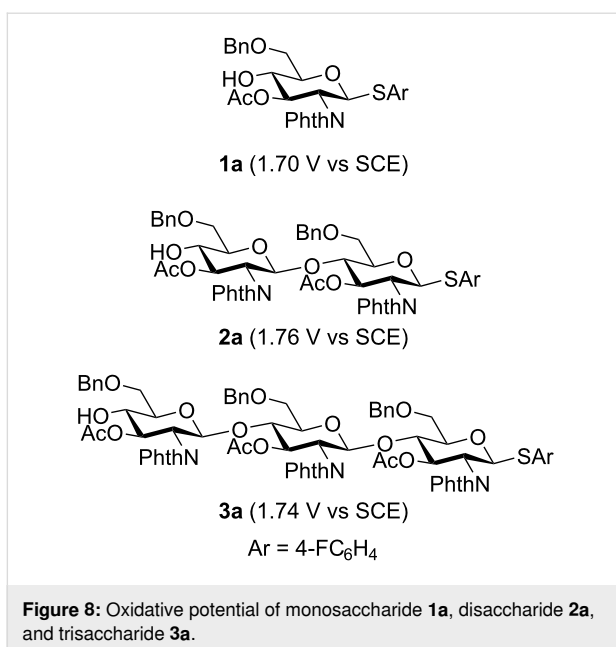


Figure 8: Oxidative potential of monosaccharide **1a**, disaccharide **2a**, and trisaccharide **3a**.

rides encouraged us to modify the electrochemical polyglycosylation protocol (Figure 9). We developed a modified electrochemical polyglycosylation method by repeating the addition of monosaccharide **1a** and anodic oxidation as a single cycle. To prove our concept, we ran the electrochemical polyglycosylation under the optimized conditions, and one equivalent of monosaccharide **1a** was added before the second anodic oxidation. After the second cycle, we could isolate heptasaccharide **7a** (3%, 1.5 µmol, 4.7 mg) together with an increased amount of hexasaccharide **6a** (5%, 3.1 µmol, 8.2 mg). We ran the process up to the third cycle and isolated octasaccharide **8a** (3%, 2.3 µmol, 7.6 mg), which was never isolated after the first cycle and the second cycle. These results also supported the proposed reaction mechanism path a in Figure 7.

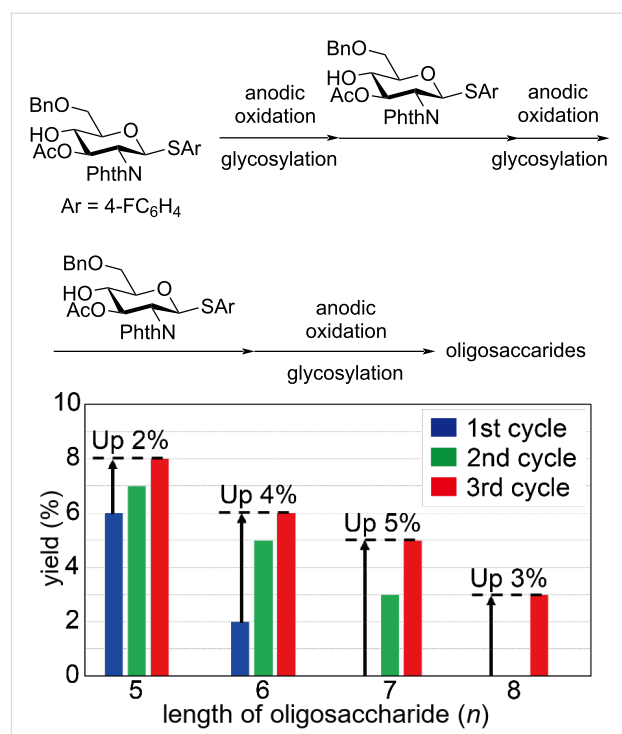
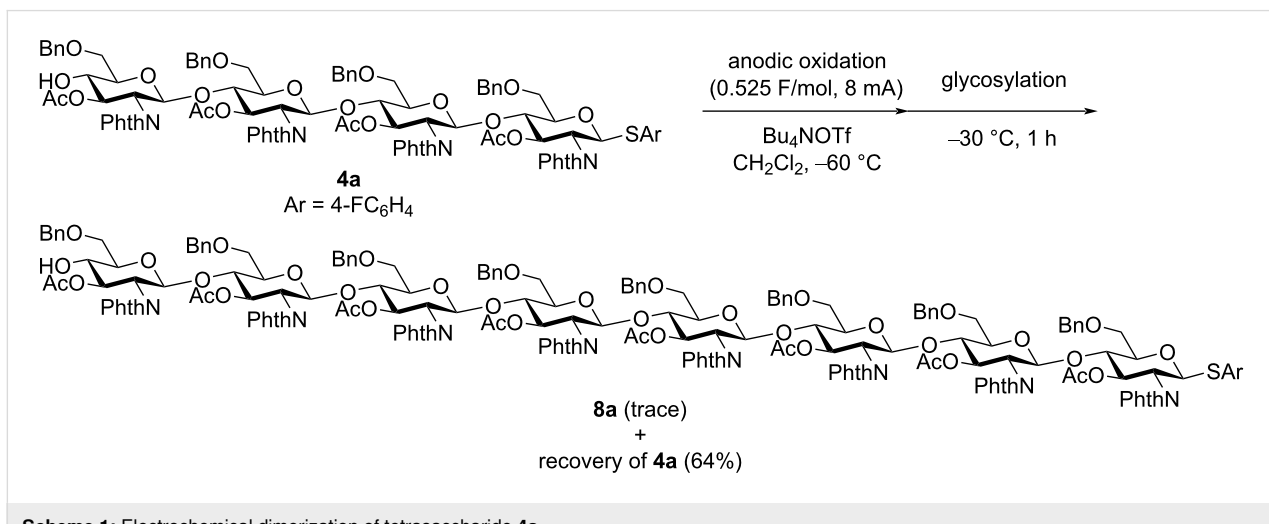


Figure 9: Influence of cycle number on the yield of longer oligosaccharides **5a** ($n = 5$)–**8a** ($n = 8$). Conditions of anodic oxidation: constant current (8.0 mA, 0.52 F/mol), temperature $-60\text{ }^{\circ}\text{C}$ for anodic oxidation and $-30\text{ }^{\circ}\text{C}$ for glycosylation, building block **1a** (0.20 mmol, 109 mg) per cycle as 0.2 M solution in dry CH_2Cl_2 .

Conclusion

In conclusion, we have developed a practical method to synthesize longer-chain oligosaccharides within a short period of time through electrochemical polyglycosylation. A rational reaction mechanism was proposed based on oxidation potentials of the oligosaccharides, and further modification of the protocol was examined. By repeating cycles in one pot, the modified method



Scheme 1: Electrochemical dimerization of tetrasaccharide **4a**.

enabled us to prepare longer oligosaccharides up to the octasaccharide. Further optimizations of reaction parameters, such as concentration, size and shape of electrodes for large-scale production of oligosaccharides, and deprotection of oligosaccharides thus obtained are in progress in our laboratory.

Experimental

Electrochemical polyglycosylation (see Figure 4, $T1 = -60\text{ }^{\circ}\text{C}$ and $T2 = -30\text{ }^{\circ}\text{C}$) was performed using our second-generation automated electrochemical synthesizer equipped with the H-type electrolysis cell. Thioglycoside **1a** (0.20 mmol, 109 mg), $\text{Bu}_4\text{N}^+\text{OTf}^-$ (1.0 mmol, 393 mg), and dry CH_2Cl_2 (10 mL) were added to the anodic chamber. Triflic acid (0.2 mmol, 17.6 μL) and CH_2Cl_2 (10 mL) were added to the cathodic chamber. Electrolysis was performed at $-60\text{ }^{\circ}\text{C}$ under constant current conditions until 0.52 F/mol of electricity had been consumed. Then, the reaction temperature was elevated to $-30\text{ }^{\circ}\text{C}$, and the temperature was kept for 1 h. The reaction was quenched with Et_3N (0.30 mL), and the reaction mixture was diluted with Et_2O and EtOAc and washed with water to remove the electrolyte. The combined organic layer was dried with Na_2SO_4 , and the solvent was removed under reduced pressure. The thus-obtained crude product (110 mg) was purified by preparative GPC using CHCl_3 as eluent.

2. Yang, Y.; Yu, B. *Tetrahedron* **2014**, *70*, 1023–1046. doi:10.1016/j.tet.2013.11.064
3. Nokami, T.; Hayashi, R.; Saigusa, Y.; Shimizu, A.; Liu, C.-Y.; Mong, K.-K. T.; Yoshida, J. *Org. Lett.* **2013**, *15*, 4520–4523. doi:10.1021/o1402034g
4. Isoda, Y.; Sasaki, N.; Kitamura, K.; Takahashi, S.; Manmode, S.; Takeda-Okuda, N.; Tamura, J.; Nokami, T.; Itoh, T. *Beilstein J. Org. Chem.* **2017**, *13*, 919–924. doi:10.3762/bjoc.13.93
5. Hashimoto, H.; Abe, Y.; Horito, S.; Yoshimura, J. *J. Carbohydr. Chem.* **1989**, *8*, 307–311. doi:10.1080/07328308908048012
6. Kadokawa, J.; Watanabe, Y.; Karasu, M.; Tagaya, H.; Chiba, K. *Macromol. Rapid Commun.* **1996**, *17*, 367–372. doi:10.1002/marc.1996.030170601
7. Endo, H.; Ochi, M.; Rahman, M. A.; Hamada, T.; Kawano, T.; Nokami, T. *Chem. Commun.* **2022**, *58*, 7948–7951. doi:10.1039/d2cc02287g
8. Nokami, T.; Isoda, Y.; Sasaki, N.; Takaiso, A.; Hayase, S.; Itoh, T.; Hayashi, R.; Shimizu, A.; Yoshida, J. *Org. Lett.* **2015**, *17*, 1525–1528. doi:10.1021/acs.orglett.5b00406
9. Nokami, T.; Shibuya, A.; Tsuyama, H.; Suga, S.; Bowers, A. A.; Crich, D.; Yoshida, J. *J. Am. Chem. Soc.* **2007**, *129*, 10922–10928. doi:10.1021/ja072440x
10. The theoretical amount of electricity necessary for 100% conversion of the monosaccharide building block into disaccharide is 0.5 F/mol. This theoretical value was based on the hypothesis of selective activation of the monosaccharide.
11. Li, K.; Xing, R.; Liu, S.; Li, P. *J. Agric. Food Chem.* **2020**, *68*, 12203–12211. doi:10.1021/acs.jafc.0c05316

Supporting Information

Supporting Information File 1

Additional experimental details and compound characterization data.

[<https://www.beilstein-journals.org/bjoc/content/supplementary/1860-5397-18-117-S1.pdf>]

Funding

T. N. acknowledges financial support from the JSPS (Grant No. JP 19K05714).

ORCID® IDs

Md Azadur Rahman - <https://orcid.org/0000-0003-2049-1196>

Toshiki Nokami - <https://orcid.org/0000-0001-5447-4533>

Preprint

A non-peer-reviewed version of this article has been previously published as a preprint: <https://doi.org/10.3762/bxiv.2022.58.v1>

References

1. Fittolani, G.; Tyrikos-Ergas, T.; Vargová, D.; Chaube, M. A.; Delbianco, M. *Beilstein J. Org. Chem.* **2021**, *17*, 1981–2025. doi:10.3762/bjoc.17.129

License and Terms

This is an open access article licensed under the terms of the Beilstein-Institut Open Access License Agreement (<https://www.beilstein-journals.org/bjoc/terms>), which is identical to the Creative Commons Attribution 4.0

International License

(<https://creativecommons.org/licenses/by/4.0>). The reuse of material under this license requires that the author(s), source and license are credited. Third-party material in this article could be subject to other licenses (typically indicated in the credit line), and in this case, users are required to obtain permission from the license holder to reuse the material.

The definitive version of this article is the electronic one which can be found at:

<https://doi.org/10.3762/bjoc.18.117>



Electro-conversion of cumene into acetophenone using boron-doped diamond electrodes

Mana Kitano¹, Tsuyoshi Saitoh², Shigeru Nishiyama¹, Yasuaki Einaga^{*1} and Takashi Yamamoto^{*1}

Letter

Open Access

Address:

¹Department of Chemistry, Keio University, 3-14-1 Hiyoshi, Yokohama 223-8522, Japan and ²International Institute for Integrative Sleep Medicine (WPI-IIIS), University of Tsukuba, 1-1-1 Tennodai, Tsukuba 305-8575, Japan

Email:

Yasuaki Einaga^{*} - einaga@chem.keio.ac.jp; Takashi Yamamoto^{*} - takyama@chem.keio.ac.jp

^{*} Corresponding author

Keywords:

aromatic alkyl; boron-doped diamond electrode; electrosynthesis; oxidation

Beilstein J. Org. Chem. **2022**, *18*, 1154–1158.

<https://doi.org/10.3762/bjoc.18.119>

Received: 20 June 2022

Accepted: 26 August 2022

Published: 07 September 2022

This article is part of the thematic issue "Molecular and macromolecular electrochemistry: synthesis, mechanism, and redox properties".

Guest Editor: S. Inagi

© 2022 Kitano et al.; licensee Beilstein-Institut.

License and terms: see end of document.

Abstract

A straightforward electro-conversion of cumene into acetophenone has been reported using boron-doped diamond (BDD) electrodes. This particular conversion is driven by the addition reaction of a cathodically generated hydroperoxide anion to an anodically generated cumyl cation, where the BDD's wide potential window enables the direct anodic oxidation of cumene into the cumyl cation. Since electricity is directly employed as the oxidizing and reducing reagents, the present protocol is easy to use, suitable for scale-up, and inherently safe.

Introduction

Selective oxidation of aromatic alkyl side chains is an important molecular transformation process to obtain various rubbers, resins, fine chemicals, and other industrial products [1,2]: terephthalic acid from *p*-xylene, cumene hydroperoxide/dicumyl peroxide/phenol from cumene, acetophenone from ethylbenzene, and others. Generally, molecular oxygen has been utilized in the straightforward oxidation of aromatic alkyls. However, since molecular oxygen is highly stable, activation of the molecular oxygen itself is necessary, which requires a specific catalyst and/or harsh conditions such as high temperature

and pressure. Recent environmental and sustainable concerns lead to a growing demand for the development of greener oxidation processes. For example, even for the cumene process that involves the oxidation reaction of cumene, first reported in 1944 [3], a wide variety of catalytic systems are still being reported [4-12].

Electro-organic synthesis refers to an organic synthetic method combined with electrochemistry [13,14]. A striking feature in electro-organic synthesis is the use of electricity as a reagent,

which allows to reduce the reagent waste to a minimum. Obviously, as this characteristic matches well with the increasing demands to realize a sustainable society. In electro-organic synthesis, electrode materials are one of the most significant parameters because reactions occur at the anode and/or cathode. Boron-doped diamond (BDD) is a relatively new electrode material [15,16] and shows a wide potential window, which can be applied to the transformation of compounds with high redox potentials. Therefore, BDD electrodes would enable a straightforward oxidation reaction of aromatic alkyls, which is difficult to achieve with other conventional electrode materials.

Herein, we report the straightforward electro-conversion of cumene, one of the most important and extensively investigated aromatic alkyls, by BDD electrodes. Acetophenone was obtained as the main product when BDD was used as the anode. The role of electrode materials was investigated with electrochemical measurements. Only the BDD anode with a wide potential window can oxidize cumene directly to afford a cumyl cation as the reaction intermediate. Furthermore, acetophenone is produced via cumene hydroperoxide, and this molecular conversion is found to proceed electrochemically.

Results and Discussion

First, we carried out the electrolysis of cumene (**1**) in 0.1 M Bu_4NBF_4 /MeCN under constant current conditions in an undi-

vided beaker-type cell (Table 1, entry 1). The main product was acetophenone (**3**) and α -cumyl alcohol (**4**) was also obtained. When the anion of the supporting electrolyte was changed to the perchlorate ion (Table 1, entries 2–4), isolated yields of **3** were increased, in which using Et_4NClO_4 gave the best result. Next, the current density (j) and the amount of charge (Q ; referring to mole of **1**) were investigated (Table 1, entries 5–7). As the isolated yield of **3** was not particularly improved by changing j and Q , we set the optimum conditions as j of 2.1 mA/cm² and Q of 5 F. On the other hand, when the combination of anode and cathode was graphite/graphite or Ni/Ni (Table 1, entries 8 and 9), almost no acetophenone was obtained. Therefore, it is suggested that the BDD anode is essential in the electro-conversion of **1** into **3**, and the cathode material has no significant effect. Here, the low total yields would be due to the formation of highly polar compounds. We were not able to obtain them as isolated compounds. In addition, ¹H NMR and FTIR spectra for the crude compound did not show characteristic peaks derived from carboxylic acid and amide.

In order to clarify the role of the anode material, we carried out electrochemical measurements (Figure 1). Cyclic voltammetry was performed using BDD as a working electrode. A clear oxidation peak of **1** was observed at around 2.40 V (vs Ag/Ag⁺) (Figure 1a), which is comparable to a previous report using a Pt disk electrode [17]. On the other hand, no clear oxidation peak

Table 1: Electro-conversion of **1**.

Entry ^a	Anode	Cathode	Supporting electrolyte	j ^b	Q ^c	Isolated yields (%)			
						1	2	3	4
1	BDD	BDD	Bu_4NBF_4	2.1	5	n.d.	n.d.	18	14
2	BDD	BDD	Bu_4NClO_4	2.1	5	n.d.	1	27	9
3	BDD	BDD	LiClO_4	2.1	5	n.d.	n.d.	19	13
4	BDD	BDD	Et_4NClO_4	2.1	5	trace	1	34	11
5	BDD	BDD	Et_4NClO_4	2.1	3	3	4	17	28
6	BDD	BDD	Et_4NClO_4	2.1	7.5	n.d.	n.d.	32	n.d.
7	BDD	BDD	Et_4NClO_4	1.05	5	5	2	23	26
8	graphite	graphite	Et_4NClO_4	2.1	5	4	n.d.	1	4
9	Ni	Ni	Et_4NClO_4	2.1	5	4	n.d.	n.d.	n.d.
10	BDD	graphite	Et_4NClO_4	2.1	5	trace	trace	33	5
11	graphite	BDD	Et_4NClO_4	2.1	5	n.d.	trace	20	

^aReaction conditions: 1 mmol cumene (**1**), 5 mL MeCN, 0.1 M supporting electrolyte, undivided beaker-type cell, rt; ^bcurrent density (mA/cm²);

^camount of charge (F) referring to mole of **1**. n.d. = not detected.

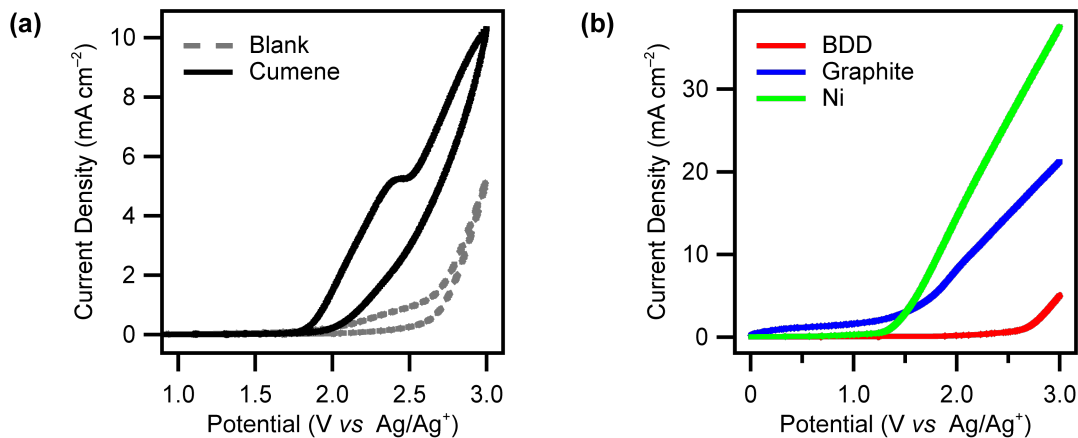


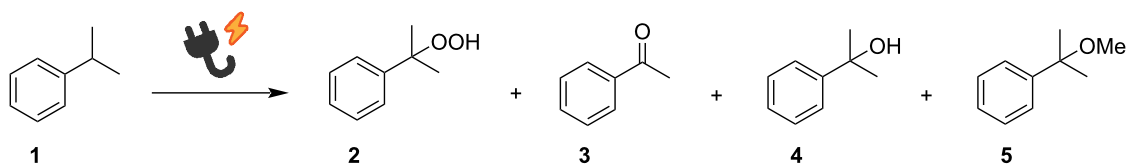
Figure 1: (a) Cyclic voltammograms of a BDD electrode in MeCN solution containing cumene (**1**; 5 mM) and Et_4NClO_4 (0.1 M). The gray dashed line shows the voltammogram in the solution without cumene. (b) Linear sweep voltammograms of BDD (red), graphite (blue), and Ni (green) electrodes in MeCN solution containing Et_4NClO_4 (0.1 M). Scan rate: 100 mV/s.

was observed when using graphite or Ni as a working electrode. This is because potential windows of graphite and Ni are too narrow to oxidize **1** directly, as can be seen in Figure 1b. Overall, the electrochemical measurements indicate the BDD's wide potential window enables direct oxidation of **1** to produce a key reaction intermediate to afford **3**.

A series of electrolysis experiments was performed to propose a reaction mechanism (Table 2). First, we carried out the electrolysis of **1** in MeCN–MeOH to confirm whether the reaction intermediate is a radical or cationic species (Table 2, entry 1). As a result, methyl cumyl ether, a methoxy adduct to the benzyl position of **1**, was obtained as the main product in 21% yield.

Therefore, it is indicated that the reaction intermediate is the cumyl cation. Second, we carried out the electrolysis of **1** in MeCN–H₂O to confirm whether the oxygen source is dissolved oxygen or residual water. When dehydrated MeCN was used, **3** was obtained as the main product (Table 2, entry 2). On the other hand, the isolated yield of **3** was decreased by the addition of H₂O (Table 2, entries 3 and 4). This is probably because the addition of H₂O promoted the generation of hydroxyl radicals, and a decomposition reaction became dominant. These results indicated that the oxygen source is not residual water in MeCN, but dissolved oxygen. The role of dissolved oxygen was further investigated. As the reaction did not proceed without electricity, it is suggested that the superoxide generated on the

Table 2: Control electrolysis experiments of **1**^a.



Entry	Solvent	Isolated yields (%)				
		1	2	3	4	5
1	MeCN–MeOH 9:1	trace	4	trace	12	21
2	MeCN (dehydrated)	trace	1	29	15	n.a.
3	MeCN–H ₂ O 9:1	n.d.	6	9	20	n.a.
4	MeCN–H ₂ O 1:1	n.d.	trace	trace	15	n.a.

^aReaction conditions: BDD anode and cathode, 1 mmol cumene (**1**), 5 mL solvent, 0.1 M Et_4NClO_4 , 2.1 mA/cm^2 and Q of 5 F (referring to mole of **1**), undivided beaker-type cell, rt. n.d. = not detected, n.a. = not applicable.

cathode is involved in the reaction, rather than dissolved molecular oxygen itself. Therefore, we treated **1** with KO_2 and 18-crown-6 to examine whether the reaction proceeds only with the superoxide. As a result, only the starting material, **1**, was recovered, which indicates that **3** is produced by a concerted reaction of the direct oxidation of **1** on the anode and the reduction of dissolved oxygen on the cathode.

Figure 2 shows a proposed mechanism. Anodic oxidation of cumene on the BDD electrode with a wide potential window preferentially affords the cumyl cation as the reaction intermediate. On the other hand, cathodic reduction of dissolved oxygen produces the superoxide and even the hydroperoxide anion. Addition of the hydroperoxide anion to the cumyl cation yields cumene hydroperoxide, which is further converted into acetophenone. This reaction pathway is supported by the following two facts. One is that cumene hydroperoxide was obtained as a byproduct, and the other is that electrolysis of cumene hydroperoxide as a starting material afforded acetophenone [18]. It should be noted that the tertiary carbon at the benzyl position is a key for the present molecular transformation, since acetophenone was yielded in 19% as the main product by the electrolysis of *sec*-butylbenzene as a starting material, while propylbenzene was not. Moreover, the electrolysis under a flow of oxygen did not improve the yields, which indicates that the BDD cathode can utilize the electrogenerated oxygen species efficiently, as we have reported previously [19].

Conclusion

We have demonstrated a straightforward electro-conversion of cumene into acetophenone using boron-doped diamond (BDD) electrodes. The BDD's wide potential window enabled the direct anodic oxidation of cumene to afford a key reaction intermediate, which cannot be realized by other electrodes such as

graphite and Ni. Electrosynthesis is a sustainable, scalable, and cost-efficient protocol; a specific catalyst is not required, and reagent waste can be avoided. In addition, the present work offers new perspectives for an electrosynthetic strategy toward oxidation reactions of aromatic alkyls.

Experimental

General protocol for electro-conversion of cumene

Electrolysis was carried out by using an IKA screening system (IKA, Germany). A solution of cumene (**1**, 0.12 g, 1.00 mmol) and supporting electrolyte (0.1 M) in 5 mL solvent was transferred into the electrolysis cell equipped with electrodes (purchased from IKA, Germany; $0.3 \times 1.0 \times 7.0$ cm; immersed 1.8 cm into solution). A constant current electrolysis was performed at room temperature. After application of the desired amount of charge, the electrolysis was stopped, and the solvent was removed in *vacuo*. The residue was purified by silica gel column chromatography (CH_2Cl_2).

Supporting Information

Supporting Information File 1

Characterization data and ^1H NMR spectra of isolated compounds **2**, **3**, **4**, and **5**.

[<https://www.beilstein-journals.org/bjoc/content/supplementary/1860-5397-18-119-S1.pdf>]

Funding

This work was supported by Keio University Academic Development Funds.

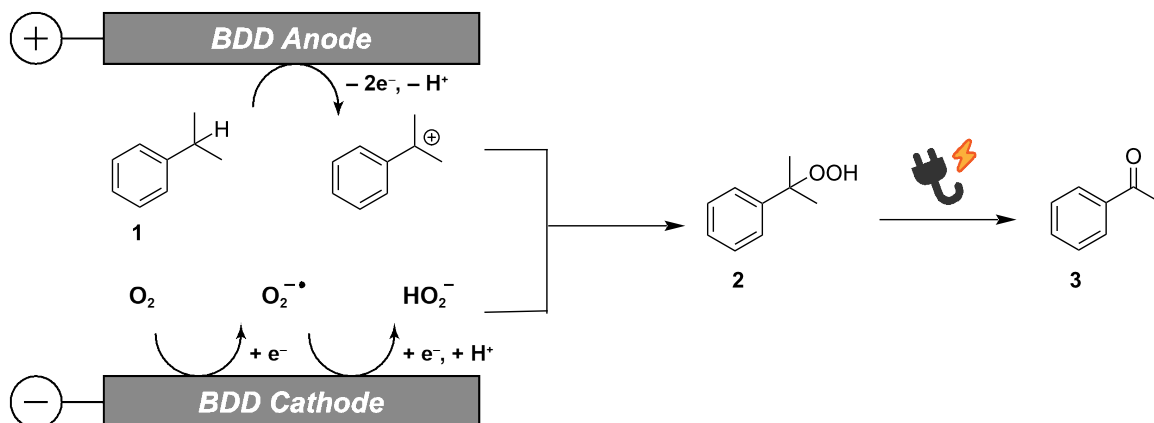


Figure 2: Proposed reaction mechanism of electro-conversion of cumene (**1**) into acetophenone (**3**).

ORCID® IDs

Yasuaki Einaga - <https://orcid.org/0000-0001-7057-4358>

Takashi Yamamoto - <https://orcid.org/0000-0002-4252-8132>

References

1. Suresh, A. K.; Sharma, M. M.; Sridhar, T. *Ind. Eng. Chem. Res.* **2000**, *39*, 3958–3997. doi:10.1021/ie0002733
2. Carrà, S.; Santacesaria, E. *Catal. Rev.: Sci. Eng.* **1980**, *22*, 75–140. doi:10.1080/03602458008066530
3. Hock, H.; Lang, S. *Ber. Dtsch. Chem. Ges. B* **1944**, *77*, 257–264. doi:10.1002/cber.19440770321
4. Bryant, J. R.; Matsuo, T.; Mayer, J. M. *Inorg. Chem.* **2004**, *43*, 1587–1592. doi:10.1021/i035298j
5. Kaizer, J.; Klinker, E. J.; Oh, N. Y.; Rohde, J.-U.; Song, W. J.; Stubna, A.; Kim, J.; Münck, E.; Nam, W.; Que, L., Jr. *J. Am. Chem. Soc.* **2004**, *126*, 472–473. doi:10.1021/ja037288n
6. Brutchez, R. L.; Drake, I. J.; Bell, A. T.; Tilley, T. D. *Chem. Commun.* **2005**, 3736–3738. doi:10.1039/b506426k
7. Minisci, F.; Recupero, F.; Cecchetto, A.; Gambarotti, C.; Punta, C.; Paganelli, R.; Pedulli, G. F.; Fontana, F. *Org. Process Res. Dev.* **2004**, *8*, 163–168. doi:10.1021/op034137w
8. Bonchio, M.; Carraro, M.; Gardan, M.; Scorrano, G.; Drioli, E.; Fontananova, E. *Top. Catal.* **2006**, *40*, 133–140. doi:10.1007/s11244-006-0115-5
9. Liao, S.; Peng, F.; Yu, H.; Wang, H. *Appl. Catal., A* **2014**, *478*, 1–8. doi:10.1016/j.apcata.2014.03.024
10. Safa, M. A.; Al-Shamary, T.; Al-Majren, R.; Bouresli, R.; Ma, X. *Energy Fuels* **2017**, *31*, 7464–7470. doi:10.1021/acs.energyfuels.7b01272
11. Mu, C.; Cao, Y.; Wang, H.; Yu, H.; Peng, F. *Chem. Eng. Sci.* **2018**, *177*, 391–398. doi:10.1016/j.ces.2017.11.016
12. Yang, M.; Qiu, G.; Huang, C.; Han, X.; Li, Y.; Chen, B. *Ind. Eng. Chem. Res.* **2019**, *58*, 19785–19793. doi:10.1021/acs.iecr.9b03476
13. Fuchigami, T.; Inagi, S.; Atobe, M. *Fundamentals and Applications of Organic Electrochemistry: Synthesis, Materials, Devices*; John Wiley & Sons: Chichester, UK, 2015. doi:10.1002/9781118670750
14. Hammerich, O.; Speiser, B. *Organic Electrochemistry*, 5th ed.; CRC Press: Boca Raton, FL, USA, 2015. doi:10.1201/b19122
15. Macpherson, J. V. *Phys. Chem. Chem. Phys.* **2015**, *17*, 2935–2949. doi:10.1039/c4cp04022h
16. Yang, N.; Yu, S.; Macpherson, J. V.; Einaga, Y.; Zhao, H.; Zhao, G.; Swain, G. M.; Jiang, X. *Chem. Soc. Rev.* **2019**, *48*, 157–204. doi:10.1039/c7cs00757d
17. Tajima, T.; Kurihara, H.; Nakajima, A.; Fuchigami, T. *J. Electroanal. Chem.* **2005**, *580*, 155–160. doi:10.1016/j.jelechem.2005.03.024
18. (Electrolysis) 45% yield; (without electricity) recovery of cumene hydroperoxide.
19. Zhang, Y.; Sugai, T.; Yamamoto, T.; Yamamoto, N.; Kutsumura, N.; Einaga, Y.; Nishiyama, S.; Saitoh, T.; Nagase, H. *ChemElectroChem* **2019**, *6*, 4194–4198. doi:10.1002/celc.201801308

License and Terms

This is an open access article licensed under the terms of the Beilstein-Institut Open Access License Agreement (<https://www.beilstein-journals.org/bjoc/terms>), which is identical to the Creative Commons Attribution 4.0

International License

(<https://creativecommons.org/licenses/by/4.0>). The reuse of material under this license requires that the author(s), source and license are credited. Third-party material in this article could be subject to other licenses (typically indicated in the credit line), and in this case, users are required to obtain permission from the license holder to reuse the material.

The definitive version of this article is the electronic one which can be found at:

<https://doi.org/10.3762/bjoc.18.119>



Reductive opening of a cyclopropane ring in the Ni(II) coordination environment: a route to functionalized dehydroalanine and cysteine derivatives

Oleg A. Levitskiy, Olga I. Aglamazova, Yuri K. Grishin and Tatiana V. Magdesieva^{*}

Full Research Paper

Open Access

Address:

Lomonosov Moscow State University, Dept. of Chemistry, Leninskie Gory 1/3, Moscow 119991, Russian Federation

Email:

Tatiana V. Magdesieva^{*} - tvm@org.chem.msu.ru

^{*} Corresponding author

Keywords:

amino acids; cathodic cyclopropane opening; cysteine derivatives; Ni-Schiff base complexes; stereoselective electrosynthesis; voltammetric testing

Beilstein J. Org. Chem. **2022**, *18*, 1166–1176.

<https://doi.org/10.3762/bjoc.18.121>

Received: 30 May 2022

Accepted: 24 August 2022

Published: 08 September 2022

This article is part of the thematic issue "Molecular and macromolecular electrochemistry: synthesis, mechanism, and redox properties".

Guest Editor: S. Inagi

© 2022 Levitskiy et al.; licensee Beilstein-Institut.

License and terms: see end of document.

Abstract

The involvement of an α,α -cyclopanated amino acid in the chiral Ni(II) coordination environment in the form of a Schiff base is considered as a route to electrochemical broadening of the donor–acceptor cyclopropane concept in combination with chirality induction in the targeted products. A tendency to the reductive ring-opening and the follow-up reaction paths of thus formed radical anions influenced by substituents in the cyclopropane ring are discussed. Optimization of the reaction conditions opens a route to the non-proteinogenic amino acid derivatives containing an α – β or β – γ double C=C bond in the side chain; the regioselectivity can be tuned by the addition of Lewis acids. One-pot combination of the reductive ring opening and subsequent addition of thiols allows obtaining the cysteine derivatives in practical yields and with high stereoselectivity at the removed β -stereocenter.

Introduction

Electrochemistry provides a direct access to highly reactive species by means of harnessing electrons or electron holes as reagents [1,2]. This capacity can be efficiently exploited in organic synthesis for rational construction of complex multi-functional molecules [3–8].

Recently, we elaborated a versatile electrochemical approach for the stereoselective functionalization of a side chain of amino acids involved in the Ni(II) chiral coordination environment

[9–15]. A combination of redox-activity and chirality provided by the Ni–Schiff base template, supported with the protection from redox-destruction of the amino acid skeleton, makes the suggested approach a convenient route to various types of non-proteinogenic amino acids [9,10,12,13]. Recently, several practical approaches to α,α -cyclopanated amino acids in the form of Ni(II)–Schiff base complexes were suggested [16–19], including electrochemical ones [15]. Cyclopropane-containing amino acids are important components of various

pharmaceuticals [20,21] and bio-additives [22]. Meanwhile, the cyclopropane fragment not only provides targeted pharmacophoric properties of the bio-active molecule [23] but also opens a route to its further functionalization, being a building block with wide variety of reactivity. A donor–acceptor cyclopropane concept suggested in the 1980s [24] became extremely popular in the recent decade [25,26]. Donor–acceptor cyclopropanes constitute an easily available equivalent of all-carbon 1,3-zwitter-ions used in targeted synthesis of various alicyclic as well as carbo- or heterocyclic compounds [27–30]. The reactive synergy of the three-membered ring and the C–C bond polarization due to donor–acceptor substituents contribute to the rich chemistry of these compounds. However, strict requirements for the nature of substituents somewhat narrow the applicability of the method.

The electrochemical one-electron opening of a cyclopropane ring results in the formation of an ion-radical species instead of zwitter-ions, thus creating preconditions for a different type of reactivity. Such processes are much less investigated.

The very first example of anodic cyclopropane ring opening was reported by Shono [31]. This publication sparked interest in this topic; a number of publications appeared but the reaction scope was mainly limited to rather simple compounds containing methyl and phenyl substituents [32–37].

When discussing examples of reductive cyclopropane ring opening, one should refer to early publications concerning the carbonyl- and nitro-substituted compounds [38–42]. The principal possibility of the process was demonstrated but the synthetic potential of the method was not sufficiently implemented.

Great success of the donor–acceptor cyclopropane concept in organic synthesis stimulated a renaissance of interest to electrochemical ring opening. Quite recently, two publications from the Werz group appeared concerning anodic activation of donor–acceptor cyclopropanes followed by their functionalization with arenes [43] or yielding oxy-ketones or 1,2-dioxanes [44]; the latter process was inspired by a previous report of Buriez [45]. The anodic fluorination of arylcyclopropane derivatives was reported recently [46,47], difluorinated or oxyfluorinated products were obtained [47]. Notably, anodic fluorination of cyclopropane derivatives bearing arylthio groups gives rise to a variety of possible reaction paths yielding monofluorinated sulfoxides as well as ring-opened fluorinated products [46].

Thus, recent publications on the topic concern only anodic opening of a cyclopropane ring followed by further functionalization of the carbon skeleton, demonstrating great synthetic potential of the process.

Electrochemical cyclopropane opening followed by stereoselective functionalization has not been probed as yet. Herein, reductive three-membered ring opening in the chiral α,α -cyclopropanated amino acids involved in the Ni(II)–Schiff base coordination environment is reported. Follow-up transformations of thus formed radical anions will be discussed, including reactions with electrophiles, intramolecular cyclization and disproportionation process. The synthetic viability of the approach will be considered. A one-pot multistep synthetic protocol is suggested, based on addition of thiols to the mixture of isomeric alkenes formed in an electroreductive opening of a cyclopropane ring in α,α -cyclopropanated amino acids yielding the cysteine derivatives in practical yields and with high stereoselectivity at the removed β -stereocenter. Thus, the present paper is a further development of the extended research on electrochemically induced stereoselective transformations in the Ni(II) coordination environment yielding structurally and functionally novel types of tailor-made amino acids.

Results and Discussion

Voltammetry study

As models, a series of Ni(II)–Schiff base complexes containing α,α -cyclopropanated amino acids was synthesized (see Figure 1). Complexes **1–3** containing an unsubstituted cyclopropane ring (**1**) or bearing Me (**2**) and COOMe (**3**) groups were obtained using previously reported protocols [15,19]. Complex **4** is new.

Compound **4** was obtained by the reaction of an electrophilic dehydroalanine complex with a bromomalonate anion (Scheme 1). The reaction proceeds smoothly at room temperature giving rise to cyclopropane **4** in excellent diastereoselectivity ($de = 92\%$) and high yield.

The optical purity of the starting compounds was confirmed by comparison of the optical rotation data with previously published values (see Supporting Information File 1). Complex **4** was easily separated from the minor diastereomer by column chromatography. The structure and purity of (*S*)-**4** was confirmed by NMR data, including HMBC, HSQC and COSY 2D techniques. The assignment of the α -stereocenter as (*S*) was based on the NOESY data (see Supporting Information File 1 and Figure 2). The protons of the ester group linked to the cyclopropane moiety exhibit correlation with the methylene protons of proline in the NOESY spectrum. Thus, the ester groups are at the same side of the Ni coordination plane as the proline methylene groups indicating the (*S*) configuration of the α -stereocenter. The large positive value of the specific rotation ($[\alpha]_D +1770$) additionally supports α -(*S*) configuration since positive $[\alpha]_D$ values are characteristic for the Ni–Schiff base

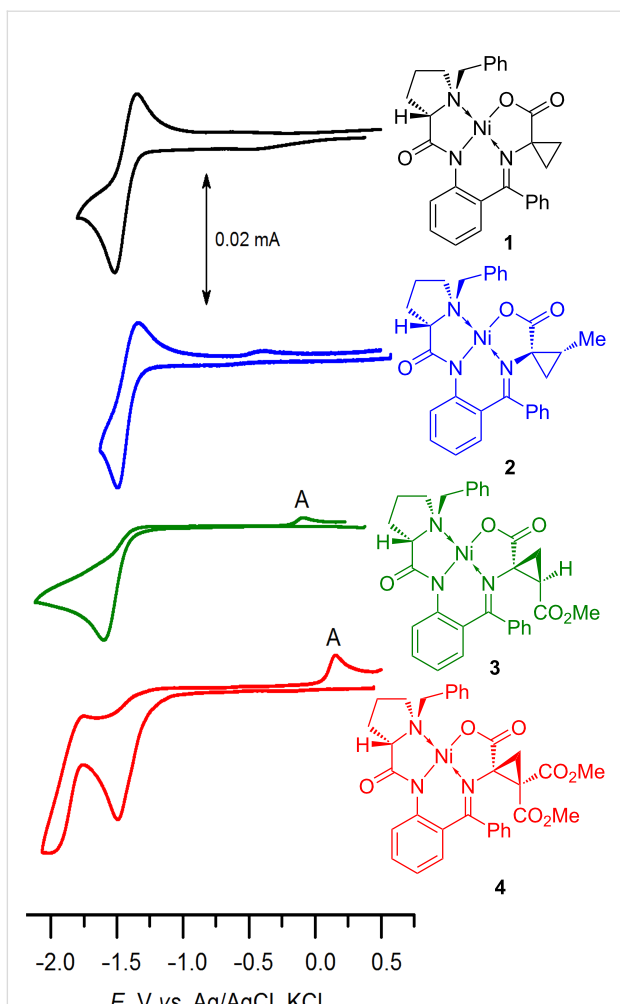


Figure 1: Cyclic voltammograms obtained for complexes **1** (black), **2** (blue), **3** (green), **4** (red) (MeCN , 0.05 M Bu_4NBF_4 , 100 mV/s, Pt).

complexes of *(S*)-*N*-(*N*-benzylprolyl)aminobenzophenone and L-amino acids [48].

To choose the most promising candidates for electrochemical three-membered ring opening, a voltammetric study was performed.

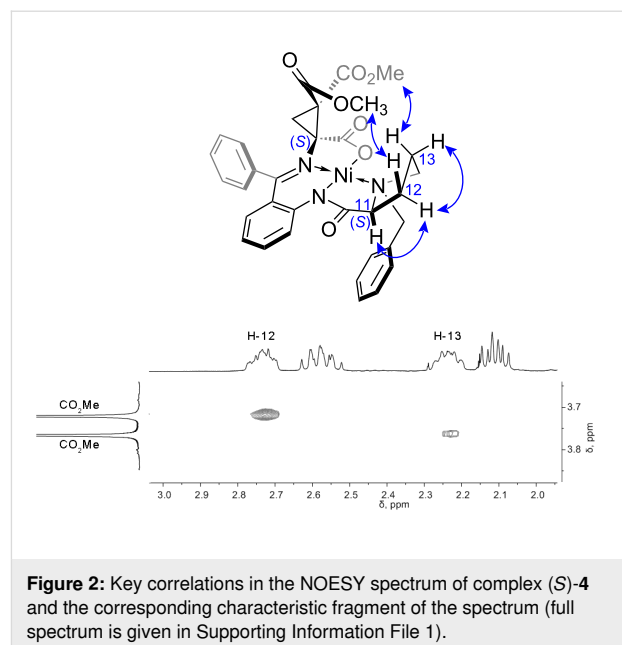
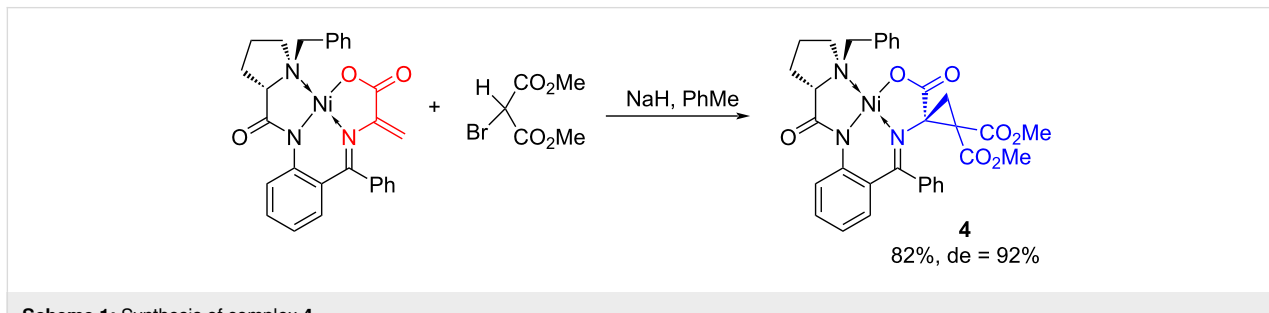


Figure 2: Key correlations in the NOESY spectrum of complex (S)-**4** and the corresponding characteristic fragment of the spectrum (full spectrum is given in Supporting Information File 1).

As it has been shown in our previous publications [49–51], the electrochemical behavior and the orbitals location sites are dependent on the type of the amino acid involved in the Schiff base complex. The LUMOs of the glycine, alanine, serine and cysteine derivatives are formed as an antibonding combination of the $\text{Ni } d_{x^2-y^2}$ orbital with the group orbitals of the ligands; the π^* orbital of the imine and the π orbital of the phenylene fragments are also partially involved. Reduction occurs at similar potential values and is almost independent on the substituent at the α -carbon atom in the amino acid fragment. Electrochemical reduction of complexes containing an unsubstituted cyclopropane ring (**1**) or bearing Me (**2**) substituents is similar to that for α -alkyl derivatives: they exhibit reversible one-electron reduction (the radical anions formed are relatively stable, at least in the CV time scale) at close potential values ($E_{1/2} = -1.42$ V (**1**), -1.42 V (**2**); for comparison: $E_{1/2}$ for $\text{AlaNi} = -1.53$ V [52] vs $\text{Ag}/\text{AgCl}, \text{KCl}_{(\text{sat.})}$).

The complexes containing one (**3**) or two (**4**) electron-deficient COOMe groups in the cyclopropane moiety may be expected to



Scheme 1: Synthesis of complex **4**.

be more prone to the ring opening, and the irreversibility of the cathodic redox process observed in the voltammograms ($E_{pc} = -1.60$ V vs Ag/AgCl, KCl_(sat.) for **3** and $E_{pc} = -1.50$ V for **4**; Figure 1) supported the suggestion. In the reverse anodic scan, a new oxidation peak (**A** in Figure 1; $E_p^A = -0.06$ V (**3**), 0.16 V (**4**) vs Ag/AgCl, KCl_(sat.)) can be observed for both complexes **3** and **4** (though in the latter case it is more intensive); more likely, the peak corresponds to reoxidation of the anionic species formed after the ring opening. The reduction patterns for compounds **3** and **4** differ significantly. In the voltammogram corresponding to complex **4** containing two COOMe groups, two consecutive reduction peaks can be observed. The more cathodic peak is reversible ($E_{1/2} = -1.87$ V vs Ag/AgCl, KCl_(sat.)). Analysis of semi-differential curves (see Supporting Information File 1) indicates that the consumption of electrons at the first reduction peak is independent on the potential scan rate. In contrast, the more cathodic peak in semi-differential voltammogram gradually decreases with the scan rate increase. Thus, the second peak should be assigned to reduction of the product of the chemical step following the first reduction process.

Preparative electrolysis

Based on the voltammetry results, complexes **3** and **4** were chosen as the models for the preparative study. The electrolysis was performed in a two-compartment electrochemical cell in DMF using a glassy carbon plate as a working electrode and an iron rod as an auxiliary electrode. The process was carried out in the potentiostatic mode at a potential of 100 mV more cathodic than the peak potential value observed in the voltammogram; a charge corresponding to 1 mol equivalent of the starting complex was passed through the solution. The color of the solution was gradually changed from deep red to dark violet, typically for the anionic complexes. The solutions obtained were ESR-silent, indicating formation of the closed-shell species. The UV-vis study showed an intensive absorption at 546 nm for **3** and at 519 nm for **4**. The significant bathochromic shift as compared to the deprotonated glycine complex ($\lambda_{max} = 458$ nm [9]) indicates an elongation of the conjugation chain and formation of the anionic complex which can be considered as a vinylog of the parent glycine derivative (Scheme 2)

The anionic species formed in the electrolysis of complex **3** can be protonated using acetic acid (pK_a in DMSO = 12.3 [53]), in contrast to their counterparts formed from complex **4**. In the latter case, a stronger protonating agent is required, e.g., PhNEt₂·HCl (pK_a in DMSO = 2.45 for PhN⁺HMe₂ [53]). The pK_a value of **6** determined in DMSO solution using the UV-vis method (see Supporting Information File 1 for the details) is 5.1, indicating high stability of the anion.

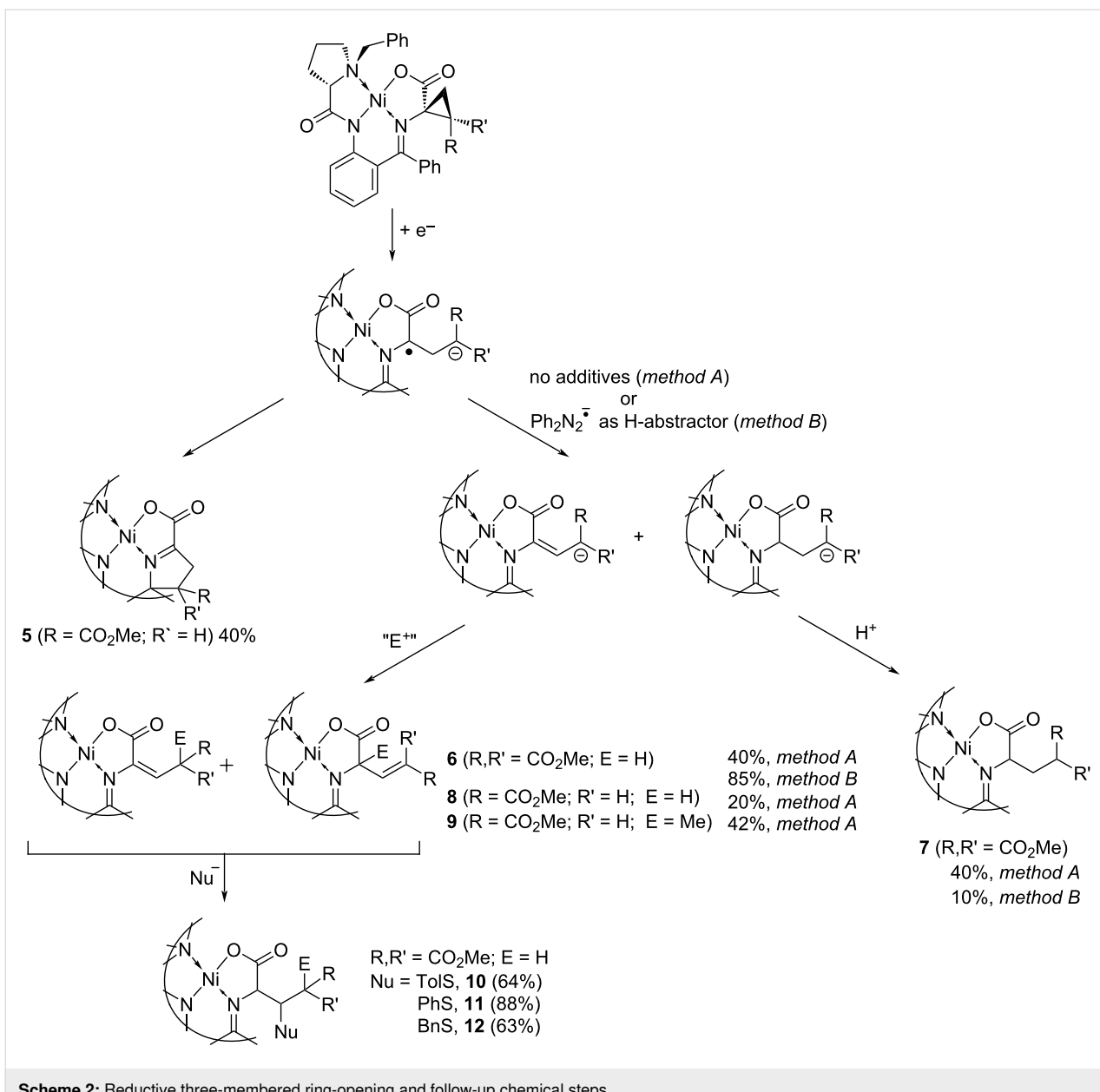
Synthesis of dehydroalanine derivatives **6**

The reaction products were isolated by column chromatography and analyzed using spectral methods. Both alkene and hydrogenated complexes are formed in the equimolar ratio, indicating disproportionation of the radical anions formed. The hydrogenated complexes **7** are of less synthetic value since they are more easily available than the corresponding substituted dehydroalanine derivatives. Additionally, the latter are of interest due to bioactivity [54,55]. To increase the yield of the alkene complexes, the addition of an external “H-abstractor” may be helpful, to suppress disproportionation. A possible candidate may be a reduced radical form of azobenzene. Indeed, the preparative electrolysis performed in the presence of the equimolar Ph₂N₂ additive changed the relative ratio of alkene to hydrogenated derivatives in favor of the former one (see Table 1).

As follows from Table 1, the azobenzene additive allows increasing the yield of the alkene complexes up to 85% suppressing formation of the hydrogenated complexes. Spectral NMR analysis of the reaction mixture showed that two isomeric alkenes (containing the α - β or β - γ double bond) are formed. In the isomers, two protons of the amino acid side chain create an AB system; in the α - β isomer, both protons show correlations in the HMBC spectrum with the C atoms of the COOMe groups, whereas in the β - γ isomer, only one H correlates with the COOMe and the other H atom correlates with the Schiff and carboxylic carbons (see Figure 3 and Supporting Information File 1).

The experimental ratio of the isomeric alkenes (1.5:1) is close to the calculated value predicted from their relative thermodynamic stability (1.3:1, see Supporting Information File 1). Notably, the coordination to the Lewis acid increases the regioselectivity of protonation in the allylic anions formed in the electrolysis. Thus, using LiCl as a supporting electrolyte increases the ratio to 5:1. An even more pronounced effect can be achieved if the electrolysis is performed in the undivided cell equipped with a Zn or Mg anode. In this case, the anodically generated Zn²⁺ or Mg²⁺ worked as Lewis acid and the isomeric α - β and β - γ alkene complexes are formed in 54:1 ratio (though the total yield is decreased to 50%).

In case of complex **3**, the isolated yield of the alkene complex was low (20%); the Ph₂N₂ additive gives only insignificant increase (27%). Analysis of the values of spin coupling constants (see Supporting Information File 1 for the details) testifies in favor of the β - γ isomer selective formation. The dominant reaction product formed in the reductive opening of the cyclopropane ring in complex **3** was new derivative **5** containing a five-membered ring (see below and Scheme 2).

**Scheme 2:** Reductive three-membered ring-opening and follow-up chemical steps.**Table 1:** Yields of the alkene complexes **6** and the hydrogenated derivative are dependent on the electrolysis conditions used for the ring opening in complex **4** (8 mM) (GC, DMF, 0.09 M Bu₄NBF₄ or 0.8 M LiCl).

supporting electrolyte, additives	WE potential	conditions		cell type	alkene complexes 6 yield, %	hydrogenated derivative 7 yield, %
		charge / 1 mol of 4	α-β/β-γ isomers ratio			
Bu ₄ NBF ₄	-1.7 V	1 F	divided	40	1.5:1	40
Bu ₄ NBF ₄ , Ph ₂ N ₂ (1 equiv)	-1.5 V	2 F	divided	85	1.5:1	10
Bu ₄ NBF ₄ , Ph ₂ N ₂ (1.5 equiv)	-1.5 V	2.5 F	divided	85	1.5:1	10
LiCl	-1.4 V	1 F	divided	40	5:1	40
Bu ₄ NBF ₄ electrogenerated Zn ²⁺ or Mg ²⁺	(galvanostatic regime)	8 F	undivided	50	54:1	12

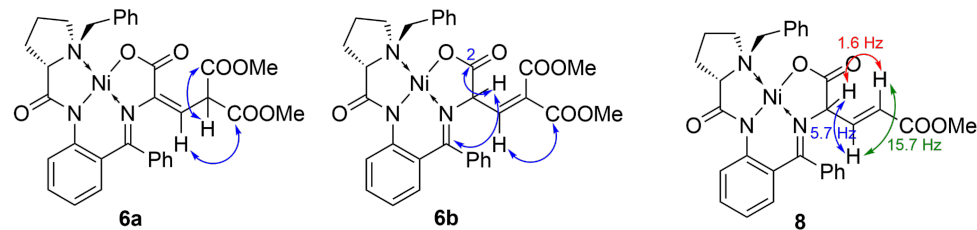


Figure 3: Correlations in the HMBC spectra of **6a** and **6b** and spin coupling constants in the ^1H NMR spectrum of **8**.

Intramolecular cyclization

The anionic species formed in the ring opening in complex **3** undergo fast intramolecular cyclization via the nucleophilic attack at the imine fragment yielding new complex **5** (Scheme 3), which was isolated in the form of two diastereomers in a total yield of 37%, indicating that this reaction route dominates. The compounds were characterized with NMR (2D technique, see Supporting Information File 1). Notably, insertion of the second COOR group in the starting cyclopropane complex **4** completely suppresses this reaction channel: intramolecular cyclization of the anions formed in the reductive cleavage of the three-membered ring was not observed. This may be attributed to the decreased nucleophilicity as well as to steric reasons.

Reaction with electrophiles

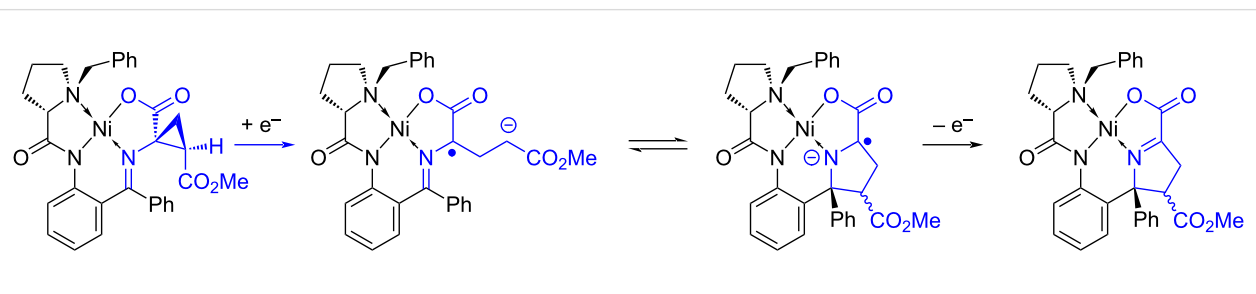
Anions formed in the reductive ring opening in complex **4** are stable enough: they survive even in the presence of acetic acid and do not react with electrophiles (CH_3I , benzaldehyde). In contrast, addition of external electrophiles in the reaction mixture obtained in the electrolysis of **3** launches an additional reaction path, along with intramolecular cyclization described above. Thus, addition of CH_3I results in the formation of γ -methylated alkene complex **9** in the form of two diastereomers (5:1) in 42% yield.

The results obtained clearly indicate that follow-up functionalization of the anions formed after the ring opening with electro-

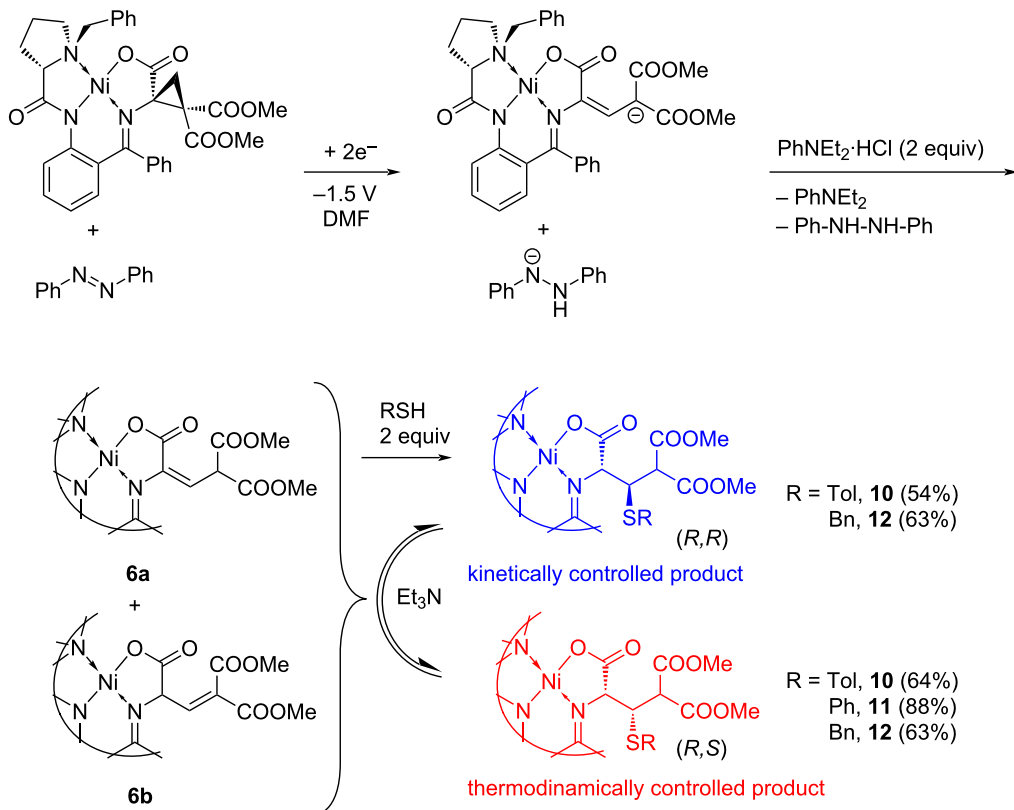
philes (except H^+) has low synthetic value due to multiple competing reaction channels observed in case of **3** and decreased nucleophilicity of **4**. Consequently, it seems reasonable to focus on the one-pot nucleophilic functionalization of the double bond of the dehydroalanine derivatives formed after the reductive ring opening and subsequent protonation. Such an approach opens a route to double functionalization of the amino acids side chain. Insertion of the sulfur-containing fragments is of special interest due to the bioactivity of such compounds [56,57]; thus, elaboration of new synthetic protocols to these multifunctional molecules is a topical problem.

Complex **4** was subjected to reductive ring opening at a potential of -1.5 V ($\text{Ag}/\text{AgCl}, \text{KCl}_{(\text{sat.})}$) in the presence of an equimolar amount of azobenzene as described above (two-compartment cell, DMF, Bu_4NBF_4 , a glassy carbon WE, an iron wire as a CE). After 2 F/mol amount of electricity passed and subsequent protonation with $\text{PhNEt}_2\cdot\text{HCl}$, aryl- or benzylthiol was added. The reaction mixture was kept overnight and then the products were isolated using column chromatography and analyzed using spectral methods. The results obtained are given in Table 2 and Scheme 4.

The synthetic procedure was tested on three thiols, of both aromatic and aliphatic types. The first experiment with *p*-tolylthiol gave the targeted cysteine derivative in practical 64% isolated yield, along with some amount of the alkene complex (see Scheme 4). In an attempt to increase the yield of the cysteine



Scheme 3: Electrochemically induced ring-opening followed by intramolecular cyclization.



Scheme 4: One-pot multistep approach to the cysteine derivatives.

Table 2: Yield and diastereomeric ratio of the cysteine derivatives obtained in a one-pot electrochemical reduction (method B: -1.5 V (Ag/AgCl, KCl_(sat.)), 4 (8 mM), Ph₂N₂ (8 mM), 2F/mol, DMF) of complex 4 with subsequent thiol addition (PhNEt₂·HCl (2 equiv); RSH (1 or 2 equiv), 24 h, rt).

	RSH	RSH (equiv)	(R,S):(R,R) dr	yield, %	additive	complex
1	TolSH	1	10:1	64	–	10
2	TolSH	2	1:5	54	–	10
3	TolSH	2	10:1	64	+ 1 equiv Et ₃ N	10
4	PhSH	2	12:1	88	+ 1 equiv Et ₃ N	11
5	BnSH	2	1:2.6	64	–	12
6	BnSH	2	pure (R,S)-isomer	42 ^a	+ 1 equiv Et ₃ N	12

^a72 h, 40 °C.

derivatives, the amount of the thiol was doubled. Unexpectedly, this resulted in the inversion of the diastereomeric ratio (entry 2 in Table 2). To find a reason, the experiment was repeated in the presence of an additional base (1 mol equivalent of Et₃N); the result was identical to that previously obtained for the equimolar **4**:*p*-tolylthiol mixture (compare entries 1 and 3 in Table 2). Thus, it seems reasonable to suggest that a base may induce epimerization of the product yielding the

most thermodynamically stable cysteine derivative [58]. The suggestion was proven by the control experiment. An equimolar mixture of the diastereomeric cysteine complexes **10** were dissolved in DMF containing Et₃N and TolSH (1:1) and left overnight at room temperature under argon. As a result, the (R,S):(R,R) diastereomeric ratio was changed from 1:1 to 13:1 in favor of the thermodynamically more stable (R,S) diastereomer.

The experiment with thiophenol performed under the same reaction conditions (a two-fold excess of thiol and the Et_3N additive) gave the cysteine derivatives in 88% yield and with 12:1 diastereoselectivity; again, the (R,S) diastereomer was the dominant (entry 4, Table 2), in line with the previous results with tolylthiol.

In case of an aliphatic thiol (benzylthiol), the results were qualitatively similar. The diastereomeric ratio is inverted in favor of the kinetically controlled product when no Et_3N is added into the solution (entry 5, Table 2). In contrast, pure (R,S) diastereomer was obtained when the solution containing 1 mol equiv of Et_3N was kept for 72 h under slight heating ($40\text{ }^\circ\text{C}$, entry 6); though in the expense of the yields decrease (a significant amount of the alkene (48% instead of 20% detected in entry 5) was also isolated from the reaction mixture).

Thus, the experiments indicated that the one-pot multistep experimentally simple procedure allows achieving high stereoselectivity at the removed β -stereocenter, what is not an easy task. In all cases, the targeted cysteine derivatives were isolated in practical yields. It should be noted that there is no need to separate the isomeric alkene complexes formed after the cyclopropane ring opening, they can be involved in the follow-up reaction with nucleophiles in the form of a mixture. This simplifies the synthetic procedure; the multistep process can be performed in an electrochemical cell, with the potential switching off prior to the addition of nucleophiles (thiols in our case).

Complexes **10–12** were obtained as pure diastereomers (a set of signals corresponding to the individual compound is present in the ^1H NMR spectrum in each case). Assigning of the relative configurations of newly formed α - and β -stereocenters in cysteine derivatives discussed above was performed using the NOESY spectra. It is illustrated in Figure 4 taking complex **10** as an example. A correlation between protons of the tolyl substituent in the side chain of the amino acid moiety and H-12 and H-13 protons of the proline methylene group is observed in the NOESY spectrum (Figure 4). Hence, the amino acid side chain and the proline methylenes are at the same side of the Ni coordination plane allowing to assign the configuration to the α -stereocenter as (R) in both thermodynamically and kinetically controlled isomers of **10**. The configurations of the β -stereocenter in the obtained diastereomers of **10** are different, as follows from the different correlations of the *ortho*-phenyl protons of the benzophenone moiety observed in the NOESY spectra of the diastereomers. The *ortho*-phenyl proton exhibits correlation with the β -H in case of the thermodynamically controlled isomer, whereas correlation with the ester methyl group is observed in the spectrum of the kinetically controlled isomer.

This allows to unambiguously assign the relative configurations for these compounds (Figure 4).

Large positive values of specific rotation for both diastereomers of complexes **10–12** (see Supporting Information File 1) additionally support the α - (R) configuration. It was shown that positive values of $[\alpha]_D$ are inherent to the Ni–Schiff base complexes of (S) -*N*-(*N*-benzylprolyl)aminobenzophenone and L-amino acids (i.e., (R) -cysteine derivatives) [48].

Conclusion

Electroreductive opening of a cyclopropane ring in α,α -cyclopropanated amino acids in the form of Ni(II)–Schiff base complexes was studied. Preliminary voltammetry testing allowed to choose the most promising candidates for the preparative synthesis. The bulk electrolysis showed that substituents in the cyclopropane ring not only affect its tendency to the ring-opening, but also determine the follow-up reaction paths of thus formed radical anions. Possible reaction paths include disproportionation reaction yielding a mixture of alkenes and the corresponding hydrogenated derivatives, intramolecular cyclization and reaction with external electrophiles. Optimization of the reaction conditions opens a route to amino acid derivatives containing the α - β or β - γ double C=C bond in the side chain; the regioselectivity can be tuned by the addition of Lewis acids. This type of non-proteinogenic amino acid derivatives is not easily available but strongly required due to their bioactivity.

One-pot nucleophilic in situ functionalization of the double bond of dehydroalanine derivatives formed after the reductive ring opening and subsequent protonation opens a route to double functionalization of the amino acids side chain. Thus, addition of thiols to the mixture of alkenes formed in reductive opening of a cyclopropane ring in α,α -cyclopropanated amino acids allows obtaining the cysteine derivatives in practical yields and with high stereoselectivity at the removed β -stereocenter. The developed one-pot multistep procedure highlights new perspectives provided by combination of electrochemically broaden DA-cyclopropane concept and chirality induction within a metal coordination sphere.

Notably, the Ni template is an important component of the reaction. It is responsible for chirality induction and facilitates the cyclopropane ring opening, significantly decreasing the reduction potential value. It stabilizes the anion formed and serves as a directing group. Thus, the Ni–Schiff base platform creates an optimal balance between the covalent binding with the substrate (which does not “kill” its reactivity but precludes its redox destruction) with non-covalent interactions in the metal chiral coordination environment governing the reaction’s stereocontrol.

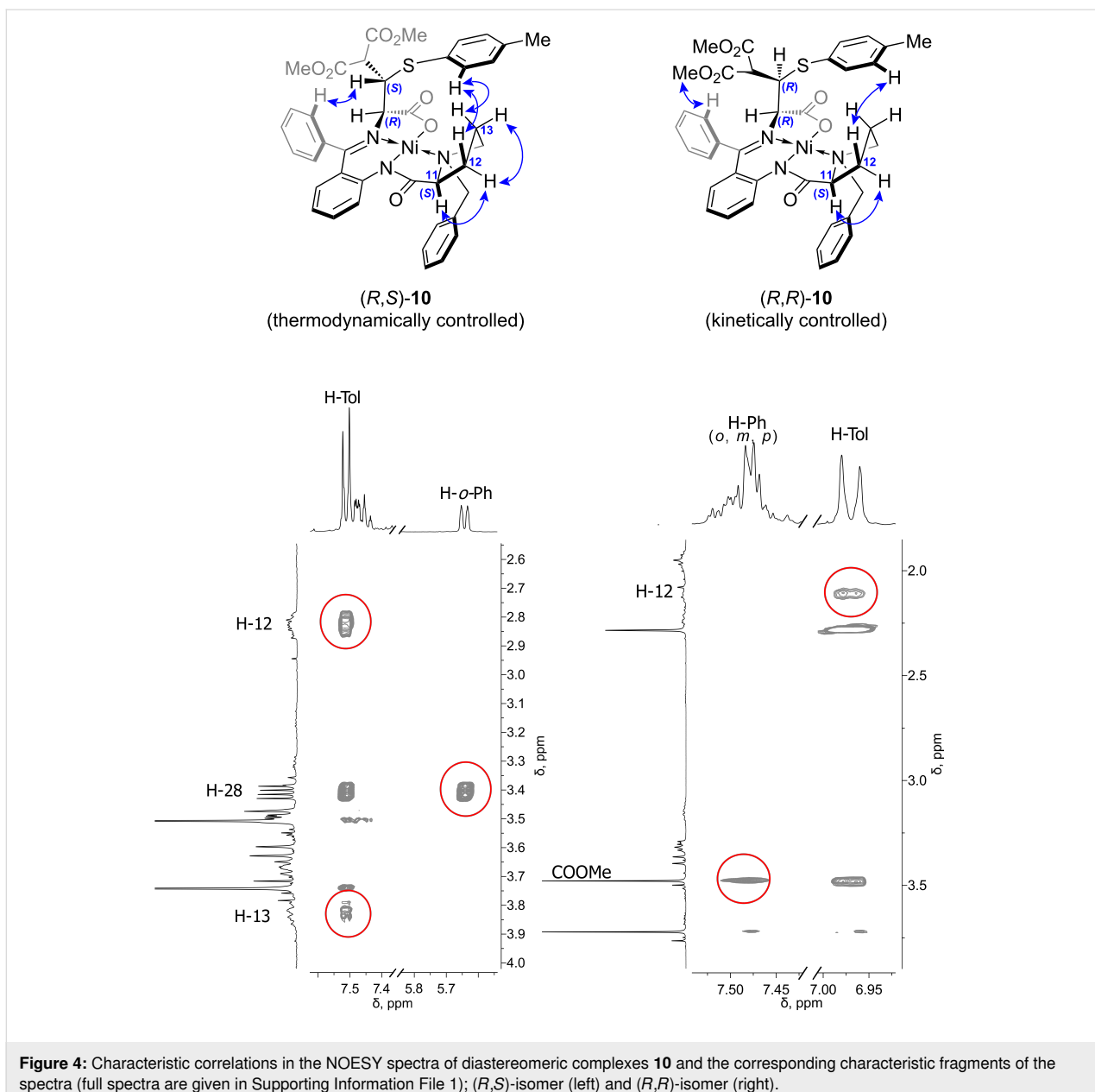


Figure 4: Characteristic correlations in the NOESY spectra of diastereomeric complexes **10** and the corresponding characteristic fragments of the spectra (full spectra are given in Supporting Information File 1); (*R,S*)-isomer (left) and (*R,R*)-isomer (right).

Supporting Information

Supporting Information File 1

Additional experimental details, characterization data as well as NMR and MS spectra of synthesized compounds. [<https://www.beilstein-journals.org/bjoc/content/supportive/1860-5397-18-121-S1.pdf>]

ORCID® iDs

Tatiana V. Magdesieva - <https://orcid.org/0000-0003-2173-652X>

Preprint

A non-peer-reviewed version of this article has been previously published as a preprint: <https://doi.org/10.3762/bxiv.2022.40.v1>

References

- Yoshida, J.-i.; Shimizu, A.; Hayashi, R. *Chem. Rev.* **2018**, *118*, 4702–4730. doi:10.1021/acs.chemrev.7b00475
- Luca, O. R.; Gustafson, J. L.; Maddox, S. M.; Fenwick, A. Q.; Smith, D. C. *Org. Chem. Front.* **2015**, *2*, 823–848. doi:10.1039/c5qo00075k

Funding

This work was supported by the Russian Foundation for Basic Research (project number 19-29-08012).

3. Yan, M.; Kawamata, Y.; Baran, P. S. *Chem. Rev.* **2017**, *117*, 13230–13319. doi:10.1021/acs.chemrev.7b00397
4. Zhu, C.; Ang, N. W. J.; Meyer, T. H.; Qiu, Y.; Ackermann, L. *ACS Cent. Sci.* **2021**, *7*, 415–431. doi:10.1021/acscentsci.0c01532
5. Horn, E. J.; Rosen, B. R.; Baran, P. S. *ACS Cent. Sci.* **2016**, *2*, 302–308. doi:10.1021/acscentsci.6b00091
6. Ghosh, M.; Shinde, V. S.; Rueping, M. *Beilstein J. Org. Chem.* **2019**, *15*, 2710–2746. doi:10.3762/bjoc.15.264
7. Möhle, S.; Zirbes, M.; Rodrigo, E.; Gieshoff, T.; Wiebe, A.; Waldvogel, S. R. *Angew. Chem., Int. Ed.* **2018**, *57*, 6018–6041. doi:10.1002/anie.201712732
8. Chang, X.; Zhang, Q.; Guo, C. *Angew. Chem., Int. Ed.* **2020**, *59*, 12612–12622. doi:10.1002/anie.202000016
9. Magdesieva, T. V.; Levitskiy, O. A.; Grishin, Y. K.; Ambartsumyan, A. A.; Kiskin, M. A.; Churakov, A. V.; Babievsky, K. K.; Kochetkov, K. A. *Organometallics* **2014**, *33*, 4629–4638. doi:10.1021/om500070n
10. Levitskiy, O. A.; Grishin, Y. K.; Semivrazhskaya, O. O.; Ambartsumyan, A. A.; Kochetkov, K. A.; Magdesieva, T. V. *Angew. Chem., Int. Ed.* **2017**, *56*, 2704–2708. doi:10.1002/anie.201609792
11. Levitskiy, O. A.; Grishin, Y. K.; Magdesieva, T. V. *Eur. J. Org. Chem.* **2019**, 3174–3182. doi:10.1002/ejoc.201900466
12. Levitskiy, O. A.; Grishin, Y. K.; Paseshnichenko, K. A.; Kochetkov, K. A.; Magdesieva, T. V. *Tetrahedron Lett.* **2018**, *59*, 2831–2834. doi:10.1016/j.tetlet.2018.06.025
13. Levitskiy, O. A.; Aglamazova, O. I.; Grishin, Y. K.; Paseshnichenko, K. A.; Magdesieva, T. V. *ChemElectroChem* **2020**, *7*, 3361–3367. doi:10.1002/celc.202000970
14. Levitskiy, O. A.; Aglamazova, O. I.; Dmitrieva, A. V.; Soloshonok, V. A.; Moriwaki, H.; Grishin, Y. K.; Magdesieva, T. V. *Mendeleev Commun.* **2021**, *31*, 337–340. doi:10.1016/j.mencom.2021.04.018
15. Levitskiy, O. A.; Aglamazova, O. I.; Grishin, Y. K.; Nefedov, S. E.; Magdesieva, T. V. *Electrochim. Acta* **2022**, *409*, 139980. doi:10.1016/j.electacta.2022.139980
16. Belokon, Y. N.; Maleev, V. I.; Savel'eva, T. F.; Moskalenko, M. A.; Pripadchev, D. A.; Khrustalev, V. N.; Saghiyan, A. S. *Amino Acids* **2010**, *39*, 1171–1176. doi:10.1007/s00726-010-0551-1
17. Kawashima, A.; Xie, C.; Mei, H.; Takeda, R.; Kawamura, A.; Sato, T.; Moriwaki, H.; Izawa, K.; Han, J.; Aceña, J. L.; Soloshonok, V. A. *RSC Adv.* **2015**, *5*, 1051–1058. doi:10.1039/c4ra12658k
18. Debaché, A.; Collet, S.; Bauchat, P.; Danion, D.; Euzenat, L.; Hercouet, A.; Carboni, B. *Tetrahedron: Asymmetry* **2001**, *12*, 761–764. doi:10.1016/s0957-4166(01)00106-9
19. Levitskiy, O. A.; Aglamazova, O. I.; Grishin, Y. K.; Paseshnichenko, K. A.; Soloshonok, V. A.; Moriwaki, H.; Magdesieva, T. V. *Dalton Trans.* **2020**, *49*, 8636–8644. doi:10.1039/d0dt01578d
20. Brackmann, F.; de Meijere, A. *Chem. Rev.* **2007**, *107*, 4493–4537. doi:10.1021/cr078376j
21. Revill, P.; Serradell, N.; Bolós, J.; Rosa, E. *Drugs Future* **2007**, *32*, 788–798. doi:10.1358/dof.2007.032.09.1138229
22. Kende, H. *Annu. Rev. Plant Physiol. Plant Mol. Biol.* **1993**, *44*, 283–307. doi:10.1146/annurev.pp.44.060193.001435
23. Wermuth, C.; Aldous, D.; Raboisson, P.; Rognan, D. *The Practice of Medicinal Chemistry*, 4th ed.; Academic Press: London, UK, 2015. doi:10.1016/c2012-0-03066-9
24. Reissig, H.-U.; Hirsch, E. *Angew. Chem., Int. Ed. Engl.* **1980**, *19*, 813–814. doi:10.1002/anie.198008131
25. Schneider, T. F.; Kaschel, J.; Werz, D. B. *Angew. Chem., Int. Ed.* **2014**, *53*, 5504–5523. doi:10.1002/anie.201309886
26. Xia, Y.; Liu, X.; Feng, X. *Angew. Chem., Int. Ed.* **2021**, *60*, 9192–9204. doi:10.1002/anie.202006736
27. Kulinkovich, O. G. *Cyclopropanes in Organic Synthesis*; John Wiley & Sons: Hoboken, NJ, USA, 2015. doi:10.1002/9781118978429
28. Tomilov, Y. V.; Menchikov, L. G.; Novikov, R. A.; Ivanova, O. A.; Trushkov, I. V. *Russ. Chem. Rev.* **2018**, *87*, 201–250. doi:10.1070/rctr4787
29. Chen, D. Y.-K.; Pouwer, R. H.; Richard, J.-A. *Chem. Soc. Rev.* **2012**, *41*, 4631–4642. doi:10.1039/c2cs35067j
30. Ivanova, O. A.; Trushkov, I. V. *Chem. Rec.* **2019**, *19*, 2189–2208. doi:10.1002/tcr.201800166
31. Shono, T.; Matsumura, Y.; Nakagawa, Y. *J. Org. Chem.* **1971**, *36*, 1771–1775. doi:10.1021/jo00812a011
32. Shono, T.; Matsumura, Y. *Bull. Chem. Soc. Jpn.* **1975**, *48*, 2861–2864. doi:10.1246/bcsj.48.2861
33. Torii, S.; Inokuchi, T.; Takahasi, N. *J. Org. Chem.* **1978**, *43*, 5020–5022. doi:10.1021/jo00420a030
34. Torii, S.; Okamoto, T.; Ueno, N. *J. Chem. Soc., Chem. Commun.* **1978**, 293–294. doi:10.1039/c39780000293
35. Wayner, D. D. M.; Arnold, D. R. *J. Chem. Soc., Chem. Commun.* **1982**, 1087–1088. doi:10.1039/c39820001087
36. Matsubara, Y.; Uchida, T.; Ohnishi, T.; Kanehira, K.; Fujita, Y.; Hirashima, T.; Nishiguchi, I. *Tetrahedron Lett.* **1985**, *26*, 4513–4516. doi:10.1016/s0040-4039(00)88944-3
37. Wang, Y.; Tanko, J. M. *J. Am. Chem. Soc.* **1997**, *119*, 8201–8208. doi:10.1021/ja970932b
38. Tanko, J. M.; Li, X.; Chahma, M.; Jackson, W. F.; Spencer, J. N. *J. Am. Chem. Soc.* **2007**, *129*, 4181–4192. doi:10.1021/ja063857q
39. Tanko, J. M.; Drumright, R. E. *J. Am. Chem. Soc.* **1990**, *112*, 5362–5363. doi:10.1021/ja00169a060
40. Tanko, J. M.; Gillmore, J. G.; Friedline, R.; Chahma, M. *J. Org. Chem.* **2005**, *70*, 4170–4173. doi:10.1021/jo047917r
41. Couture-Martin, F.; Sardashti, A.; Cristea, C.; Chapuzet, J. M.; Lessard, J. *Meet. Abstr.* **2008**, MA2008-01, 567. doi:10.1149/ma2008-01/14/567
42. Lessard, J.; Fry, A. J. *Meet. Abstr.* **2017**, MA2017-01, 1688. doi:10.1149/ma2017-01/36/1688
43. Kolb, S.; Ahlborg, N. L.; Werz, D. B. *Org. Lett.* **2021**, *23*, 5549–5553. doi:10.1021/acs.orglett.1c01890
44. Kolb, S.; Petzold, M.; Brandt, F.; Jones, P. G.; Jacob, C. R.; Werz, D. B. *Angew. Chem., Int. Ed.* **2021**, *60*, 15928–15934. doi:10.1002/anie.202101477
45. Madelaine, C.; Six, Y.; Buriez, O. *Angew. Chem., Int. Ed.* **2007**, *46*, 8046–8049. doi:10.1002/anie.200702903
46. Oyanagi, S.; Ishii, H.; Inagi, S.; Fuchigami, T. *J. Electrochem. Soc.* **2020**, *167*, 155511. doi:10.1149/1945-7111/abb83b
47. Peng, P.; Yan, X.; Zhang, K.; Liu, Z.; Zeng, L.; Chen, Y.; Zhang, H.; Lei, A. *Nat. Commun.* **2021**, *12*, 3075. doi:10.1038/s41467-021-23401-8
48. Soloshonok, V. A.; Belokon', Y. N.; Kukhar', V. P.; Chernoglazova, N. I.; Saporovskaya, M. B.; Bakhmutov, V. I.; Kolycheva, M. T.; Belikov, V. M. *Russ. Chem. Bull.* **1990**, *39*, 1479–1485. doi:10.1007/bf00957865
49. Levitskiy, O. A.; Aglamazova, O. I.; Dmitrieva, A. V.; Magdesieva, T. V. *Electrochim. Acta* **2021**, *388*, 138537. doi:10.1016/j.electacta.2021.138537

50. Levitskiy, O. A.; Aglamazova, O. I.; Soloshonok, V. A.; Moriwaki, H.; Magdesieva, T. V. *Chem. – Eur. J.* **2020**, *26*, 7074–7082. doi:10.1002/chem.201905708

51. Magdesieva, T. V. *Chem. Rec.* **2021**, *21*, 2178–2192. doi:10.1002/tcr.202100019

52. Magdesieva, T. V.; Levitskiy, O. A.; Grishin, Y. K.; Ambartsumyan, A. A.; Paseshnichenko, K. A.; Kolotyrkina, N. G.; Kochetkov, K. A. *Organometallics* **2014**, *33*, 4639–4654. doi:10.1021/om500034x

53. Bordwell, F. G. *Acc. Chem. Res.* **1988**, *21*, 456–463. doi:10.1021/ar00156a004

54. Fichtner, M.; Voigt, K.; Schuster, S. *Biochim. Biophys. Acta, Gen. Subj.* **2017**, *1861*, 3258–3269. doi:10.1016/j.bbagen.2016.08.008

55. Siodlak, D. *Amino Acids* **2015**, *47*, 1–17. doi:10.1007/s00726-014-1846-4

56. Kang-Sickel, J.-C. C.; Fox, D. D.; Nam, T.-g.; Jayaraj, K.; Ball, L. M.; French, J. E.; Klapper, D. G.; Gold, A.; Nylander-French, L. A. *Chem. Res. Toxicol.* **2008**, *21*, 852–858. doi:10.1021/tx7003773

57. Emre, Y.; Imhof, B. A. *Semin. Immunopathol.* **2014**, *36*, 253–259. doi:10.1007/s00281-014-0420-1

58. Since the reaction is performed as a one-pot procedure, 1 equiv of PhNEt₂ formed after protonation of the carbanion is already present in the reaction mixture. An excess of the thiol (which is sufficiently acidic) eliminates the base preventing epimerization of the product.

License and Terms

This is an open access article licensed under the terms of the Beilstein-Institut Open Access License Agreement (<https://www.beilstein-journals.org/bjoc/terms>), which is identical to the Creative Commons Attribution 4.0

International License

(<https://creativecommons.org/licenses/by/4.0>). The reuse of material under this license requires that the author(s), source and license are credited. Third-party material in this article could be subject to other licenses (typically indicated in the credit line), and in this case, users are required to obtain permission from the license holder to reuse the material.

The definitive version of this article is the electronic one which can be found at:

<https://doi.org/10.3762/bjoc.18.121>



A one-pot electrochemical synthesis of 2-aminothiazoles from active methylene ketones and thioureas mediated by NH₄I

Shang-Feng Yang^{‡1}, Pei Li^{‡1}, Zi-Lin Fang¹, Sen Liang^{*1}, Hong-Yu Tian¹, Bao-Guo Sun¹, Kun Xu² and Cheng-Chu Zeng^{*2}

Full Research Paper

Open Access

Address:

¹Beijing Advanced Innovation Center for Food Nutrition and Human Health, Beijing Key Laboratory of Flavor Chemistry, Beijing

Technology and Business University, Beijing 100048, China and

²Faculty of Environment and Life, Beijing University of Technology, Beijing 100124, China

Email:

Sen Liang^{*} - liangsen@bjtu.edu.cn; Cheng-Chu Zeng^{*} - zengcc@bjut.edu.cn

* Corresponding author ‡ Equal contributors

Keywords:

2-aminothiazoles; electrosynthesis; indirect electrolysis; halide ion

Beilstein J. Org. Chem. **2022**, *18*, 1249–1255.

<https://doi.org/10.3762/bjoc.18.130>

Received: 27 May 2022

Accepted: 05 September 2022

Published: 15 September 2022

This article is part of the thematic issue "Molecular and macromolecular electrochemistry: synthesis, mechanism, and redox properties".

Guest Editor: S. Inagi

© 2022 Yang et al.; licensee Beilstein-Institut.

License and terms: see end of document.

Abstract

The electrochemical preparation of 2-aminothiazoles has been achieved by the reaction of active methylene ketones with thioureas assisted by DL-alanine using NH₄I as a redox mediator. The electrochemical protocol proceeds in an undivided cell equipped with graphite plate electrodes under constant current conditions. Various active methylene ketones, including β -keto ester, β -keto amide, β -keto nitrile, β -keto sulfone and 1,3-diketones, can be converted to the corresponding 2-aminothiazoles. Mechanistically, the in situ generated α -iodoketone was proposed to be the key active species.

Introduction

Thiazoles are prevalent structural motifs in a wide range of natural products [1] and synthetic molecules possessing various pharmaceutical activities such as antimicrobial [2,3], antiviral [4], antitumor [5,6], anti-inflammatory [7,8] and so on. Moreover, as a type of important intermediates, thiazole is of prime importance in organic synthesis [9,10] which is used extensively in the preparation of flavors [11], polymers [12], dyes [13], etc. These important features of thiazoles have driven intense interests in their facile synthesis [14–17]. Among various synthetic routes to the thiazole unit, the Hantzsch condensation of

α -halo ketones (dielectrophiles) with various thioureas (dinucleophiles) should be the most well-known method (Scheme 1a) [18]. Since active methylene ketones are able to be in situ α -halogenated, the modified Hantzsch condensation of active methylene ketones with thioureas has attracted increasing attention in thiazoles' synthesis, thereby saving costs and time needed to prepare the required α -halogenated dielectrophiles. Along this line, in situ α -halogenation strategies have been developed, using various halogenating reagents including Br₂ [19,20], I₂ [21,22], NBS [23–25], tribromoisocyanuric acid

[26], 1,3-dichloro-5,5-dimethylhydantoin [27], HBr or HI, DMSO [28] etc. (Scheme 1b). Alternatively, the oxidation of α -C–H of active methylene ketones generate α -carbon-centered radicals, thus providing another way to obtain thiazoles. Recently, Sun et al. reported a *tert*-butyl hydroperoxide/azodisisobutyronitrile-mediated synthesis of 2-aminothiazoles from active methylene ketones and thiourea via an oxidative cyclization initiated by a radical process and a following condensation reaction (Scheme 1c) [29]. Although these methods are practical, most of these strategies require stoichiometric or excess amounts of halogenating reagents or oxidants, which are toxic, hazardous and would lead to a large quantity of waste. Considering the importance of thiazoles in synthetic and medicinal chemistry, the development of greener and more atom economic processes for the thiazole synthesis has become increasingly necessary with growing awareness of environmental constraints.

Organic electrosynthesis has been recognized as a green, modern, and safe technique, since electrons can be used as an alternative for oxidants or reductants [30–38]. During our continuous interests in halide-mediated indirect electrolysis [39–42], we have achieved the *in situ* generation of α -iodocarbonyl ketones from constant current electrolysis (CCE) of ketones in the presence of iodide ions. It is worth noting that we have also reported an electrochemical method for the synthesis of 2-aminothiazoles via the one-pot direct α -C–H functionalization of ketones with thioureas [42]. However, the reported method only tolerates aromatic and aliphatic ketones; the active methylene ketones were not suitable. Given that amino acids

have been reported to work as green organocatalysts for the synthesis of 2-aminothiazole heterocycles [43,44]. We herein report a DL-alanine-assisted one-pot electrochemical synthesis of 2-aminothiazoles from active methylene ketones and thioureas mediated by NH₄I (Scheme 1d). This electrochemical method features external-oxidant-free conditions and avoids the prefunctionalization of the substrates.

Results and Discussion

To demonstrate the feasibility of our idea, ethyl acetoacetate (**1a**) and thiourea (**2a**) were chosen as model substrates for the optimization of reaction conditions. Based on our previous studies on the halide-mediated α -C–H functionalization of carbonyl compounds [32–35], graphite was chosen as the working electrode rather than exploring other options. As shown in Table 1, when the electrolysis of **1a** with **2a** was performed in aqueous DMSO at a constant current of 5 mA/cm² using NH₄I as the mediator, LiClO₄ as electrolyte and asparagine as additive in an undivided cell, the desired product **3a** was isolated in 51% after passing 6 F/mol of charge (Table 1, entry 1). The yield of **3a** decreased obviously when the ratio of **1a** to **2a** changed from 2:1 to 1:1 or 1:2 (Table 1, entries 2 and 3). Subsequent solvent screening disclosed that aqueous DMSO was the optimal solvent and lower yields were obtained in other solvents, such as aqueous DMF, aqueous MeCN or aqueous EtOH (Table 1, entries 4–6). Owing to the tedious workup process in using a large amount of DMSO as solvent, we decided to increase the proportion of H₂O and disclosed that the yield of **3a** improved from 52% to 61% when the ratio of DMSO to H₂O changed from 2:1 to 1:14 (Table 1, entry 7). When the

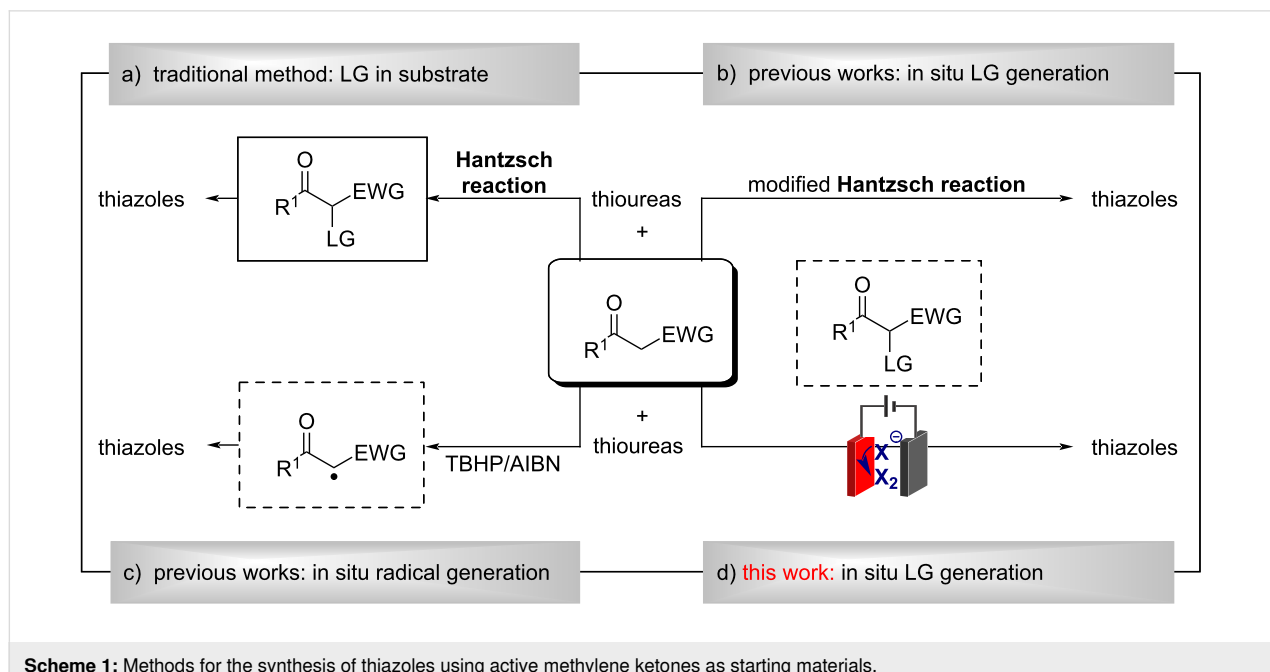


Table 1: Optimization of the reaction conditions^a.

Entry	1a : 2a	Mediator	Solvent (15 mL)	Additive	<i>T</i> [°C]	F [mol]	Yield [%] ^b		
								undivided cell	5 mA/cm ²
1	2:1	NH ₄ I	DMSO/H ₂ O (2:1)	asparagine	70	6	51		
2	1:1	NH ₄ I	DMSO/H ₂ O (2:1)	asparagine	70	6	17		
3	1:2	NH ₄ I	DMSO/H ₂ O (2:1)	asparagine	70	6	15		
4	2:1	NH ₄ I	DMF/H ₂ O (2:1)	asparagine	70	6	41		
5	2:1	NH ₄ I	MeCN/H ₂ O (2:1)	asparagine	70	6	33		
6	2:1	NH ₄ I	EtOH/H ₂ O (2:1)	asparagine	70	6	46		
7	2:1	NH ₄ I	DMSO/H ₂ O (1:14)	asparagine	70	6	61		
8	2:1	NH ₄ I	H ₂ O	asparagine	70	6	51		
9	2:1	NH ₄ I	DMSO/H ₂ O (1:14)	L-phenylalanine	70	6	60		
10	2:1	NH ₄ I	DMSO/H ₂ O (1:14)	L-aspartic acid	70	6	62		
11	2:1	NH ₄ I	DMSO/H ₂ O (1:14)	L-allysine	70	6	60		
12	2:1	NH ₄ I	DMSO/H ₂ O (1:14)	DL-alanine	70	6	65		
13	2:1	NH ₄ I	DMSO/H ₂ O (1:14)	DL-alanine	50	6	65		
14	2:1	NH ₄ I	DMSO/H ₂ O (1:14)	DL-alanine	30	6	75		
15 ^c	2:1	NH ₄ I	DMSO/H ₂ O (1:14)	DL-alanine	30	6	65		
16 ^d	2:1	NH ₄ I	DMSO/H ₂ O (1:14)	DL-alanine	30	6	73		
17	2:1	NH ₄ I	DMSO/H ₂ O (1:14)	DL-alanine	30	4	66		
18	2:1	NH ₄ I	DMSO/H ₂ O (1:14)	DL-alanine	30	8	75		
19	2:1	NH ₄ Cl	DMSO/H ₂ O (1:14)	DL-alanine	30	6	35		
20	2:1	NH ₄ Br	DMSO/H ₂ O (1:14)	DL-alanine	30	6	55		
21	2:1	Et ₄ NI	DMSO/H ₂ O (1:14)	DL-alanine	30	6	64		
22	2:1	Bu ₄ NI	DMSO/H ₂ O (1:14)	DL-alanine	30	6	59		
23	2:1	NaI	DMSO/H ₂ O (1:14)	DL-alanine	30	6	72		
24 ^e	2:1	NH ₄ I	DMSO/H ₂ O (1:14)	DL-alanine	30	6	73		
25 ^f	2:1	NH ₄ I	DMSO/H ₂ O (1:14)	DL-alanine	30	6	70		

^aReaction conditions: ethyl acetoacetate (**1a**, 2 mmol), thiourea (**2a**, 1 mmol), NH₄I (1 mmol), acid (1 mmol), LiClO₄ (0.5 mmol), DMSO/H₂O (v/v), undivided cell, graphite plate anode and cathode, 5 mA/cm². ^bIsolated yield. ^c4 mA/cm². ^d6 mA/cm². ^eNH₄I (0.1 mmol). ^fWithout LiClO₄.

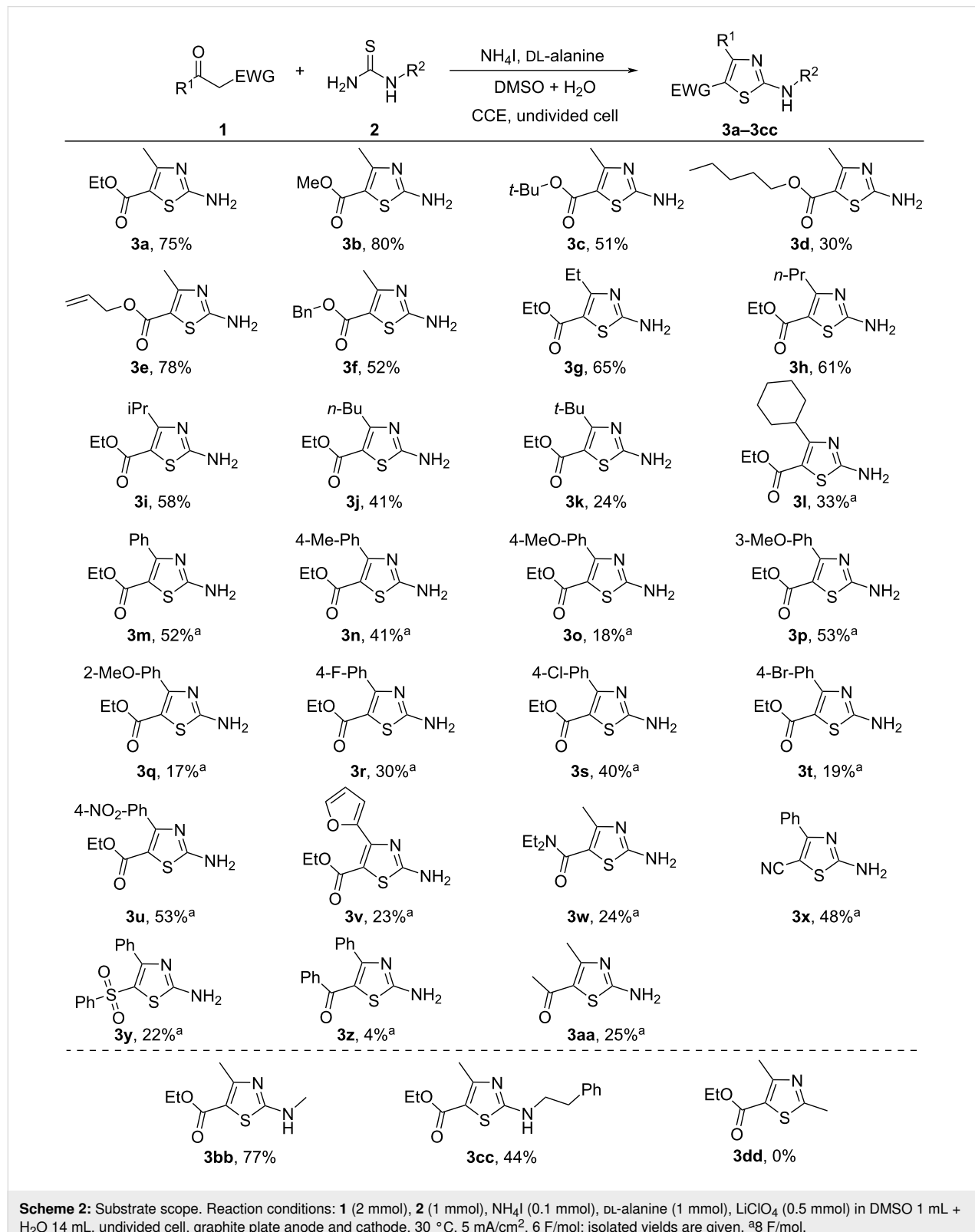
reaction was performed in H₂O, **3a** was obtained in 51% yield (Table 1, entry 8). It was observed that the additive plays an important role, among which DL-alanine was proved to be the best, although asparagine, L-phenylalanine, L-aspartic acid and L-allysine also gave comparable yields of **3a** (Table 1, entries 9–12). It is interesting to note that **3a** was achieved in higher yields (75%) when the temperature decreased from 70 °C to 30 °C (Table 1, entry 14). The effect of current density was also examined. It was found that a slightly lower yield of **3a** was produced when 4 mA/cm² (Table 1, entry 15) or 6 mA/cm² (Table 1, entry 16) was used instead of the optimal 5 mA/cm². In addition, 6 F/mol of charge was preferable because less yield of **3a** was obtained when 4 F/mol (Table 1, entry 17) and 8 F/mol (Table 1, entry 18) charge were consumed.

Next, the effect of halide-based mediators on the reaction was examined. When NH₄Cl or NH₄Br was used as the mediator, the yield of **3a** decreased to 35% (Table 1, entry 19) and 55% (Table 1, entry 20), respectively. Slightly lower yields of **3a** were obtained when the mediator NH₄I was replaced by Et₄NI, Bu₄NI or NaI (Table 1, entries 21–23). Interestingly, almost same yield of **3a** was isolated when the amount of NH₄I was reduced to 0.1 mmol (Table 1, entry 24). In addition, without conductive salt (LiClO₄) the electrochemical reaction also proceeded smoothly with a comparable yield (Table 1, entry 25).

Based on the results mentioned above, the optimal reaction conditions are as follows: constant current electrolysis was performed in an undivided cell equipped with a graphite plate as

working electrode and counter electrode, using 0.1 mmol of NH_4I as the mediator and $\text{DMSO}/\text{H}_2\text{O}$ (1 mL + 14 mL) as the solvent in the presence of DL-alanine (Table 1, entry 24).

Under the optimized reaction conditions (entry 24, Table 1), the scope of the electrochemical reaction was studied using a series of active methylene ketones (Scheme 2). Various linear and



branched alkyl acetoacetates including methyl, ethyl, *tert*-butyl, and amyl reacted smoothly with thiourea **2a** under the optimized conditions, giving the corresponding products in 30–80% yields (**3a–d**). In addition, allyl and benzyl acetoacetate were also suitable substrates to give the desired 2-aminothiazoles **3e** and **3f** in 78% and 52% yields, respectively. β -Ketoesters containing ethyl, *n*-propyl, isopropyl, *n*-butyl, *tert*-butyl and cyclohexyl moieties were also compatible with the optimized conditions, providing the corresponding 2-aminothiazoles in 24% to 65% yields (**3g–l**).

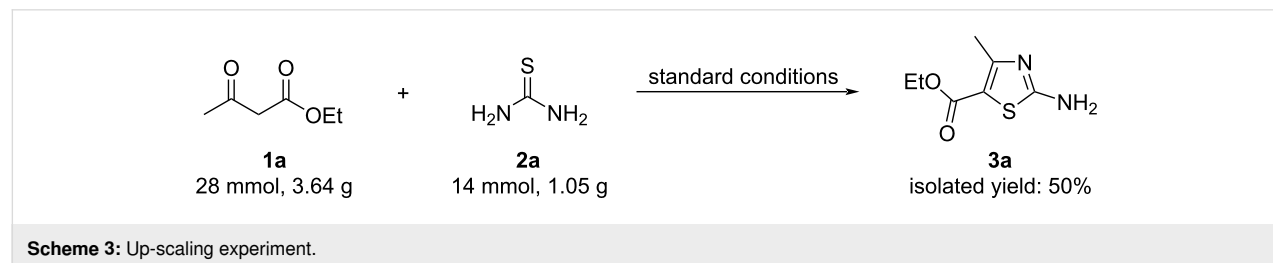
As shown in Scheme 2, when the R¹ group changed from alkyl to aryl, the target products could also be obtained. For example, ethyl 3-oxo-3-phenylpropanoate and ethyl 3-oxo-3-(*p*-tolyl)propanoate afforded the corresponding 2-aminothiazoles **3m** and **3n** in 52% and 41% isolated yields under the standard conditions. When an electron-donating methoxy substituent was introduced to the *ortho*-, *meta*-, or *para*-position of the phenyl moiety, the corresponding 2-aminothiazoles, **3o–q**, were given in 17–53% yields. With electron-withdrawing groups (F, Cl, Br, NO₂), the desired products **3r–u** were obtained in moderate yields. Other heteroaryl ketones, ethyl 3-(furan-2-yl)-3-oxopropanoate (**1v**) reacted with thiourea to give **3v** in 23% yield. In addition to β -keto esters, other active methylene derivatives, including β -ketoamide, β -keto nitrile and β -keto sulfone were also suitable coupling partners with relatively lower yields (**3w–y**) and most of the starting materials were recovered. The

method could also be applied to 1,3-diones. For example, in the cases of 1,3-diphenylpropane-1,3-dione and acetoacetone, the corresponding products **3z** and **3aa** were given in 4% and 25% yields, respectively.

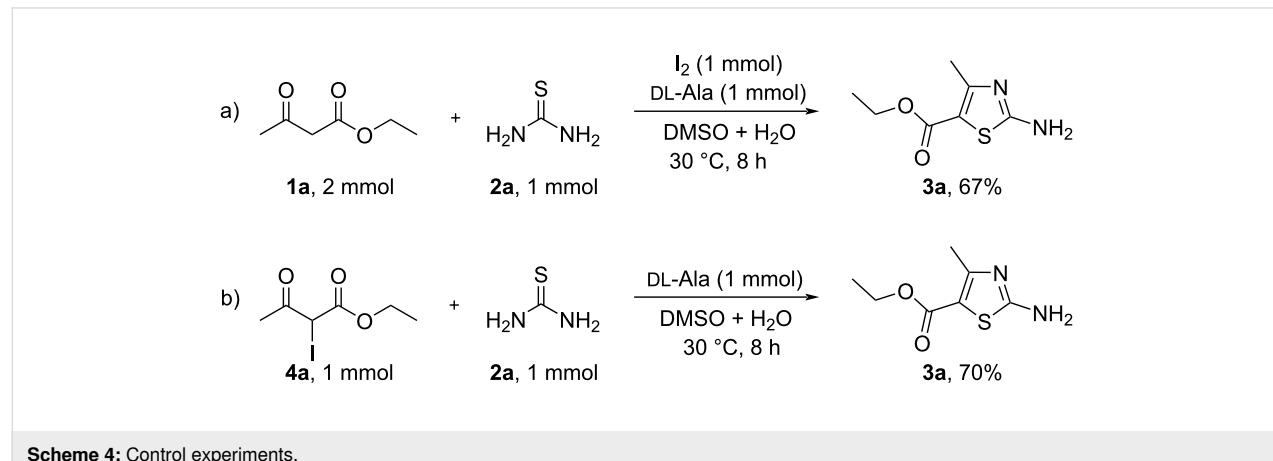
Different *N*-substituted thioureas were also screened for the electrochemical reactions. *N*-methylthiourea and *N*-(2-phenylethyl)thiourea reacted smoothly with ethyl acetoacetate **1a** under the optimized conditions, providing the corresponding 2-aminothiazoles, **3bb** and **3cc**, in 77% and 44% yields, respectively. It is regretful that thioacetamide is not the best suitable partner due to its low reactivity under the optimized conditions.

To demonstrate the practicability of the reaction, a scale-up reaction of ethyl acetoacetate (**1a**, 28 mmol, 3.64 g) and thiourea (**2a**, 14 mmol, 1.05 g) was carried out under the optimized conditions to give **3a** in 50% yield (Scheme 3).

In order to better understand the iodide-mediated reaction mechanism and to determine the possible active intermediates involved, several control experiments were carried out. As shown in Scheme 4, when molecular iodine was employed as oxidant, the desired product **3a** was obtained in a 67% yield under otherwise identical conditions (Scheme 4a), but without passing electricity. Therefore, the *in situ*-generated I₂ was one of the active species. Further investigation revealed that the condensation of ethyl 2-iodo-3-oxobutanoate (**4a**) with thiourea



Scheme 3: Up-scaling experiment.



Scheme 4: Control experiments.

2a could give the target product **3a** in 70% yield (Scheme 4b). Therefore, the in situ-generated ethyl 2-iodo-3-oxobutanoate (**4a**) should be a key intermediate for this tandem reaction.

On the basis of the above mechanistic studies and the previous works on iodide-mediated electrochemical transformation [37–40], a possible mechanism for this electrochemical reaction was proposed (Scheme 5). It is well known that amino acid can act as a bi-functional organocatalyst due to the existence of both Lewis base (NH_2) and Brønsted acidic (COOH) sites. In the suggested mechanism, the carboxy group may polarize the carbonyl group of the active methylene ketone and the amino group as a Lewis base serves the formation of enolate to produce α -iodo ketone with the molecular I_2 produced by anodic oxidation. Subsequently, the nucleophilic substitution between intermediate **4** and thiourea tautomer gives α -sulfur substituted ketone **5**. Intermediate **5** undergoes intramolecular nucleophilic addition to the carbonyl group and followed by dehydration to give the heterocyclic product **3**. At the cathode, protons are reduced to release H_2 .

Conclusion

In conclusion, we have developed a one-pot electrochemical strategy for the synthesis of 2-aminothiazoles by the reaction of active methylene ketones with thioureas. The electrochemical synthesis was performed in an undivided cell with NH_4I as the mediator and cheap graphite plate as the working electrode. Various active methylene ketones, including β -keto ester, β -keto amide, β -keto nitrile, β -keto sulfone and 1,3-diones proved to be compatible with the protocol. Since external oxidants and prefunctionalization of substrates are avoided, the present electrochemical protocol represents an appealing alternative for the synthesis of 2-aminothiazoles. Gram-scale synthe-

sis also highlighted the synthetic practicability of this electrochemical strategy. Mechanistically, the in situ-generated α -iodoketone was proposed to be a key active species. Further application of this method is underway in our laboratory.

Supporting Information

Supporting Information File 1

Experimental procedures, characterization data and copies of spectra of the all synthesized compounds (^1H NMR, ^{13}C NMR and HRMS).

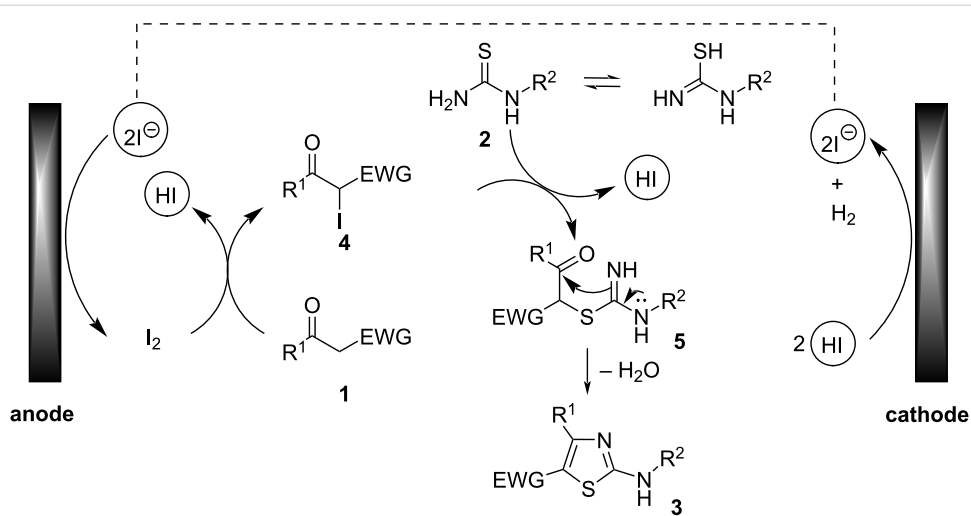
[<https://www.beilstein-journals.org/bjoc/content/supplementary/1860-5397-18-130-S1.pdf>]

Funding

This work was financially supported by the National Natural Science Foundation of China (No. 31901619).

References

1. de Souza, M. V. N. *J. Sulfur Chem.* **2005**, *26*, 429–449. doi:10.1080/17415990500322792
2. Samadhiya, P.; Sharma, R.; Srivastava, S. K.; Srivastava, S. D. *J. Serb. Chem. Soc.* **2012**, *77*, 599–605. doi:10.2298/jsc110616002s
3. Sarıgüney, A. B.; Kocababaş, E.; Erci, F.; Torlak, E.; Coşkun, A. *J. Heterocycl. Chem.* **2018**, *55*, 2107–2110. doi:10.1002/jhet.3254
4. Jeong, K.-w.; Lee, J.-h.; Park, S.-m.; Choi, J.-H.; Jeong, D.-Y.; Choi, D.-H.; Nam, Y.; Park, J.-H.; Lee, K.-N.; Kim, S.-M.; Ku, J.-M. *Eur. J. Med. Chem.* **2015**, *102*, 387–397. doi:10.1016/j.ejmchem.2015.08.020
5. Hutchinson, I.; Jennings, S. A.; Vishnuvajjala, B. R.; Westwell, A. D.; Stevens, M. F. G. *J. Med. Chem.* **2002**, *45*, 744–747. doi:10.1021/jm011025r



Scheme 5: The proposed mechanism for the one-pot electrochemical synthesis of 2-aminothiazoles mediated by NH_4I .

6. Ottmann, O.; Saglio, G.; Apperley, J. F.; Arthur, C.; Bullorsky, E.; Charbonnier, A.; Dipersio, J. F.; Kantarjian, H.; Khouri, H. J.; Kim, D.-W.; Healey, D.; Strauss, L.; Cortes, J. E. *Blood Cancer J.* **2018**, *8*, 88. doi:10.1038/s41408-018-0122-3
7. Kalkhambkar, R. G.; Kulkarni, G. M.; Shivkumar, H.; Rao, R. N. *Eur. J. Med. Chem.* **2007**, *42*, 1272–1276. doi:10.1016/j.ejmech.2007.01.023
8. Singh, N.; Bhati, S. K.; Kumar, A. *Eur. J. Med. Chem.* **2008**, *43*, 2597–2609. doi:10.1016/j.ejmech.2007.12.024
9. Kaupp, G.; Amer, F. A.; Metwally, M. A.; Abdel-Latif, E. *J. Heterocycl. Chem.* **2003**, *40*, 963–971. doi:10.1002/jhet.5570400603
10. Alajarín, M.; Cabrera, J.; Pastor, A.; Sánchez-Andrade, P.; Bautista, D. *J. Org. Chem.* **2006**, *71*, 5328–5339. doi:10.1021/jo060664c
11. Liu, Y.; Chen, H.; Yin, D.; Sun, B. *Molecules* **2010**, *15*, 5104–5111. doi:10.3390/molecules15085104
12. Al-Dujaili, A. H.; Atto, A. T.; Al-Kurde, A. M. *Eur. Polym. J.* **2001**, *37*, 927–932. doi:10.1016/s0014-3057(00)00221-4
13. Abu-Melha, S. *Pigm. Resin Technol.* **2019**, *48*, 375–382. doi:10.1108/prt-09-2018-0102
14. Kashyap, S. J.; Garg, V. K.; Sharma, P. K.; Kumar, N.; Dudhe, R.; Gupta, J. K. *Med. Chem. Res.* **2012**, *21*, 2123–2132. doi:10.1007/s00044-011-9685-2
15. Das, D.; Sikdar, P.; Bairagi, M. *Eur. J. Med. Chem.* **2016**, *109*, 89–98. doi:10.1016/j.ejmech.2015.12.022
16. Gümüş, M.; Yakan, M.; Koca, İ. *Future Med. Chem.* **2019**, *11*, 1979–1998. doi:10.4155/fmc-2018-0196
17. Jadhav, P. M.; Kantevari, S.; Tekale, A. B.; Bhosale, S. V.; Pawar, R. P.; Tekale, S. U. *Phosphorus, Sulfur Silicon Relat. Elem.* **2021**, *196*, 879–895. doi:10.1080/10426507.2021.1945601
18. Hantzsch, A.; Weber, J. H. *Ber. Dtsch. Chem. Ges.* **1887**, *20*, 3118–3132. doi:10.1002/cber.188702002200
19. Zav'yalov, S. I.; Kravchenko, N. E.; Ezhova, G. I.; Kulikova, L. B.; Zavozin, A. G.; Dorofeeva, O. V. *Pharm. Chem. J.* **2007**, *41*, 105–108. doi:10.1007/s11094-007-0023-4
20. Dziuk, B.; Kyziol, J. B.; Zaleski, J.; Ejsmont, K.; Zarychta, B. *J. Heterocycl. Chem.* **2018**, *55*, 763–768. doi:10.1002/jhet.3086
21. Abedi-Jazini, Z.; Safari, J.; Zar negar, Z.; Sadeghi, M. *Polycyclic Aromat. Compd.* **2018**, *38*, 231–235. doi:10.1080/10406638.2016.1200104
22. Safari, J.; Shokrani, Z.; Zar negar, Z. *Polycyclic Aromat. Compd.* **2020**, *40*, 1105–1111. doi:10.1080/10406638.2018.1528287
23. Narender, M.; Reddy, M. S.; Kumar, V. P.; Srinivas, B.; Sridhar, R.; Nageswar, Y. V. D.; Rao, K. R. *Synthesis* **2007**, 3469–3472. doi:10.1055/s-2007-990849
24. Meng, G.; Wang, M.; Zheng, A.; Dou, J.; Guo, Z. *Green Chem. Lett. Rev.* **2014**, *7*, 46–49. doi:10.1080/17518253.2014.895858
25. Kuarm, B. S.; Madhav, J. V.; Rajitha, B. *Lett. Org. Chem.* **2011**, *8*, 549–553. doi:10.2174/157017811797249443
26. de Andrade, V. S. C.; de Mattos, M. C. S. *Synthesis* **2018**, 4867–4874. doi:10.1055/s-0037-1610243
27. Sadeghi, M.; Safari, J.; Zar negar, Z. *RSC Adv.* **2016**, *6*, 64749–64755. doi:10.1039/c6ra11175k
28. Zar negar, Z.; Sadeghi, M.; Alizadeh, R.; Safai, J. *J. Mol. Liq.* **2018**, *255*, 76–79. doi:10.1016/j.molliq.2018.01.119
29. Sun, J.; Ge, H.; Zhen, X.; An, X.; Zhang, G.; Zhang-Negrerie, D.; Du, Y.; Zhao, K. *Tetrahedron* **2018**, *74*, 2107–2114. doi:10.1016/j.tet.2018.02.064
30. Frontana-Uribe, B. A.; Little, R. D.; Ibanez, J. G.; Palma, A.; Vasquez-Medrano, R. *Green Chem.* **2010**, *12*, 2099–2119. doi:10.1039/c0gc00382d
31. Francke, R. *Beilstein J. Org. Chem.* **2014**, *10*, 2858–2873. doi:10.3762/bjoc.10.303
32. Yan, M.; Kawamata, Y.; Baran, P. S. *Chem. Rev.* **2017**, *117*, 13230–13319. doi:10.1021/acs.chemrev.7b00397
33. Jiang, Y.; Xu, K.; Zeng, C. *Chem. Rev.* **2018**, *118*, 4485–4540. doi:10.1021/acs.chemrev.7b00271
34. Liang, S.; Zeng, C.-C. *Curr. Opin. Electrochem.* **2020**, *24*, 31–43. doi:10.1016/j.coelec.2020.06.005
35. Novaes, L. F. T.; Liu, J.; Shen, Y.; Lu, L.; Meinhardt, J. M.; Lin, S. *Chem. Soc. Rev.* **2021**, *50*, 7941–8002. doi:10.1039/d1cs00223f
36. Wang, Z.-Q.; Meng, X.-J.; Li, Q.-Y.; Tang, H.-T.; Wang, H.-S.; Pan, Y.-M. *Adv. Synth. Catal.* **2018**, *360*, 4043–4048. doi:10.1002/adsc.201800871
37. Li, J.-S.; Xie, X.-Y.; Yang, P.-P.; Jiang, S.; Tao, L.; Li, Z.-W.; Lu, C.-H.; Liu, W.-D. *Adv. Synth. Catal.* **2020**, *362*, 771–775. doi:10.1002/adsc.201901290
38. Ahdenov, R.; Mohammadi, A. A.; Makarem, S.; Taheri, S.; Mollabagher, H. *Heterocycl. Commun.* **2022**, *28*, 67–74. doi:10.1515/hc-2022-0008
39. Liang, S.; Zeng, C.-C.; Tian, H.-Y.; Sun, B.-G.; Luo, X.-G.; Ren, F.-z. *J. Org. Chem.* **2016**, *81*, 11565–11573. doi:10.1021/acs.joc.6b01595
40. Liang, S.; Zeng, C.-C.; Tian, H.-Y.; Sun, B.-G.; Luo, X.-G.; Ren, F.-z. *Adv. Synth. Catal.* **2018**, *360*, 1444–1452. doi:10.1002/adsc.201701401
41. Liang, S.; Xu, K.; Zeng, C.-C.; Tian, H.-Y.; Sun, B.-G. *Adv. Synth. Catal.* **2018**, *360*, 4266–4292. doi:10.1002/adsc.201800519
42. Li, P.; Yang, S.-F.; Fang, Z.-L.; Cui, H.-R.; Liang, S.; Tian, H.-Y.; Sun, B.-G.; Zeng, C.-C. *J. Environ. Chem. Eng.* **2022**, *10*, 107487. doi:10.1016/j.jece.2022.107487
43. Shaikh, I. R. *J. Catal.* **2014**, 402860. doi:10.1155/2014/402860
44. Safari, J.; Shokrani, Z.; Zar negar, Z. *Polycyclic Aromat. Compd.* **2020**, *40*, 1105–1111. doi:10.1080/10406638.2018.1528287

License and Terms

This is an open access article licensed under the terms of the Beilstein-Institut Open Access License Agreement (<https://www.beilstein-journals.org/bjoc/terms>), which is identical to the Creative Commons Attribution 4.0 International License (<https://creativecommons.org/licenses/by/4.0>). The reuse of material under this license requires that the author(s), source and license are credited. Third-party material in this article could be subject to other licenses (typically indicated in the credit line), and in this case, users are required to obtain permission from the license holder to reuse the material.

The definitive version of this article is the electronic one which can be found at:

<https://doi.org/10.3762/bjoc.18.130>



Microelectrode arrays, electrosynthesis, and the optimization of signaling on an inert, stable surface

Kendra Drayton-White[†], Siyue Liu[†], Yu-Chia Chang, Sakashi Uppal and Kevin D. Moeller^{*}

Full Research Paper

Open Access

Address:

Washington University in Saint Louis, Saint Louis, Missouri 63130, United States

Email:

Kevin D. Moeller^{*} - moeller@wustl.edu

^{*} Corresponding author [†] Equal contributors

Keywords:

calibration of binding curves; electrochemical signaling; microelectrode array

Beilstein J. Org. Chem. **2022**, *18*, 1488–1498.

<https://doi.org/10.3762/bjoc.18.156>

Received: 11 July 2022

Accepted: 10 October 2022

Published: 20 October 2022

This article is part of the thematic issue "Molecular and macromolecular electrochemistry: synthesis, mechanism, and redox properties".

Guest Editor: S. Inagi

© 2022 Drayton-White et al.; licensee Beilstein-Institut.

License and terms: see end of document.

Abstract

Microelectrode arrays are powerful tools for monitoring binding interactions between small molecules and biological targets. In most cases, molecules to be studied using such devices are attached directly to the electrodes in the array. Strategies are in place for calibrating signaling studies utilizing the modified electrodes so that they can be quantified relative to a positive control. In this way, the relative binding constants for multiple ligands for a receptor can potentially be determined in the same experiment. However, there are applications of microelectrode arrays that require stable, tunable, and chemically inert surfaces on the electrodes. The use of those surfaces dictate the use of indirect detection methods that are dependent on the nature of the stable surface used and the amount of the binding partner that is placed on the surface. If one wants to do a quantitative study of binding events that involve molecules on such a stable surface, then once again a method for calibrating the signal from a positive control is needed. Fortunately, the electrodes in an array are excellent handles for conducting synthetic reactions on the surface of an array, and those reactions can be used to tune the surface above the electrodes and calibrate the signal from a positive control. Here, we describe how available Cu-based electrosynthetic reactions can be used to calibrate electrochemical signals on a polymer-coated electrode array and delineate the factors to be considered when choosing a polymer surface for such a study.

Introduction

Microelectrode arrays composed of collections of electrodes that can each be individually addressed are powerful platforms for monitoring interactions between a protein target and small

molecules [1–8]. In these efforts, molecules are either placed or synthesized by specific, selected electrodes in the array, and then the associated electrodes are used to monitor any subse-

quent binding events involving those molecules [8,9]. The method frequently relies on the chemistry used to place or synthesize the molecules by the surface of the electrodes in the array because it is the nature of those molecules that defines the biological interactions that can be studied [10,11]. As discussed below, such efforts need to not only control the selectivity of the reactions for specific, predetermined sites on the array, but also control the surface concentration of the molecules placed at those sites.

In the majority of such studies, the molecules to be added to the electrodes in an array are attached directly to the array either through the use of a self-assembled monolayer or direct functionalization of a carbon electrode [12,13]. Following the synthetic chemistry used to place molecules on a microelectrode array, binding events on the surface of the array are typically monitored by using the electrodes in the array to measure current changes that are caused by that event. The method is ideal in that it allows for the "real-time" detection of the binding event. In many cases, these measurements are made using an electroactive group that is incorporated into, or found naturally in, either the molecule placed on the surface of the electrodes or in the protein target. The binding event changes the distance between this electroactive group and the associated electrodes resulting in a change in the ability of the electrode to either oxidize or reduce the group. This causes a change in the current measured for the redox reaction [14]. Alternatively, the binding event can be detected with an indirect, impedance-based method. This method works by inserting a functionalized electrode into a solution containing a redox mediator. The mediator is oxidized at the electrodes in the array and reduced at a remote counter electrode. This results in a current that can be measured at each electrode in the array. The protein target is then added to the solution above the array, and when it binds one of the molecules fixed to the surface of a set of electrodes in the array it causes a change in the current to be measured at those electrodes. This change in current can be recorded and the binding event monitored. By varying the concentration of the protein in solution and recording the corresponding change in current, a binding curve for the interaction can be generated.

While this approach can be very effective, it has limitations. We are interested in using microelectrode arrays to guide synthetic efforts to build molecular probes for protein active sites. For example, consider a pair of molecules (Figure 1) that selectively inhibit the G_{q/11}-signaling pathway in cells [15,16]. The molecules are complex cyclic peptides, and the construction of analogs of the molecules to probe the basis of their activity is a significant challenge. In an ideal situation, the design and synthesis of those analogs would be informed by biological data that was gathered iteratively with the synthetic efforts. That

scenario requires each new analog synthesized to be rapidly and accurately evaluated for activity. Microelectrode arrays that can be used to quickly gather real-time data on binding events appear ideal for such an iterative study. However, to use a microelectrode array in this fashion requires that the molecules being synthesized be added to the surface of an array as they become available, and then the growing library analyzed in a manner that allows the relative binding of the new analog to be compared to previous analogs and the natural products.

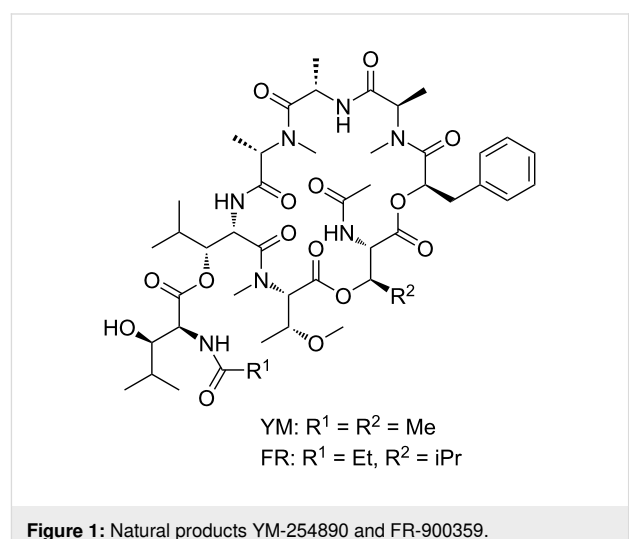
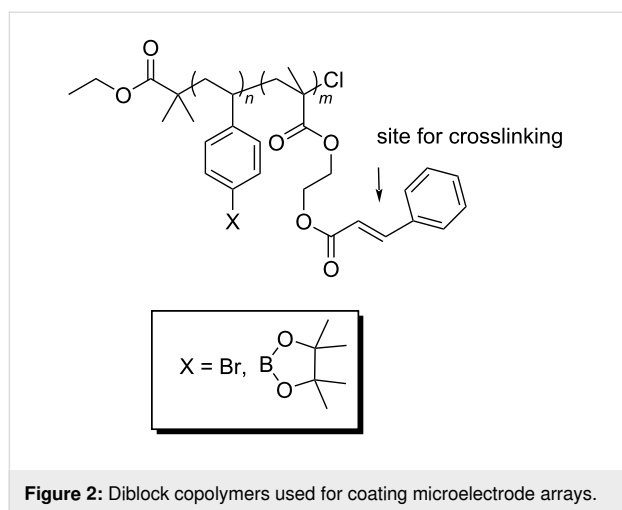


Figure 1: Natural products YM-254890 and FR-900359.

For the strategy to be viable, the surface coating on the electrodes must be very stable over time, chemically inert to the reactions used to place molecules on the array, and tunable so that nonspecific interactions can be minimized for a variety of biological targets. Self-assembled monolayers do not have this stability, and strategies that chemically modify carbon electrodes do not offer the chemical flexibility or surface tunability needed. Hence, an alternative strategy is required. This led to the development of polymer-coated arrays that capitalize on the versatility of diblock copolymers as surface coatings (Figure 2) [17–19]. In the polymer, one of the blocks is used to place attachment sites for molecules above the electrodes (the aryl-bromide or arylborate block in the polymer shown), and the other block is used to provide a site for cross-linking the polymer in order to render the surface more stable once it is coated onto an array (the cinnamate block is used to make a polymer network through photochemical cross-linking). The use of the borate ester surface provides a tunable surface that can be used to help prevent non-specific binding and minimize biofouling possibilities [18]. While the use of a diblock copolymer coating offers the desired stability advantage, it also rules out the use of both direct methods for conducting synthetic transformations on the array and the direct detection methods in the subsequent binding studies. The polymer

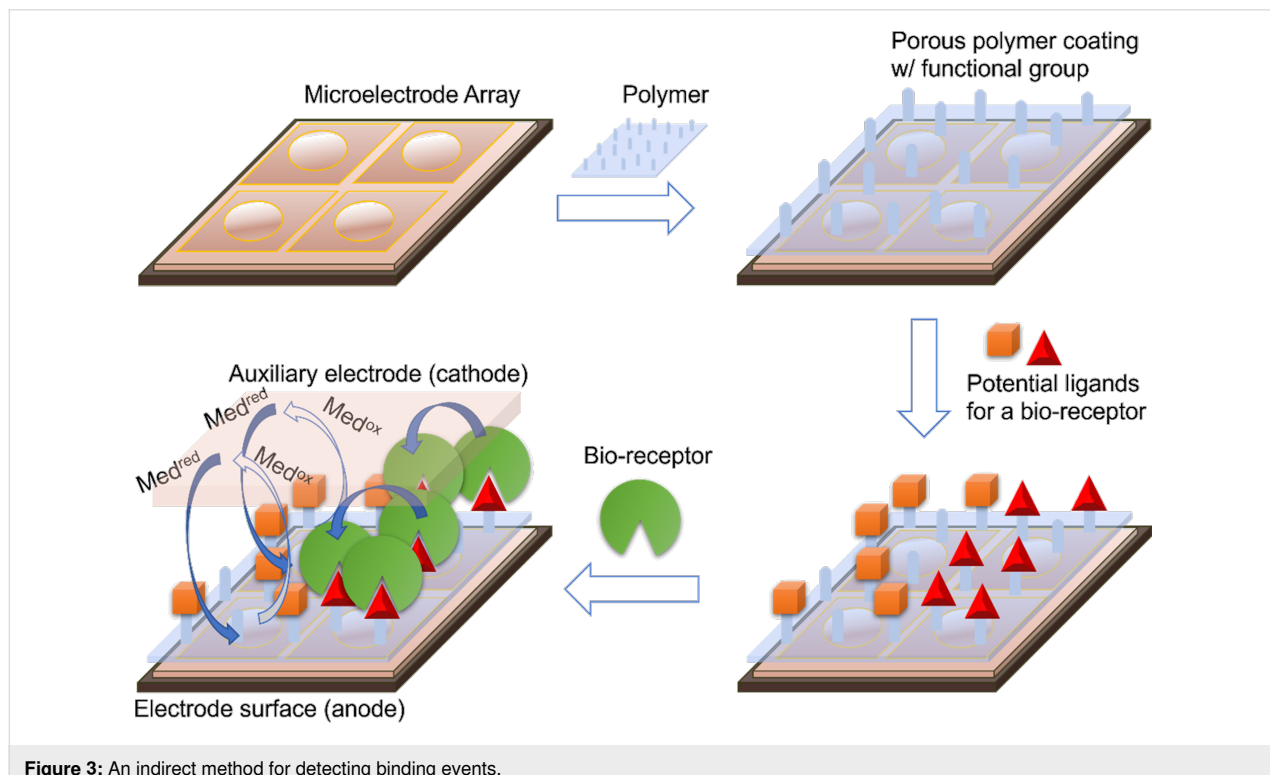
network is not permeable to molecules tethered to its surface or proteins in solution.

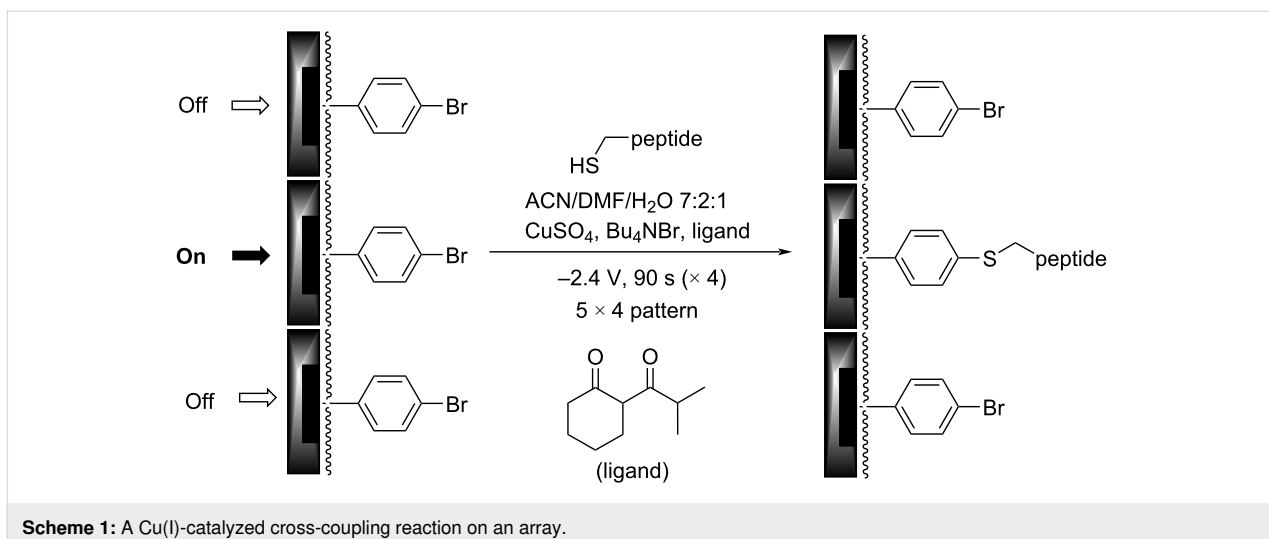


The synthetic problem was solved by using the electrodes in an array to generate chemical reagents and catalysts and then confining those reagents and catalysts (and the reactions they mediate) to the surface of the electrodes for their generation [10,11]. For the subsequent signaling experiments, the impedance-based approach outlined above has proven effective with polymer-coated electrodes (Figure 3). As described, this method works by inserting a functionalized electrode into a solution

containing a redox mediator and then monitoring the current associated with a redox mediator. The method is different relevant to the traditional methods lacking the polymer surface in that the current is dependent on changes to the polymer coating; a situation that can lead to analogous drops in current to methods involving molecules bound directly to an electrode surface or increases in current if a binding event helps to swell a polymer.

The utility of this approach for a polymer-coated electrode was verified by looking at several small molecule–protein interactions [5–7]. For example, a binding curve generated for the interaction between an RGD-peptide (C-PEG6-GGRGDGP) and its integrin ($\alpha 5, \beta 1$) target is shown in Figure 4 below. A PEG-linker was added to the RGD-peptide so that the peptide would not be buried in the polymer coating the surface of the array, a scenario that would make it unavailable for binding to the integrin receptor in the subsequent analytical experiment. The PEG-6-linker was selected because it was effective and readily available from commercial sources. This linker was functionalized with a cysteine on the end opposite the peptide so that the thiol group in the sidechain could be used to place the molecule the array with the use of an electrochemically initiated Cu(I)-catalyzed cross-coupling reaction (Scheme 1) [9]. To this end, the Cu(I) catalyst needed for the reaction was generated at the electrodes by the reduction of Cu(II). Confinement of the Cu(I) catalyst to the selected electrodes was accom-





plished with the use of oxygen in solution. The oxygen oxidized any Cu(I) before it could migrate to a non-selected electrode. The electrodes selected for the reduction were cycled on an off with each cycle turning the electrode on for 90 s and then off for 180 s. This was done to tune the rate of Cu(I) generation to match the rate of Cu(I) oxidation in solution and in so doing optimize confinement of the Cu(I) catalyst to the selected electrodes. Longer "on-times" would lead to more reagent generation making it harder for the confinement strategy to keep up. The result is a loss in confinement. It is important to point out that the reaction shown in Scheme 1 is not a typical electrosynthetic reaction. The cross-coupling reaction shown is a Cu(I)-catalyzed transformation that requires no recycling of a reagent; there is no net oxidation or reduction involved. Instead, on the array the catalyst is purposely destroyed in the solution above the electrodes and then regenerated electrochemically so that the location of the reaction can be confined to only desired sites on the array. Unlike the synthesis of a complex molecule, the synthesis of a complex, two-dimensional addressable surface requires a new type of selectivity – "site-selectivity". The use of electrosynthesis is essential for obtaining this selectivity.

With the substrate on the surface of the array, a hydroquinone/quinone redox couple was then used for the subsequent signaling experiment [20]. The hydroquinone/quinone redox couple has superior stability to the iron-based systems used previously [20], and its use leads to more reproducible binding curves. To generate the binding curve shown in Figure 4, the concentration of the integrin receptor was varied (and plotted on the *x*-axis) and then the current measured for the redox couple by CV (current = peak current for the oxidation – peak current for the reduction) for each concentration of the receptor. Blocks of 12 electrodes were used for recording the current with each data point in Figure 4 representing the average current

measured at three such blocks with the error bars indicating the range in the data. The use of the method to probe interactions between a v107-peptide and its targeted VEGF receptors proved equally effective [7].

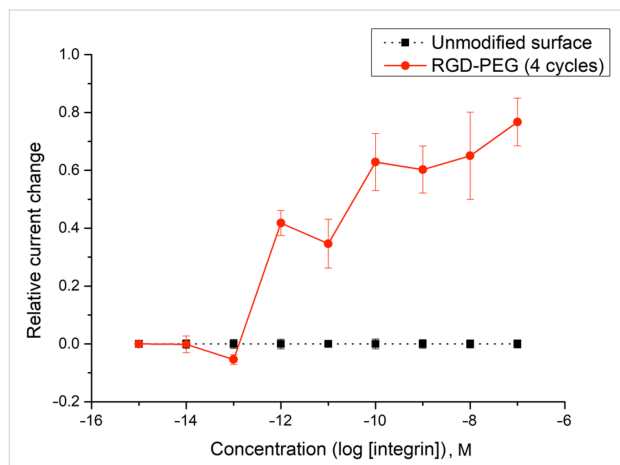


Figure 4: A model study using an RGD peptide (C-PEG6-GGRGDGP) and integrin receptor ($\alpha 5, \beta 1$).

The binding curve shown in Figure 4 did indicate a surface interaction that was stronger than the solution-phase nanomolar K_d -value known for the RGD–integrin binding event. This was not viewed as an issue since we could see the whole binding curve, and the arrays are used to examine relative binding events between molecules on the array and not determine absolute binding constants in the absence of a positive control. In this case, the positive control needed for any subsequent study was clearly visible and quantifiable.

However, the amplification of signals on the array could not be ignored as soon as we sought to use the arrays to guide the syn-

thesis of YM- and FR-analogs as proposed in connection with Figure 1. YM and FR bind the alpha-subunit of the G-protein. So, we initially sought to show that the signaling approach being taken could monitor this type of interaction. The initial test was conducted with an R6A-peptide and its $\text{G}\alpha_{i1}$ -target (Figure 5) [21]. $\text{G}\alpha_{i1}$ was selected as a positive control for subsequent studies because it can be expressed easily, has roughly 55% homology with the much more difficult to express $\text{G}\alpha_q$ [15], and chimeric proteins are available that have $\text{G}\alpha_{i1}$ modified with a $\text{G}\alpha_q$ binding site for YM and FR [22]. R6A was chosen as the ligand for $\text{G}\alpha_{i1}$ because it was known to bind the target with a binding constant of $K_D = 60 \text{ nM}$ [21]. The binding data shown in Figure 5 compared interactions between $\text{G}\alpha_{i1}$ and two surface bound peptides; R6A (MSQTKRLDDQLY-WWEYLC) and a scrambled R6A sequence (QLSEDTYLLM-RWDYWQK). The two peptides were placed on the array along with a fluorescent dye (LRSC, lissamine rhodamine) that was

used to make sure the placement chemistry was working. The array used was coated with the borate ester diblock copolymer (Figure 2), and the peptides were attached to this polymer through a PEG-6 linker in direct analogy to the RGD-peptide experiment shown above. In this case, a Cu(II)-mediated Chan–Lam coupling reaction was used to place each molecule on a arylborate ester coating the array (Scheme 2) [23]. The Cu(II) needed for the transformation was generated at the selected electrodes by the oxidation of a Cu(I) precursor, and then confined to the surface of those electrodes with the use of a solution-phase Cu(II)-mediated disulfide bond-forming reaction using excess substrate in solution. The molecules were placed by individually addressable blocks of electrodes on the array that were each comprised of 65 individual electrodes. This was done to increase the amount of current measured for the block of electrodes relative to many experiments that use blocks of 12 electrodes.

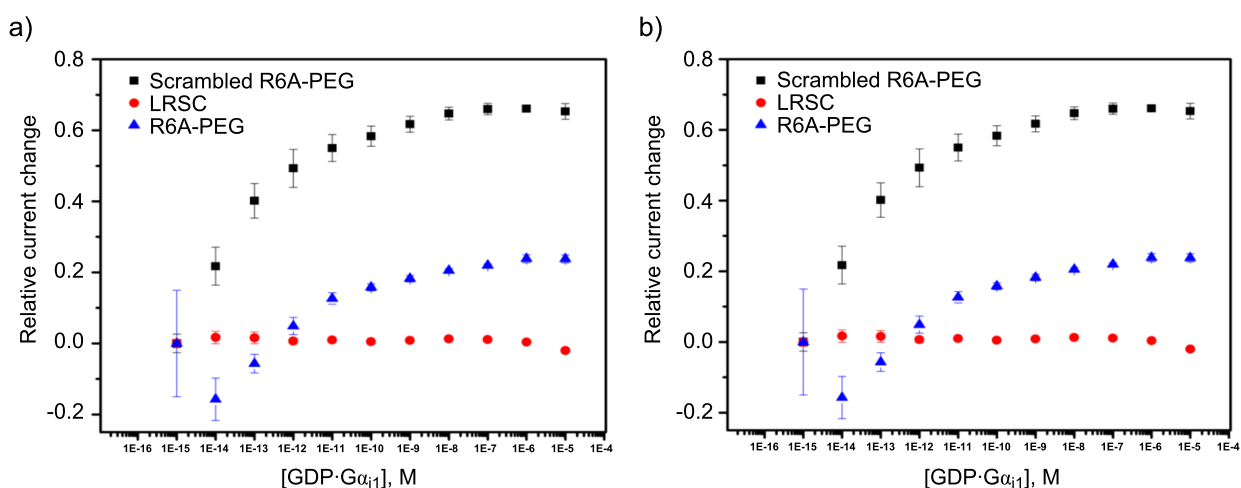
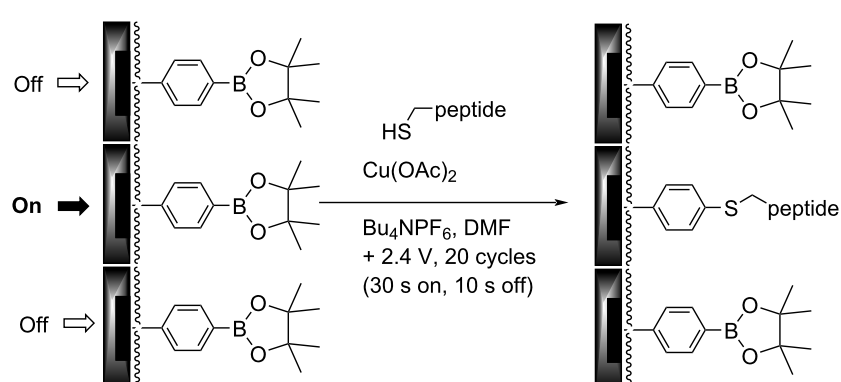


Figure 5: A failure in connection with the monitoring of binding events between a peptide and its G-protein target. a) Binding curve generated for $\text{G}\alpha_{i1}$ binding to scrambled R6A peptide (black), LRSC peptide (red), and R6A peptide (blue). b) Binding curve generated after subtraction of nonspecific binding for $\text{G}\alpha_{i1}$ binding to scrambled R6A peptide (black) and R6A peptide (red).



Scheme 2: An array-based Chan–Lam coupling reaction.

Once the molecules were in place, the array was placed in a buffer solution (see Supporting Information File 1 for details) containing ferrocene carboxylic acid as a redox mediator. Initially, the array was placed in a solution containing the smallest concentration of $\text{G}\alpha_{i1}$ and then a current measured for the mediator at the electrodes in the array. The solution was then removed, replaced with a mediator/buffer solution containing the next highest concentration of $\text{G}\alpha_{i1}$, and the current for the mediator again measured. This procedure was repeated for each concentration of $\text{G}\alpha_{i1}$. From the data, it was clear that there was little binding to the electrodes proximal to the LRSC dye. At those electrodes, no change in current was evident as the concentration of receptor was varied. However, significant binding occurred for both the scrambled R6A and R6A itself. For the specific plots shown, we had been looking for the binding event to decrease the current. It did not. Instead, the binding event swelled the polymer, made it easier for the redox couple to reach the electrode, and thus caused an increase in the current. This led to an increase in current being shown as negative because it was opposite of what was planned and what we had seen in previous studies.

At this point, the non-specific binding of $\text{G}\alpha_{i1}$ to the functionalized surface was removed from the data by subtracting the curve obtained for the scrambled peptide from both the scrambled peptide and R6A (Figure 5b). This revealed a clear, immediate change in current for the binding of $\text{G}\alpha_{i1}$ to R6A. A rapid change in current of this nature can indicate either a binding event that is already occurring at the start of the experiment or a precipitation event (Figure 6). However, a precipitation event would cause a drop in current since precipitation of the protein onto a polymer-coated electrode prevents the mediator from reaching the electrodes below the polymer. Hence, the increase in current seen in the experiment shown in Figure 5b was associated with a binding event that was already occurring at the start of the experiment. The net result was that a full binding curve for the positive control selected for subsequent comparisons could not be observed. Hence, any subsequent evaluation of binding events using synthesized analogs of YM and FR could not be quantified. A method for calibrating the positive control had to be found.

With the signal for the R6A/ $\text{G}\alpha_{i1}$ interaction amplified out of the window for the experiment, the question became what caused the amplification and how the problem could be remedied. Amplifications of surface-based signals are typically caused by the presence of multiple ligands for the receptor above any given electrode. If the protein dissociates from one ligand and then rapidly binds another on the surface of the electrode, then it never leaves the surface. The surface does not recover its original conductivity and the experiment shows a

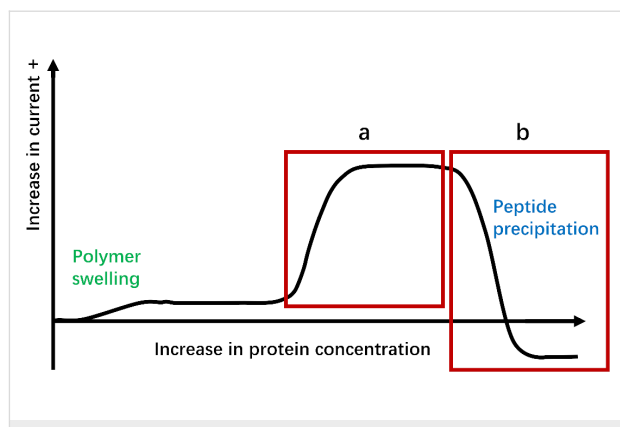


Figure 6: Potential for an immediate, rapid change in current. a) The binding event being monitored has already started. b) Precipitation of the protein target.

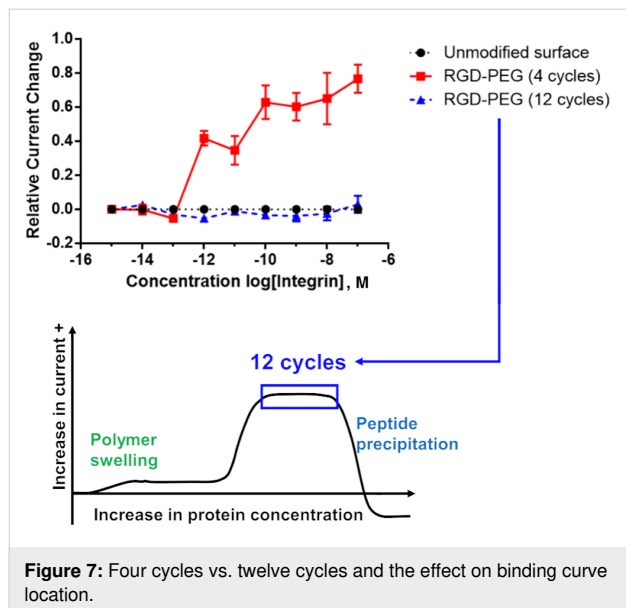
binding constant that is greater than either of the individual interactions. Alternatively, the surface-bound substrate could lead to avidity events where more than one of the ligands binds to the protein at the same time by taking advantage of allosteric binding sites.

Either way, the result is the same. The data shown in Figure 5 cannot be used to assess the binding strength of the interaction. The experiment needed to be calibrated so that the signal could be moved into the window where the full binding curve could be observed.

Both of the possible causes for amplification of the signal result from too high of a concentration of ligand on the surface of the electrodes. Solving the problem requires a reduction in the amount of peptide on the surface of the electrodes in the array. This can be accomplished in two ways. First, the amount of material placed on the array can be decreased by cutting the reaction time used for the placement reaction. The amount of material placed onto the surface of an array is linearly dependent on the time used for the placement reaction up until the surface becomes saturated [23]. Second, the peptide to be placed on the surface of the array can be diluted with a substrate that does not bind the receptor before placement on the array. For any given reaction time, this would lower the density of the active peptide ligand on the surface of the electrode where it was placed. Of course, a combination of the two methods can be used.

In order to probe the effectiveness of these two methods with a cheaper option than $\text{G}\alpha_{i1}$, the effect of peptide surface concentration on the location of the binding curve obtained was initially studied with the more readily available RGD-peptide/integrin pair. Initially, the amount of RGD-peptide placed on the array was increased to see if we could mimic the experiment with the R6A/ $\text{G}\alpha_{i1}$ pair that amplified the binding curve

out of the observable window. This effort is highlighted in Figure 7.



For this experiment, the number of cycles used for placement of the RGD-PEG₆ substrate onto the array was varied from 4 cycles (the initial experiment shown in Figure 4) to 12 cycles. As in the earlier experiments, each cycle involved turning the electrode on for 90 s and then off for 180 s. The more cycles used the longer the time employed for the placement reaction. The "binding curves" generated at the electrodes with these two placement times were compared with the background signal derived from the unfunctionalized polymer. The more stable (relative to iron-based mediator pairs) hydroquinone/quinone redox pair was used, again in direct analogy to the experiment shown in Figure 4. The current associated with this redox couple at each of the electrode in the array was again monitored by using the array as an anode and the remote Pt electrode in the electrolysis cell as a cathode. The surface of the array was the arylbromide-based diblock copolymer. Binding between the integrin receptor and the RGD peptide on the polymer increased the solubility of the polymer above the associated electrodes and in so doing increased the current associated with the mediator. This change in current relative to the concentration of integrin in solution is what is recorded in Figure 7. From here on in, all changes in current on the array will be plotted as positive since the increase in current was observed for every experiment conducted in this study.

The background signal measured using the unfunctionalized electrodes showed no signal. This indicated the absence of any significant non-specific binding event between the integrin receptor and the polymer coating on the array. When 4 cycles

were used to place the RGD-peptide (with the C-PEG₆ linker) on the surface of the electrodes, the subsequent analytical experiment led to a clear binding curve. Once again, the binding curve measured in this manner was amplified relative to the known nanomolar binding constant for the interaction. When three times the reaction time was used for the placement reaction (12 cycles), the binding curve was amplified out of the window. In this case, no signal could be observed. This was not a surprise since the experiment measures a change in current from the initial starting point. If the binding event is complete at the initial concentration, then no current change will be measured, and the experiment gives rise to an "curve" that cannot be distinguished from background.

The observation highlights why it is essential that all array-based studies contain a positive control that can be used to demonstrate that a binding event can be measured using the synthetic conditions employed. This is particularly important since the amount of material on the surface of an electrode is dependent not only on the length of time for the placement experiment, but also on the surface itself. A thicker polymer coating affords more attachment sites for the peptide placed on the array, a thinner polymer fewer. Hence, the surface coverage for a given placement reaction is dependent both on the time used for the experiment and the thickness of the polymer coating. While the thickness of the surface was initially characterized for the coating of an array [17], that thickness is not perfectly reproducible from one array to the next. Consider the two different signaling experiments shown in Figure 8. Both were performed in a manner identical to the experiment shown in Figure 7. In the first experiment, a single array was used to compare a placement reaction conducted for 4 cycles with one conducted for 25 cycles. The two experiments were conducted at different regions of the array. The binding curve for the experiment using 4 cycles closely resembled the experiment shown in Figure 7. However, there was a significant difference with the experiment using a longer placement reaction. In this case, part of the binding curve could be seen. The lower total change in current observed was due to the fact that only the top piece of the binding curve was observed with much of the binding curve remaining out of the window of the experiment. Hence the total change in current from the starting point of the experiment was smaller. When compared to the earlier experiment shown in Figure 7, the binding curve was still shifted out of the window of the experiment with the longer placement reaction but not as far as the earlier experiment. The difference was due to the change in the coating on the array. A thinner polymer coating on the portion of the array used for the 25-cycle placement reaction would mean less material on the surface of the array, even relative to a different array using 12 cycles for the placement reaction. So, the overall conclusion

of the two experiments was the same. The location of the binding curve could be calibrated so that the entire binding curve could be seen by controlling the amount of peptide on the surface of the electrodes. But, the specific details of the experiments were not identical.

The same conclusion was reached with the second experiment shown in Figure 8. In this case, the difference between the placement reactions was kept small in order to see how sensitive the experiment was to the placement reaction. The electrodes functionalized with a placement reaction using 4 cycles and the electrodes functionalized with a placement reaction using 3 cycles gave rise to almost identical binding curves that could be seen in their entirety. However, those binding curves were not in the same location as that observed for the experiment in Figure 7. The polymer thickness on this array was again thinner leading to peptide on the surface of the electrodes.

Clearly, the method is not compatible with providing an absolute measure for a binding constant in the absence of a positive control. There is simply too much variance in the coating of the surface from one array to the next. Fortunately, it was also clear from the observations that once an experiment was calibrated to place a positive control in the center of observable window, variations in the surface from experiment to experiment will not move the positive control out of that window.

Evidence for the variations on a single array being relatively small is shown in Figure 9. In this experiment, a 12K array was coated with the arylbromide-based diblock copolymer and then blocks of 12 electrodes each functionalized with pyrene-butanol at various places on the array. For the placement reaction, the Cu(I)-catalyzed cross-coupling reaction used above

(Scheme 1) was employed for 4 cycles (90 s on and 180 s off). The chemistry placed enough of the alcohol by the electrodes for the pyrene to form the exciplex dimer that fluoresces in the red region of the spectrum and does not self-quench. A fluorescence microscope was then used to take an image of the array, and the image used to quantify the fluorescence, and thereby the amount of material present, at each region of the array. The process was repeated three times on the same array in order to generate an average intensity for each region examined. Two blocks of electrodes were examined from the top, center, and bottom regions of the array. While the data did not vary to a large extent, there were differences in the amount of material placed at the top, center, and bottom regions of the array. Variations within the regions were smaller. Since all of the placement reactions were run at the same time for the same duration,

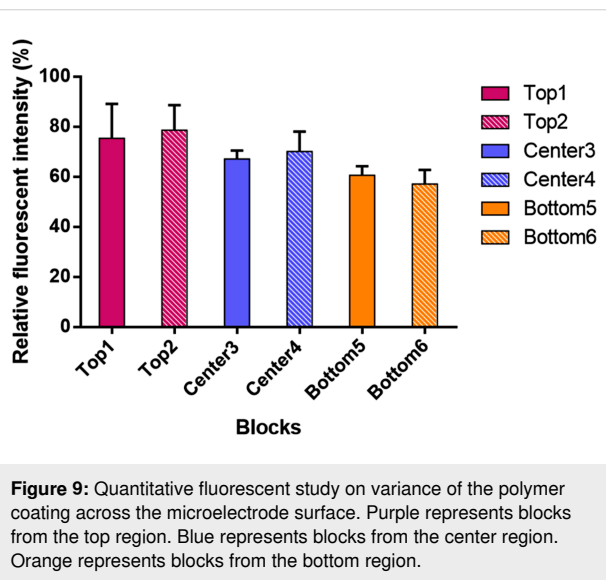


Figure 9: Quantitative fluorescent study on variance of the polymer coating across the microelectrode surface. Purple represents blocks from the top region. Blue represents blocks from the center region. Orange represents blocks from the bottom region.

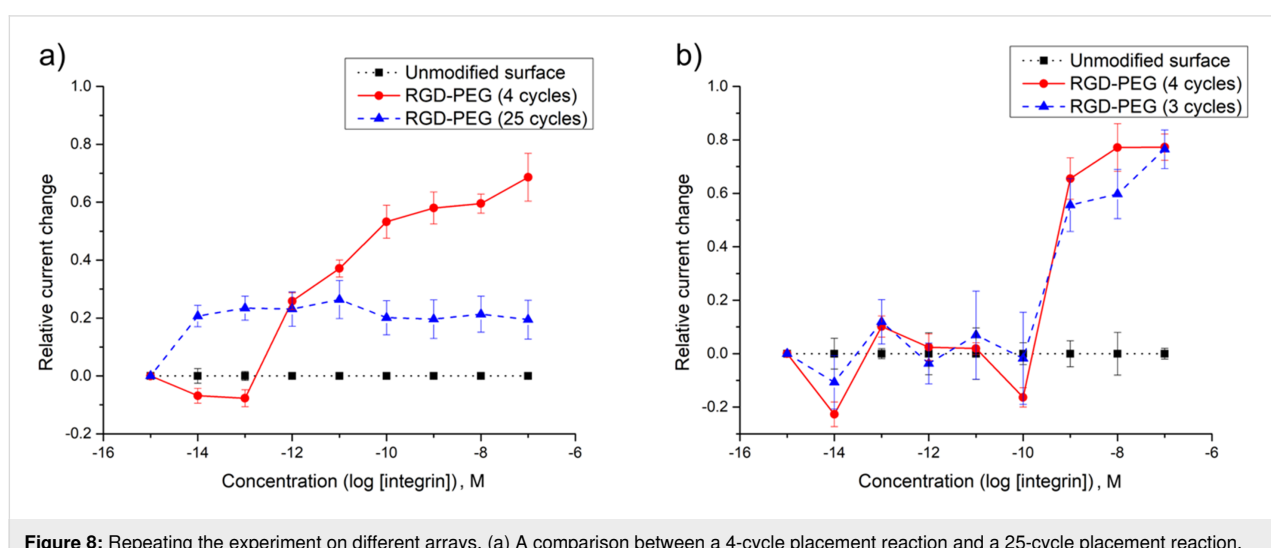


Figure 8: Repeating the experiment on different arrays. (a) A comparison between a 4-cycle placement reaction and a 25-cycle placement reaction. (b) 3 vs. 4 cycles.

the only difference between the sites examined was a lack of uniformity in the polymer coating on the array. From a practical standpoint, the variance in the nature of the surface on an array translates into signaling studies with smaller error bars if a single region of the array is used for any given analysis. With a total of 12,544 electrodes on the array, this is not typically a problem. There are more than enough electrodes in any one region of the array for an extensive study.

With that information in place, attention was turned back to the initial small molecule/G-protein interaction that lies at the heart of guiding the synthetic study proposed in connection with Figure 1. Initially, the same approach used for the RGD/integrin model system was employed for this study. Namely, the amount of the R6A-peptide placed on the array was controlled by the number of cycles used for the placement reaction. The R6A-peptide was first attached to a C-PEG₆-linker, and then the Cu(I)-catalyzed reaction used for its placement on an array coated with the arylbromide-based diblock copolymer. The reaction conditions for the placement reaction were identical to those described above.

In this case, the effort to shift the curve into the window of the experiment was not successful. No matter how few cycles were used for the placement reaction, the full binding curve for the interaction between R6A and its $\text{G}\alpha_{i1}$ -target could not be observed. A method was needed to further reduce the concentration of the R6A peptide on the surface of the electrodes. To this end, cysteine methyl ester was selected as a molecule with which to dilute the R6A peptide because cysteine methyl ester

does not show any background binding to $\text{G}\alpha_{i1}$, and it can be efficiently placed onto the arylbromide-based surface using the same Cu(I)-catalyzed cross-coupling reaction used to place the R6A-PEG-C substrate on the array (Scheme 3).

The first attempt at the dilution study compared a set of control electrodes that had only the cysteine methyl ester placed on the polymer coating their surfaces, a set of electrodes that were functionalized with only the R6A-PEG-C substrate, and a set of electrodes that were functionalized with a 1:1 mixture of R6A-PEG-C to cysteine methyl ester (Figure 10). The placement

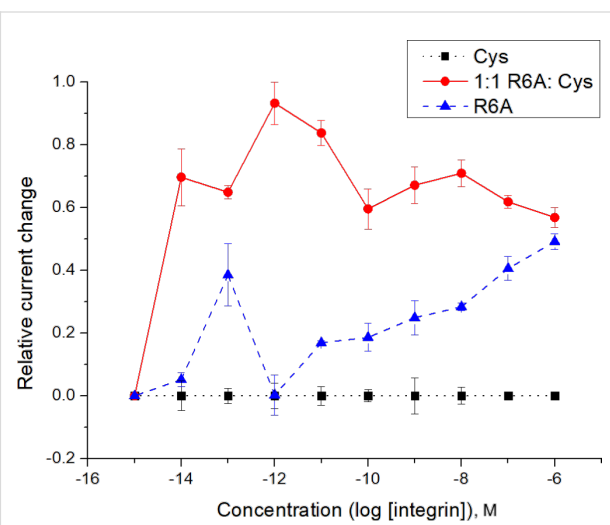
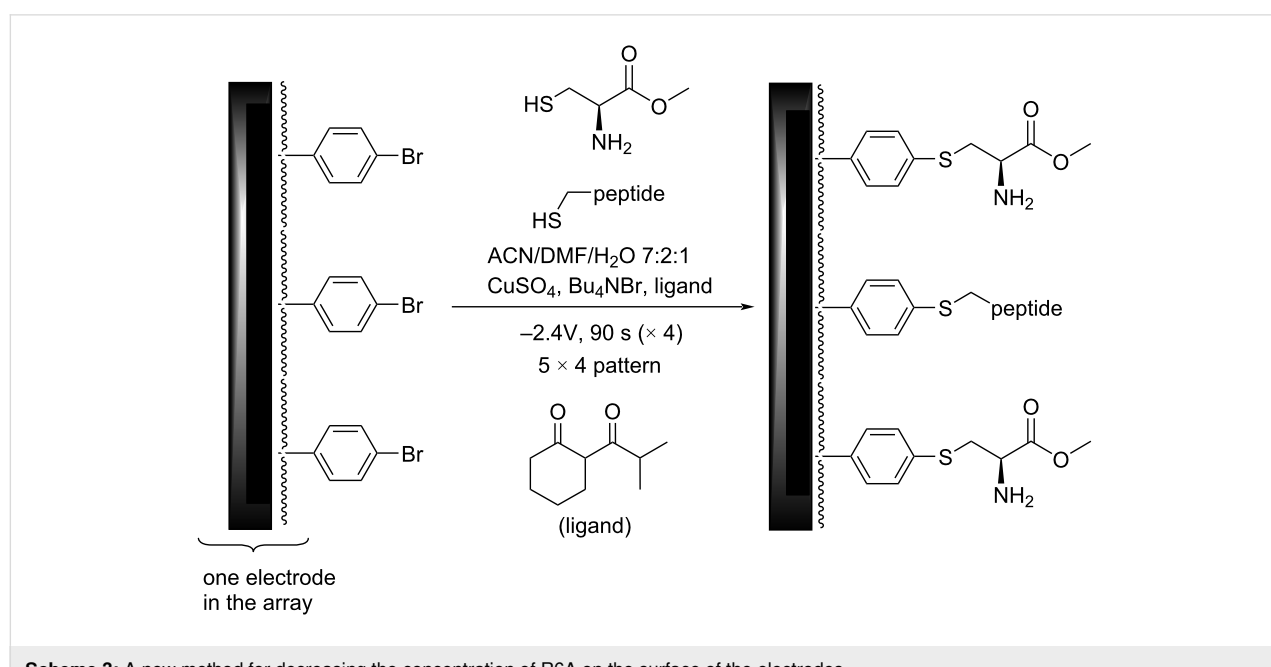


Figure 10: An initial study and the comparison of an R6A surface and a 1:1 R6A/cysteine methyl ester surface.



reactions were conducted for 4 cycles using the method described above.

The analytical study used the hydroquinone/quinone redox couple as the mediator and then added increasing amounts of the $\text{G}\alpha_{i1}$ -protein in solution as indicated in Figure 10. The electrodes functionalized with only cysteine showed no interaction with $\text{G}\alpha_{i1}$. Those electrodes were used as a baseline to subtract any non-specific binding from the other curves. The signal from the electrodes functionalized with only the R6A-PEG substrate showed negligible binding over the background indicating that the signal was amplified completely out of the window for the experiment. A significant binding event was observed at the electrodes functionalized with a 1:1 mixture of R6A-PEG and cysteine, although it was still shifted out of the window so that only the latter portion of the binding curve could be observed.

With this initial experiment in place, the ratio of cysteine to the R6A-PEG substrate was varied (Figure 11). The experiments shown in Figure 11a and b were run on different arrays by different individuals at different times. The two experiments used very similar dilutions, and they afforded very similar results. The full binding curve could be seen for each experiment although both were close the edge of the window. It did appear that for the R6A- $\text{G}\alpha_{i1}$ small variations in the surface of the array were not a significant issue. Further dilution of the R6A

peptide with cysteine methyl ester (Figure 11c and d) then illustrated how the location of the binding curve could be moved within the window of the experiment, an observation that shows how the array experiment can be calibrated in order to place the positive control where it can best be used for comparison with other interactions involving $\text{G}\alpha_{i1}$. Further adjustments could be made to place the signal in the middle of the window, but that level of optimization was deemed unnecessary for a model study.

Conclusion

Indirect measurements on microelectrode arrays have two consistent issues. One is that the signals are amplified by either avidity effects or multiple binding events happening on the surface of an electrode. The second is that variations between arrays and the coatings placed on the arrays can cause shifts in the binding constants measured for any given interaction. These two problems can both be addressed by controlling the concentration of a ligand on the surface of the electrodes, something that can be readily accomplished using an electrosynthetic reaction. This allows for calibration of a signaling experiment and the placement of a positive control in the center of the observable window. The result is an opportunity to measure relative binding constants for ligands for a given receptor. The results presented set the stage for using microelectrode arrays to guide synthetic efforts aimed at probing G-protein/peptide interactions.

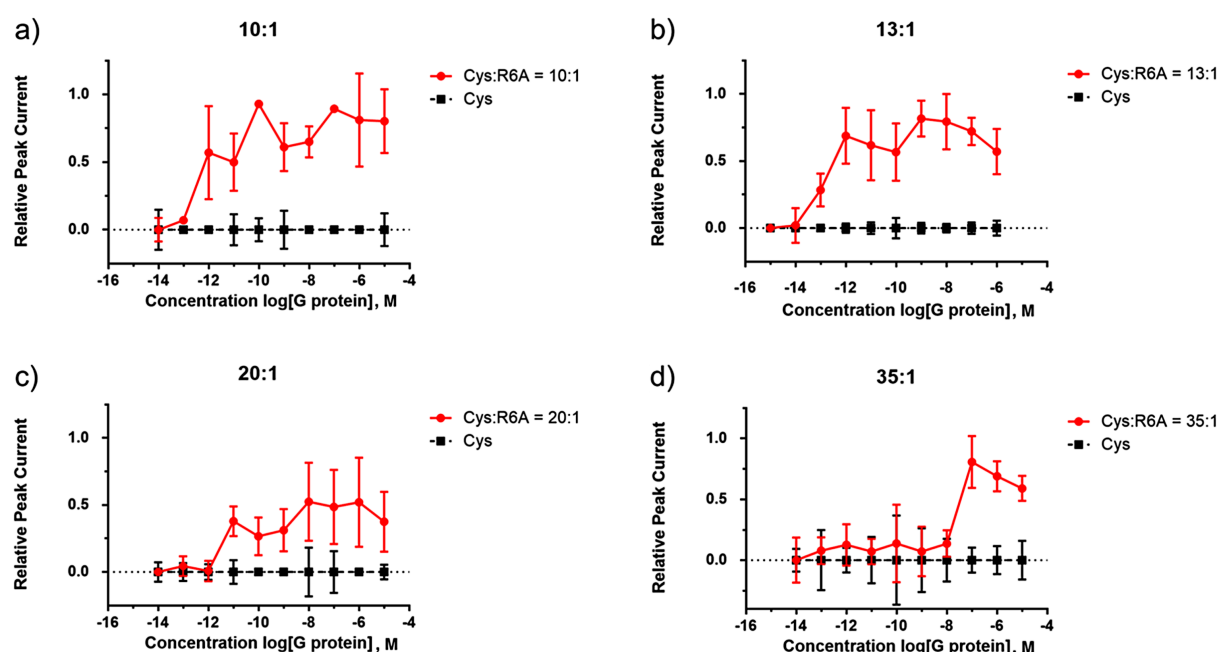


Figure 11: Calibrating the array-based signaling experiment for monitoring small molecule G-protein interactions.

Supporting Information

Supporting Information File 1

Procedures for electrolysis and cyclic voltammetry experiments, characterization of electrolysis products, procedures for synthesis and characterization of electrolysis starting materials.

[<https://www.beilstein-journals.org/bjoc/content/supplementary/1860-5397-18-156-S1.docx>]

Funding

We thank the National Institutes of Health (1R01 GM122747) for their generous support of this work.

ORCID® iDs

Siyue Liu - <https://orcid.org/0000-0003-3797-0687>

Yu-Chia Chang - <https://orcid.org/0000-0002-9307-3780>

Kevin D. Moeller - <https://orcid.org/0000-0002-3893-5923>

References

- Chandra, S.; Siraj, S.; Wong, D. K. Y. *ChemElectroChem* **2017**, *4*, 822–833. doi:10.1002/celc.201600810
- Lee, E.-j.; Chan, E. W. L.; Luo, W.; Yousaf, M. N. *RSC Adv.* **2014**, *4*, 31581–31588. doi:10.1039/c4ra03795b
- Li, J.; Sun, C.-L.; An, P.; Liu, X.; Dong, R.; Sun, J.; Zhang, X.; Xie, Y.; Qin, C.; Zheng, W.; Zhang, H.-L.; Jiang, X. *J. Am. Chem. Soc.* **2019**, *141*, 8816–8824. doi:10.1021/jacs.9b01003
- Soscia, D. A.; Lam, D.; Tooker, A. C.; Enright, H. A.; Triplett, M.; Karande, P.; Peters, S. K. G.; Sales, A. P.; Wheeler, E. K.; Fischer, N. O. *Lab Chip* **2020**, *20*, 901–911. doi:10.1039/c9lc01148j
- Stuart, M.; Maurer, K.; Moeller, K. D. *Bioconjugate Chem.* **2008**, *19*, 1514–1517. doi:10.1021/bc800025z
as well as references [6] and [7] (examples using the arrays employed here).
- Fellet, M. S.; Bartels, J. L.; Bi, B.; Moeller, K. D. *J. Am. Chem. Soc.* **2012**, *134*, 16891–16898. doi:10.1021/ja308121d
- Graaf, M. D.; Marquez, B. V.; Yeh, N.-H.; Lapi, S. E.; Moeller, K. D. *ACS Chem. Biol.* **2016**, *11*, 2829–2837. doi:10.1021/acscchembio.6b00685
- Dill, K.; Montgomery, D. D.; Wang, W.; Tsai, J. C. *Anal. Chim. Acta* **2001**, *444*, 69–78. doi:10.1016/s0003-2670(01)01155-2
- Bartels, J.; Lu, P.; Maurer, K.; Walker, A. V.; Moeller, K. D. *Langmuir* **2011**, *27*, 11199–11205. doi:10.1021/la201881k
- Graaf, M. D.; Moeller, K. D. *Langmuir* **2015**, *31*, 7697–7706. doi:10.1021/la504254e
- Yeh, N.-H.; Zhu, Y.; Moeller, K. D. *ChemElectroChem* **2019**, *6*, 4134–4143. doi:10.1002/celc.201900851
- Sheridan, M. V.; Lam, K.; Sharafi, M.; Schneebeli, S. T.; Geiger, W. E. *Langmuir* **2016**, *32*, 1645–1657. doi:10.1021/acs.langmuir.6b00012
- Karbelkar, A. A.; Furst, A. L. *ACS Infect. Dis.* **2020**, *6*, 1567–1571. doi:10.1021/acsinfecdis.0c00342
- Wehmeyer, K. R.; White, R. J.; Kissinger, P. T.; Heineman, W. R. *Annu. Rev. Anal. Chem.* **2021**, *14*, 109–131. doi:10.1146/annurev-anchem-061417-125655
- Nishimura, A.; Kitano, K.; Takasaki, J.; Taniguchi, M.; Mizuno, N.; Tago, K.; Hakoshima, T.; Itoh, H. *Proc. Natl. Acad. Sci. U. S. A.* **2010**, *107*, 13666–13671. doi:10.1073/pnas.1003553107
- Tietze, D.; Kaufmann, D.; Tietze, A. A.; Voll, A.; Reher, R.; König, G.; Hausch, F. *J. Chem. Inf. Model.* **2019**, *59*, 4361–4373. doi:10.1021/acs.jcim.9b00433
- Hu, L.; Bartels, J. L.; Bartels, J. W.; Maurer, K.; Moeller, K. D. *J. Am. Chem. Soc.* **2009**, *131*, 16638–16639. doi:10.1021/ja907000m
- Hu, L.; Graaf, M. D.; Moeller, K. D. *J. Electrochem. Soc.* **2013**, *160*, G3020–G3029. doi:10.1149/2.004307jes
- Yeh, N.-H.; Medcalf, M.; Moeller, K. D. *J. Am. Chem. Soc.* **2018**, *140*, 7395–7398. doi:10.1021/jacs.8b02922
- Gulaboski, R.; Bogeski, I.; Mirčeski, V.; Saul, S.; Pasieka, B.; Haeri, H. H.; Štefová, M.; Stanoeva, J. P.; Mitrev, S.; Hoth, M.; Kappl, R. *Sci. Rep.* **2013**, *3*, 1865. doi:10.1038/srep01865
- Ja, W. W.; Roberts, R. W. *Biochemistry* **2004**, *43*, 9265–9275. doi:10.1021/bi0498398
- Onken, M. D.; Makepeace, C. M.; Kaltenbronn, K. M.; Kanai, S. M.; Todd, T. D.; Wang, S.; Broekelmann, T. J.; Rao, P. K.; Cooper, J. A.; Blumer, K. J. *Sci. Signaling* **2018**, *11*, 10.1126/scisignal.aa06852. doi:10.1126/scisignal.aa06852
- Graaf, M. D.; Moeller, K. D. *J. Org. Chem.* **2016**, *81*, 1527–1534. doi:10.1021/acs.joc.5b02656

License and Terms

This is an open access article licensed under the terms of the Beilstein-Institut Open Access License Agreement (<https://www.beilstein-journals.org/bjoc/terms>), which is identical to the Creative Commons Attribution 4.0 International License

(<https://creativecommons.org/licenses/by/4.0>). The reuse of material under this license requires that the author(s), source and license are credited. Third-party material in this article could be subject to other licenses (typically indicated in the credit line), and in this case, users are required to obtain permission from the license holder to reuse the material.

The definitive version of this article is the electronic one which can be found at:

<https://doi.org/10.3762/bjoc.18.156>